

# CHALMERS



## Estimation of axial load in timber beams using resonance frequency analysis

*Master's Thesis in the Master's Programme Structural Engineering and Building  
Performance Design*

**STEVE LAUX**

Department of Civil and Environmental Engineering  
Division of Structural Engineering  
Steel and Timber Structures  
CHALMERS UNIVERSITY OF TECHNOLOGY  
Göteborg, Sweden 2012  
Master's Thesis 2012:60



MASTER'S THESIS 2012:60

# Estimation of axial load in timber beams using resonance frequency analysis

*Master's Thesis in the Master's Programme Structural Engineering and Building  
Performance Design*

STEVE LAUX

Department of Civil and Environmental Engineering  
*Division of Structural Engineering  
Steel and Timber Structures*  
CHALMERS UNIVERSITY OF TECHNOLOGY  
Göteborg, Sweden 2012

Estimation of Axial Load in Timber Beams Using Resonance Frequency Analysis

*Master's Thesis in the Master's Programme Structural Engineering and Building Performance Design*

STEVE LAUX

© STEVE LAUX, 2012

Examensarbete 2012:60

Department of Civil and Environmental Engineering

Division of Structural Engineering

*Steel and Timber Structures*

Chalmers University of Technology

SE-412 96 Göteborg

Sweden

Telephone: + 46 (0)31-772 1000

Cover:

The picture shows frequency measurements on timber beams under different conditions. (Photo: Steve Laux, 2012)

Chalmers Reproservice / Department of Civil and Environmental Engineering  
Göteborg, Sweden 2012

---

# Estimation of Axial Load in Timber Beams Using Resonance Frequency Analysis

*Master's Thesis in the Master's Programme Structural Engineering and Building Performance Design*

STEVE LAUX

Department of Civil and Environmental Engineering  
Division of Structural Engineering  
*Steel and Timber Structures*  
Chalmers University of Technology

## ABSTRACT

During the last years, the media reported about several timber roof collapses all across Europe, especially during rough winters. This is a serious problem that bears the risk of many fatal incidents and needs to be encountered in order to improve the safety of structures. One solution could be to estimate the axial loads in the structural members using resonance frequency analysis. The results could then be used to assess the safety of timber structures and to decide about their continued use or temporary closure. While this method had already been reported for steel structures, only little research had been carried out in the area of timber structures.

The aim of this project was therefore to investigate if it is possible to estimate the axial loads in timber beams using resonance frequency analysis and if yes, what are the precision requirements for the material properties and the measured frequencies. This was achieved by performing transversal frequency measurements on 32 timber specimens and an aluminium bar under tension. The latter hereby served as homogeneous reference for better interpretation of results. The two first frequencies, together with different values for the E-modulus were then used to estimate the axial load and the rotational stiffness at the boundaries. The numerical model behind the calculations was based on Timoshenko beam theory, allowing to include effects of shear deformations and rotary inertia. The material properties of the specimens were previously determined by static and dynamic tests. Finally, a sensitivity analysis was carried out to investigate the influence of errors in input parameters on the final results.

The best results were obtained using the E-modulus derived from transversal vibration tests and showed a mean error ranging from 7.6% to 46.6%, where the results generally improved for higher loads. When using the E-moduli from longitudinal vibration tests, the mean errors increased to 12.4% to 89.5%. It was also attempted to use the static E-modulus for the calculations, which led however to incorrect results. Dynamic values should be used for the parameter estimation with the presented resonance frequency method. The results of the sensitivity analysis showed that the sensitivity of the estimated axial load decreases for higher load levels, which could also be observed in the test results. The most influential parameters on the quality of the results were the measured frequencies and the clear beam length, followed by the density and the E-modulus.

Key words: resonance frequency analysis, timber beams, axial load, non destructive testing, Timoshenko beam theory, dynamic E-modulus, modal analysis, parameter estimation

---

---

# Contents

1	INTRODUCTION	1
1.1	Background	1
1.2	Aim of the thesis	2
1.3	Method	2
1.4	Limitations	3
1.5	Outlines	3
2	BUILDING MATERIAL TIMBER	5
2.1	Characteristics of timber	5
2.2	Non-destructive methods for timber grading	8
3	DETERMINATION OF AXIAL LOAD AND BOUNDARY CONDITIONS IN SLENDER BEAMS	13
3.1	Determination of axial loads	13
3.2	Determination of boundary conditions	14
3.3	Conclusion	16
4	VIBRATION THEORY	17
4.1	Derivations	17
4.1.1	Longitudinal vibrations	17
4.1.2	Torsional vibrations	18
4.1.3	Transversal vibrations – Euler beam theory	19
4.1.4	Transversal vibrations – Timoshenko beam theory	21
4.2	Applications	22
4.2.1	Longitudinal vibrations	22
4.2.2	Torsional vibrations	24
4.2.3	Transversal vibrations – Euler beam theory	26
4.2.4	Transversal vibrations – Timoshenko beam theory	29
5	NUMERICAL MODELLING AND PARAMETER ESTIMATION	31
5.1	Rayleigh-Ritz method	31
5.2	Discrete model	33
5.2.1	Element mass matrix	33
5.2.2	Element stiffness matrix	33
5.2.3	Element damping matrix	34
5.2.4	Global matrix formulation	34
5.3	Continuous model	36
5.4	Model comparison	37
5.5	Parameter estimation	38

---

5.6	Sensitivity analysis for continuous model with $k_1 = k_2$	39
5.6.1	Sensitivity of S	40
5.6.2	Sensitivity of k	42
5.6.3	Discussion	44
6	MODAL ANALYSIS	45
6.1	Theoretical modal analysis (TMA)	45
6.2	Experimental modal analysis (EMA)	46
6.3	Data acquisition	47
6.4	Data processing	48
7	DETERMINATION OF MATERIAL PROPERTIES	51
7.1	Specimen dimensions and properties	51
7.2	Test equipment and data processing	53
7.3	Determination of static E- and G-modulus	54
7.4	Determination of longitudinal E-modulus	56
7.5	Determination of transversal E- and G-modulus	59
7.6	Summary of results	63
8	TENSION TESTS	67
8.1	Setup and equipment	67
8.2	Test results	69
8.3	Estimation of tensile force S	71
8.4	Determination of ultimate tensile strength	76
9	CONCLUSIONS AND FURTHER RESEARCH	79
9.1	Conclusions	79
9.2	Suggestions for further research	80
10	REFERENCES	81
11	APPENDICES	83
11.1	Appendix A – Matlab codes	83
11.1.1	Calculation of transversal frequencies	83
11.1.2	Calculation of longitudinal E-moduli	89
11.1.3	Calculation of transversal E-moduli	94
11.1.4	Dual parameter estimation	102
11.2	Appendix B – Material properties	114
11.2.1	Density measurements	114
11.2.2	Moisture measurements	115
11.2.3	Four-point bending tests	116

---

11.2.4	Longitudinal vibration tests	117
11.2.5	Transversal vibration tests	130
11.3	Appendix C - Tension tests	144
11.3.1	Results for each specimen	144
11.3.2	Summary of results	244

---

---

## Preface

This study investigated the possibility of using resonance frequency analysis for the estimation of axial loads in timber beams. The project was carried out as cooperation between the Divisions of Structural Engineering, Steel and Timber Structures of ETH Zurich, Switzerland and Chalmers University of Technology, Sweden. All tests were performed in the laboratory of the Division of Structural Engineering at Chalmers University of Technology.

The project was carried out under the supervision of PhD-student Thomas Kruglowa from Chalmers as well as Daniel Sandin from Midapro. Furthermore, much valuable input and support was also received from Michael Klippel, PhD-student at ETH Zurich. The examiners from the different universities were Professor Robert Kliger from Chalmers and Professor Andrea Frangi from ETH Zurich. I would like to thank all these participants for their help and support during this research.

Finally, it should be noted that the tests could never have been conducted without the sense of high quality and professionalism of the laboratory staff. Special thanks are directed to Lars Wahlström.

Gothenburg, June 2012

Steve Laux

---

## Notations

In the notation table, all variables occurring in the report are listed alphabetically.

### Roman upper case letters

$A$	Area of cross section
$A$	Equation coefficient
$B$	Equation coefficient
$C$	Equation coefficient
$C_i$	Equation coefficients
$C'_i$	Equation coefficients
$D$	Equation coefficient
$D_i$	Equation coefficients
$E$	E-modulus
$E_{0,mean}$	Mean E-modulus parallel to the grain for timber
$E_{i,b}$	Dynamic E-modulus from transversal vibration tests
$E_{i,L}$	Dynamic E-modulus from longitudinal vibration tests
$E_{static}$	Static E-modulus
$G$	G-modulus
$G_i$	Dynamic G-modulus from transversal vibration tests
$G_{mean}$	Mean G-modulus for timber
$H$	Factor in the continuous numerical model
$I$	Moment of inertia
$I_p$	Polar moment of inertia
$K_i$	Load levels for the static four-point bending test
$K_t$	Torsional constant
$L$	Beam length or clear span length
$L_{max}$	Maximum clear length for the beam in the tensile machine
$L_{min}$	Minimum clear length for the beam in the tensile machine
$M$	Bending moment
$M_t$	Torsional moment
$N$	Number of terms in the Rayleigh-Ritz method
$S$	Axial load (positive in tension)
$S_E$	Euler buckling load for a simply supported beam
$S_{est}$	Estimated axial load
$S_{max}$	Maximum tensile load
$T^*$	Reference kinetic energy
$T_{max}$	Maximum kinetic energy
$V$	Shearing force
$V_{max}$	Maximum potential energy
$X$	Normal function or modal shape of a vibrating beam
$X_i$	Modal shapes of a vibrating beam
$Y$	Modal shape of a transversally vibrating beam
$Z$	Factor in the continuous numerical model

---

**Roman lower case letters**

$a$	$\sqrt{E/\rho}$
$a$	Distance from the support to the first load (four-point bending test)
$a_i$	Coefficients in Rayleigh-Ritz method
$b$	$\sqrt{(G \cdot K_t)/(\rho \cdot I_p)}$
$b$	Beam height
$b$	Factor in the continuous numerical model
$b_i$	Coefficients in Rayleigh-Ritz method
$c_i$	Factors in continuous numerical method
$f$	Resonance frequency
$f_i$	Resonance frequencies for different vibration modes
$f_{ib}$	Transversal resonance frequencies for different vibration modes
$f_{it}$	Torsional resonance frequencies for different vibration modes
$f_{iL}$	Longitudinal resonance frequencies for different vibration modes
$f_{t,0,k}$	Characteristic tensile strength parallel to the grain
$f_{t,0,max}$	Maximum tensile strength parallel to the grain from tensile tests
$f_u$	Ultimate tensile strength
$h$	Beam height
$i$	Natural integer
$k$	Rotational stiffness at boundary
$k$	$\sqrt{\omega/a}$
$k_i$	Translational and rotational stiffness at boundary
$k_i$	$\sqrt{\omega_i/a}$
$k_{est}$	Estimated rotational stiffness at boundary
$k_s$	Shear factor, in general $k_s = 5/6$
$l$	Beam length, span or finite element length
$n$	Natural integer
$p$	Factor in the continuous numerical model
$s$	Factor in the continuous numerical model
$t$	Time
$u$	Longitudinal displacement
$v$	Transversal displacement
$w$	Moisture content or deflection

---

$w_i$	Moisture content or deflection in different points
$x, y$	Main directions in coordinate system

### Greek letters

$\Delta$	Factor in the continuous numerical model
$\Theta$	$Y$ or $\Psi$
$\Psi$	Modal shape of a transversally vibrating beam
$\beta$	Angle of shear
$\varepsilon$	Strain
$\theta$	Rotation angle
$\theta$	$y$ or $\psi$
$\lambda_1$	Factor in the continuous numerical model
$\lambda_2$	Factor in the continuous numerical model
$\rho$	Density
$\rho_k$	Density
$\sigma$	Stress level
$\phi$	$k_s GA$ for the continuous numerical model
$\phi$	$12EI/(k_s GA l^2)$ for the discrete numerical model
$\psi$	Angle of rotation of cross section
$\omega$	Angular resonance frequency
$\omega_i$	Angular resonance frequencies for different vibration modes

### Signs and mathematical symbols

%	Percentage
$\int$	Integral
[ ]	Matrix/vector parentheses
$\cos$	Cosinus function
$\sin$	Sinus function
$^T$	Transposition of a matrix
$\cdot$	First derivate of a function
$\ddot{\phantom{x}}$	Second derivate of a function
$\partial^i$	$i^{\text{th}}$ order derivate in multiple calculi
$d$	Infinite small increment
$\partial$	Derivate in multiple calculi

### Matrix notations (bold style)

<b><math>C</math></b>	Coefficient vector
<b><math>C</math></b>	Damping matrix
<b><math>CM</math></b>	Matrix for continuous numerical model
<b><math>K</math></b>	Stiffness matrix
<b><math>K^e</math></b>	Element stiffness matrix
<b><math>K_L^e</math></b>	Part of element stiffness matrix accounting for the axial load
<b><math>K_S^e</math></b>	Part of element stiffness matrix accounting for the strain
<b><math>M</math></b>	Mass matrix
<b><math>M^e</math></b>	Element mass matrix
<b><math>M_R^e</math></b>	Part of element mass matrix accounting for effects of rotary inertia

---

$M_T^e$	Part of element mass matrix accounting for effects of translatory inertia
$f(t)$	Time dependent force vector
$v$	Vector of displacement
$\phi$	Eigenvector to the eigenvalue problem

### Abbreviations

°C	Degree Celsius
CEN	Comité Européen de Normalisation
E-modulus	Modulus of elasticity
FE(M)	Finite element (method)
FFT	Fast Fourier Transformation
FRF	Frequency response functions
G	Giga-
Glulam	Glued-laminated timber
G-modulus	Shear modulus
M	Mega-
N	Newton
OSB	Oriented Strand Boards
Pa	Pascal
TC	Technical Committee
k	kilo-
m	Meter
m	milli-
s	Second

---

---

# 1 Introduction

## 1.1 Background

Over the last years, the media reported about several roof collapses across Europe that occurred mostly during winter times after high snow precipitations. The fact that roof structures failed under the loads of snow and ice cost several human lives and caused many injuries. In January 2006, the Bad Reichenhall Ice Rink in Bavaria, Germany collapsed after continuing snowfalls. The failure of the 36-year-old roof claimed 15 lives and caused 34 injured. In February of the same year, the collapse of a market hall in Moscow claimed the lives of 50 Caucasian guest workers. These are only a few examples of collapses that occurred during this particularly strong winter. In February 2009, the roof of a three-year-old school sports hall in St. Gallen, Switzerland collapsed just two hours before start of classes. In January 2012 a one-year old roof structure of an ice-hockey hall in Slovakia collapsed during a match. All these examples show the severity of this safety issue that exists in many different countries and damages the public confidence in the construction sector.

The main reasons for the collapses consist in general of high snow loads, combined with moisture effects or wrong assumptions considering the structural behaviour. Branco (2010) stated that the “assessment of constructed timber trusses shows various differences in their structural model” and that “visual inspections are the basis of any analysis of timber structures” to ensure the detection of decay or mechanical damages. In the case that a snow removal does not occur, it is therefore important to assess the real behaviour of the structure that can considerably derive from the assumed model. Also a condition assessment of the structural members should be carried out to assure a realistic evaluation, especially for older structures. An example for this is further shown in Branco (2010), where two timber trusses from a construction situated near Caldonazzo Lake, Italy were analysed. The over 70 year old trusses were disassembled and reconstructed in the laboratory, where their real structural behaviour was assessed by visual grading as well as dynamic and static testing. Both trusses showed asymmetric behaviour even under symmetric loading, which is a clear deviation from the structural model. All this indicates that a lack of information about the structural behaviour of roofs can lead to incorrect or even unnecessary reinforcements or replacements.

The problem of uncertainties in structural integrity is furthermore enhanced by uncertainties in future snowfall development affected by climate change. Strasser (2008) indicates that climate change could have a harmful effect on snow loads, at least in colder regions. Even if higher temperatures will result in less frequent snowfall, extreme weather events and precipitations are likely to become more frequent. In regions that will remain cold enough these precipitations will occur in form of strong snowfalls, which most likely will exceed today’s design values. In other words, instead of many moderate snowfalls it is probable that there will be fewer snowfalls with higher peaks. It is therefore important to know if today’s structures can bear these increased loads.

The solution to these problems could lie in non-destructive testing (NDT) methods, namely frequency based identification methods. In contrast to strain gauges, these methods allow to estimate actual stress levels at any time and without the need of a reference state. This means that stresses inside the structural members caused by self-weight, creep or changes in temperature or moisture are included in the results, which

---

allows a realistic assessment of the structural behaviour and the detection of the most loaded, hence most vulnerable members. With this information, a better computer model can be created from which a more realistic assessment of the load bearing capacity can be drawn. This gives for example answers to the questions “What snow load levels can the roof bear?” and “When should a structure be temporary closed and reinforced for safety reasons?”.

Livingston (1994) was one of the first to introduce a method based on frequency measurements to estimate the axial load in members. His model furthermore allowed identifying the rotational restraint at the supports of prismatic beams. The principle is to transversally excite a beam under axial force and to determine the first frequencies with the help of an accelerometer linked to a computer software. Resonance frequency analysis then allows deriving the axial loads and boundary conditions from these frequencies. The method was tested on a square steel rod under tension to verify the results. Even though it could be observed that the axial loads were in general overestimated, the method showed promising results, especially for high-tension forces. The same technique was also used by Amabili (2010) to determine the in-situ tensile forces in steel rods being part of ancient masonry buildings in Italy. The results could then be used as a basis to decide whether the bars needed to be replaced or not. In Maille (2008) the method was used to assess the safety of an old breeding barn’s roof structure. The testing led to the axial loads in the steel members of the truss construction, which were then compared to the ones predicted by different computer models. The most accurate model could then be used to determine the bearing capacity of the structure. As these works show, the technique has been approved for steel, which is a homogeneous material with isotropic properties. However it seems that no experiments have yet been carried out to verify the method for inhomogeneous materials like timber, on which is the focus in this thesis.

Since one of the main application fields of timber products are roof structures and since the exact material behaviour is not entirely clear, a reliable non-destructive testing method would represent a major contribution to the safety assessment of existing structures.

## **1.2 Aim of the thesis**

The aim of this thesis was to investigate the possibility of estimating axial loads in timber members by means of resonance frequency analysis. For promising results, this method could be used in the future to assess the safety of timber structures by determining the actual stress of state in the loaded members. The main difference to steel structures is that the material properties of timber are subject to a large spread given by its inhomogeneity and natural growth. It is therefore important to analyse what precision is required for the use of this method and what parameters have the highest influence on the estimation of the axial load.

## **1.3 Method**

Based on a literature study carried out on resonance frequency testing for the determination of axial forces, the framework for the specimen dimensions and the test setup was elaborated. Static and dynamic testing was then performed on 32 timber specimens of Norway spruce to determine their material properties. Furthermore, the

---

same tests were carried out on an aluminium bar serving as reference for homogeneous material. Finally, transversal frequency measurements were performed on the specimen under different load levels. The collected data was then evaluated using Timoshenko beam theory to estimate boundary conditions and axial load. A sensitivity study was carried out to analyse the influence of the different input parameters on the estimation of the axial load and the boundary conditions.

## 1.4 Limitations

The main limitations in this research were a lack of time and available laboratory space and equipment. This led to small-scale experiments on 32 timber specimens of identical dimensions and an aluminium bar. No moisture variation or long-term effects could be considered. The available machine limited the research to tensile loads only.

## 1.5 Outlines

In the following, the contents of the different chapters and their chronological order are presented.

1. **Introduction**: This chapter gives the necessary background information as well as the aims of the thesis. Moreover, the methods to the respective aims are explained.
2. **Building material timber**: In this chapter, the material properties of timber are discussed. Furthermore, non-destructive methods for timber grading are explained.
3. **Determination of axial load and boundary conditions in slender beams**: A literature review is presented on resonance frequency analysis for the purpose of parameter estimation. Conclusions are drawn on how to choose the specimen size and test framework.
4. **Vibration theory**: The theory behind different types of beam vibrations is explained and the according assumptions are listed. The difference between Euler and Timoshenko theory is explained.
5. **Numerical modelling and parameter estimation**: In this chapter, different numerical models are presented and compared. The parameter estimation used in later data processing is explained. Finally, a sensitivity analysis is carried out to analyse the sensitivity of the axial load and the boundary conditions with regard to measured input parameters.
6. **Modal analysis**: This chapter explains the difference between theoretical and experimental modal analysis. The most important aspects of data acquisition and data processing are illustrated.

- 
7. **Determination of material properties**: The specimens are presented along with information on the test equipment and the data processing. The material properties of each beam are determined using static and dynamic testing.
  8. **Tension tests**: The tensile machine and setup of the final tests are explained. The results of the frequency measurements as well as the according estimation of axial loads and boundary conditions are presented. This is followed by a comparison and discussion of the results for timber and aluminium. Finally, tensile tests on some specimens are presented to determine their ultimate tensile strength.
  9. **Conclusions and further research**: This chapter presents the final conclusions made from the data acquisition and the parameter analysis. In addition, suggestions for further research are made.
  10. **References**: An alphabetical summary of the used literature is listed in this chapter.
  11. **Appendices**: This chapter contains a summary of all test results, frequency response function plots and Matlab codes used in this paper.

---

## 2 Building material timber

The demand for construction timber has been rising considerably during the last decades. One main reason is the new awareness with regard to the environment caused by the climate change and resource scarcity. Timber meets this new requirement by being a naturally regrowing material with low energy consumption during the whole life cycle. Another reason for the raising use of timber materials is the high level of prefabrication. The different parts can be produced in indoor workshops prior to construction. This ensures high quality standards and weather independence. After the prefabrication, the different parts can then be transported on site and assembled in a quick and precise way.

A major disadvantage of timber is however its anisotropy. Unlike steel or other homogeneous materials, timber has different material properties in different directions, which requires much care and consideration during the design phase. This is given by its cell structure, which is illustrated in more detail in the next paragraph, together with the material properties of timber.

### 2.1 Characteristics of timber

When analysing the cell structure of wood, one has to distinguish softwood (coniferous wood) and hardwood (deciduous wood). From the cell structure illustrations in *Figure 2-1*, it can be seen that softwood has a more uniform composition parallel to the grain than hardwood, where the grain is penetrated by vessels variable in size and shape. This leads to a higher variation in material properties.

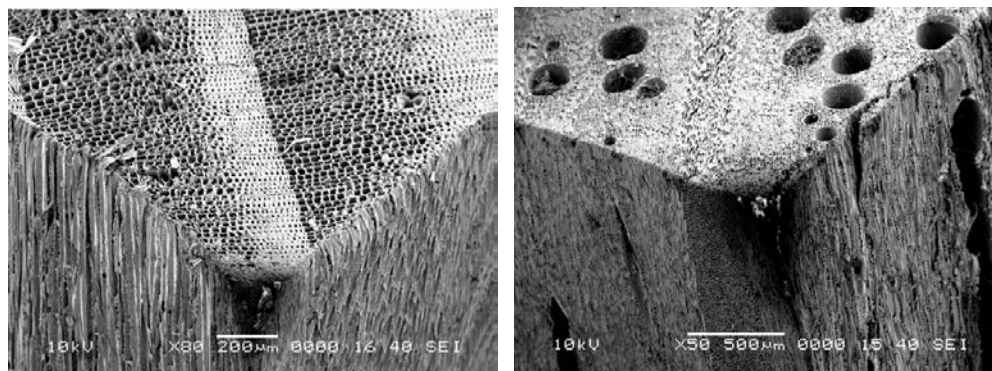


*Figure 2-1* SEM images showing the difference between softwood (left) and hardwood (right), Wikipedia.org (2006)

It is however true for all types of clear wood, that the stiffness and strength properties generally increase with higher densities. Also the stiffness and strength properties are always considerably higher in grain direction than perpendicular to the grain. *Figure 2-2* shows the variation of tensile and compression strength with the angle variation from the grain direction for strength class C24 according to SIA (2003). It is obvious that the strength perpendicular to the grain is very low, even negligible for tension, compared to the one in grain direction. This is also one of the most common failure modes observed in practice. The E-modulus for the same strength class is around 35 times higher in the grain direction than perpendicular to it SIA (2003).

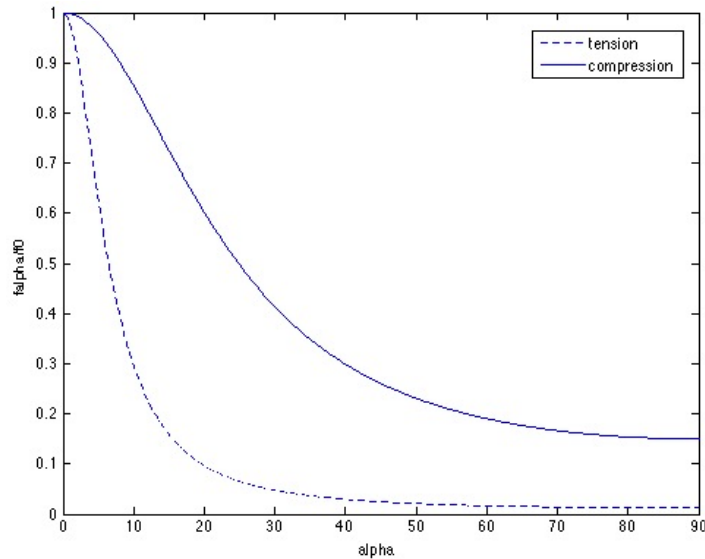


Figure 2-2 Tensile and compression strength of C24 for different angles  $\alpha$  to the grain direction SIA (2003)

The strength of a timber beam also depends on the loading mode, i.e. moment, tension, compression or shear. The according strengths are usually determined by direct testing methods under the assumption of elastic behaviour. Beams under tension generally show a brittle failure, while some plastic deformations are possible for compression forces, due to the buckling of the fibres.

The good properties of clear wood in grain direction are significantly reduced by random defects such as knots, oblique fibre orientation and resin pockets. The varying number and location of these defects cause a large spread in properties shown in Figure 2-3.

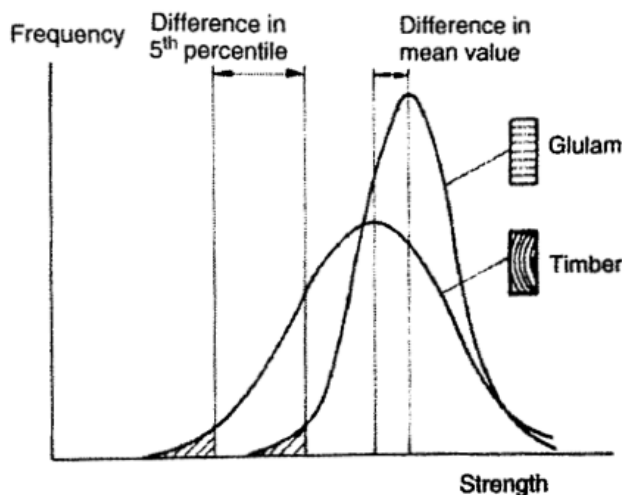


Figure 2-3 Probability density functions for solid wood and glulam Thelandersson and Larsen (2003)

This spread led to the development of Engineered wood products (EWP), which in general aim to reduce the high variability of timber. For glue-laminated timber for instance, several lamellas of solid wood are glued together. This improves the material properties since local weak zones can redistribute stresses to adjacent stronger regions. Another approach is to shred the wood to smaller pieces and

---

reassembling it with the use of adhesives as it is done for OSB panels. *Figure 2-4* shows some examples of EWPs.



*Figure 2-4* Examples of Engineered wood products *Buyleedlumber.com* (2012)

According to Thelandersson and Larsen (2003), these are some of the main advantages of EWPs:

- Size is not limited by tree dimensions.
- Reduced effect of defects by distributing them over the whole beam.
- Reduced anisotropy
- Higher dimensional stability and tolerances

One should however also note that EWPs are generally more expensive than solid wood and that adhesives like glue are necessary for their production. The latter somewhat decrease the ecological character of the timber use.

Another consideration, that needs to be taken into account when dealing with timber, is that it interacts with the humidity in the environment until it reaches the equilibrium moisture content. This change in moisture can result in internal stresses causing deformations or even cracks, for example perpendicular to the grain. Also it has to be considered that the material properties vary with the moisture content. For high moisture contents, strength and stiffness values need to be reduced, while values around 12% at an ambient temperature of 20°C are optimal SIA (2003).

Another important aspect is that timber has a low shear modulus compared to homogeneous materials like steel. This means that shear deformations need to be taken into account for timber structures since they can be of the same order as deformations from bending. This effect becomes even more important for a high presence of knots since the reduction they cause in G-modulus is more important than the one in the E-modulus. The deformations of timber beams increase furthermore over time, since the strength decreases under permanent loading.

All these illustrations show that there are various uncertainties related to timber construction and that there is a need for non-destructive methods to estimate the material properties and make sure they are within desirable limits. The next paragraph gives an overview of methods used in practice for the grading of timber and the determination of some important properties of timber beams, namely the density, strength and stiffness.

---

## 2.2 Non-destructive methods for timber grading

According to Thelandersson and Larsen (2003), two types of strength grading can be distinguished:

- **Visual grading:** it is based on visual inspections to determine number and distribution of defects like knots, grain slope, compression wood, resin pockets etc. According to specific rules, the specimen can then be assigned to a strength class.
- **Machine grading:** there are different methods that can be used to measure several parameters including knots, ring width, density etc. The resulting information can then be combined to predict the strength and stiffness of the specimen.

The most numerous, yet also harmful defects are knots since they considerably reduce the stiffness and are in general also the cause for failure in ultimate bending or tensile tests.

One should keep in mind that even after timber grading there are still uncertainties concerning the material properties and that these values can only be considered as estimates based on more or less accurate correlations between different parameters. There is for example a good correlation between E-modulus and strength, even in presence of knots. The correlation between density and E-modulus on the other hand is only strong for clear wood specimens, which are not the general case Thelandersson and Larsen (2003).

### Determination of density

The easiest way to determine the global density of a specimen is to calculate its weight-to-volume ratio. Since this is however not possible for existing structures without taking a probe, there is a need for other non-destructive methods that can be used on-site.

Accurate results can in this case be achieved by means of radiation techniques (x-ray or gamma rays). They allow to determine not only the global density, but even the density distribution of a beam. Furthermore it is possible to find the location as well as size of hidden knots since they have a higher density than the surrounding material (cf. *Figure 2-5*). An application of this technique can be found in Oja (2001) and (Schajer, 2001) where it was used to determine the density of logs and lumber from which it was then attempted to derive strength and stiffness.

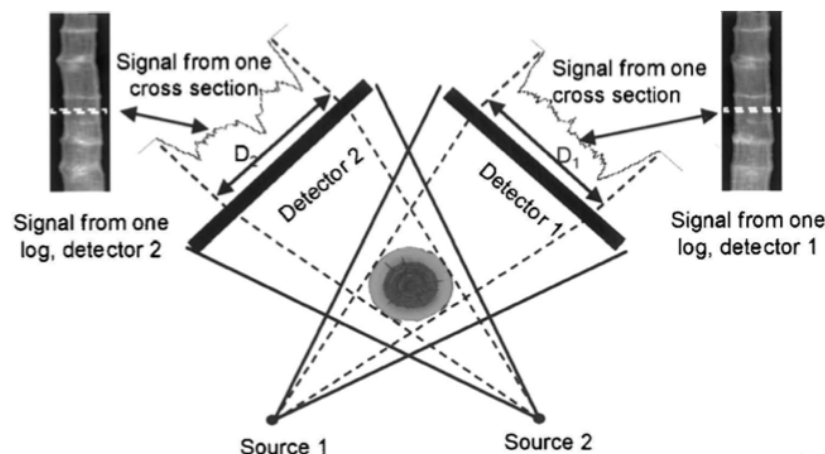
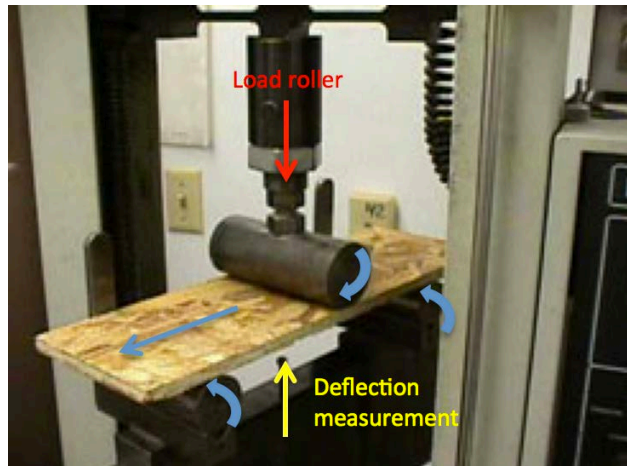


Figure 2-5 Illustration of the determination of wood density using x-rays Oja (2001)

---

## Determination of E-modulus

One of the most widely used methods to determine the static E-modulus is to perform continuous flatwise-bending tests. This is in fact a three-point loading test carried out along the beam length (cf. *Figure 2-6*). The result is the E-modulus distribution over the beam length, excluding the ends since it is not possible to carry out the measurements there.



*Figure 2-6* Bending type machine for continuous timber grading, based on (*Performancepanels.com, 2012*)

A more recent approach to determine the E-modulus are dynamic testing methods. They have gained much importance during the last decades, since they provide a quick assessment of wood quality with relatively low means of equipment. In the following, some of these non-destructive dynamic grading methods are described in more detail.

Resonance frequency measurements are based on the fact that for free boundary conditions, the frequencies depend only on the density, the E-modulus and the geometry of the specimen. With known density it is then possible to estimate the E-modulus. The free boundary conditions can be simulated by suspending the specimen on rubber bands or by using soft foam pieces as support. The specimen is excited with a hammer and the response can be recorded using an accelerometer or a microphone. The frequencies can then be calculated by performing a Fast Fourier Transformation (FFT) on the raw time data, which can be done using a computer software Haines (1996). From these frequencies, longitudinal and transversal E-moduli can then be derived. The test setups for both kinds of frequency measurements are illustrated in *Figure 2-7*.

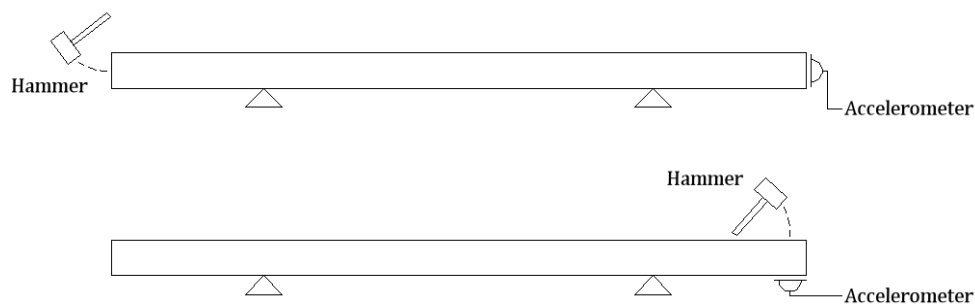


*Figure 2-7* Illustration of the test-setup for longitudinal (top) and transversal (bottom) frequency measurement

The E-moduli calculated from dynamic testing are usually higher than the ones obtained from static testing. The reason for this is the difference in duration of the tests. Static tests are carried out during several minutes where the timber starts to creep, giving its viscoelastic material behaviour. This results in lower stiffness values. Dynamic tests only last seconds and therefore represent a short-time stiffness that is higher in value (Haines, 1996). The correlation between the different E-moduli is however quite strong, depending on the number of defects and the type of wood. In general it can be said that the correlation is higher for clear wood since defects like knots cause a local reduction of the stiffness and reduce the accuracy of the dynamic tests.

Ohlsson and Perstorper (1992) carried out both, flexure and longitudinal tests on a clear piece of Norway spruce to determine its E- and G-modulus using different numbers of frequencies together with Timoshenko theory. The test setup comprised several accelerometers to be able to determine the vibrations modes also for higher frequencies. The excitations were made using an instrumented hammer. The best results for the E-modulus could be achieved using only the two lowest longitudinal frequencies and the lowest flatwise bending frequency. The use of additional information from higher frequencies did not improve the results, but rather lowered the accuracy. For non-defect-free specimens it seems therefore reasonable to only use the lowest frequency.

Another possibility to determine the E-modulus from a known density is the ultrasonic test developed by Sandoz (1989), also known as Syla-test. The test is based on the velocity of stress wave propagation in materials. In simple words, an impulse is induced at one end of a beam and the response is measured at the other end. The time delay of the impact over the length of the beam can then be used to compute the wave velocity from which the E-modulus can eventually be derived. The results presented in Sandoz (1989) show very good correlation between dynamic and static E-modulus. The general test-setup as well as the application in practice are illustrated in *Figure 2-8*.

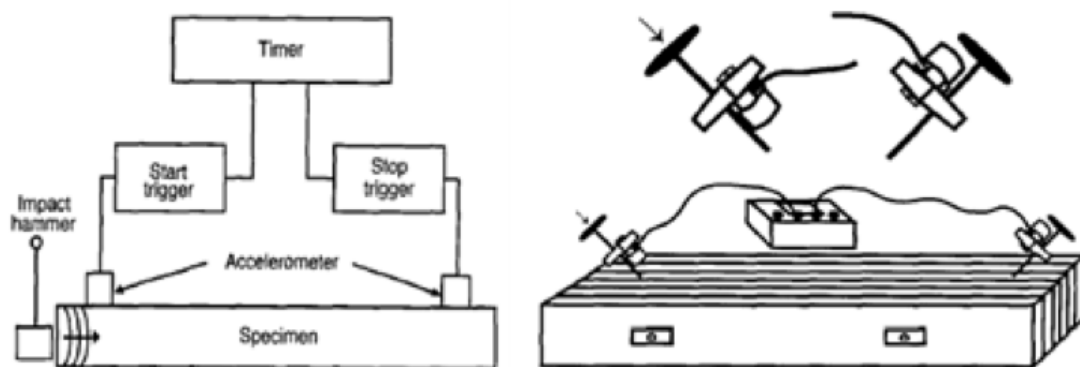


*Figure 2-8 Schematic model of the Syla-test (left) and application on a stress-laminated timber deck (right), Ross (1994)*

---

## Determination of G-modulus

The G-modulus can be determined in the same way as the E-modulus using torsional instead of bending vibrations Ohlsson and Perstorper (1992). To record the torsional modes, the accelerometer needs to be placed at the edge of the cross section at some distance from the neutral axis (cf. *Figure 2-9*). The beam then needs to be excited in an eccentric point to cause torsional vibrations. An additional accelerometer can be placed in the neutral axis to simplify the detection of the torsional frequencies. Comparison of the frequency plots for both accelerometers will then show that the torsional frequencies are only recorded by the eccentric accelerometer. As already mentioned, Ohlsson and Perstorper (1992) also presents good results for the measurement of the G-modulus, for which only the first two lowest torsional frequencies were used.

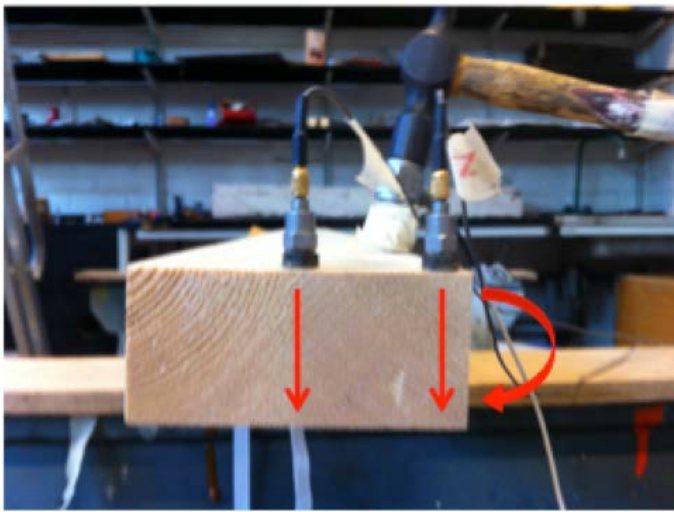


*Figure 2-9* Test setup for transversal and torsional frequency measurement

Apart from the transversal excitation, all these methods can, at least in theory, be also applied to loaded structures. This means that material properties like density, E- and G-modulus can theoretically be determined on existing structures.

---

---

## 3 Determination of axial load and boundary conditions in slender beams

This chapter analysis research that was carried out in the past concerning the determination of axial loads and boundary conditions using of transversal frequency analysis. The different case studies are examined regarding the overall test setup, the testing equipment, the theoretical models and the accuracy of the results. Based on this analysis, conclusions are drawn on how to plan the laboratory tests and to process the data collected within this research.

### 3.1 Determination of axial loads

One of the first frequency based laboratory tests to determine the axial load in a prismatic Euler beam under tension was carried out by Livingston (1994). The setup consisted of a square steel rod subjected to loading and unloading cycles in a vertical Tinius Olsen tensile machine. A single accelerometer was attached at a distance of  $4/5$  of the specimen length, which was then excited with an impact hammer equipped with a soft tip. From the resulting frequency response function (FRF), the first three frequencies were then extracted for each loading and unloading cycle. Using a non-linear least square parameter technique described in Béliveau (1987) together with a continuous model, the axial force and the boundary conditions represented by rotational springs were then estimated, considering at first only the first two, then the first three frequencies. Even though the axial loads were in general overestimated, the results were promising, especially for higher forces. It can be said that the additional data provided by the third frequency did not improve the results of the experiment. The estimated boundary conditions varied over the loading and unloading of the rod and were not discussed in further detail.

A different approach was used by Tullini and Laudiero (2008). Instead of using several frequencies to determine the axial loads and boundary conditions, only the mode shape and frequency of the first mode were used. The necessary information was gathered by three accelerometers situated in each quarter point of the specimen. The displacements of the accelerometers were used to determine the shape of the first mode, whereas the frequency was again derived from the FRF. An impact hammer was used to measure the force function. This method was applied on both, a steel rod under tension and a slender box beam under compression. For both test setups, the results for the axial loads showed very good accordance with the real values. The estimation of the end constraint stiffness however was rather far away from the analytical values for the limit conditions pinned-pinned and fixed-fixed and was therefore not convincing.

Maille (2008) carried out in-situ experiments on an old breeding barn to assess its structural integrity for a full snow load. For this purpose, transversal frequency testing was carried out on the structural steel members to determine the axial tensile forces under different load combinations. The results of these measurements were then compared with different computer models to find out which one comes closest to the actual behaviour of the structure. Based on this model, the axial forces under a full snow load were then computed which could then be used for the structural assessment.

---

The tests were performed by striking every steel member in three different ways to excite as many frequencies as possible. These three methods included a steel hammer, a rubber mallet and plucking the members by hand. One single accelerometer was used to detect the frequencies. However, since in many cases not all of the frequencies could be detected, the author suggests for further research to use an additional accelerometer situated close to the end of the members. As the members were assumed to be pinned at both ends, the axial loads could be determined by a single parameter estimation using the first 6 measured frequencies and the formula for Euler beams Eq. (3.34) in Maille (2008). In addition, a dual parameter estimation was carried out by means of least square linear regression to also verify the E-modulus of each member. Even though most of them coincided well with the assumed value, there were still some outliers. For the testing of inhomogeneous materials with a high variation in material properties like timber, it is therefore reasonable to always verify the assumed parameters with additional measurements and estimations.

A somewhat different model was used in Italy to assess the safety of tie-rods in ancient masonry buildings, Amabili (2010). Using finite elements, the rods were modelled as Timoshenko beams, taking into account shear deformations and effects of rotary inertia. The equipment for the in-situ tests consisted of a single accelerometer situated at 2/5 of the span and an impact hammer to determine the first 6 resonance frequencies. The portion of the beam inside the wall at both sides was assumed to be elastically founded. The calculated values were found by applying Rayleigh-Ritz method (cf. Chapter 5). The unknown parameters were estimated by minimizing the weighted difference between the computed and measured frequencies. This was done in several ways, from first using only the two first modes from the estimation, then the first three and so on till finally all six modes. The advantage of this method is that measurement and modelling errors are minimized through the use of redundant data given by the several frequencies. It is however questionable if this could be done in the same way for timber since the accuracy requirements might not be fulfilled for higher frequencies.

As it can be seen, this literature study only yielded research that has been done on steel structures. It seems that not much research has been done on the possibility to determine the axial loads in timber members using resonance frequency analysis. There are however investigations on the boundary conditions of timber elements in frames or trusses.

### **3.2 Determination of boundary conditions**

Crovella and Kyanka (2011) made use of vibration techniques to determine the rotational stiffness of timber joints. The main incentive for his research was the little amount of research available investigating the member joint properties, even though the failures usually occur in the joints. Transversal vibration tests were carried out on timber beams and frames of softwood and hardwood for different boundary conditions. The beams were unloaded, so that no axial tension needed to be taken into account. Furthermore the beams were modelled as Euler beams meaning that effects of shear deformations or rotary inertia were neglected. Shear deformations can however have a big influence on the vibration of timber beams, especially for the present span-to-depth ratios, that are 16 and 36. Chui and Smith (1990) suggests that shear deformations need to be taken into account for values below the region of 32 for simply supported beams. For stiffer boundary conditions, this limit value is even

lower. Here, the use of Timoshenko theory could have been further investigated to see if there is an improvement in results. A single accelerometer was used to record the beam vibrations that were then used to derive the first resonance frequency. With the above-mentioned assumptions a simple relation between the frequency and the joint stiffness could be used for the estimation. When looking at the continuum of joint stiffness plot in *Figure 3-1*, one can see that the ratio of the joint rotational stiffness and the beam flexural stiffness is of importance. If one of them is considerably higher than the other one, a change of the joint stiffness has a minimal effect on the frequency.

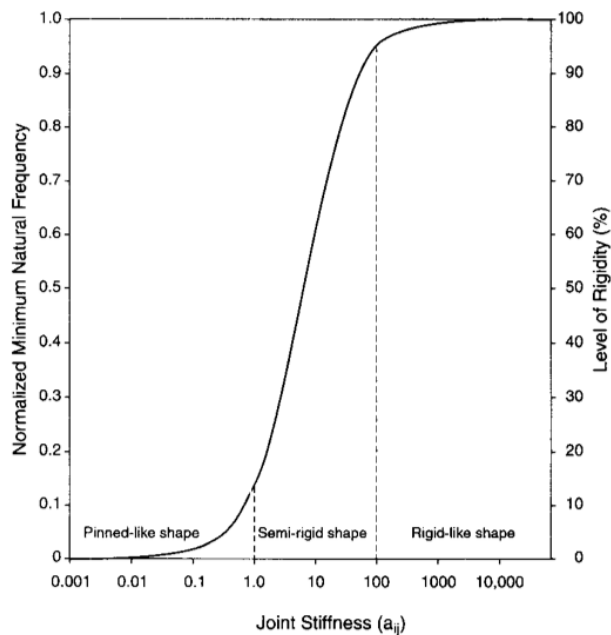


*Figure 3-1* Plot of continuum joint stiffness against the normalised minimum natural frequency, McGuire (1995)

According to Leichti (2000), a 50% rigid connection is the maximum that can be achieved for timber joints. This theory seems to be supported by the results of Crovella and Kyanka (2011) that were all below that value, even for stiff connectors. To be able to assess the accuracy of the results, the rotational stiffness at the beam-ends was derived from deflection tests. The conclusion was that the results were good for semi-rigid joints, but rather poor for joints of low stiffness. This can possibly be explained by the small slope of the formula plot in low frequency regions, where small changes in frequency result in rather high changes for the estimated rotational stiffness. All these considerations can lead to the conclusion that it could be possible to determine also the rotational stiffness for beams under axial tension, at least if the boundary conditions are stiff enough and if Timoshenko theory is used.

---

### 3.3 Conclusion

For the determination of axial loads, most of the investigated members were steel bars with a high length compared to their sectional dimensions. The span-to-depth ratios ranged from around a 100 in Livingston (1994) to over 300 in Maille (2008). The reason for this is that for a given change in axial load, a change in frequency increases for a higher slenderness of the loaded member. This needs to be considered when choosing a sample size for the experiments in this research, since changes in axial load might not even be possible to detect for beams with a low slenderness. The tension machine used in this research is similar to the vertical one used in Livingston (1994). Since the friction grips at both ends of the beam are the same, it is reasonable to assume equal boundary conditions. The static system consequently is a simply supported beam with identical rotational springs at both ends. This leads to two unknown parameters, namely the axial force  $S$  and the rotational stiffness  $k$ . This means that at least two bending frequencies are necessary to determine the parameters. It will however be investigated if additional information from higher frequencies can be used for error minimisation, even if this is doubtful given the inhomogeneous properties of timber and their influence on the precision of frequency measurement. In this case, a least linear regression is necessary to solve the over-determined system. It is necessary to keep the number of unknown parameters to a minimum to make sure not too much accuracy is lost, even if it would theoretically be possible to include more parameters, like for example material properties. For the actual tests, the use of one single accelerometer seems appropriate since the vibration modes are well known for the given system. The accelerometer needs to be placed away from modal nodes to make sure the desired frequencies can be recorded. A distance of 20% of the length is a good position to enable measurements of the first five frequencies. If necessary, an additional accelerometer placed closer to one end, can be used to record more frequencies. The beams should be excited on the weak axis, since the lower moment of inertia causes a higher variation of frequency for a change in axial force. Since the results seem to be sensible to the stress level, the specimen should be tested for a wide range of axial loads. As mentioned above, shear deformations have a big influence on the frequencies of timber beams, even if they are rather slender. It is therefore necessary to include them according to Timoshenko theory. This can be done in different ways, either by using an exact continuous model or using approximations through discrete modelling (finite elements) or Rayleigh-Ritz theory.

## 4 Vibration theory

The following paragraphs present derivations and applications of differential equations for several kinds of beam vibrations. All derivations were made according to Timoshenko (1974) and Howson and Williams (1973).

### 4.1 Derivations

#### 4.1.1 Longitudinal vibrations

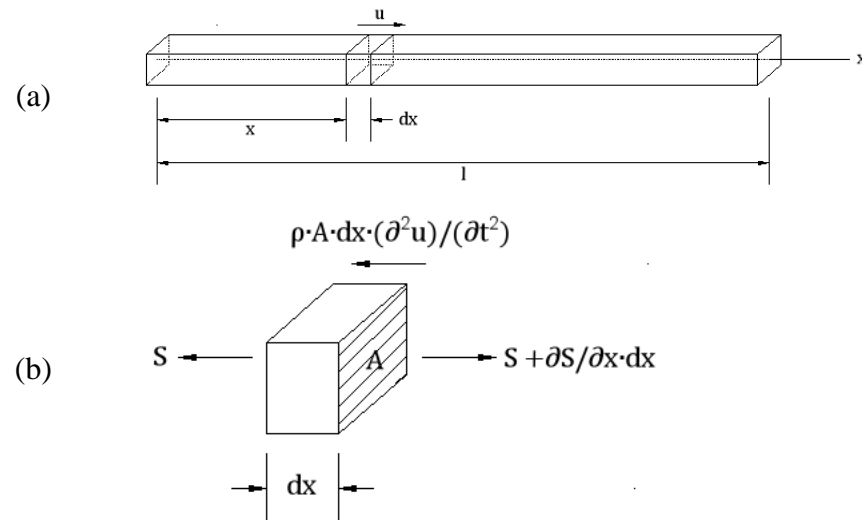


Figure 4-1 Illustration of a beam subjected to longitudinal vibration (a) and the according forces acting on an infinitesimal element (b)

Figure 4-1 (a) shows a prismatic beam of length  $l$  and the cross-section  $A$  subjected to longitudinal vibration. An according infinitesimal segment of length  $dx$ , in a distance  $x$  from the left end of the beam, is illustrated in Figure 4-1 (b). Forming equilibrium of the acting forces yields

$$S + \rho \cdot A \cdot dx \cdot \frac{\partial^2 u}{\partial t^2} - S - \frac{\partial S}{\partial x} \cdot dx = 0 \quad (4.1)$$

where  $S$  is the internal force acting on the beam,  $\rho$  the density and  $u$  the longitudinal displacement of the segment, which makes  $\partial^2 u / \partial t^2$  its acceleration.

Applying Hooke's law on the axial force  $S$ , we obtain

$$S = A \cdot \sigma = E \cdot A \cdot \varepsilon = E \cdot A \cdot \frac{\partial u}{\partial x} \quad (4.2)$$

where  $E$  is the modulus of elasticity,  $\sigma$  the axial stress and  $\varepsilon = \partial u / \partial x$  the axial strain. Substitution of Eq. (4.2) into Eq. (4.1) yields

$$\frac{\partial^2 u}{\partial x^2} = \frac{\rho}{E} \cdot \frac{\partial^2 u}{\partial t^2} \quad (4.3)$$

If we introduce the wave velocity  $a = \sqrt{E/\rho}$ , Eq. (4.3) can be rewritten as

$$\frac{\partial^2 u}{\partial x^2} = \frac{1}{a^2} \cdot \frac{\partial^2 u}{\partial t^2} \quad (4.4)$$

which is called the *one-dimensional wave equation*. For the natural vibration modes of the beam, the solution to Eq. (4.4) can be written as

$$u = X \cdot (A \cdot \cos(\omega \cdot t) + B \cdot \sin(\omega \cdot t)) \quad (4.5)$$

where  $X$  is called the *normal function* that defines the shape of the natural modes.

Substitution of Eq. (4.5) into Eq. (4.4) yields the time-independent differential equation for longitudinal vibration

$$\frac{d^2X}{dx^2} + \frac{\omega^2}{a^2} \cdot X = 0 \quad (4.6)$$

which is the differential equation of motion for beams subjected to longitudinal vibrations according to Euler theory.

The solution to Eq. (4.6) is of the kind:

$$X = (C \cdot \cos\left(\frac{\omega \cdot x}{a}\right) + D \cdot \sin\left(\frac{\omega \cdot x}{a}\right)) \quad (4.7)$$

The constants  $C$  and  $D$  are determined by applying the boundary conditions of the beam. Examples are presented in Chapter 4.2.

#### 4.1.2 Torsional vibrations

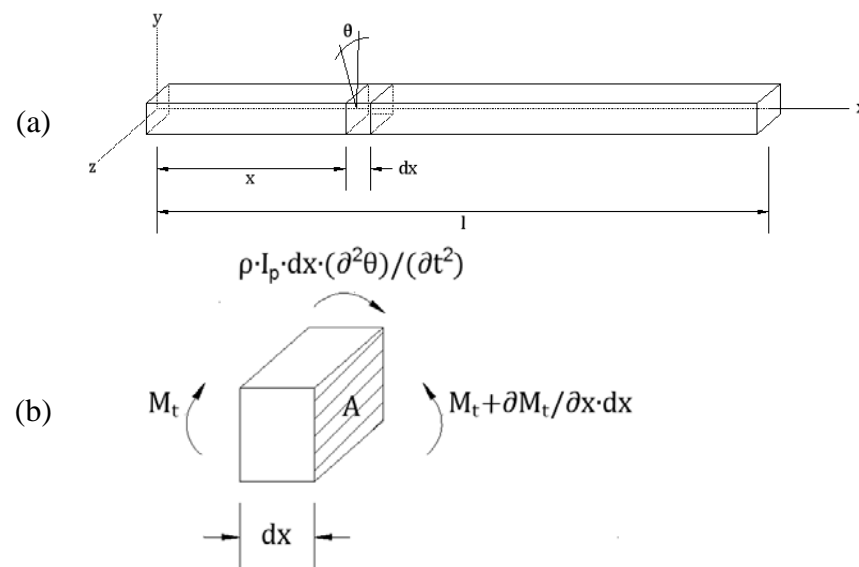


Figure 4-2 Illustration of a beam subjected to torsional vibration (a) and the corresponding moments acting on an infinitesimal element (b)

Considering the same beam subjected to torsion (Figure 4-2 (a)), the moment equilibrium can be derived according to Figure 4-2 (b):

$$M_t + \rho \cdot I_p \cdot dx \cdot \frac{\partial^2 \theta}{\partial t^2} - M_t - \frac{\partial M_t}{\partial x} \cdot dx = 0 \quad (4.8)$$

where  $M_t$  is the torsional moment acting on the beam,  $I_p$  the polar moment and  $\theta$  the angular displacement of the segment, which makes  $\partial^2 \theta / \partial t^2$  its acceleration.

Elementary torsion theory gives

$$M_t = G \cdot K_t \cdot \frac{\partial \theta}{\partial x} \quad (4.9)$$

where  $G$  is the modulus of shear, and  $K_t$  is the torsional constant that varies with the shape of the cross-section. For circular sections  $K_t$  is equal to the polar moment  $I_p$ . For other cross-sections refer to Roymech.co.uk (2010).

Substitution of Eq. (4.9) into Eq. (4.8) yields

$$\frac{\partial^2 \theta}{\partial x^2} = \frac{\rho \cdot I_p}{G \cdot K_t} \cdot \frac{\partial^2 \theta}{\partial t^2} \quad (4.10)$$

Introducing  $b = \sqrt{(G \cdot K_t)/(\rho \cdot I_p)}$ , Eq. (4.10) can be rewritten as

$$\frac{\partial^2 \theta}{\partial x^2} = \frac{1}{b^2} \cdot \frac{\partial^2 \theta}{\partial t^2} \quad (4.11)$$

which has the same form than the *one-dimensional wave equation* from before, which is why the same solution as in Eq. (4.5) can again be used:

$$\theta = X \cdot (A \cdot \cos(\omega \cdot t) + B \cdot \sin(\omega \cdot t)) \quad (4.12)$$

Substitution of Eq. (4.12) into Eq. (4.11) yields the time-independent differential equation for torsional vibration

$$\frac{d^2 X}{dx^2} + \frac{\omega^2}{b^2} \cdot X = 0 \quad (4.13)$$

which is the differential equation of motion for beams subjected to torsional vibrations according to Euler theory.

Since Eq. (4.13) is of the same kind as Eq. (4.6), its solution has also the same form as Eq. (4.7):

$$X = (C \cdot \cos\left(\frac{\omega \cdot x}{b}\right) + D \cdot \sin\left(\frac{\omega \cdot x}{b}\right)) \quad (4.14)$$

which can again be solved for different boundary conditions.

### 4.1.3 Transversal vibrations – Euler beam theory

The Euler beam theory is based on the assumptions that the cross-sections of a prismatic beam remain plane during vibration. This means that deformations caused by shear forces as well as rotary inertia effects are not taken into account when using this theory. The consequence is that it only gives accurate results if the deformations from shear are small compared to the ones from bending. This is in general the case for slender beams.

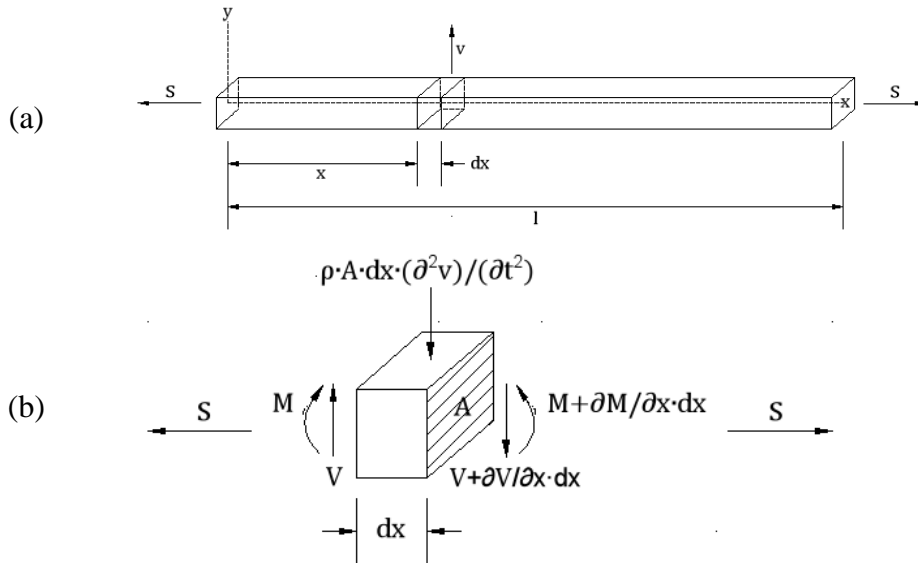


Figure 4-3 Illustration of a beam subjected to an axial load and transversal vibration (a) and the according forces and moments acting on an infinitesimal element according to Euler beam theory (b)

Figure 4-3 (a) shows a vibrating beam subjected to a tensile force  $S$  and transversal vibration. Forming the equilibrium on an infinitesimal element (Figure 4-3 (b)) for both, vertical forces and moments, yields

$$V - \rho \cdot A \cdot dx \cdot \frac{\partial^2 v}{\partial t^2} - V - \frac{\partial V}{\partial x} \cdot dx = 0 \quad (4.15)$$

and

$$V \cdot dx - \frac{\partial M}{\partial x} \cdot dx = 0 \quad (4.16)$$

where  $V$  is the shearing force acting on the beam, and  $v$  the transversal displacement of the segment, which makes  $\partial^2 v / \partial t^2$  its acceleration.

Solving Eq. (4.16) with respect to  $V$  and substituting into Eq. (4.15) yields

$$\frac{\partial^2 M}{\partial x^2} = -\rho \cdot A \cdot dx \cdot \frac{\partial^2 v}{\partial t^2} \quad (4.17)$$

The differential equation for the deflection of a beam subjected to a tensile force and a transverse load is

$$M = EI \cdot \frac{\partial^2 v}{\partial x^2} - S \cdot v \quad (4.18)$$

Substitution of Eq. (4.18) into Eq. (4.17) leads to

$$EI \cdot \frac{\partial^4 v}{\partial x^4} - S \cdot \frac{\partial^2 v}{\partial x^2} = -\rho \cdot A \cdot \frac{\partial^2 v}{\partial t^2} \quad (4.19)$$

If a beam vibrates in one of its natural modes, a solution to this equation is given by

$$v = X \cdot (A \cdot \cos(\omega \cdot t) + B \cdot \sin(\omega \cdot t)) \quad (4.20)$$

Substitution of Eq. (4.20) into Eq. (4.19), yields:

$$EI \cdot \frac{\partial^4 X}{\partial x^4} - S \cdot \frac{\partial^2 X}{\partial x^2} = \rho \cdot A \cdot \omega^2 \cdot X \quad (4.21)$$

which is the differential equation of motion for beams under axial load subjected to transversal vibrations according to Euler theory.

#### 4.1.4 Transversal vibrations – Timoshenko beam theory

This paragraph gives a derivation of the transversal vibrations of prismatic beams under axial load according to Timoshenko beam theory. In general, shear deformations can be neglected for flexural vibrations if a beam's cross-sectional dimensions are small compared to its length. For timber, however, shear deformations can be of the same order as deformations from bending, even for slender beams. The reason is that the shear stiffness of the material is small compared to other materials. For this reason, it is important to include shear effects in the calculation, especially when studying the vibration modes of higher frequencies where they gain more and more of importance Timoshenko (1974), Howson and Williams (1973).

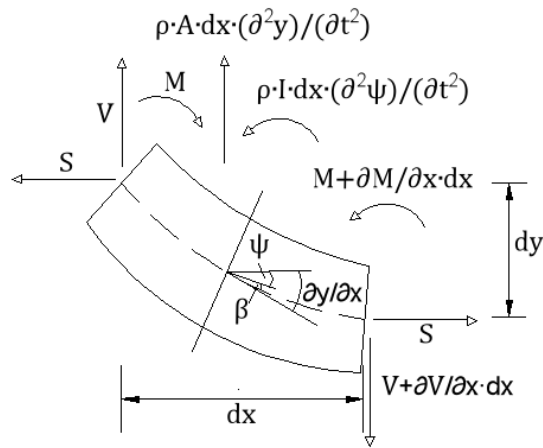


Figure 4-4 Illustration of forces and moments acting on an infinitesimal element of a transversally vibrating beam under axial load according to Timoshenko beam theory, based on Howson and Williams (1973)

Figure 4-4 shows a deformed infinitesimal element to a transversally vibrating beam in the x-y plane. To include the shear deformations, it must be considered that the beam not only performs a translatory movement, but also rotates. The angle of rotation  $\partial M/\partial x$  is the deflection slope and can be expressed as the sum of the angle of shear  $\beta$  and a parameter  $\psi$  that represents the angle of rotation of the cross-section:

$$\frac{\partial y}{\partial x} = \psi + \beta \quad (4.22)$$

The rotation of the beam produces a moment  $\rho \cdot I \cdot \frac{\partial^2 \psi}{\partial t^2} \cdot dx$ , that needs to be taken into account when forming the dynamic moment equilibrium on an infinitesimal element of length  $dx$ :

$$V \cdot dx - \frac{\partial M}{\partial x} \cdot dx - \rho \cdot I \cdot \frac{\partial^2 \psi}{\partial t^2} \cdot dx - S \cdot \frac{\partial y}{\partial x} \cdot dx = 0 \quad (4.23)$$

The dynamic equilibrium for the forces in the vertical direction is

$$-V - \rho \cdot A \cdot dx \cdot \frac{\partial^2 y}{\partial t^2} + V + \frac{\partial V}{\partial x} \cdot dx = 0 \quad (4.24)$$

The differential equation for the deflection of a beam subjected to a tensile force and a transverse load is

$$M = -EI \cdot \frac{\partial \psi}{\partial x} \quad (4.25)$$

Furthermore, consideration of the shearing yields

$$V = (k_s \cdot A \cdot G + S) \cdot \frac{\partial y}{\partial x} - k_s \cdot A \cdot G \cdot \psi \quad (4.26)$$

Eliminating  $V, M$ , and either  $\psi$  or  $y$  by combining Eq. (4.22) - (4.26), leads to the complete differential equation for transverse vibrations of prismatic beams under axial load:

$$EI \cdot \left(1 + \frac{S}{k_s \cdot A \cdot G}\right) \frac{\partial^4 \theta}{\partial x^4} - S \cdot \frac{\partial^2 \theta}{\partial x^2} + \rho \cdot A \cdot \frac{\partial^2 \theta}{\partial t^2} - \rho \cdot I \cdot \left(1 + \frac{S}{k_s \cdot A \cdot G} + \frac{E}{k_s \cdot G}\right) \cdot \frac{\partial^4 \theta}{\partial x^2 \cdot \partial t^2} + \frac{\rho^2 \cdot I}{k_s \cdot G} \cdot \frac{\partial^4 \theta}{\partial t^4} = 0 \quad (4.27)$$

where

$$\theta = y \text{ or } \psi$$

If a beam vibrates in one of its natural modes, a solution to this equation is given by

$$\theta = \Theta \cdot (A \cdot \cos(\omega \cdot t) + B \cdot \sin(\omega \cdot t)) \quad (4.28)$$

Substitution of Eq. (4.28) into Eq. (4.27), leads to

$$EI \cdot \left(1 + \frac{S}{k_s \cdot A \cdot G}\right) \frac{\partial^4 \Theta}{\partial x^4} - S \cdot \frac{\partial^2 \Theta}{\partial x^2} - \rho \cdot A \cdot \omega^2 \cdot \Theta + \rho \cdot I \cdot \omega^2 \cdot \left(1 + \frac{S}{k_s \cdot A \cdot G} + \frac{E}{k_s \cdot G}\right) \cdot \frac{\partial^2 \Theta}{\partial x^2} + \frac{\rho^2 \cdot I}{k_s \cdot G} \cdot \omega^4 \cdot \Theta = 0 \quad (4.29)$$

where

$$\Theta = Y \text{ or } \Psi$$

and which is the differential equation of motion for beams under axial load subjected to transversal vibrations according to Timoshenko theory.

## 4.2 Applications

In the following, the equations of motion derived in Chapter 4.1 are used to determine the mode shapes and resonance frequencies for different boundary conditions.

### 4.2.1 Longitudinal vibrations

#### Beam with free ends

For a free-free beam, the axial force, which is proportional to  $dX/dx$ , has to be zero at both ends.

$$\left(\frac{dX}{dx}\right)_{(x=0)} = 0 \quad \left(\frac{dX}{dx}\right)_{(x=l)} = 0 \quad (4.30)$$

The first condition is only fulfilled if  $D = 0$ . To obtain a non-trivial solution, the second condition requests  $C \neq 0$ , which leads to

$$\sin\left(\frac{\omega \cdot l}{a}\right) = 0 \quad (4.31)$$

This is only fulfilled if

$$\frac{\omega_i l}{a} = i \cdot \pi \quad (4.32)$$

where  $i$  is an integer. Substituting  $\omega_i = 2\pi \cdot f_i$  and  $a = \sqrt{E/\rho}$  into Eq. (4.32) results in

$$f_i = \frac{1}{2l} \cdot \sqrt{\frac{E}{\rho}} \cdot i \quad (4.33)$$

which for  $i = 1, 2, 3 \dots$  yields the natural frequencies of the longitudinal vibration modes of the beam. Together with Eq. (4.7), the first three frequencies with the corresponding modes can be determined to

$$f_1 = \frac{1}{2l} \cdot \sqrt{\frac{E}{\rho}} \quad X_1 = C_1 \cdot \cos\left(\frac{\pi \cdot x}{l}\right) \quad (4.34)$$

$$f_2 = \frac{1}{l} \cdot \sqrt{\frac{E}{\rho}} \quad X_2 = C_2 \cdot \cos\left(\frac{2\pi \cdot x}{l}\right) \quad (4.35)$$

$$f_3 = \frac{3}{2l} \cdot \sqrt{\frac{E}{\rho}} \quad X_3 = C_3 \cdot \cos\left(\frac{3\pi \cdot x}{l}\right) \quad (4.36)$$

The shape of the three first modes is illustrated in *Figure 4-5*.

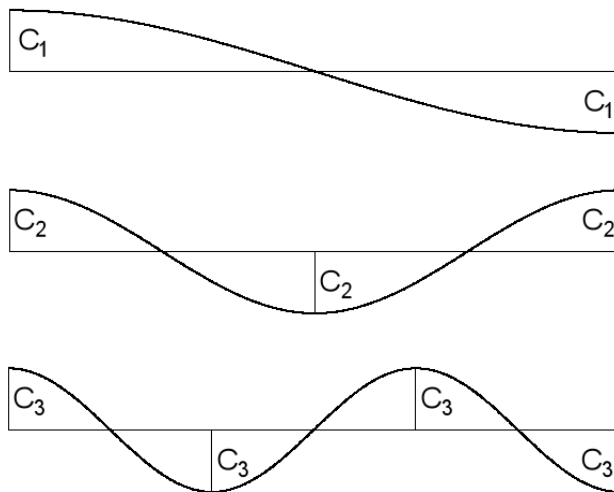


*Figure 4-5 Three first longitudinal vibration modes of a beam with free boundary conditions*

### Beam with fixed ends

For a beam with fixed ends, the displacement has to be zero at both ends.

$$X_{(x=0)} = 0 \quad X_{(x=l)} = 0 \quad (4.37)$$

The first condition is only fulfilled if  $C = 0$ . To obtain a non-trivial solution, the second condition requests  $D \neq 0$ , which brings us again to

$$\sin\left(\frac{\omega \cdot l}{a}\right) = 0 \quad (4.38)$$

and the according frequencies

$$f_i = \frac{1}{2l} \cdot \sqrt{\frac{E}{\rho}} \cdot i \quad (4.39)$$

which are the same as for the free-free condition. The modal shapes change however.

$$f_1 = \frac{1}{2l} \cdot \sqrt{\frac{E}{\rho}} \quad X_1 = D_1 \cdot \sin\left(\frac{\pi \cdot x}{l}\right) \quad (4.40)$$

$$f_2 = \frac{1}{l} \cdot \sqrt{\frac{E}{\rho}} \quad X_2 = D_2 \cdot \sin\left(\frac{2\pi \cdot x}{l}\right) \quad (4.41)$$

$$f_3 = \frac{3}{2l} \cdot \sqrt{\frac{E}{\rho}} \quad X_3 = D_3 \cdot \sin\left(\frac{3\pi \cdot x}{l}\right) \quad (4.42)$$

The shape of the three first modes is illustrated in *Figure 4-6*.

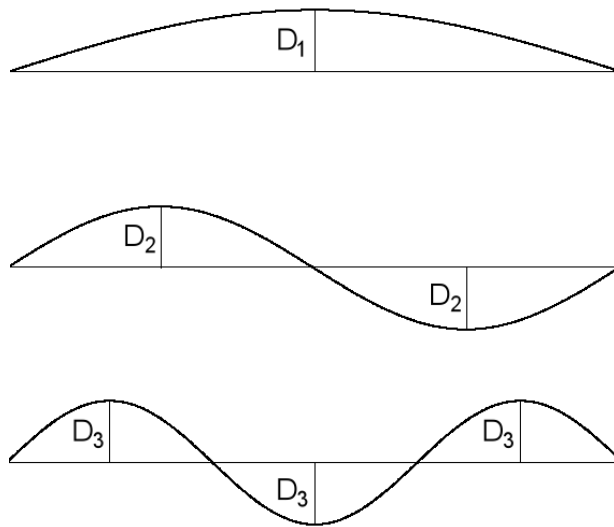


*Figure 4-6* Three first longitudinal vibration modes of a beam with fixed boundary conditions

## 4.2.2 Torsional vibrations

### Beam with free ends

The bending moment has to disappear at the ends:

$$\left(\frac{dX}{dx}\right)_{(x=0)} = 0 \quad \left(\frac{dX}{dx}\right)_{(x=l)} = 0 \quad (4.43)$$

The first condition is only fulfilled if  $D = 0$ . To obtain a non-trivial solution, the second condition requests  $C \neq 0$ , which leads to

$$\sin\left(\frac{\omega \cdot l}{b}\right) = 0 \quad (4.44)$$

This is only fulfilled if

$$\frac{\omega_i \cdot l}{b} = i \cdot \pi \quad (4.45)$$

where  $i$  is an integer. Substituting  $\omega_i = 2\pi \cdot f_i$  and  $b = \sqrt{(G \cdot K_t)/(\rho \cdot I_p)}$  into Eq. (4.45) results in

$$f_i = \frac{1}{2l} \cdot \sqrt{\frac{G \cdot K_t}{\rho \cdot I_p}} \cdot i \quad (4.46)$$

which for  $i = 1, 2, 3 \dots$  yields the natural frequencies of the torsional vibration modes of the beam. Together with Eq. (4.14), the first three frequencies with the corresponding modes can be determined to

$$f_1 = \frac{1}{2l} \cdot \sqrt{\frac{G \cdot K_t}{\rho \cdot I_p}} \quad X_1 = C_1 \cdot \cos\left(\frac{\pi \cdot x}{l}\right) \quad (4.47)$$

$$f_2 = \frac{1}{l} \cdot \sqrt{\frac{G \cdot K_t}{\rho \cdot I_p}} \quad X_2 = C_2 \cdot \cos\left(\frac{2\pi \cdot x}{l}\right) \quad (4.48)$$

$$f_3 = \frac{3}{2l} \cdot \sqrt{\frac{G \cdot K_t}{\rho \cdot I_p}} \quad X_3 = C_3 \cdot \cos\left(\frac{3\pi \cdot x}{l}\right) \quad (4.49)$$

The shape of the three first modes is illustrated in *Figure 4-7*.

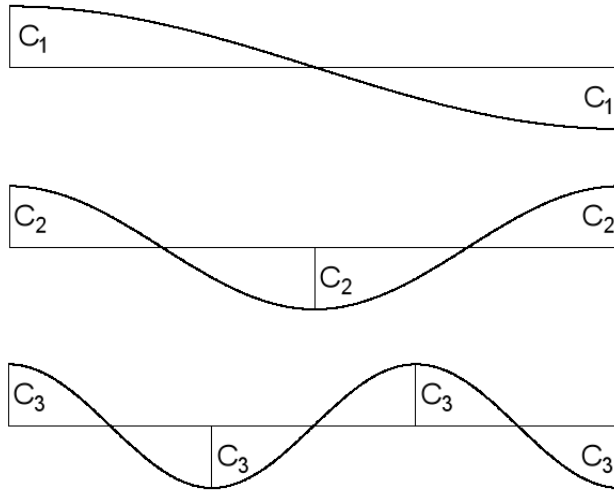


*Figure 4-7* Three first torsional vibration modes of a beam with free boundary conditions

### Beam with fixed ends

For a beam with fixed ends, the rotation has to be zero at both ends.

$$X_{(x=0)} = 0 \quad X_{(x=l)} = 0 \quad (4.50)$$

The first condition is only fulfilled if  $C = 0$ . To obtain a non-trivial solution, the second condition requests  $D \neq 0$ , which leads again to

$$\sin\left(\frac{\omega \cdot l}{b}\right) = 0 \quad (4.51)$$

and the according frequencies

$$f_i = \frac{1}{2l} \cdot \sqrt{\frac{G \cdot K_t}{\rho \cdot I_p}} \cdot i \quad (4.52)$$

which are the same as for the free-free condition. The modal shapes however are different again.

$$f_1 = \frac{1}{2l} \cdot \sqrt{\frac{G \cdot K_t}{\rho \cdot I_p}} \quad X_1 = D_1 \cdot \sin\left(\frac{\pi \cdot x}{l}\right) \quad (4.53)$$

$$f_2 = \frac{1}{l} \cdot \sqrt{\frac{G \cdot K_t}{\rho \cdot I_p}} \quad X_2 = D_2 \cdot \sin\left(\frac{2\pi \cdot x}{l}\right) \quad (4.54)$$

$$f_3 = \frac{3}{2l} \cdot \sqrt{\frac{G \cdot K_t}{\rho \cdot I_p}} \quad X_3 = D_3 \cdot \sin\left(\frac{3\pi \cdot x}{l}\right) \quad (4.55)$$

The shape of the three first modes is illustrated in *Figure 4-8*.

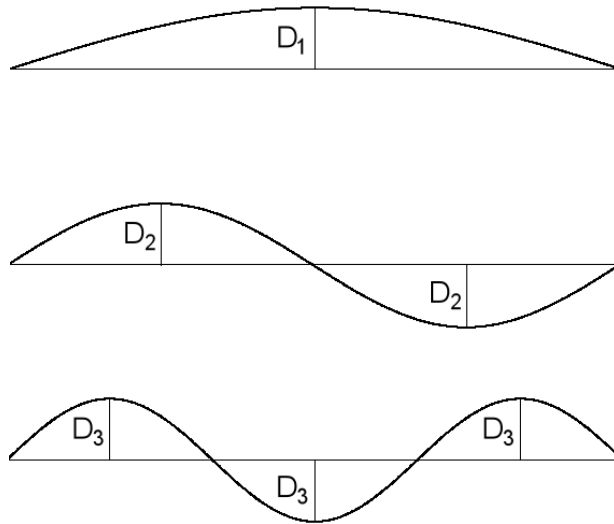


*Figure 4-8* Three first torsional vibration modes of a beam with fixed boundary conditions

As it can be seen, the modes and frequencies have the same shape for longitudinal and rotational vibrations for the same boundary conditions.

### 4.2.3 Transversal vibrations – Euler beam theory

#### Beam with free ends, $S=0$

The following boundary conditions apply for free-free beams:

$$\left(\frac{d^2 X}{dx^2}\right)_{(x=0)} = 0 \quad \left(\frac{d^3 X}{dx^3}\right)_{(x=0)} = 0 \quad (4.56)$$

$$\left(\frac{d^2 X}{dx^2}\right)_{(x=l)} = 0 \quad \left(\frac{d^3 X}{dx^3}\right)_{(x=l)} = 0 \quad (4.57)$$

The conditions in Eq. (4.56) are satisfied by the solution

$$X = C \cdot (\cos(k \cdot x) + \cosh(k \cdot x)) + D \cdot (\sin(k \cdot x) + \sinh(k \cdot x)) \quad (4.58)$$

while the other two conditions in Eq. (4.57) yield the equations

$$C \cdot (-\cos(k \cdot l) + \cosh(k \cdot l)) + D \cdot (-\sin(k \cdot l) + \sinh(k \cdot l)) = 0 \quad (4.59)$$

$$C \cdot (\sin(k \cdot l) + \sinh(k \cdot l)) + D \cdot (-\cos(k \cdot l) + \cosh(k \cdot l)) = 0 \quad (4.60)$$

A solution for this system different from zero only exists if the determinant of Eq. (4.59) and Eq. (4.60) disappears:

$$(-\cos(k \cdot l) + \cosh(k \cdot l))^2 - (\sin(k \cdot l)^2 - \sinh(k \cdot l)^2) = 0 \quad (4.61)$$

With the equations

$$\cosh(k \cdot l)^2 - \sinh(k \cdot l)^2 = 1$$

$$\cos(k \cdot l)^2 + \sin(k \cdot l)^2 = 1$$

Eq. (4.61) can be rewritten as

$$\cos(k \cdot l) \cdot \cosh(k \cdot l) = 1 \quad (4.62)$$

for which the solution can be approximated to

$$k_i \cdot l \approx (i + 1/2) \cdot \pi \quad (4.63)$$

Substitution of  $k_i^4 = \frac{\omega_i^2}{a^2}$ ,  $a = \sqrt{(E \cdot I)/(\rho \cdot A)}$  and  $\omega_i = 2\pi \cdot f_i$ , yields

$$f_i = \frac{\pi}{8 \cdot l^2} \cdot \sqrt{\frac{E \cdot I}{\rho \cdot A}} \cdot (2 \cdot i + 1)^2 \quad (4.64)$$

The shape of the three first modes is illustrated in *Figure 4-9*.

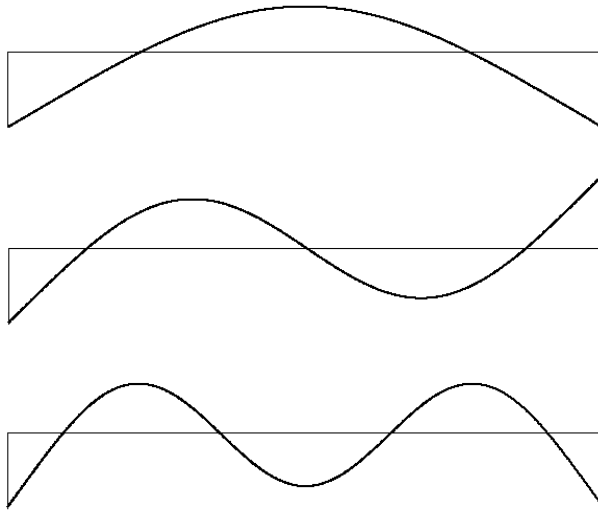


*Figure 4-9 Three first transversal vibration modes of a beam with free boundary conditions*

### **Beam with clamped ends, S=0**

For clamped ends, the boundary conditions are

$$X_{(x=0)} = 0 \quad \left(\frac{dX}{dx}\right)_{(x=0)} = 0 \quad (4.65)$$

$$X_{(x=l)} = 0 \quad \left(\frac{dX}{dx}\right)_{(x=l)} = 0 \quad (4.66)$$

The first two conditions in Eq. (4.65) are satisfied by the solution

$$X = C \cdot (\cos(k \cdot x) - \cosh(k \cdot x)) + D \cdot (\sin(k \cdot x) - \sinh(k \cdot x)) \quad (4.67)$$

while the other two conditions in Eq. (4.66) yield the equations

$$C \cdot (\cos(k \cdot l) - \cosh(k \cdot l)) + D \cdot (\sin(k \cdot l) - \sinh(k \cdot l)) = 0 \quad (4.68)$$

$$C \cdot (\sin(k \cdot l) + \sinh(k \cdot l)) + D \cdot (-\cos(k \cdot l) + \cosh(k \cdot l)) = 0 \quad (4.69)$$

A solution for this system different from zero only exists if the determinant of Eq. (4.68) and Eq. (4.69) disappears:

$$(-\cos(k \cdot l) + \cosh(k \cdot l))^2 - (\sin(k \cdot l)^2 - \sinh(k \cdot l)^2) = 0 \quad (4.70)$$

from which the same equation as in Eq. (4.62) can be deduced, which results in the same frequencies as for the free-free beam:

$$f_i = \frac{\pi}{8 \cdot l^2} \cdot \sqrt{\frac{E \cdot I}{\rho \cdot A}} \cdot (2 \cdot i + 1)^2 \quad (4.71)$$

The shape of the three first modes is illustrated in *Figure 4-10*.

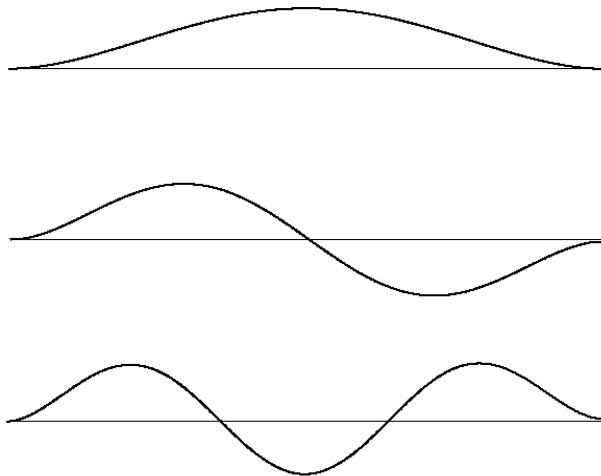


*Figure 4-10* Three first transversal vibration modes of a beam with fixed boundary conditions

### **Beam with simple supports under axial load, $S \neq 0$**

For a simply supported beam, the boundary conditions are

$$X_{(x=0)} = 0 \quad X_{(x=l)} = 0 \quad (4.72)$$

which are satisfied for

$$X_i = \sin\left(\frac{i \cdot \pi \cdot x}{l}\right) \quad (4.73)$$

where  $i$  is an integer. Substituting Eq. (4.73) into Eq. (4.21) and replacing  $\omega_i = 2\pi \cdot f_i$  yields

$$f_i = i^2 \cdot \frac{\pi}{2 \cdot l^2} \cdot \sqrt{\frac{E \cdot I}{\rho \cdot A}} \cdot \sqrt{1 + \frac{S \cdot l^2}{i^2 \cdot E \cdot I \cdot \pi^2}} \quad (4.74)$$

---

The three first mode shapes are illustrated in *Figure 4-11*.

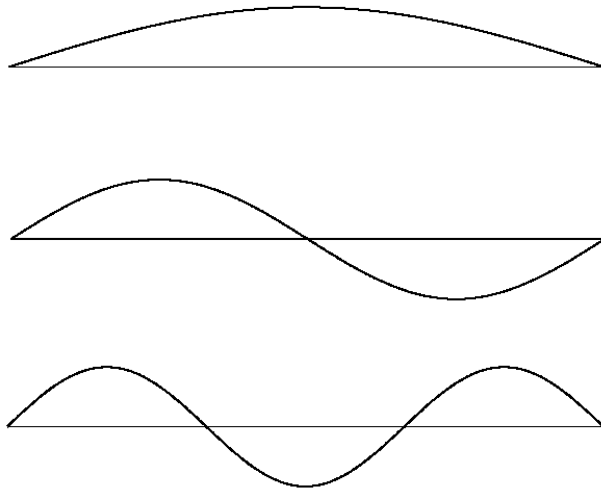


*Figure 4-11* Three first transversal vibration modes of a beam under axial load with simply supported boundary conditions

For other boundary conditions there are no simple expressions, which states the need for numerical solutions. These can for example be found in Shaker (1975).

#### **4.2.4 Transversal vibrations – Timoshenko beam theory**

No simple expressions for an exact solution are available to solve Eq. (4.29). This makes it necessary to use numerical methods to determine the frequencies for beams with different boundary conditions, like for instance clamped-clamped or elastic supports, cf. Chapter 5.

---

## 5 Numerical modelling and parameter estimation

This chapter contains an overview of different means to calculate the resonance frequencies for a beam under axial load subjected to transversal vibrations for different boundary conditions using Timoshenko theory. The end conditions are modelled using translational and rotational springs (cf. *Figure 5-1*), based on the assumption that the supports show linearly elastic behaviour.

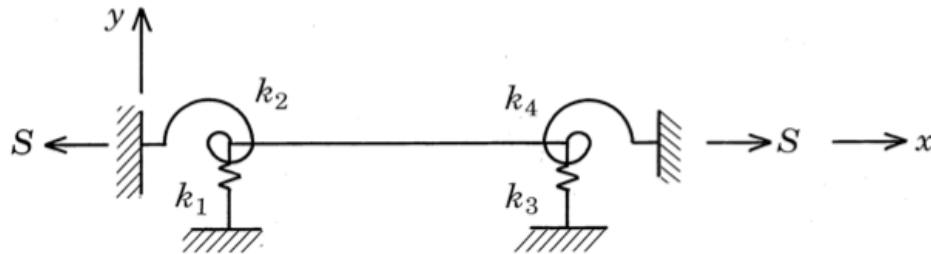


*Figure 5-1* Illustration of an axially loaded beam with translational and rotational spring supports, Livingston (1994)

The according boundary conditions can be written as:

$$V_{x=0} = k_1 \cdot (Y)_{x=0} \quad (5.1)$$

$$V_{x=l} = -k_3 \cdot (Y)_{x=l} \quad (5.2)$$

$$M_{x=0} = -k_2 \cdot (Y')_{x=0} \quad (5.3)$$

$$M_{x=l} = k_4 \cdot (Y')_{x=l} \quad (5.4)$$

A dual parameter estimation method is furthermore presented that can be used to estimate axial load  $S$  and boundary conditions  $k$ , assuming rigid transversal supports and identical rotational supports (cf. *Figure 5-2*).

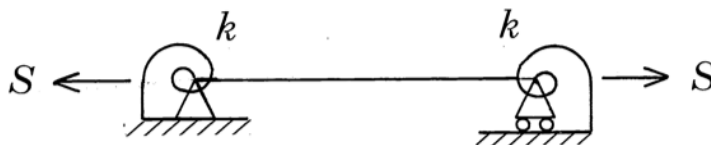


*Figure 5-2* Illustration of a simply supported beam under axial load with rotational spring supports, Livingston (1994)

At the end of the chapter, a sensitivity analysis is carried out to determine the sensitivity of the output parameters  $S$  and  $k$  with regard to errors in different input parameters.

### 5.1 Rayleigh-Ritz method

Since the exact determination of the first frequencies of a vibrating system is not always possible or even necessary, it can be reasonable to use approximation methods for this purpose. Such methods are for example Rayleigh's method or its further development according to Ritz Harris (2002). While Rayleigh's method gives only good results for the fundamental frequency, Ritz's method can also be used to estimate some of the higher frequencies. Rayleigh's method is based on the fact that the total energy in a vibrating system without damping is constant. When a beam

reaches its maximal deflection from its neutral state, the global potential energy is maximal and the kinetic energy is zero. When it passes through its equilibrium position, the opposite is true. For conservation of energy, these two energies therefore have to be equal, which is from where the fundamental frequency can be computed. Ritz's method is based on the same principle with the difference that the deflection functions contain several undetermined parameters, which are adjusted in a way to minimize the frequency. It can be shown that frequencies found by using inexact shapes are always higher than the actual frequencies Den Hartog (1985). The accuracy of the result therefore depends largely on the choice of the deflection function. For the exact deflection function the computed frequency is the exact solution. Rayleigh–Ritz method is appropriate to determine the lower frequencies of simple systems.

In the case of the Timoshenko beam presented in *Figure 5-1*, the maximal potential and kinetic energies can be expressed as follows, according to Harris (2002):

$$V_{max} = \frac{1}{2} \int_0^l \left[ EI \left( \frac{\partial \theta}{\partial x} \right)^2 + k_s GA \left( \frac{\partial v}{\partial x} - \theta \right)^2 \right] dx + \frac{1}{2} \int_0^l \left[ S \left( \frac{\partial v}{\partial x} \right)^2 \right] dx + \frac{1}{2} k_1 (v_{x=0})^2 + \frac{1}{2} k_3 (v_{x=l})^2 + \frac{1}{2} k_2 (\theta_{x=0})^2 + \frac{1}{2} k_4 (\theta_{x=l})^2 \quad (5.5)$$

$$T_{max} = \omega^2 \cdot T^* = \omega^2 \cdot \frac{1}{2} \int_0^l [\rho A \dot{v}(x)^2 + \rho I \dot{\theta}(x)^2] dx \quad (5.6)$$

where  $T^*$  is the reference kinetic energy of the system.

For conservation of energy Eq. (5.5) and Eq. (5.6) have to be equal, which leads to the following equation, where  $V_{max}$  and  $T^*$  are functions of  $v$  and  $\theta$ .

$$V_{max}(v, \theta) - \omega^2 \cdot T^*(v, \theta) = 0 \quad (5.7)$$

If we are only interested in the first resonance frequency, we can assume functions for  $v(x)$  and  $\theta(x)$ , substitute into Eq. (5.7) and solve for  $\omega$ . The accuracy of the result will improve the more boundary conditions are fulfilled and the closer the functions are to the actual deflection shapes. However good results can already be obtained for rather poor input functions.

If we are however interested in resonance frequencies of higher order, Ritz's improvement needs to be used to find accurate results. In this case the input functions are expressed as sums of functions multiplied by unknown parameters, as for example in:

$$v(x) = \sum_{i=1}^N a_i \cdot \sin(i\pi x/l) \quad (5.8)$$

$$\theta(x) = \sum_{i=1}^N b_i \cdot i \cdot \cos(i\pi x/l) \quad (5.9)$$

Substituting Eq. (5.8) and Eq. (5.9) into Eq. (5.7) and minimizing with regard to each unknown parameter yields a system of  $2N$  equations with  $2N$  unknowns. Written in matrix form, this system has a trivial solution only if the determinant equals to zero. The according equation can then be solved for the resonance frequencies. The accuracy will improve with a higher number of terms  $N$ , so will however also the computational effort.

## 5.2 Discrete model

The discrete model is in fact a finite element approach, which means that the results are only approximations to the actual behaviour of a system. It is most suitable to determine the dynamic characteristics of complicated structures that are modelled using discrete mass, stiffness and damping matrices. These matrices have different shapes, depending on which element theory is used and how many degrees of freedom are included. In this paper, all the presented matrices were formed using Timoshenko beam elements.

### 5.2.1 Element mass matrix

The element mass matrix can be calculated using cubic polynomial shape functions and the principle of virtual work Friedman and Kosmatka (1993). The results are two element matrices, one accounting for effects of translatory, the other one for rotary inertia. The final element mass matrix is then obtained by forming the sum of these two matrices:

$$\mathbf{M}^e = \mathbf{M}_T^e + \mathbf{M}_R^e \quad (5.10)$$

where

$$\mathbf{M}_T^e = \frac{\rho A l}{(1 + \Phi)^2} \begin{bmatrix} \frac{13}{35} + \frac{7}{10}\Phi + \frac{1}{3}\Phi^2 & \left(\frac{11}{210} + \frac{11}{120}\Phi + \frac{1}{24}\Phi^2\right)l & \frac{9}{70} + \frac{3}{10}\Phi + \frac{1}{6}\Phi^2 & -\left(\frac{13}{420} + \frac{3}{40}\Phi + \frac{1}{24}\Phi^2\right)l \\ \left(\frac{1}{105} + \frac{1}{60}\Phi + \frac{1}{120}\Phi^2\right)l^2 & \left(\frac{13}{420} + \frac{3}{40}\Phi + \frac{1}{24}\Phi^2\right)l & -\left(\frac{1}{140} + \frac{1}{60}\Phi + \frac{1}{120}\Phi^2\right)l^2 & \\ \frac{13}{35} + \frac{7}{10}\Phi + \frac{1}{3}\Phi^2 & -\left(\frac{11}{210} + \frac{11}{120}\Phi + \frac{1}{24}\Phi^2\right)l & \frac{9}{70} + \frac{3}{10}\Phi + \frac{1}{6}\Phi^2 & -\left(\frac{13}{420} + \frac{3}{40}\Phi + \frac{1}{24}\Phi^2\right)l \\ \left(\frac{1}{105} + \frac{1}{60}\Phi + \frac{1}{120}\Phi^2\right)l^2 & & \left(\frac{1}{105} + \frac{1}{60}\Phi + \frac{1}{120}\Phi^2\right)l^2 & \end{bmatrix}$$

*symmetric*

$$\mathbf{M}_R^e = \frac{\rho I}{(1 + \Phi)^2 l} \begin{bmatrix} \frac{6}{5} & \left(\frac{1}{10} - \frac{1}{2}\Phi\right)l & -\frac{6}{5} & \left(\frac{1}{10} - \frac{1}{2}\Phi\right)l \\ \left(\frac{2}{15} + \frac{1}{6}\Phi + \frac{1}{3}\Phi^2\right)l^2 & \left(-\frac{1}{10} + \frac{1}{2}\Phi\right)l & -\left(\frac{1}{30} + \frac{1}{6}\Phi - \frac{1}{6}\Phi^2\right)l^2 & \\ \frac{6}{5} & \left(-\frac{1}{10} + \frac{1}{2}\Phi\right)l & \left(-\frac{1}{10} + \frac{1}{2}\Phi\right)l & \\ \left(\frac{2}{15} + \frac{1}{6}\Phi + \frac{1}{3}\Phi^2\right)l^2 & & \left(\frac{2}{15} + \frac{1}{6}\Phi + \frac{1}{3}\Phi^2\right)l^2 & \end{bmatrix}$$

*symmetric*

$$\Phi = 12EI/(k_s GA l^2)$$

If shear effects and rotary effects can be neglected, these matrices can be reduced to Euler theory by setting  $\Phi = 0$  and  $\mathbf{M}_R^e = 0$ . The reduced matrices are then the same as in Livingston (1994).

### 5.2.2 Element stiffness matrix

In a similar way, the element stiffness matrix can be formulated using again the principle of work. Two element matrices are obtained, one accounting for the strain of the beam, cf. Friedman and Kosmatka (1993), the other one for its axial load Paz (1997). The sum of these matrices yields the element stiffness matrix:

$$\mathbf{K}^e = \mathbf{K}_\zeta^e + \mathbf{K}_L^e \quad (5.11)$$

---

where

$$K_S^e = \frac{EI}{(1 + \Phi)l^3} \begin{bmatrix} 12 & 6l & -12 & 6l \\ 6l & (4 + \Phi)l^2 & -6l & (2 - \Phi)l^2 \\ -12 & -6l & 12 & -6l \\ 6l & (2 - \Phi)l^2 & -6l & (4 + \Phi)l^2 \end{bmatrix}$$

$$K_L^e = \frac{S}{30l} \begin{bmatrix} 36 & 3l & -36 & 3l \\ 3l & 4l^2 & -3l & -l^2 \\ -36 & -3l & 36 & -3l \\ 3l & -l^2 & -3l & 4l^2 \end{bmatrix}$$

$$\Phi = 12EI/(k_sGA l^2)$$

The according Euler element stiffness matrix can again be obtained by setting  $\Phi = 0$ , Livingston (1994).

### 5.2.3 Element damping matrix

The damping matrix can be taken into account in different ways, depending on the damping properties of the system (for example viscous or hysteretic), cf. Harris (2002) for more information. In this thesis, damping is considered as a negligible parameter.

### 5.2.4 Global matrix formulation

According to Livingston (1994), there are three steps in the formulation of the global matrices:

1. Divide the system in a number of elements
2. Identify nodes between the elements and number consequently the degrees of freedom
3. Determine the mass and stiffness matrices for each element and add them into the global mass and stiffness matrices

This procedure is called the direct method.

As an example, consider the beam from *Figure 5-1* with  $L = 3$ ,  $E = 1$ ,  $I = 1$  and  $S = 0$ , modelled with three elements, each having a length of  $l = 1$ . Neglecting effects from shear and rotary inertia, the global mass and stiffness matrices are:



### 5.3 Continuous model

The continuous model is most suitable for simple systems, like for example single bars or beams. For complex systems, the computational effort is too large, resulting in an inefficient use of memory. The advantage of the continuous model is however that it yields an exact solution since the differential Eq. (4.29) is solved directly. According to Howson and Williams (1973), this equation can be solved with the following functions:

$$Y = C_1 \cosh\left(\lambda_1 \cdot \frac{x}{l}\right) + C_2 \sinh\left(\lambda_1 \cdot \frac{x}{l}\right) + C_3 \cos\left(\lambda_2 \cdot \frac{x}{l}\right) + C_4 \sin\left(\lambda_2 \cdot \frac{x}{l}\right) \quad (5.13)$$

$$\Psi = C_1' \sinh\left(\lambda_1 \cdot \frac{x}{l}\right) + C_2' \cosh\left(\lambda_1 \cdot \frac{x}{l}\right) + C_3' \sin\left(\lambda_2 \cdot \frac{x}{l}\right) + C_4' \cos\left(\lambda_2 \cdot \frac{x}{l}\right) \quad (5.14)$$

where

$$\lambda_1 = \frac{b}{\sqrt{2(1-s^2p^2)}} \sqrt{-\Delta + \sqrt{\Delta^2 + \frac{4}{b^2}(1-s^2p^2)(1-b^2r^2s^2)}}$$

$$\lambda_2 = \frac{b}{\sqrt{2(1-s^2p^2)}} \sqrt{\Delta + \sqrt{\Delta^2 + \frac{4}{b^2}(1-s^2p^2)(1-b^2r^2s^2)}}$$

with

$$b^2 = \rho A l^2 \omega^2 / EI$$

$$r^2 = I / A l^2$$

$$\phi = k_s GA$$

$$s^2 = EI / \phi l^2$$

$$p^2 = Pl^2 / EI$$

$$\Delta = (p^2/b^2) + r^2(1-s^2p^2) + s^2$$

Furthermore it can be shown that Howson and Williams (1973):

$$C_1' = HC_1 \quad (5.15)$$

$$C_2' = HC_2 \quad (5.16)$$

$$C_3' = -ZC_3 \quad (5.17)$$

$$C_4' = HC_4 \quad (5.18)$$

where

$$H = \frac{(1-s^2p^2)\lambda_1^2 + b^2s^2}{\lambda_1 l}$$

$$Z = \frac{(1-s^2p^2)\lambda_2^2 - b^2s^2}{\lambda_2 l}$$

Substituting Eq. (4.25) and Eq. (4.26) together with Eq. (5.13)-(5.18) into the boundary conditions (5.1)-(5.4) yields a system of four equations with four unknowns that can be written in the following matrix form:

$$\mathbf{CM} \cdot \mathbf{C} = \mathbf{0} \quad (5.19)$$

where

$$\mathbf{CM} = \begin{bmatrix} \langle -k_1 \rangle & \langle -\phi H + \phi \frac{\lambda_1}{l} + S \frac{\lambda_1}{l} \rangle \\ \langle k_3 c_2 - \phi H c_1 + \phi c_1 \frac{\lambda_1}{l} + S c_1 \frac{\lambda_1}{l} \rangle & \langle k_3 c_1 - \phi H c_2 + \phi c_2 \frac{\lambda_1}{l} + S c_2 \frac{\lambda_1}{l} \rangle \\ \langle -EIH \frac{\lambda_1}{l} \rangle & \langle H k_2 \rangle \\ \langle -EIH c_2 \frac{\lambda_1}{l} - H k_4 c_1 \rangle & \langle -EIH c_1 \frac{\lambda_1}{l} - H k_4 c_2 \rangle \\ \langle -k_1 \rangle & \langle -\phi Z + \phi \frac{\lambda_2}{l} + S \frac{\lambda_2}{l} \rangle \\ \langle k_3 c_4 + \phi Z c_3 - \phi c_3 \frac{\lambda_2}{l} - S c_3 \frac{\lambda_2}{l} \rangle & \langle k_3 c_3 - \phi Z c_4 + \phi c_4 \frac{\lambda_2}{l} + S c_4 \frac{\lambda_2}{l} \rangle \\ \langle EIZ \frac{\lambda_2}{l} \rangle & \langle Z k_2 \rangle \\ \langle EIZ c_4 \frac{\lambda_2}{l} + Z k_4 c_3 \rangle & \langle EIZ c_3 \frac{\lambda_2}{l} - Z k_4 c_4 \rangle \end{bmatrix}$$

$$\mathbf{C} = \begin{bmatrix} C_1 \\ C_2 \\ C_3 \\ C_4 \end{bmatrix}$$

and

$$c_1 = \sinh(\lambda_1)$$

$$c_2 = \cosh(\lambda_1)$$

$$c_3 = \sin(\lambda_2)$$

$$c_4 = \cos(\lambda_2)$$

A non-trivial solution to this system can only be found if the determinant of  $\mathbf{CM}$  vanishes, leading to

$$|\mathbf{CM}| = 0 \quad (5.20)$$

This equation can be solved for the angular eigenfrequencies  $\omega_n$ , from which the corresponding frequencies  $f_n$  can be computed. This can be done for different boundary conditions  $k_1$ - $k_4$ . In this thesis, the  $k_i$  are set to zero to model free support conditions, or they are set to values of  $10^{15}$  to simulate rigid supports.

## 5.4 Model comparison

Table 5-1 and Table 5-2 shows the frequencies for different boundary conditions with and without axial load, calculated using the discrete and continuous model, cf. Appendix A, as well as the above-mentioned SFVIBAT software. Furthermore the frequencies according to Euler theory are presented to show the difference in the results compared to the Timoshenko theory. The chosen parameters are:  $E = 13000$  MPa,  $G = 760$  MPa,  $\rho = 400$  kg/m<sup>3</sup>,  $L = 1.5$ m,  $h = 75$ mm and  $b = 35$ mm.

Table 5-1 Comparison of transversal frequencies of a beam with different boundary conditions calculated with different numerical models

S=0		Timoshenko			Euler
Beam	Freq [Hz]	Continuous Model	Discrete Model (n=50)	SFVIBAT (n=50)	Discrete Model (n=50)
free-free	f1	90.54	90.64	90.19	91.16
	f2	245.49	246.06	243.51	251.28
pinned-pinned	f1	40.02	40.03	39.99	40.21
	f2	157.84	157.97	157.37	160.85
rotational springs (k=10000 Nm)	f1	59.49	59.50	59.44	60.11
	f2	181.34	181.49	180.81	186.03
fixed-fixed	f1	89.10	89.17	89.02	91.16
	f2	239.19	239.49	238.45	251.28

Table 5-2 Comparison of transversal frequencies of an axially loaded beam with different boundary conditions calculated with different numerical models

S=20000		Timoshenko			Euler
Beam	Freq [Hz]	Continuous Model	Discrete Model (n=50)	SFVIBAT (n=50)	Discrete Model (n=50)
free-free	f1	135.85	136.00	135.34	136.56
	f2	288.11	288.78	285.83	293.71
pinned-pinned	f1	60.97	60.98	60.92	61.10
	f2	182.66	182.82	182.11	185.30
rotational springs (k=10000 Nm)	f1	75.45	75.47	75.39	75.96
	f2	203.46	203.65	202.87	207.70
fixed-fixed	f1	102.52	102.54	102.43	104.54
	f2	258.44	258.65	257.65	270.16

The discrete models calculate with  $n = 50$  finite elements while the continuous models yield exact solutions for the respective model assumptions. Rigid supports are modelled setting  $k = 10^{15}$  Nm. The Euler model assumes a much stiffer behaviour of the system since shear deformations are neglected, leading to higher frequencies. They derive already considerably for the second bending mode. The comparison of the Timoshenko models shows good accordance for the first mode, while the differences are already higher for the second mode. The reason is the limited number of finite elements and leading to the fact that these models always yield approximate solutions. It can furthermore be observed that the continuous solution always lies in between the two discrete solutions, indicating a good validation of this model.

## 5.5 Parameter estimation

For the actual parameter estimation, the continuous model based on Timoshenko theory is used in the following. In most practical cases, as well as in the tests in Chapter 8, it is reasonable to assume that the translational supports can be modelled as rigid, while the rotational supports are modelled as springs. In some cases, it is even acceptable to assume identical support conditions at both sides. These considerations yield to the two systems illustrated in *Figure 5-3 (a)*.

The first system in has two unknown parameters for which the solution requires therefore at least two resonance frequencies. In theory, also more frequencies could be used for error minimisation. The measurement of higher vibration modes might however be more likely to contain errors, which makes the error minimisation

unsuitable for some materials. This is for example the case for inhomogeneous timber, especially in presence of knots. Homogeneous materials like steel do not show these problems and allow also the accurate measurement of higher frequencies. If only two resonance frequencies are used, a plot similar to the one in *Figure 5-3 (c)* is the result. For a known rotational stiffness  $k$ , there exists only one axial load  $S$  for which the beam vibrates in a given frequency. This way, a so-called contour curve can be depicted for each frequency by varying one of the parameters  $k$  and  $S$ .

The second system in *Figure 5-3 (b)* has three unknown parameters for which the solution requires therefore at least three resonance frequencies. Instead of curves, each frequency is determined by a surface (cf. *Figure 5-3 (d)*). The intersections of these surfaces are the solutions to the system. Here, there are two solutions since  $k_1$  and  $k_2$  are exchangeable for symmetry reasons.

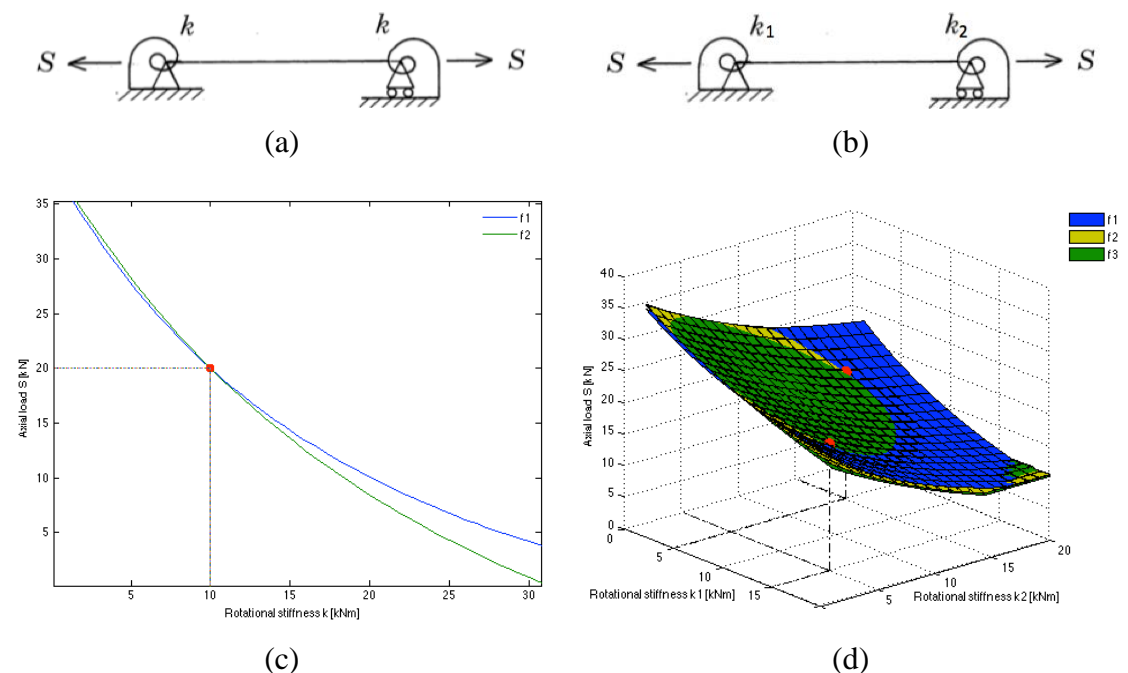


*Figure 5-3* Simply supported beam under axial load with spring supports of identical stiffness (a), simply supported beam under axial load with spring supports of different stiffness (b), illustration of dual parameter estimation (c) and illustration of triple parameter estimation (d).

## 5.6 Sensitivity analysis for continuous model with $k_1 = k_2$

In the following, the sensitivities of the parameters  $S$  and  $k$  are investigated for different load levels and under the assumption of equal boundary conditions with regard to the following input parameters:

- Clear length  $L$
- Density  $\rho$
- E-modulus  $E$
- G-modulus  $G$
- Measured frequencies  $f_i$

The errors of  $S$  and  $k$  are standardised to 25%, which allows a direct comparison of the values. A steep curve means a high sensitivity to the according parameter.

## 5.6.1 Sensitivity of S

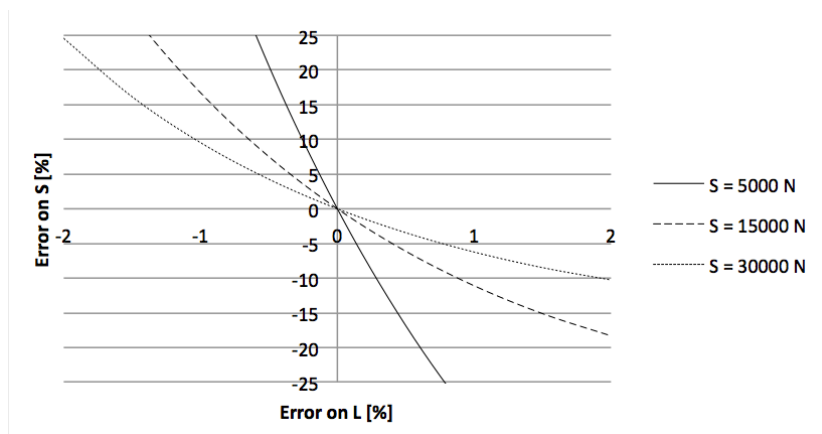


Figure 5-4 Sensitivity of the axial load  $S$  with regard to the clear length  $L$  for different load levels

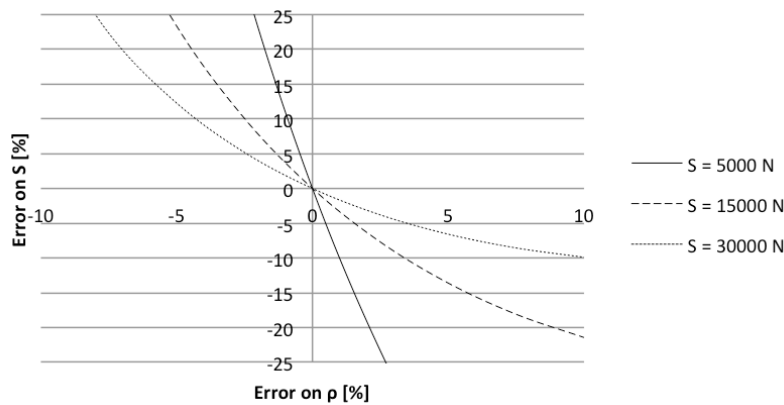


Figure 5-5 Sensitivity of the axial load  $S$  with regard to the density  $\rho$  for different load levels

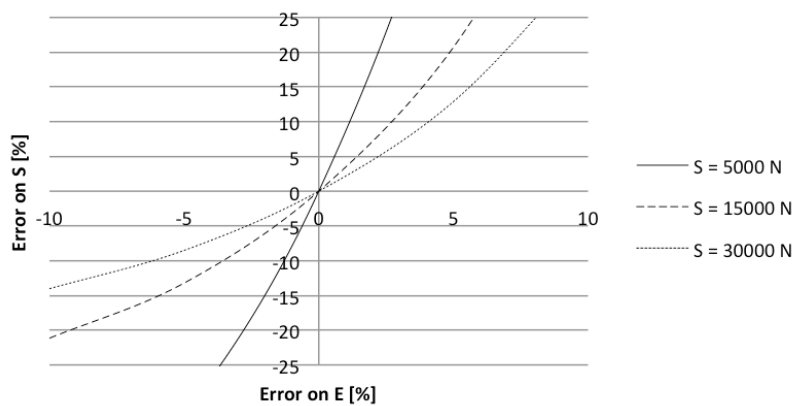


Figure 5-6 Sensitivity of the axial load  $S$  with regard to the  $E$ -modulus  $E$  for different load levels

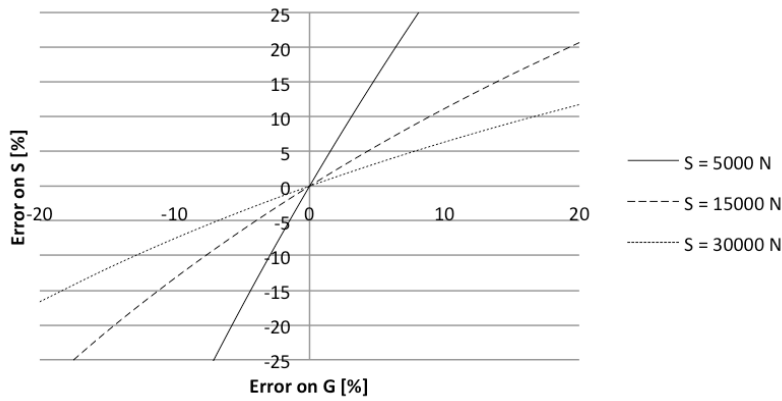


Figure 5-7 Sensitivity of the axial load  $S$  with regard to the shear modulus  $G$  for different load levels

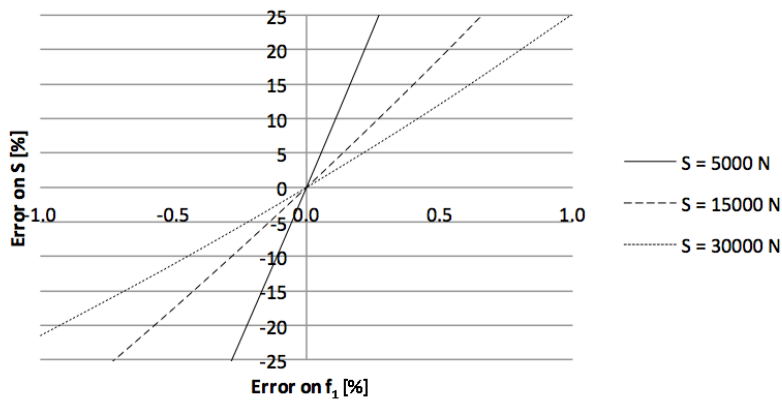


Figure 5-8 Sensitivity of the axial load  $S$  with regard to the first measured frequency for different load levels

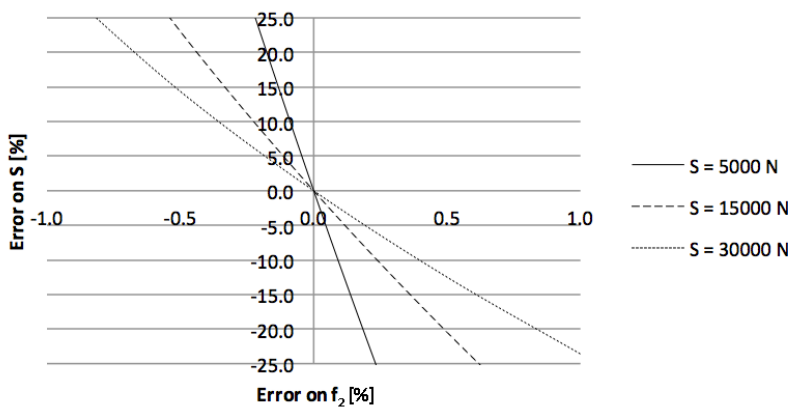


Figure 5-9 Sensitivity of the axial load  $S$  with regard to the second measured frequency for different load levels

## 5.6.2 Sensitivity of $k$

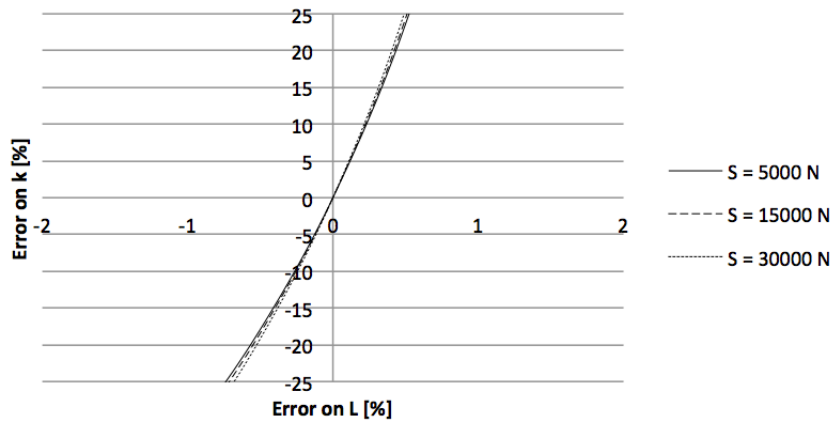


Figure 5-10 Sensitivity of the rotational stiffness  $k$  with regard to the clear length  $L$  for different load levels

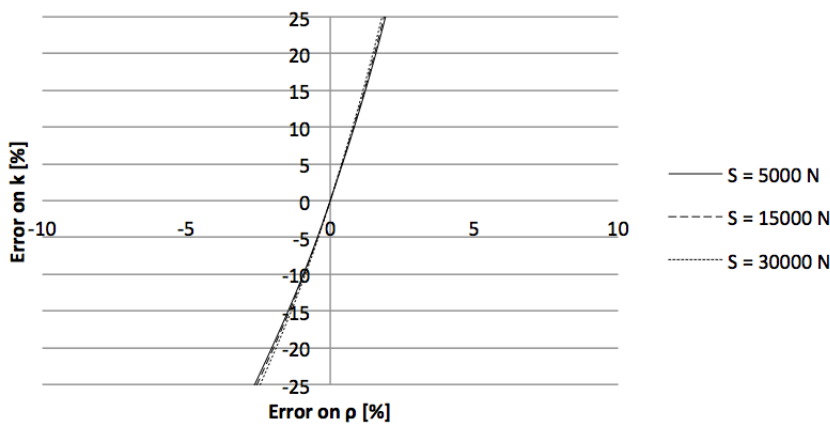


Figure 5-11 Sensitivity of the rotational stiffness  $k$  with regard to the density  $\rho$  for different load levels

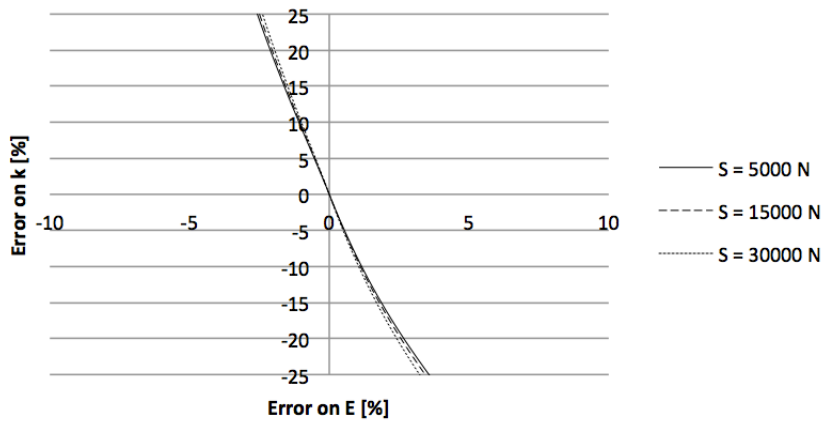


Figure 5-12 Sensitivity of the rotational stiffness  $k$  with regard to the E-modulus  $E$  for different load levels

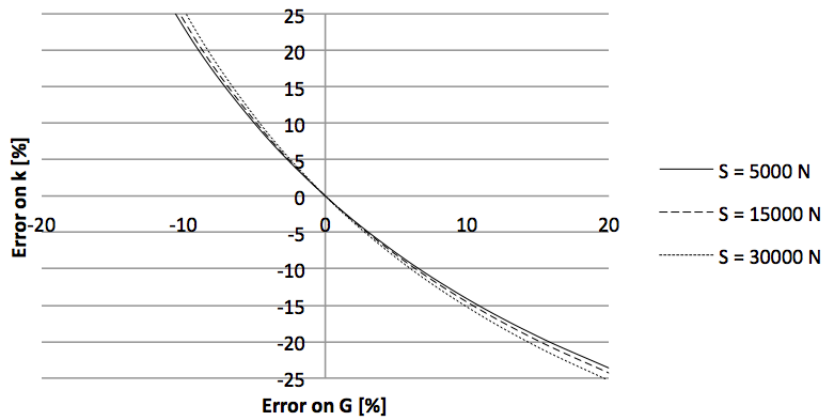


Figure 5-13 Sensitivity of the rotational stiffness  $k$  with regard to the shear modulus  $G$  for different load levels

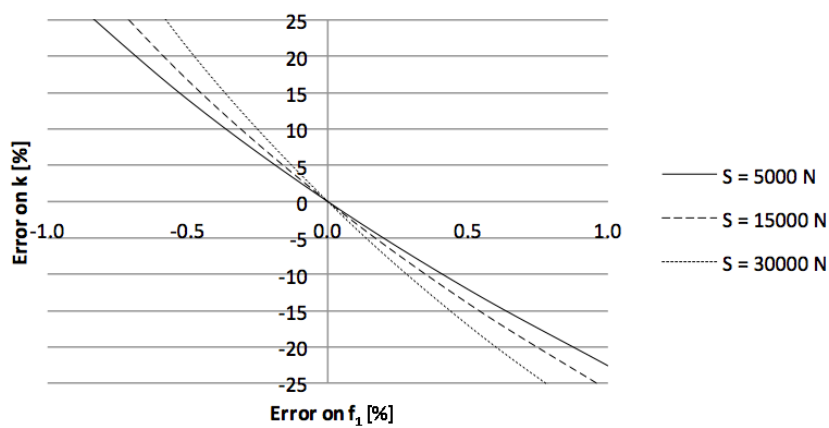


Figure 5-14 Sensitivity of the rotational stiffness  $k$  with regard to the first measured frequency for different load levels

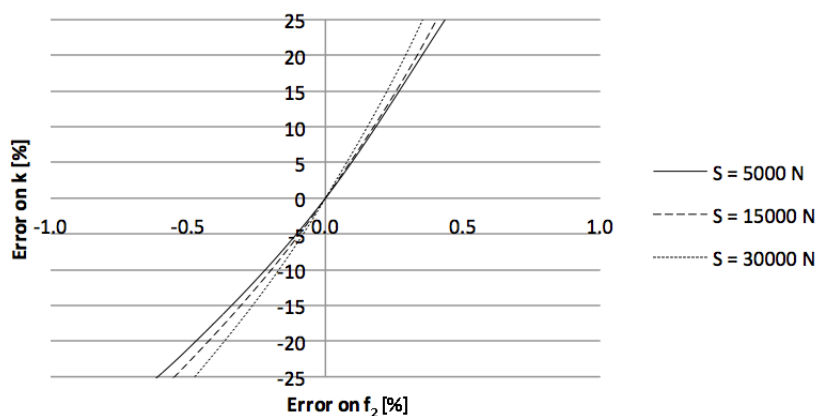


Figure 5-15 Sensitivity of the rotational stiffness  $k$  with regard to the second measured frequency for different load levels

---

### 5.6.3 Discussion

In *Figure 5-4 - Figure 5-9*, it can be seen that the sensitivity of  $S$  with regard to other parameters decreases for high loads. The highest sensitivity can be observed for the measured frequencies, which shows the importance of a high measurement quality. The second highest sensitivity is associated with  $L$ . It is therefore important to choose a reasonable restraint length at the supports, which is not always easy, especially for complicated connections or when the load is transferred over more than one connection part. The next highest sensitivity is related to  $\rho$  and  $E$ , followed by the shear modulus  $G$ . While the density can usually be determined with good accuracy, the estimation of  $E$  and  $G$  is not so straightforward.

The sensitivity of  $k$  is less influenced by the size of the axial load. *Figure 5-14* and *Figure 5-15* show however that its sensitivity with regard to the measured frequencies increases for high axial loads, contrary to the sensitivity of  $S$ . *Figure 5-10 - Figure 5-15* illustrate, that just as for the axial load, the sensitivity of  $k$  is highest for the frequencies, followed by the length  $L$  and finally the material properties  $\rho$ ,  $E$  and  $G$ . In general, one can say that the sensitivity of  $k$  is higher than the one of  $S$ .

---

## 6 Modal analysis

Modal analysis is used to describe a structure's dynamic properties, like resonance frequencies, mode shapes and damping. Those are specific for every system and do not depend on the excitation, but only on the nature of the system and its components.

This chapter gives a short summary of different aspects from theoretical and experimental modal analysis with a main focus on data acquisition and processing.

### 6.1 Theoretical modal analysis (TMA)

In theoretical modal analysis, the modal parameters are determined by solving the differential equation of motion.

Every vibrating system can be described by using the equation of motion

$$\mathbf{M} \cdot \ddot{\mathbf{v}} + \mathbf{C} \cdot \dot{\mathbf{v}} + \mathbf{K} \cdot \mathbf{v} = \mathbf{f}(t) \quad (6.1)$$

where  $\mathbf{M}$  is the mass matrix,  $\mathbf{C}$  the damping matrix and  $\mathbf{K}$  the stiffness matrix.  $\mathbf{f}(t)$  is a vector containing a time-dependant excitation force. The vector  $\mathbf{u}$  describes the displacement of the system over time,  $\dot{\mathbf{v}}$  and  $\ddot{\mathbf{v}}$  the velocity and acceleration, respectively.

If we only consider the free vibration of Eq. (6.1) and neglect the damping

$$\mathbf{M} \cdot \ddot{\mathbf{v}} + \mathbf{K} \cdot \mathbf{v} = 0 \quad (6.2)$$

and chose a solution of the form

$$\mathbf{v} = \boldsymbol{\phi} \cdot \cos(\omega \cdot t - \varphi) \quad (6.3)$$

where  $\boldsymbol{\phi}$  is a vector,  $\omega$  the angular frequency and  $\varphi$  the phase angle, we obtain the following Eigenvalue problem:

$$(-\omega^2 \cdot \mathbf{M} + \mathbf{K}) \cdot \boldsymbol{\phi} = 0 \quad (6.4)$$

For a non-trivial solution, the determinant of Eq. (6.4) must vanish

$$|-\omega^2 \cdot \mathbf{M} + \mathbf{K}| = 0 \quad (6.5)$$

By solving Eq. (6.5) for  $\omega$ , we obtain the angular resonance frequencies  $\omega_i$  of the system. Substitution of each eigenfrequency into Eq. (6.4) then yields the eigenvectors  $\boldsymbol{\phi}_i$  of the system. Each eigenvector  $\boldsymbol{\phi}_i$  represents a deflection over time at a frequency  $\omega_i$  and defines a specific modal shape of the free vibration. The deflection pattern of a structure subjected to any excitation force can in theory be expressed as the linear summation of its modal shapes.

While the solution of the eigenvalue problem is simple for harmonic force functions, it is not adaptable for pulses or other non-harmonic excitations. In this case, the resonance frequencies can be determined using a Fourier transformation.

---

## 6.2 Experimental modal analysis (EMA)

In practice, it is often not possible to use the analytical model because of different uncertainties. In this case the modal parameters can be determined experimentally. According to Dossing (1988) there are two different approaches in experimental modal analysis:

- Signal analysis (operational data)
- System analysis (modal data)

In signal analysis, only the response signal of the system is detected, while in system analysis also the force function is measured. As an example, consider the bridge in *Figure 6-1*. During service, it is subjected to wind forces that can cause undesirable vibrations. These vibrations can be measured and the obtained operational data can be used to study the bridges' behaviour and to see what resonance frequencies are excited during operation and if there is need for adjustments. If one is however interested for example in specific resonance frequencies of the bridge, it is necessary to subject it to a force able to excite these frequencies. In this case the force can also be measured and considered in the modal analysis of the structure. The main difference is that the force has to be taken as given in the first case, while it is actively controlled in the second case.

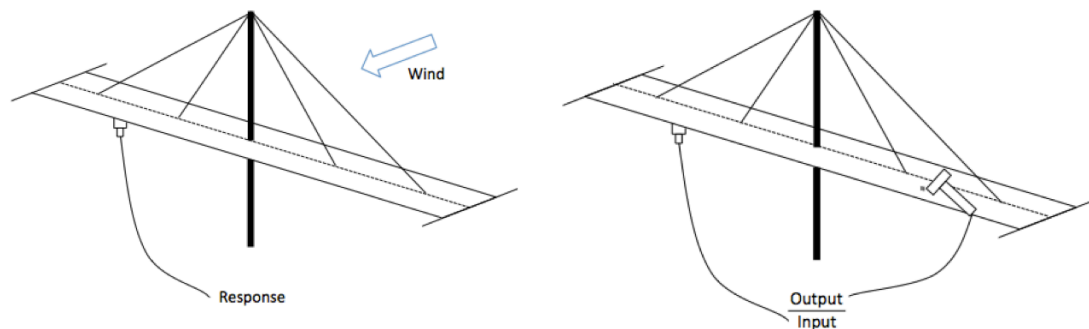


*Figure 6-1* Illustration of a bridge with measurement of operational data (left) and modal data (right)

For a given force function it is possible to detect which resonance frequencies are actually excited by having a look at the frequency response function (FRF). The FRF is defined as the ratio of response function (Output) to the force function (Input):

$$FRF = \frac{Output}{Input} \quad (6.6)$$

The force and response functions can be measured using accelerometers and force transducers. The collected data are time signals. Since however the frequencies are of interest, it is necessary to convert the signals from the time domain into the frequency domain (cf. *Figure 6-2*), which is done by performing a Fast Fourier Transformation (FFT).

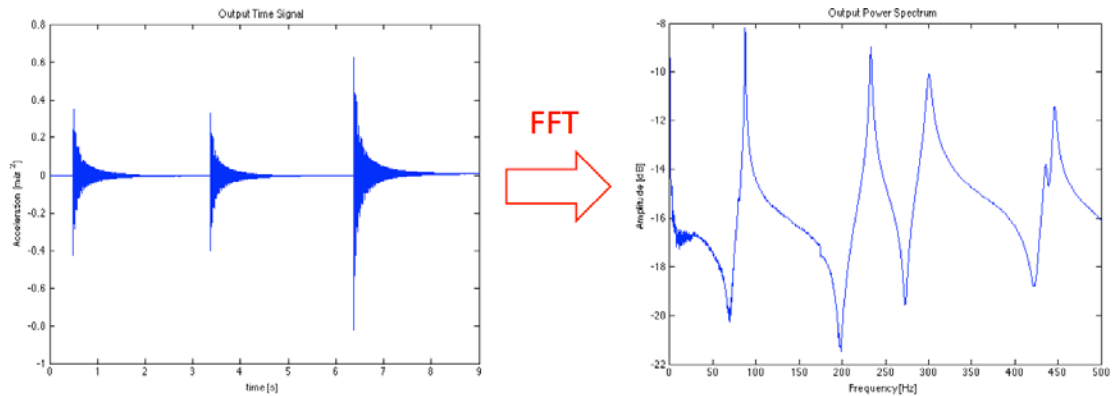


Figure 6-2 Illustration of the Fast Fourier Transformation (FFT) from the time into the frequency domain

### 6.3 Data acquisition

According to Avitabile (2001), there are two ways in system analysis to find the frequencies and mode shapes of a vibrating system (cf. Figure 6-3):

- Measure in one point and excite in several points
- Excite in one point and measure in several points

If only the frequencies are of interest and if the mode shapes can be predicted (or are actually known) since it is a simple structure like a beam with known boundary conditions, it is also possible to determine the according frequencies by only making one measurement and one excitation in the same point (drive point measurement). When doing this it is however very important that the point being measured is not a node for any of the desired mode shapes, since in this case the mode and its corresponding frequency are not being excited.

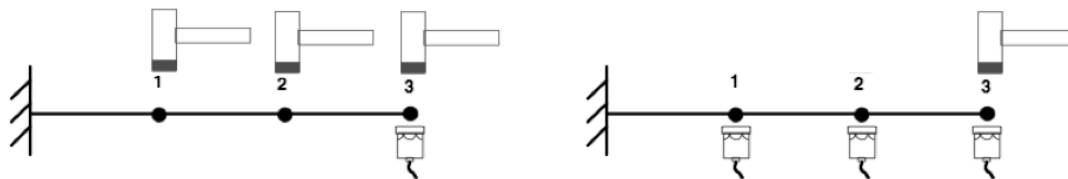
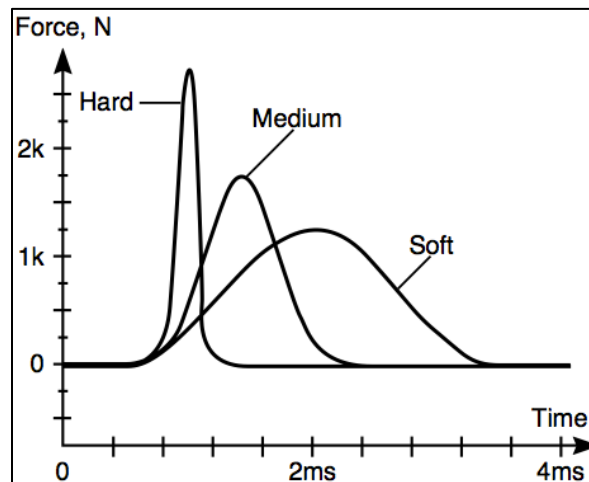


Figure 6-3 Two different approaches for the determination of resonance frequencies: measuring in one point and exciting in several points (left) or measuring in several points and exciting in one point (right), Avitabile (2001)

Accelerometers can be used for the measurement of the response signal. According to Dossing (1988), the main advantages are their low weight, wide frequency range and the simple mounting using either magnets, steel studs or bee-wax. The system can be excited either using a shaker or a hammer equipped with a piezoelectric transducer. While shakers are suitable to excite a system over longer time periods, hammers are used for short impulses. The hammers come in different sizes and tips, depending on what frequency range is of interest. The essential parameters are the weight of the hammer and the stiffness of the tips. The heavier a hammer is, the lower are the excited frequencies. The stiffer the tip, the higher are the excited frequencies. Soft tips (rubber, plastic) can therefore excite lower frequencies while hard tips (steel) are

better to excite higher frequencies. It is important to choose an adequate hammer and tips so that the energy of the hammer blow excites the desired frequency range and a good response is obtained. *Figure 6-4* shows impulse shapes for different hammer tips.



*Figure 6-4* Impulse shape for different hammer tips, Kjaer (2012)

When using accelerometers and additional equipment to acquire the modal data of a structure, it is also important that their weight is small compared to the one of the structure and its components. If this is not the case, they have to be considered as additional masses that change the mass properties of the system. The same applies for suspensions that can have a stiffening effect to the structure, which means a change in the stiffness properties. Furthermore it has to be investigated if the damping has to be taken into account to determine the frequencies or if it can be neglected.

The results acquired by accelerometers and force transducers represent timeline data that need to be further processed to obtain the eigenfrequencies. The advantage of measuring the input function is that errors originating for example from noise can be reduced.

## 6.4 Data processing

The time data acquired during measurements can be transformed to the frequency domain by performing a FFT.

Steps of the FFT according to *Figure 6-5*:

1. Analog signals must be filtered to remove high frequency signals that might be detected during testing without having any connection to the actual test (background noise)
2. The analog signals are approximated by conversion into digital signals
3. Weighting functions called *Windows* are used to reduce leakage (cf. below)
4. The actual FFT is performed to create linear spectra of the input and output data, transfer from time domain to frequency domain
5. The input, output and cross power spectra are computed.
6. These functions are then averaged and used to compute the FRF and the coherence function. While the FRF can be used to read out the resonance frequencies, the coherence function can be used for quality assessment of the data.

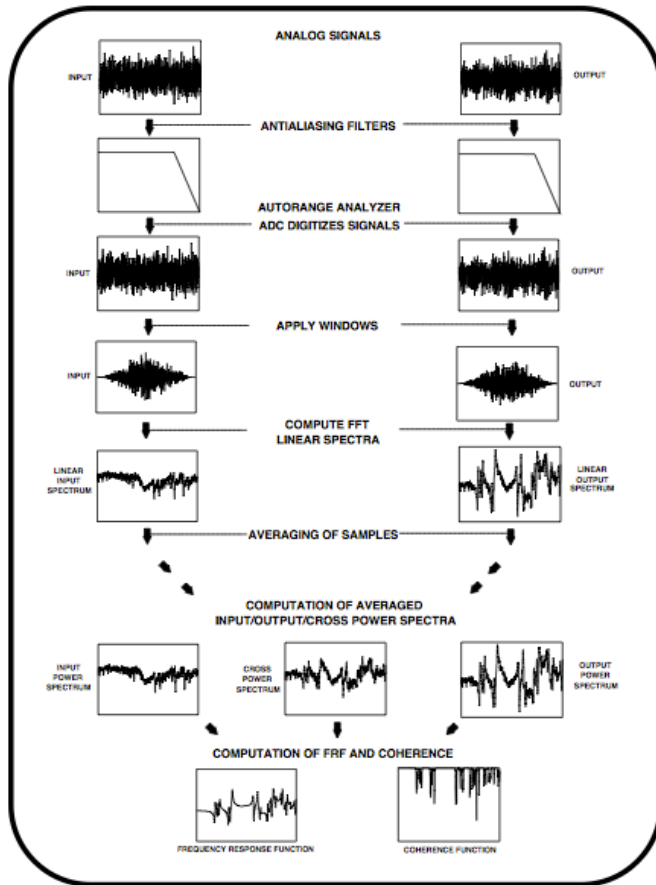


Figure 6-5 Illustration of the different steps of an FFT Analyser, Avitabile (2001)

Figure 6-6 shows an example of a FRF and the according coherence function. Peaks in the coherence function at a resonance frequency indicate a poor quality of the measurement. In this case, the quality of the results decreases for frequencies higher than approximately 4000 Hz. This is the maximum range of the hammer tip in use.

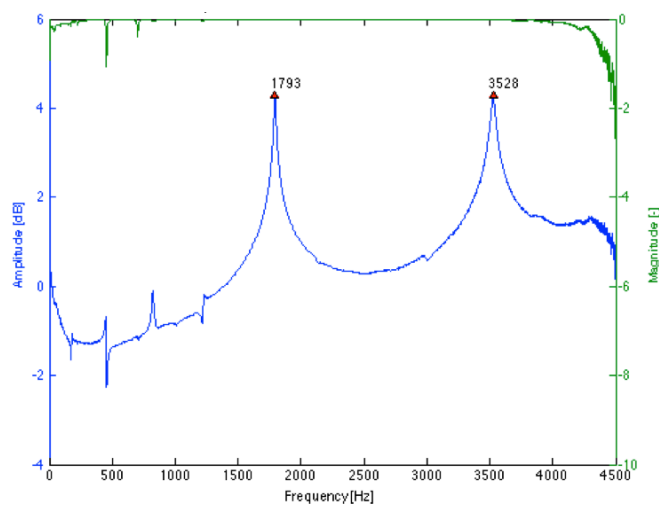
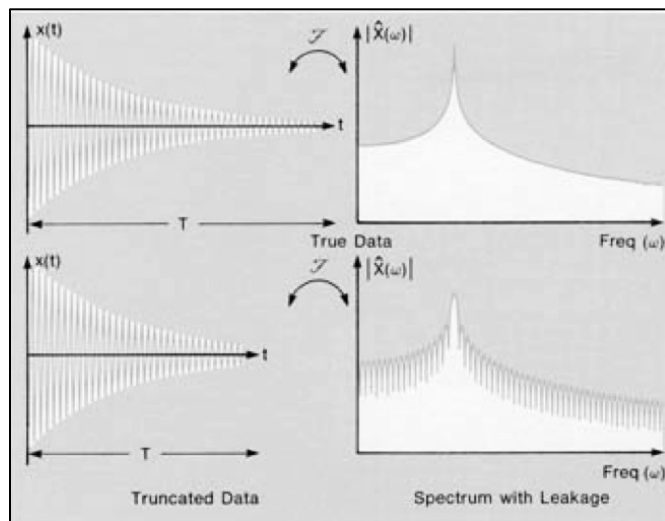


Figure 6-6 Example of a frequency response function and the according coherence function

Leakage is a signal processing error causing the distortion of data (cf. *Figure 6-7*). It is one of the most serious errors when processing data and has to be treated with special care. It occurs during the FFT transformation, which in theory requires a representation of data for all times or at least a periodic repetition. In practice, this is of course not possible since every signal has a finite observation period. There are however ways to reduce the leakage effect already during the data acquisition phase. On the one hand, the observation period should be chosen long enough so that the signal is not truncated before it has decayed to zero. On the other hand, it should not be longer than necessary since during the additional time only background noise can be recorded. In both cases, the result can be a blurry power spectrum with too low and unclear peaks.



*Figure 6-7* Illustration of the effect of truncation during data acquisition on result for the frequency response function, Dossing (1988)

After data acquisition, it is possible to further increase the resolution by applying the already mentioned window functions. While there are different window functions, they all have more or less the same effect on the signal, by improving its periodicity and forcing it to zero. A popular example for a window is the Hanning function, which is good to improve the periodicity of the sample. It is bell-shaped and heavily reduces the beginning and end of the sample function to zero. Another example is the transient window that can for example be used to remove noise following an impact pulse. Exponential windows can in addition be used to process truncated data. It should be noted however that windows cause some data distortion themselves and should be avoided, if possible. They have a negative influence on the accuracy of peak amplitudes and the damping ratios. If only the frequencies are of interest, these effects can however be considered of secondary importance and are therefore acceptable.

---

## 7 Determination of material properties

### 7.1 Specimen dimensions and properties

The material for the specimen comes from previous experiments on glulam beams from Norway spruce (*Picea abies*). These beams were first sorted to make sure only intact timber was used to produce the new specimens. Further requirements were to minimize the amount of knots, finger joints and other natural defects like resin pockets. A total of 32 beams, each consisting of two lamellas with the dimensions  $42 \times 45 \text{ mm}^2$ , were then cut out to a length of 1.5 m from the original glulam beams. The thereby obtained pieces were then evenly planed to the following final measurements of the samples:  $L \times H \times B = 1500 \times 75 \times 35 \text{ mm}^3$ . *Figure 7-1* shows one of the final specimens.

The choice of the sample size is based on the following conditions:

- The tensile machine limited the cross-sectional dimensions to a size smaller than  $77 \times 45 \text{ mm}^2$ , which is why a height of 75 mm was chosen.
- The height-to-width ratio had to be high enough to facilitate the measurement of torsional vibrations and to be able to distinguish the frequencies from the different vibration modes. The torsional frequencies are important to determine the shear modulus that is needed to take into account the effect of shear deformation on the bending modes. Also the proportions had to be realistic with regard to real-life constructions.
- The length-to-width ratio was chosen high enough to make sure that frequency changes for different stress levels are in a detectable range.

All these considerations yielded a bar-like timber beam of realistic proportions, such as they can be found for instance in roof structures, bridges or supports.

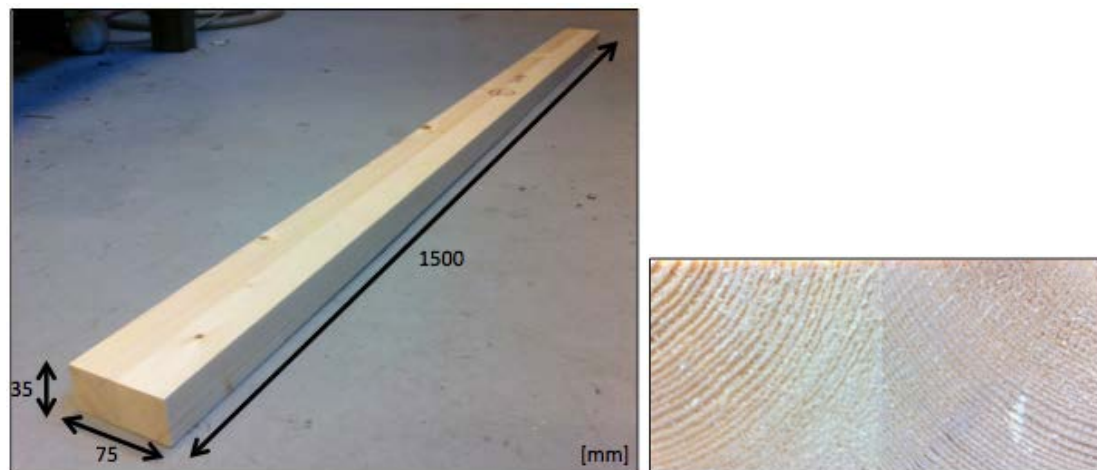


*Figure 7-1* Illustration of timber specimen with body dimensions (left) and the according cross section composed of two lamellas (right)

The original glulam beams were graded CE L40c according to European standards. This class is constituted of a combination of lamellas of different strength, the weaker ones situated on the inside, the stronger forming the outside layers (at least two strong lamellas per side). The specimens were cut out from the outer lamellas and can thus be considered as part of the higher quality timber. The mean values for the material properties of L40c are listed in *Table 7-1*.

Table 7-1 Material properties of the timber specimens according to SIA (2003)

Material properties of L40c		
Mean modulus of elasticity parallel to the grain	$E_{0,\text{mean}}$	13000 MPa
Mean modulus of shear	$G_{\text{mean}}$	760 MPa
Tensile strength parallel to the grain	$f_{t,0,k}$	17.6 MPa
Density	$\rho_k$	400 kg/m <sup>3</sup>

The specimens were packed in plastic after being cut. Over the whole testing period, they were kept in a room with an average temperature of 20°C and a relative humidity of ranging from 30 to 40%. The moisture content of each specimen was measured in three places. The registered average moisture contents are shown in Appendix B. The mean moisture content of all the specimens was determined to 12.5%.

The actual densities for each sample were determined by weighing them. The results are also shown in Appendix B. The mean value of 488.6 kg/m<sup>3</sup> is well above the one given in Table 7-1. The reason could be that only higher quality lamellas were cut out of the initial beams, which in general have higher densities.

The tests carried out on the inhomogeneous timber specimen were also conducted on an aluminium bar, representing a homogeneous reference. The comparison of the final results should eventually allow identifying the material-related deviations. The aluminium bar had the dimensions 1495×50×10 mm<sup>3</sup>. The general material properties of industrial aluminium are presented in Table 7-2 and the bar itself is illustrated in Figure 7-2.

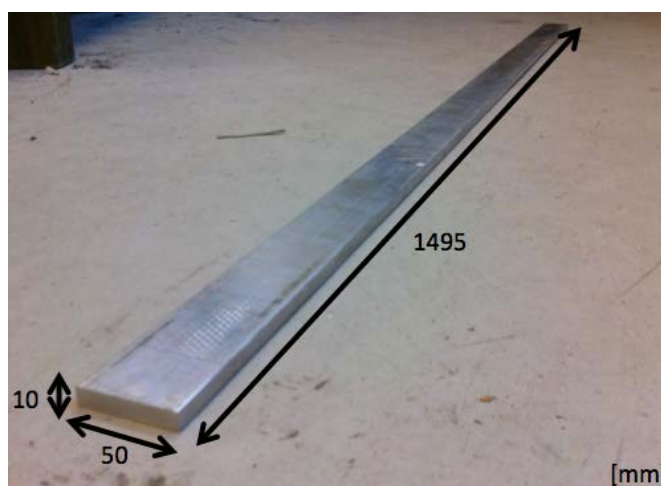


Figure 7-2 Illustration of reference aluminium specimen with body dimension

Table 7-2 Material properties of the reference aluminium specimen according to Wikipedia.org (2012)

Material properties of Aluminium		
Modulus of elasticity	E	70000 MPa
Modulus of shear	G	26000 MPa
Tensile strength	$f_u$	45 MPa
Density	$\rho_k$	2700 kg/m <sup>3</sup>

## 7.2 Test equipment and data processing

For all the dynamic tests carried out throughout this study, the same equipment was used. The beams were tapped with an instrumented hammer shown in *Figure 7-3 (a)*. It was equipped with a piezoelectric force transducer PCB 208B05 that allowed measuring the impulse function. These hammers come with different exchangeable tips, depending on the desired frequency range. The response signal from the beams was recorded using uniaxial accelerometers PCB 303A02, cf. *Figure 7-3 (b)*. Their weight of 2.8 g was small enough to exclude effects on the beam vibration. The accelerometers were attached to the beams with bee-wax. Hammer and accelerometers were connected over PCB 478A01 power suppliers to an HP 8-channel system linked to the computer.

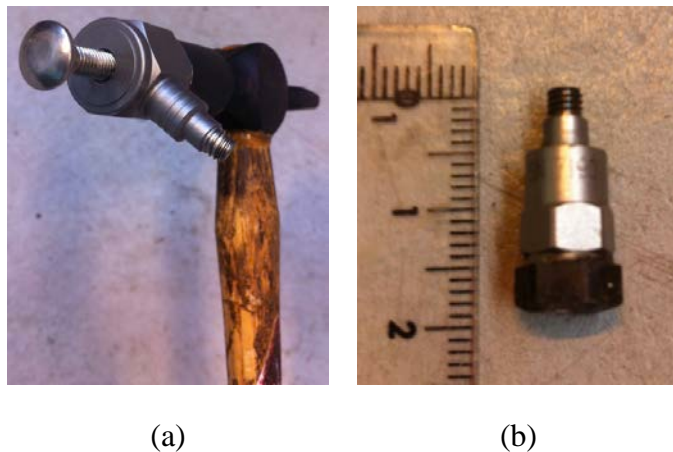


Figure 7-3 Impact hammer equipped with piezoelectric force transducer and steel tip (a) and uniaxial accelerometer (b)

The software DAC Express from VTI Instruments was used for the acquisition of the raw signal data. The actual data processing was carried out using the software Matlab from the company MathWorks to transform the signal data from the time into the frequency domain by means of a Fast Fourier Transformation (FFT). The result of this transformation is the Frequency Response Function (FRF) from which the resonance frequencies of a beam can be extracted.

### 7.3 Determination of static E- and G-modulus

Four-point bending tests according to CEN/TC (2007) were carried out to determine the static E-modulus of each specimen. The beams were tested with two sets of weights for which the deflection at mid-point was measured. Furthermore, the deflections over the supports were measured and subtracted from the mid-deflection to take into account local compressions. The E-moduli were then calculated using (7.1):

$$E = \frac{L^3(K_2 - K_1)}{bh^3(w_2 - w_1)} \left[ \left( \frac{3a}{4L} \right) - \left( \frac{a}{L} \right)^3 \right] \quad (7.1)$$

where  $h$  and  $b$  are the cross-sectional dimensions,  $L$  is the span,  $a$  is the distance between the loading and the nearest support,  $K$  are the total loads and  $w$  the according deflections (cf. *Figure 7-4*). The test setup is shown in *Figure 7-5*.

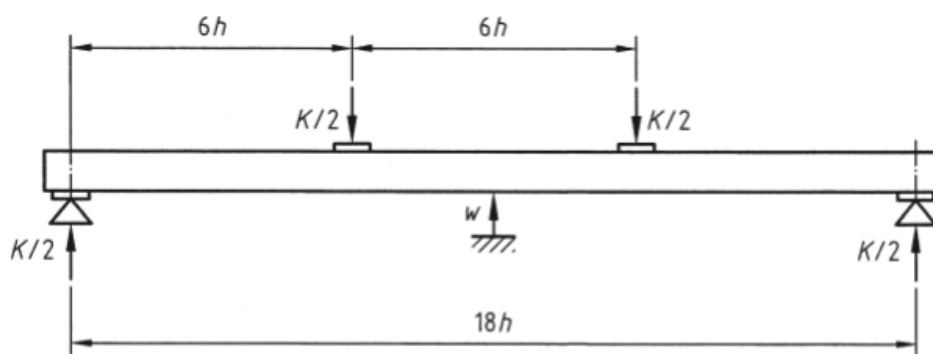


*Figure 7-4* Illustration of test setup for the four-point bending test according to CEN/TC (2007)



*Figure 7-5* Test setup for the determination of the static E-modulus according to CEN/TC (2007)

The test results are shown in *Table 7-3*.

Table 7-3 Measured deflections and computed E-moduli from the four-point bending test

Beam N°	Deflection 1				Deflection 2				Load 1 [N]	Load 2 [N]	E [MPa]
	Supp 1 [mm]	Mid [mm]	Supp 2 [mm]	Tot [mm]	Supp 1 [mm]	Mid [mm]	Supp 2 [mm]	Tot [mm]			
1	0.366	1.295	0.321	0.952	0.408	1.852	0.444	1.426	412.0	606.3	14526
2	0.235	1.372	0.340	1.085	0.272	1.963	0.450	1.602	412.0	606.3	13319
3	0.141	1.467	0.335	1.229	0.175	2.106	0.429	1.804	412.0	606.3	11987
4	0.138	1.393	0.321	1.164	0.172	2.011	0.411	1.720	412.0	606.3	12397
5	0.181	1.359	0.369	1.084	0.216	1.927	0.482	1.578	412.0	606.3	13953
6	0.290	1.364	0.360	1.039	0.359	1.949	0.466	1.537	412.0	606.3	13855
7	0.217	1.495	0.413	1.180	0.259	2.141	0.520	1.752	412.0	606.3	12061
8	0.217	1.448	0.370	1.155	0.278	2.069	0.473	1.694	412.0	606.3	12788
9	0.276	1.401	0.345	1.091	0.320	1.991	0.496	1.583	412.0	606.3	13995
10	0.163	1.323	0.363	1.060	0.199	1.893	0.467	1.560	412.0	606.3	13785
11	0.230	1.261	0.310	0.991	0.272	1.812	0.399	1.477	412.0	606.3	14197
12	0.192	1.342	0.332	1.080	0.234	1.911	0.432	1.578	412.0	606.3	13841
13	0.242	1.398	0.374	1.090	0.285	1.999	0.495	1.609	412.0	606.3	13281
14	0.226	1.400	0.362	1.106	0.268	2.006	0.482	1.631	412.0	606.3	13129
15	0.206	1.385	0.348	1.108	0.247	1.976	0.458	1.624	412.0	606.3	13371
16	0.248	1.381	0.401	1.057	0.292	1.966	0.546	1.547	412.0	606.3	14052
17	0.398	1.687	0.163	1.407	0.437	2.413	0.356	2.017	412.0	606.3	11300
18	0.149	1.375	0.324	1.139	0.188	1.979	0.418	1.676	412.0	606.3	12824
19	0.185	1.814	0.386	1.529	0.255	2.569	0.488	2.198	412.0	606.3	10303
20	0.303	1.563	0.397	1.213	0.344	2.245	0.547	1.800	412.0	606.3	11752
21	0.193	1.477	0.326	1.218	0.270	2.115	0.425	1.768	412.0	606.3	12532
22	0.229	1.408	0.357	1.115	0.278	2.019	0.470	1.645	412.0	606.3	13005
23	0.175	1.433	0.364	1.164	0.214	2.068	0.473	1.725	412.0	606.3	12286
24	0.128	1.400	0.359	1.157	0.171	2.017	0.462	1.701	412.0	606.3	12670
25	0.168	1.321	0.341	1.067	0.210	1.902	0.443	1.576	412.0	606.3	13542
26	0.226	1.481	0.361	1.188	0.288	2.121	0.462	1.746	412.0	606.3	12341
27	0.167	1.689	0.315	1.448	0.218	2.431	0.416	2.114	412.0	606.3	10349
28	0.217	1.423	0.346	1.142	0.260	2.038	0.453	1.682	412.0	606.3	12764
29	0.179	1.370	0.289	1.136	0.219	1.985	0.407	1.672	412.0	606.3	12860
30	0.191	1.696	0.428	1.387	0.220	2.416	0.551	2.031	412.0	606.3	10703
31	0.217	1.528	0.363	1.238	0.268	2.193	0.479	1.820	412.0	606.3	11853
32	0.145	1.548	0.346	1.303	0.178	2.220	0.441	1.911	412.0	606.3	11337
									Mean value		12717
									Std. dev.		1117

The mean value of 12717 MPa shows good accordance with the mean E-modulus given in Table 7-1. The slightly lower values probably result from the fact that only two lamellas are left from the original beam, which increases the negative influence of local defects on material properties. Figure 7-6 shows a good correlation between E-moduli and densities of the samples. In general, it can be said that material properties improve with an increasing density. In this case, outliers from this rule result from extreme concentrations of knots and other defects.

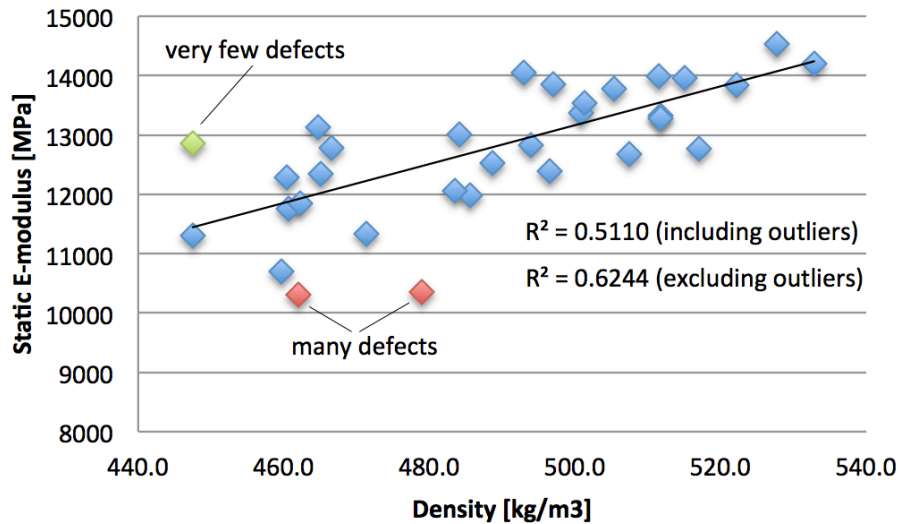


Figure 7-6 Correlation between the density and the static E-modulus for the timber specimens

## 7.4 Determination of longitudinal E-modulus

The longitudinal E-moduli were determined through dynamic tests on the beams under free boundary conditions. For this purpose, the beams were supported on foam pieces as shown in Figure 7-7. The beams were then tapped five times in one end with the instrumented hammer and the vibration was measured over a time period of 7 seconds using the uniaxial accelerometer situated on the other end. For this test, a steel tip was chosen that is suitable to excite higher frequencies.



Figure 7-7 Test setup for the determination of the dynamic longitudinal E-modulus

The results for each experiment were the timelines for the accelerometer and the force transducer, upon which a Fast Fourier Transformation (FFT) was then carried out via the software Matlab. The results of this transformation were the input and output power spectra, the Coherence Function and finally the Frequency Response Function (FRF), cf. Figure 7-8.

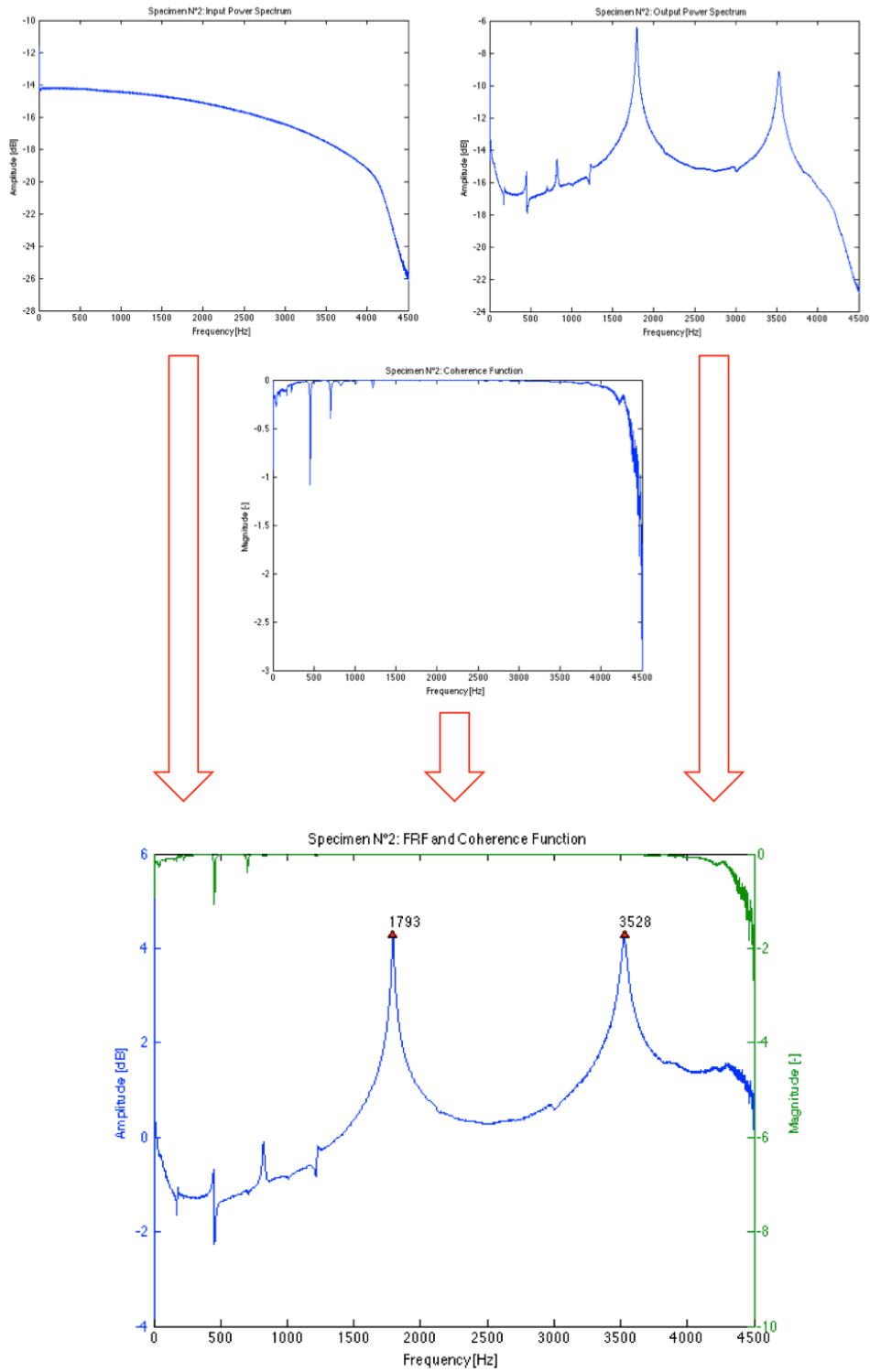


Figure 7-8 Frequency plots and coherence function resulting from the data processing of the different signals recorded during the longitudinal tests

It can be seen that the input power spectrum shows a break at around 4.2 kHz. The coherence function shows also high fluctuations from this point on. This is the maximum frequency range for the chosen hammer-tip combination. The first two longitudinal frequencies could be read out from the FRF and subsequently be used to calculate the longitudinal E-modulus with help of the following formula derived from (4.33):

$$E_L = \frac{4f^2 l^2 \rho}{i^2} \quad (7.2)$$

The E-moduli were calculated using either the first or the second frequencies. Furthermore the mean value was computed (cf. *Table 7-4*).

*Table 7-4 Measured frequencies and computed E-moduli from the longitudinal tests*

Beam N°	f <sub>1L</sub>	f <sub>2L</sub>	E <sub>1L</sub>	E <sub>2L</sub>	E <sub>mL</sub>
[-]	[Hz]	[Hz]	[MPa]	[MPa]	[MPa]
1	1891	3746	16983	16661	16822
2	1793	3528	14805	14330	14568
3	1767	3547	13646	13746	13696
4	1788	3579	14286	14310	14298
5	1788	3555	14818	14644	14731
6	1832	3641	15012	14825	14919
7	1786	3574	13883	13899	13891
8	1779	3539	13288	13146	13217
9	1836	3613	15518	15023	15271
10	1858	3668	15703	15299	15501
11	1793	3573	15416	15304	15360
12	1814	3603	15465	15253	15359
13	1824	3615	15322	15046	15184
14	1846	3707	14255	14371	14313
15	1871	3725	15778	15635	15707
16	1882	3729	15716	15425	15571
17	1749	3436	12320	11887	12104
18	1842	3666	15085	14938	15012
19	1750	3544	12734	13056	12895
20	1776	3536	13078	12961	13020
21	1756	3531	13560	13707	13634
22	1781	3546	13820	13696	13758
23	1789	3603	13262	13448	13355
24	1831	3676	15310	15427	15369
25	1833	3632	15159	14879	15019
26	1784	3534	13319	13067	13193
27	1698	3388	12429	12371	12400
28	1742	3511	14123	14342	14233
29	1902	3778	14570	14371	14471
30	1688	3386	11789	11859	11824
31	1826	3600	13870	13478	13674
32	1786	3578	13533	13579	13556
		Mean value	14308	14187	14247
		Std. dev.	1203	1128	1161
Aluminium	1710	3421	69106	69146	69126

The best correlation with the static E-moduli from the bending tests could be obtained using only the first frequency. The mean value was found to be 14308 MPa, which means that the longitudinal E-moduli are on average 12.5% higher than the static ones. This is in accordance with previous studies Ilic (2001).

A summary of the correlation as well as the FRF plots can be found in Appendix B.

---

## 7.5 Determination of transversal E- and G-modulus

Transversal vibration tests were carried out to determine the E- and G-moduli of the beams. The determination of the G-moduli was necessary to include effects of shear deformations that become more important for higher modes. Just as for the longitudinal tests, the beams were tested under free boundary conditions. The setup is however different from the one in Chapter 7.4. The free-free conditions were achieved by hanging the beams vertically on soft rubber strings. These elastic strings are necessary to reduce the overall stiffness of the system to get as close as possible to a state of the free boundary conditions. The beams were tested in a vertical position to minimize the influence of the supports on the transversal waves. The support is illustrated in *Figure 7-9 (a)*.

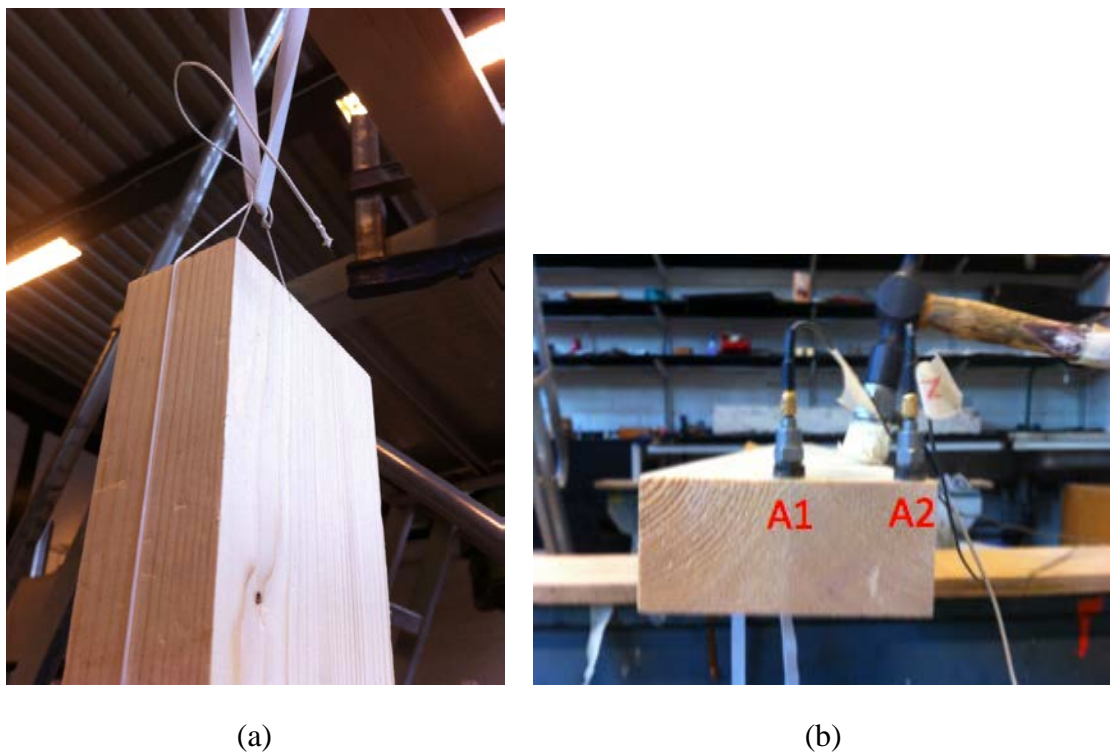


*Figure 7-9* Support conditions for the determination of the transversal E-modulus (a) and the according test setup (b)

The equipment used for the tests consisted of two uniaxial accelerometers attached to the beam with bee-wax. For a free-free beam, the ends are antinodes that allow the measurement of frequencies for different vibration modes. This is why the accelerometers were placed on the end of the beam in two different spots according to *Figure 7-9 (b)*. The specimens were excited five times with the instrumented hammer, equipped this time with a plastic tip, since the expected frequencies were in a lower range than for the longitudinal tests. The specimens had to be tapped on the edge to also excite torsional frequencies. The response signals were recorded for 15s and then transmitted to the computer where they could finally be processed to calculate the FRFs (cf. *Figure 7-10*).

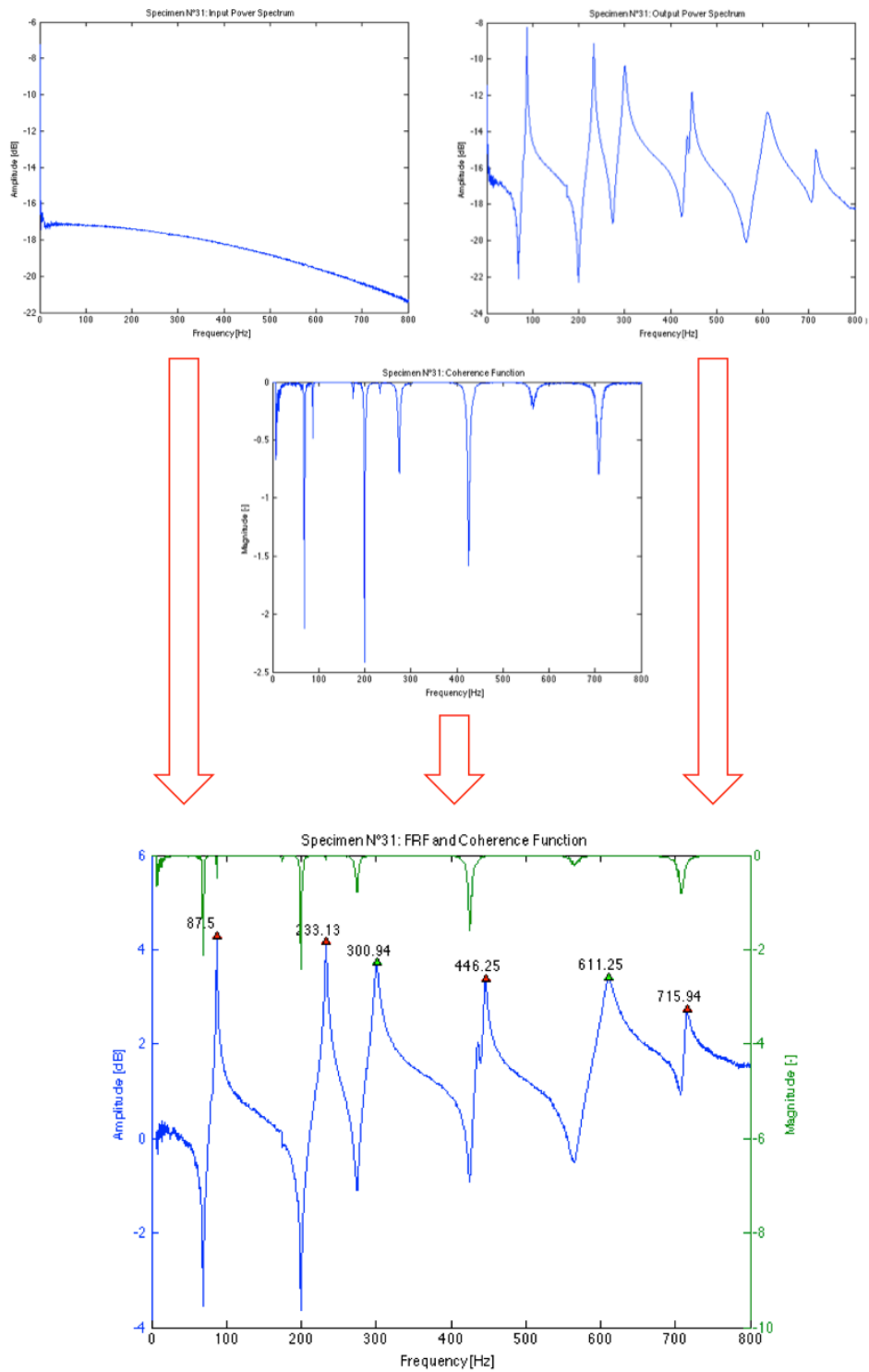
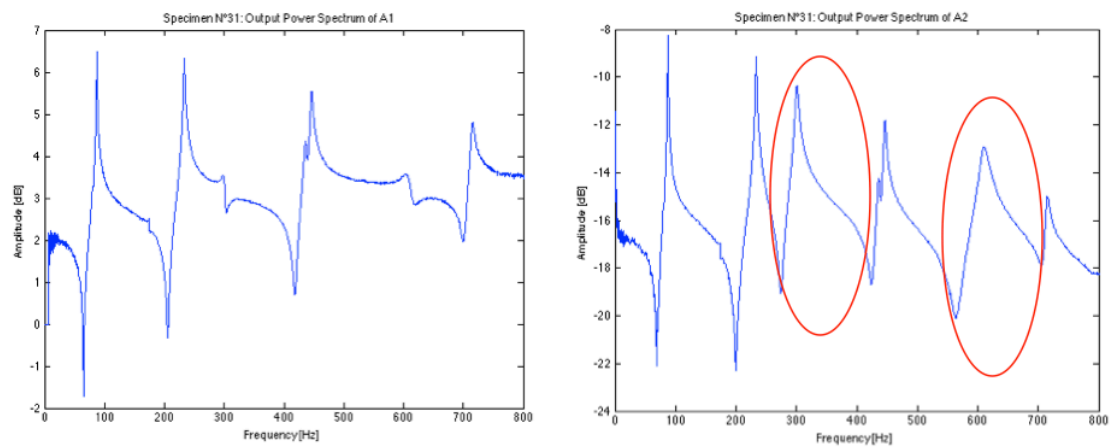


Figure 7-10 Frequency plots and coherence function resulting from the data processing of the different signals recorded during the transversal tests

Since A1 was placed in the neutral axis of the beam, it could only detect vibrations corresponding to bending modes. A2 however was placed on the edge and would therefore also record torsional vibrations. By comparing the FRFs of A1 and A2 it was then possible to distinguish bending and torsional frequencies (cf. *Figure 7-11*).



*Figure 7-11* Comparison between the frequency response function from the accelerometer situated in the neutral axis of the beam (left) and the one situated on the edge of the beam (right)

The G-moduli were calculated using Eq (7.3) derived form of Eq (4.46)

$$G_F = \frac{4f^2 l^2 \rho I_p}{i^2 K_t} \quad (7.3)$$

with the either the first or second frequency. Also the mean value of both G-moduli is presented (cf. *Table 7-5*).

Table 7-5 Measured torsional frequencies and computed G-moduli from the transversal tests

Beam N°	$f_{1t}$	$f_{2t}$	$G_1$	$G_2$	$G_m$
[-]	[Hz]	[Hz]	[MPa]	[MPa]	[MPa]
1	289.8	587.0	789	809	799
2	309.7	632.6	873	911	892
3	303.9	606.6	798	795	797
4	305.0	617.1	822	841	832
5	304.3	615.9	848	869	859
6	300.1	610.4	796	824	810
7	304.3	614.8	797	813	805
8	301.3	610.1	753	772	763
9	296.9	601.5	802	823	813
10	303.8	611.0	830	839	835
11	297.1	598.4	837	849	843
12	301.4	610.0	844	864	854
13	299.0	602.2	814	825	820
14	296.3	594.7	726	731	729
15	292.0	592.1	760	781	771
16	290.0	587.5	738	757	748
17	322.9	652.9	830	848	839
18	293.9	588.5	759	761	760
19	267.2	587.9	587	710	649
20	287.9	584.4	679	700	690
21	303.9	616.1	803	825	814
22	310.2	628.6	829	851	840
23	301.7	600.7	746	739	743
24	298.1	605.7	802	828	815
25	310.2	626.5	858	875	867
26	306.5	621.3	777	798	788
27	319.4	648.8	869	897	883
28	300.2	612.0	829	861	845
29	288.4	586.3	662	684	673
30	332.9	666.0	906	907	907
31	300.9	611.3	745	768	757
32	307.9	621.6	795	810	803
		Mean value	791	811	801
		Std. dev.	65	59	61
Aluminium	374.7	/	24676	/	/

The transversal E-moduli were calculated using Timoshenko theory as well as Euler theory for comparison. Since no simple expression is available for a free-free beam, the self-developed Matlab code in Appendix A was used for the calculations. Again, the E-moduli were calculated for different frequencies, as shown in *Table 7-6*.

Table 7-6 Measured transversal frequencies and computed E-moduli from the transversal tests

Beam N°				Euler				Timoshenko				Ratio E <sub>1b</sub>	Ratio E <sub>2b</sub>	Ratio E <sub>3b</sub>
	f <sub>1b</sub>	f <sub>2b</sub>	f <sub>3b</sub>	E <sub>1b</sub>	E <sub>2b</sub>	E <sub>3b</sub>	E <sub>1b</sub>	E <sub>2b</sub>	E <sub>3b</sub>	E <sub>mb</sub>				
[-]	[Hz]	[Hz]	[Hz]	[MPa]	[-]	[-]	[-]							
1	89.5	240.5	455.4	16533	15711	14658	16805	16616	16415	16612	0.98	0.95	0.89	
2	85.4	226.6	438.7	14596	13524	13190	14794	14139	14472	14468	0.99	0.96	0.91	
3	84.0	226.7	442.0	13401	12846	12706	13584	13451	14008	13681	0.99	0.96	0.91	
4	84.4	229.4	441.0	13833	13449	12933	14022	14092	14242	14119	0.99	0.95	0.91	
5	84.6	227.1	437.0	14416	13672	13172	14615	14316	14489	14473	0.99	0.96	0.91	
6	87.0	234.8	452.7	14713	14104	13642	14931	14830	15147	14969	0.99	0.95	0.90	
7	84.5	227.3	435.5	13505	12861	12284	13691	13468	13503	13554	0.99	0.95	0.91	
8	84.3	225.9	436.5	12966	12254	11905	13147	12836	13116	13033	0.99	0.95	0.91	
9	86.5	232.5	439.1	14969	14232	13209	15192	14967	14609	14923	0.99	0.95	0.90	
10	87.7	237.7	455.2	15204	14699	14026	15427	15455	15552	15478	0.99	0.95	0.90	
11	84.7	229.7	433.0	14950	14470	13379	15165	15198	14756	15040	0.99	0.95	0.91	
12	85.6	231.6	437.2	14966	14418	13369	15179	15135	14731	15015	0.99	0.95	0.91	
13	84.3	229.1	429.4	14223	13824	12637	14423	14509	13899	14277	0.99	0.95	0.91	
14	85.7	234.7	441.4	13352	13179	12129	13548	13873	13433	13618	0.99	0.95	0.90	
15	87.4	234.1	450.3	14962	14127	13601	15196	14889	15170	15085	0.98	0.95	0.90	
16	87.5	235.9	449.3	14763	14122	13329	14997	14904	14882	14928	0.98	0.95	0.90	
17	82.1	218.7	424.5	11797	11017	10800	11937	11452	11708	11699	0.99	0.96	0.92	
18	85.7	234.3	439.6	14191	13959	12786	14402	14704	14173	14426	0.99	0.95	0.90	
19	82.2	224.1	433.1	12209	11943	11607	12409	12645	13091	12715	0.98	0.94	0.89	
20	83.8	225.2	420.9	12654	12026	10931	12842	12646	12064	12517	0.99	0.95	0.91	
21	82.0	222.0	423.1	12850	12395	11715	13018	12956	12815	12930	0.99	0.96	0.91	
22	83.4	222.7	430.5	13170	12358	12016	13341	12900	13138	13126	0.99	0.96	0.91	
23	83.9	226.8	438.1	12676	12190	11835	12850	12772	13043	12888	0.99	0.95	0.91	
24	85.6	229.3	445.8	14541	13732	13506	14753	14417	14970	14713	0.99	0.95	0.90	
25	86.6	232.1	441.9	14704	13900	13111	14908	14559	14400	14622	0.99	0.95	0.91	
26	82.7	223.3	433.2	12439	11935	11688	12601	12473	12819	12631	0.99	0.96	0.91	
27	79.4	216.5	426.4	11811	11557	11664	11946	12013	12674	12211	0.99	0.96	0.92	
28	80.8	223.4	427.9	13204	13284	12681	13376	13907	13929	13737	0.99	0.96	0.91	
29	89.1	240.7	457.7	13895	13345	12556	14124	14123	14094	14114	0.98	0.94	0.89	
30	78.9	219.2	422.5	11193	11369	10991	11311	11796	11853	11653	0.99	0.96	0.93	
31	87.4	233.2	446.2	13809	12938	12325	14014	13592	13637	13748	0.99	0.95	0.90	
32	84.2	226.8	437.2	13071	12481	12068	13246	13055	13247	13183	0.99	0.96	0.91	
			Mean value	13736	13185	12577	13931	13834	13877	13881	0.99	0.95	0.91	
			Std. dev.	1195	1090	925	1223	1185	1094	1152				
Aluminium	23.2	63.9	125.2	67267	67158	67084	67289	67223	67211	67241	1.00	1.00	1.00	

The difference between Euler and Timoshenko theory becomes more important with higher modes. Nevertheless, the difference is already very significant for the second and third mode. The best correlation with the static E-moduli was obtained using only the first frequency. The mean value was calculated to 13931 MPa, 9.5% higher than the static one.

Appendix B presents a summary of the correlation and FRF plots.

## 7.6 Summary of results

In conclusion, one can say that the first frequencies are most suitable for the estimation of material properties since they are least influenced by material defects and hence can be measured with higher precision. The negative effect of defects increases with the number of modes, which excludes the use of higher frequencies for error minimisation.

Table 7-7 Summary of the determined material properties for each specimen

Beam N°	$\rho_k$	$E_{static}$	$E_{1L}$	$E_{1b}$	$G_{1b}$
[-]	[kg/m <sup>3</sup> ]	[MPa]	[MPa]	[MPa]	[MPa]
1	527.7	14526	16983	16760	788
2	511.7	13319	14805	14763	873
3	485.6	11987	13646	13604	797
4	496.5	12397	14286	14015	822
5	515.0	13953	14818	14646	849
6	497.0	13855	15012	14889	796
7	483.6	12061	13883	13753	797
8	466.5	12788	13288	13172	753
9	511.5	13995	15518	15213	802
10	505.4	13785	15703	15466	830
11	532.8	14197	15416	15161	837
12	522.2	13841	15465	15190	843
13	511.7	13281	15322	14451	814
14	464.8	13129	14255	13526	726
15	500.8	13371	15778	15231	761
16	493.0	14052	15716	14997	738
17	447.5	11300	12320	11964	831
18	494.0	12824	15085	14379	758
19	462.0	10303	12734	12406	587
20	460.7	11752	13078	12827	679
21	488.6	12532	13560	12979	802
22	484.1	13005	13820	13354	828
23	460.4	12286	13262	12804	745
24	507.4	12670	15310	14763	802
25	501.3	13542	15159	14894	858
26	465.0	12341	13319	12589	778
27	479.0	10349	12429	11940	869
28	517.1	12764	14123	13369	829
29	447.5	12860	14570	14112	662
30	459.7	10703	11789	11314	906
31	462.2	11853	13870	14046	745
32	471.4	11337	13533	13304	795
Mean value	488.6	12717	14308	13934	791
Std. dev.	24.2	1117	1203	1222	65

Table 7-7 summarizes the results from the material properties estimation. As already mentioned, the dynamic E-moduli are higher than the static ones. Also, the mean of the estimated G-moduli is higher than the one in Table 7-1. This difference is mainly due to creeping that occurs during static testing. While the dynamic tests are carried out over a short time period of just a few seconds, the static tests last several minutes during which the timber starts to creep, resulting in the lower values for the static E-modulus.

Nevertheless, good correlations could be observed between the different E-moduli (cf. Figure 7-12 - Figure 7-14). The correlation between longitudinal and translational E-moduli is even nearly perfect.

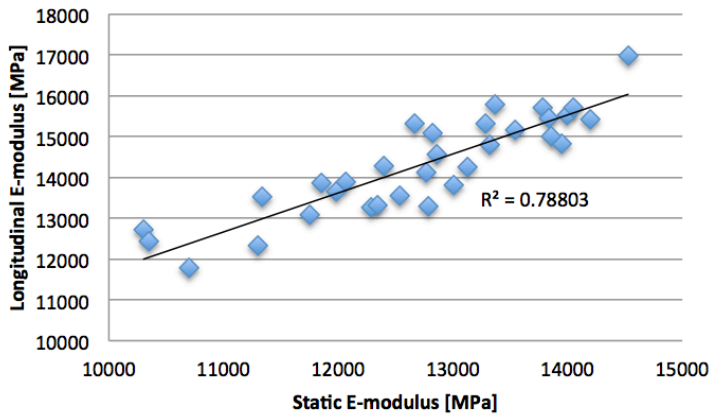


Figure 7-12 Correlation between static and longitudinal E-moduli

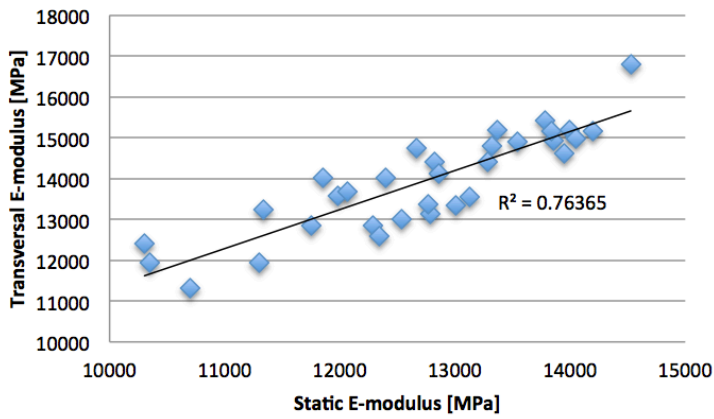


Figure 7-13 Correlation between static and transversal E-moduli

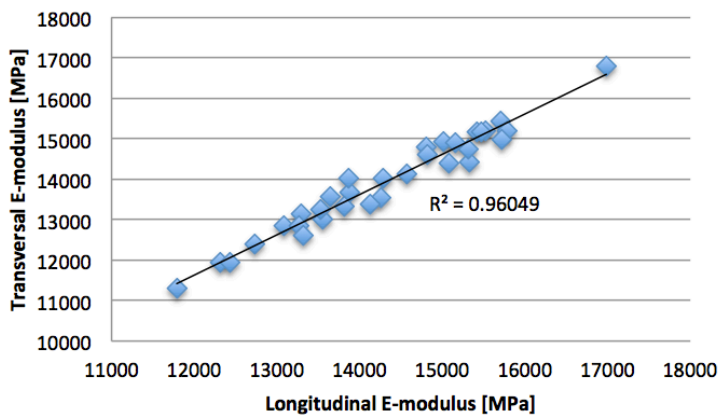


Figure 7-14 Correlation between longitudinal and transversal E-moduli

Figure 7-15 gives a summary of the estimated E-moduli and their mean values.

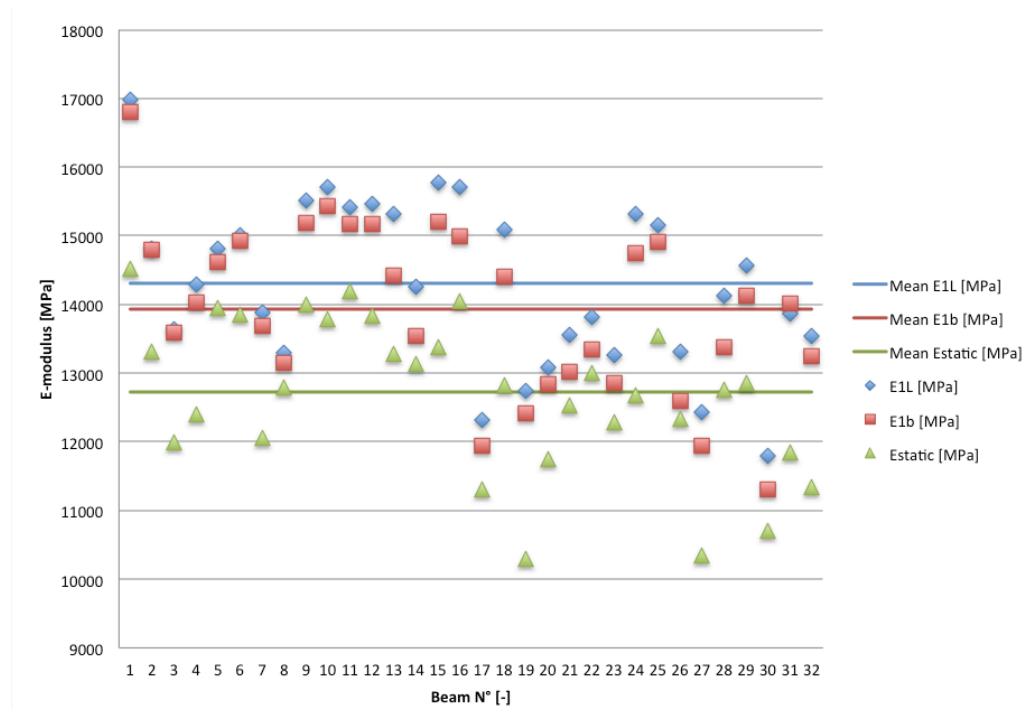


Figure 7-15 Summary of the estimated E-moduli from the different tests and according mean values

---

## 8 Tension Tests

### 8.1 Setup and equipment

The tensile tests were carried out using the Aktiebolaget Alpha Sundbyberg machine shown in *Figure 8-1*. The beams were fixed at both ends with friction grips illustrated in *Figure 8-2*. The beams were chosen to stand out 10 mm on both sides to prevent them from sliding out of the grips for higher loads. The grips had a length of 120 mm which reduced the minimum possible clear length of the beams to  $L_{min} = 1500 - 2 \cdot 10 - 2 \cdot 120 = 1240 \text{ mm}$ . Since the surface of these grips is not flat, but curved in both directions with a global maximum at approximately 60% of their length, the maximum possible clear length results in  $L_{max} = L_{min} + 2 \cdot 50 = 1340 \text{ mm}$ . This caused difficulties in assessing the actual clear length of the beams, which is further discussed in Chapter 8.3.



*Figure 8-1* Tensile machine and setup of the accelerometer (left) and scale for the determination of the axial load (right)

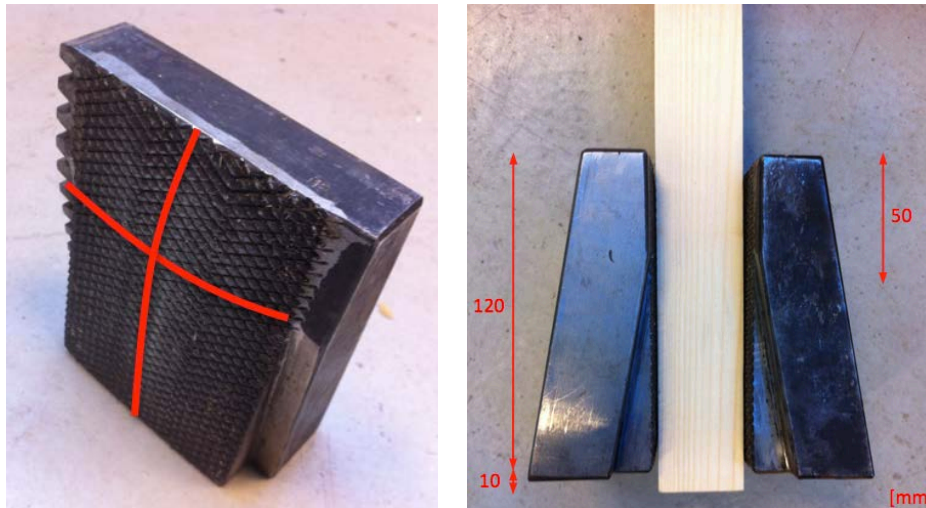


Figure 8-2 Illustration of the curved surface of the friction grips (left) and the position of the beams between the grips with according dimensions (right)

The scale chosen for the tensile machine was 10000 kg, which allowed a precision of 10 kg. The accelerometer was attached with bee-wax at a distance of 250 mm from the lower grip, which equals approximately 20% of  $L_{min}$ . This ensured the recording of the first three bending frequencies. The excitation was performed with 5 hammer blows right next to the accelerometer using an instrumented hammer equipped with a plastic tip. The technical equipment used for the modal testing is described in more detail in Chapter 7. The data acquisition settings are shown in *Table 8-1*. These settings allowed a resolution of the frequencies of approximately 0.1 Hz.

Table 8-1 Settings for data acquisition

Measurement function	Setting
Trigger type	Accelerometer
Trigger level	0.1 V
Trigger delay	-0.01 V
Sampling rate	2560
Recording time	7 s
Blocksize	1024
Frequency range	1280 Hz
NFFT	$2^{16}$

The frequency measurements were carried out for 6 different load levels between 5 kN and 30 kN with an interval of 5 kN. These levels were chosen on the assumption that the maximum tensile load was around 40 kN, corresponding to a tensile strength of 15 MPa. Later ultimate tensile tests described in Chapter 8.4 showed however that the mean tensile strength is considerably higher, namely 25.9 MPa for the tested beams.

## 8.2 Test results

The FRF plots and results from the frequency measurements are shown in Appendix C. *Figure 8-3* shows the FRFs for the aluminium bar and one timber specimen for different load levels. It can be seen that the geometry of the aluminium bar was chosen in a way that the frequency increase do to a higher load is of a comparable magnitude as for a timber specimen. This is important for the comparison of parameter estimation results since the sensitivity study showed that the axial load is very sensitive to errors in frequency (cf. Chapter 5). Moreover one can see that the peaks are much more clear for the aluminium than for the timber specimen, which is mainly due to the differences in material homogeneity.

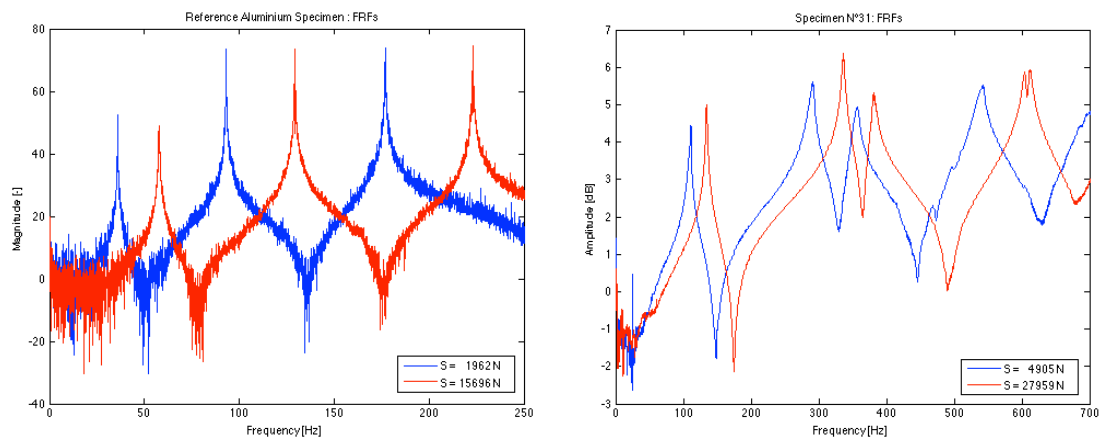


*Figure 8-3 Comparison of frequency plots for aluminium (left) and timber (right)*

*Table 8-2* lists the first three bending frequencies of the above specimen for the different load levels.

*Table 8-2 Comparison of measured frequencies for aluminium (left) and timber (right)*

Applied load S [N]	$f_{1b}$ [Hz]	$f_{2b}$ [Hz]	$f_{3b}$ [Hz]
1962	36.0	93.1	177.0
4022	40.0	98.9	184.0
6671	44.5	106.6	193.9
7750	46.4	109.6	197.6
9810	49.5	114.9	204.4
11576	52.2	119.6	210.0
13538	55.0	124.3	216.6
15696	57.8	129.4	223.3

Applied load S [N]	$f_{1b}$ [Hz]	$f_{2b}$ [Hz]	$f_{3b}$ [Hz]
4905	111.3	291.3	542.3
9221	118.2	307.8	569.1
13930	123.6	319.0	584.7
19031	128.1	327.1	596.2
23642	131.6	331.9	600.8
27959	134.2	336.6	604.2

*Figure 8-4 - Figure 8-6* show plots of the squares of the three first measured frequencies  $f_i^2$  against the applied load  $S$  under the assumption of equal boundary conditions  $k$  at both ends of the beams. Since different friction grips were used for timber and aluminium, the respective restraint lengths are also different, namely 1260 mm and 1245 mm respectively. For the aluminium bar, the measured frequencies are all more or less arranged in a line, which shows that the boundary conditions remain nearly constant for different load levels. The assumption of equal restraints at both

ends is valid for the aluminium bar as the friction grips are identical and the aluminium is homogeneous. For the timber specimen only the frequencies of the three highest loads are situated on a line. The main reason for this is that the clear length changes over different load levels. The problem is that the pressure from the grips applied on the timber is not constant, but increases with the strain applied on the beam. Thereby, the grips penetrate deeper and deeper into the soft wood and through their curved surface, more and more reduce the clear length. In the next chapter, this will be taken into account by setting different lengths for the lower load levels. Another observation when comparing the figures is that the graph of the third frequency does not correspond well with the other two graphs. Already during data acquisition, it became clear that the peak of the third frequency is not clear enough to fulfil the precision requirements, at least not for the applied measurement method. The same conclusion could already be drawn in Chapter 7 during the estimation of the material properties. The higher the frequency modes, the lower are their accuracies and thus their use for parameter estimation. This is further discussed in the next paragraph.

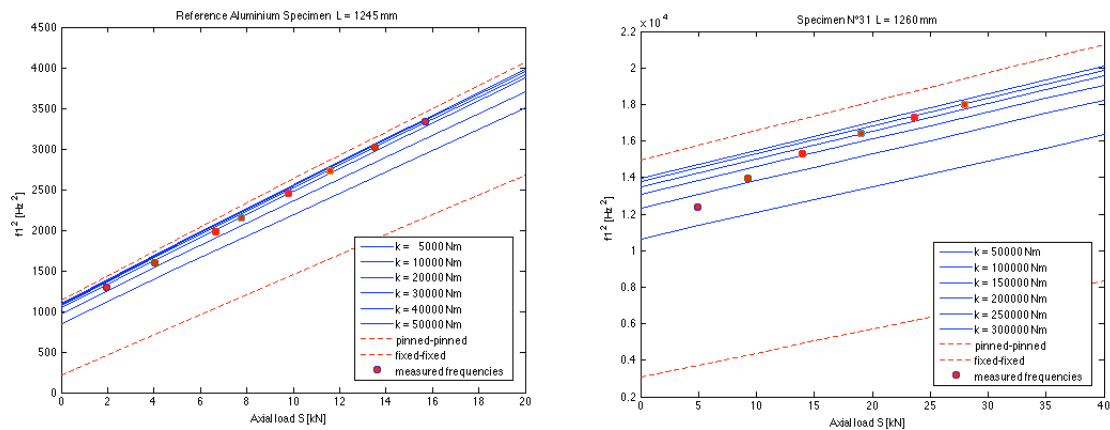


Figure 8-4 Plots of axial load against square of calculated first frequency for different boundary conditions together with measured first frequencies for aluminium (left) and timber (right)

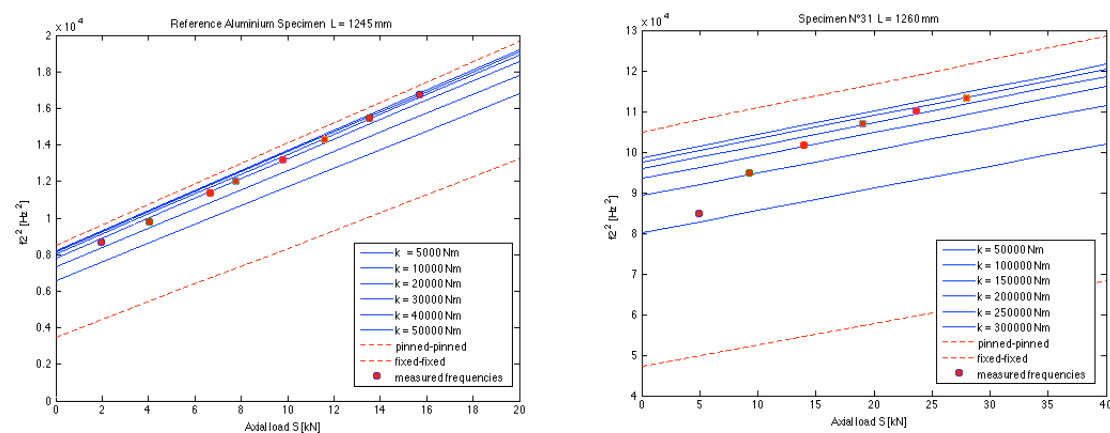


Figure 8-5 Plots of axial load against square of calculated second frequency for different boundary conditions together with measured second frequencies for aluminium (left) and timber (right)

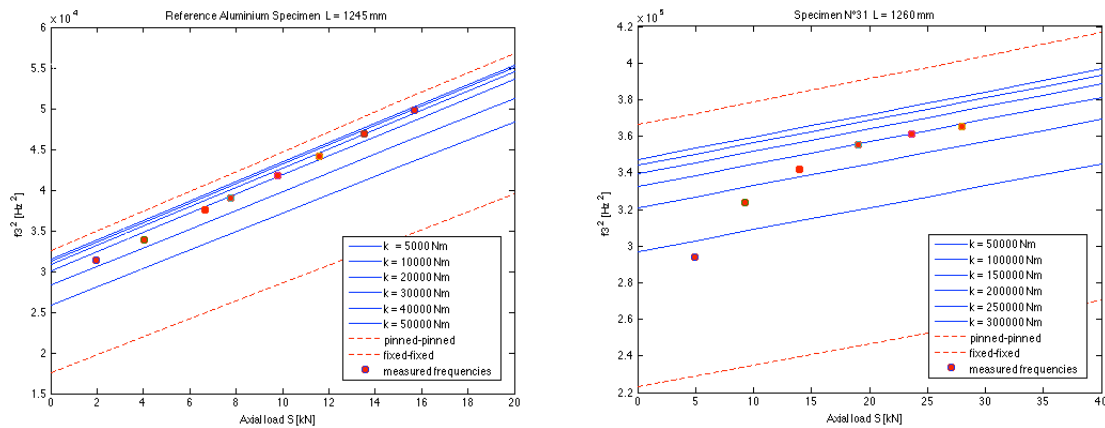


Figure 8-6 Plots of axial load against square of calculated third frequency for different boundary conditions together with measured third frequencies for different load levels for aluminium (left) and timber (right)

### 8.3 Estimation of tensile force S

The bending frequencies resulting from the data processing in Chapter 8.2 are in the following used to estimate the axial load  $S$  and the boundary conditions at the restraints. In the first step, this is done using only the two first frequencies under the assumption of equal boundary conditions. In the second step, it is attempted to use also the third frequency either for error minimisation or to expand the model by a third parameter by dropping the assumption of equal boundary conditions. Since the stiffness of the timber specimen is much smaller compared to the steel grips, the rotational stiffness at the supports is mainly influenced by the E-modulus of the specimen. For the inhomogeneous timber, the E-modulus is however not constant over the whole specimen length, which can consequently lead to a difference in boundary conditions. This means that the use of an extra frequency should have a positive effect on the results, provided that it could be determined with an appropriate precision.

For the parameter estimation, Timoshenko theory was used to include effects of shear deformations and rotary inertia since they can have a rather high influence on the results (cf. Chapter 5). The Matlab code illustrated in Appendix B was used for this purpose.

While the material properties and the sectional dimensions had already previously been determined, the choice of the clear specimen length  $L$  was still unknown. As explained above, this length changes for different load levels due to characteristics of the tensile machine. This effect is illustrated in *Figure 8-7* and *Figure 8-8* for aluminium and timber, respectively.

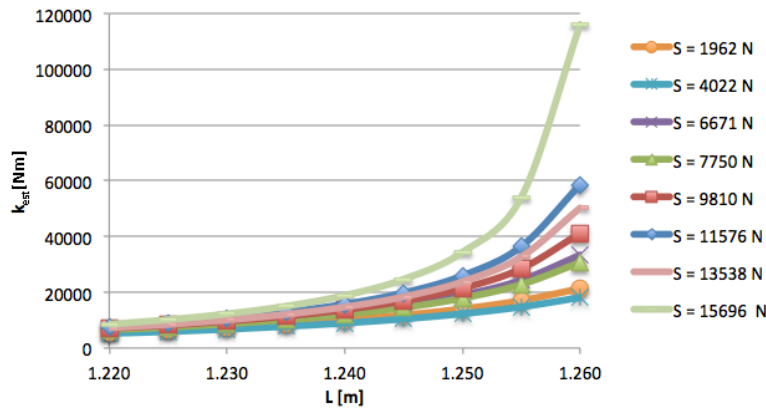


Figure 8-7 Variation of estimated rotational stiffness with different assumptions for clear length  $L$  for aluminium and different load levels

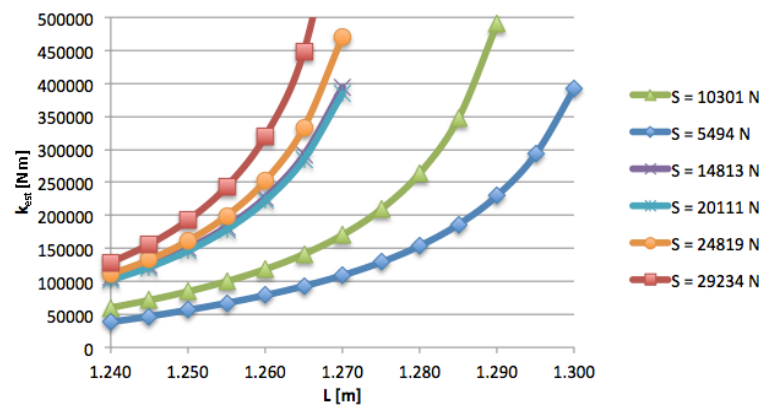


Figure 8-8 Variation of estimated rotational stiffness with different assumptions for clear length  $L$  for timber and different load levels

The plots show the variation of the rotational stiffness  $k$  for different lengths  $L$  and load levels  $S$ . When comparing the two graphs, it is obvious that the effect of the grips is much less pronounced for aluminium than for timber. In Figure 8-8, the curves associated with the two lowest load levels show strong deviations from the pattern of the other levels. In Figure 8-7, the curves are much closer together and the deviation therefore less obvious. The conclusion was that the clear length could be assumed constant for the aluminium bar while it had to be varied for the timber beam, at least for the two lowest load levels, where the clear length turned out to be bigger compared to the other levels. For the timber specimen, the length for the lowest load was chosen to the maximum length  $L_{max} = 1295 \text{ mm}$ . Under the assumption of constant boundary conditions, the length for the second highest load was then determined to  $L = 1275 \text{ mm}$ , and the length for the remaining levels to  $L = 1255 \text{ mm}$ . For aluminium,  $L$  was assumed to be  $1245 \text{ mm}$  for all load levels. The difference in length for the two materials is related to the fact that different grips with different surface properties had to be used.

After all the input parameters were now determined, the parameter estimation could be initiated. Figure 8-9 shows the graphical estimation for aluminium and timber, previously explained in Chapter 5.

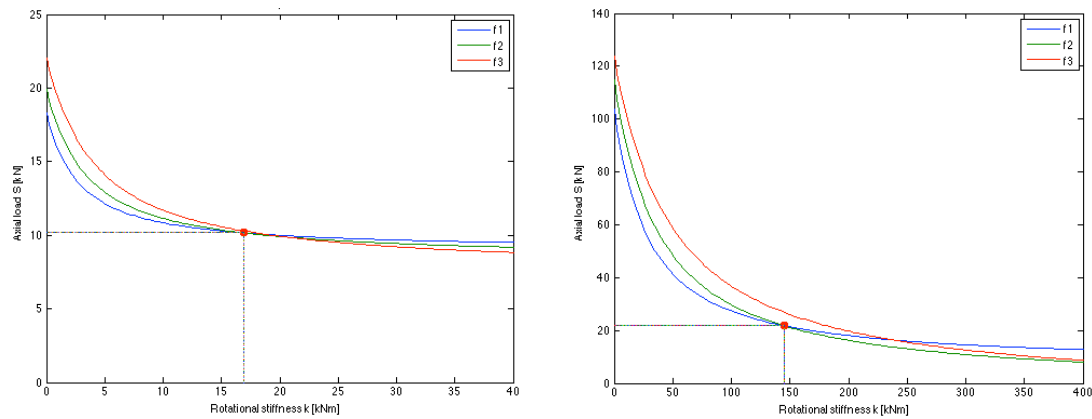


Figure 8-9 Plot for the dual parameter estimation technique for aluminium (left) and timber (right)

The use of two frequencies gave reasonable results of the axial load  $S$  for both materials. The comparison of the graphs shows however that the third frequency is only of use for aluminium, while it is far off the crossing point of the two first frequencies for the timber specimen. As previously mentioned, the third frequency could not be determined with the required precision. This is why the parameter estimation was limited to the two first frequencies, which makes the assumption of equal boundary conditions indispensable and therefore excludes the expansion of the model to a third parameter. Table 8-3 and Table 8-4 show the according results for the aluminium bar and a timber specimen using the transversal as well as the longitudinal E-moduli to investigate the difference in results. It was also attempted to use the static E-modulus, but the results were far from accurate for both materials, showing that the estimation requires dynamic values for the material stiffness.

Table 8-3 Results from the dual parameter estimation for the reference aluminium specimen using the transversal and longitudinal E-modulus

Aluminium			using $E_b$						using $E_L$			
Applied load $S$	% of yield	$S/S_e$	$f_{1b}$	$f_{2b}$	$L$	$k_{est}$	$S_{est}$	Error on $S$	$k_{est}$	$S_{est}$	Error on $S$	
[N]	[%]	[-]	[Hz]	[Hz]	[m]	[Nm]	[N]	[%]	[Nm]	[N]	[%]	
1962	8.7	1.1	36.0	93.1	1.245	11831	2261	15.2	9365	2356	20.1	
4022	17.9	2.2	40.0	98.9	1.245	10447	4568	13.6	8323	4712	17.2	
6671	29.6	3.6	44.5	106.6	1.245	15288	6884	3.2	11517	7042	5.6	
7750	34.4	4.2	46.4	109.6	1.245	14510	8181	5.6	10979	8363	7.9	
9810	43.6	5.3	49.5	114.9	1.245	16907	10161	3.6	12418	10367	5.7	
11576	51.4	6.2	52.2	119.6	1.245	19800	11982	3.5	14059	12208	5.5	
13538	60.2	7.3	55.0	124.3	1.245	18378	14241	5.2	13167	14508	7.2	
15696	69.8	8.5	57.8	129.4	1.245	24670	16228	3.4	16532	16508	5.2	

Table 8-4 Results from the dual parameter estimation for the timber specimen N°6 using the transversal and longitudinal E-modulus

T6			using $E_b$						using $E_L$			
Applied load $S$	% of yield	$S/S_e$	$f_{1b}$	$f_{2b}$	$L$	$k_{est}$	$S_{est}$	Error on $S$	$k_{est}$	$S_{est}$	Error on $S$	
[N]	[%]	[-]	[Hz]	[Hz]	[m]	[Nm]	[N]	[%]	[Nm]	[N]	[%]	
5396	7.9	0.25	110.2	290.1	1.295	149030	6841	26.8	141410	7063	30.9	
10006	14.7	0.44	116.3	300.6	1.275	103310	16825	68.1	98620	17198	71.9	
14813	21.8	0.64	121.3	311.1	1.255	93768	21630	46.0	89528	22083	49.1	
18737	27.6	0.81	125.0	318.9	1.255	144740	21782	16.3	137220	22101	18.0	
23152	34.0	1.00	129.1	325.8	1.255	171770	27198	17.5	161950	27504	18.8	
27959	41.1	1.20	132.3	331.5	1.255	213350	30845	10.3	199480	31127	11.3	

The results for aluminium are very good, with absolute errors ranging from 15.2% to 3.2% for the transversal E-modulus. As expected, the results tend to improve for higher loads since the sensitivity of the system with regard to the input parameters

decreases. There is however a small error spread that can be explained by the choice of a constant mean clear length and probably also some measurement errors. The results using the longitudinal E-modulus turned out to be less accurate than the ones using the transversal E-modulus. The same conclusions can be drawn for the timber specimens, where the results for this particular sample range from 68.1% to 10.3% when using the transversal E-modulus. The results for the other specimens are listed in Appendix C.

Table 8-5 shows the mean errors and deviations for the estimated axial load  $S$  using different E-moduli for all 32 timber specimens. The variation of the mean error for different load levels is illustrated in Figure 8-10. A complete illustration of the individual errors and deviations for all specimens is listed in Appendix C.

Table 8-5 Mean errors of the estimated axial load  $S_{est}$  for all timber specimens using the transversal and longitudinal E-moduli

Applied load $S$ [N]	% of yield [%]	$S/S_e$ [-]	using $E_b$		using $E_t$	
			Mean error on $S$ [%]	Std. dev. on error [%]	Mean error on $S$ [%]	Std. dev. on error [%]
5000	7.4	0.25	46.6	89.5	68.4	102.5
10000	14.7	0.48	34.3	45.0	48.1	52.6
15000	22.1	0.70	27.8	39.9	41.5	48.3
20000	29.4	0.94	16.2	26.9	24.1	30.4
25000	36.8	1.17	9.4	23.7	14.4	26.2
30000	44.1	1.40	7.6	20.2	12.4	22.1

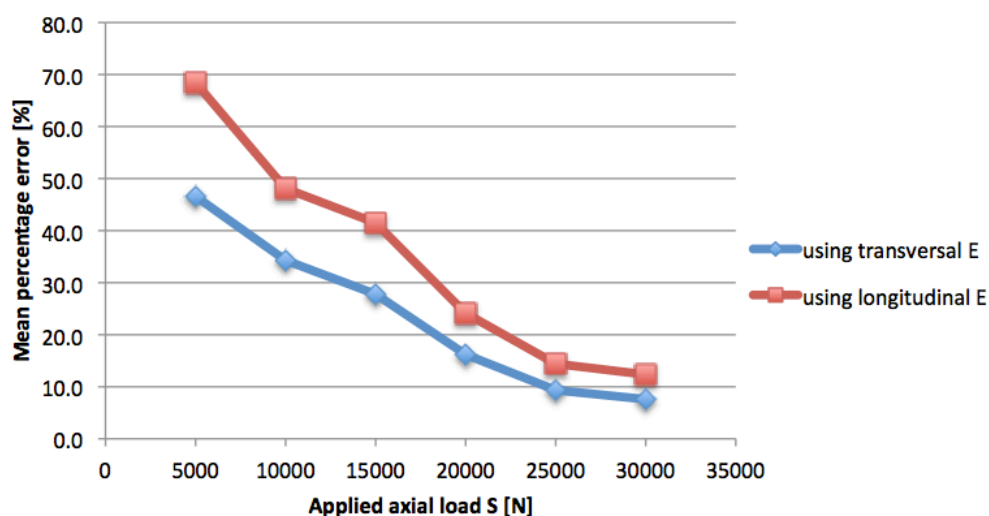
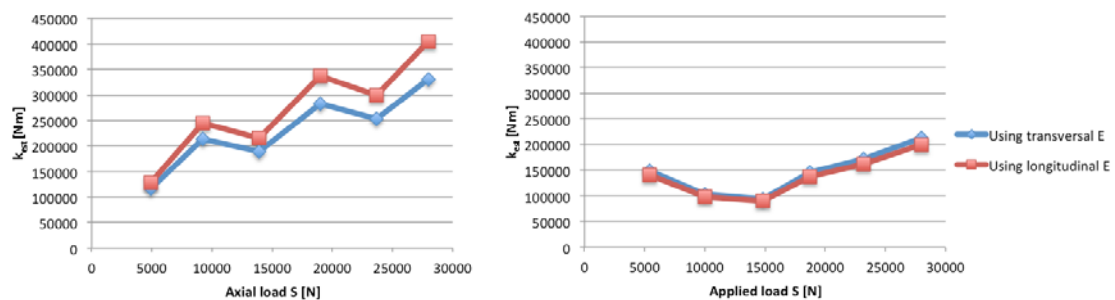


Figure 8-10 Graphical representation of the mean errors from Table 8-5 for the different load levels

The results show that the estimation of  $S$  improves for higher load levels. Again, the best results could be obtained using the transversal E-modulus. It can be seen that the differences for the two E-moduli decrease for higher loads. The axial loads are in general overestimated, with mean errors ranging from 7.6% to 46.6%. The standard deviations are of the same order, which results in a very high spread for the results. The main reason is probably the clear lengths  $L$  that was chosen the same for every specimen, even though there might be differences caused by varying material properties. This parameter was the most difficult to assess since the restraint length cannot be visually determined, but has a big influence on the results. Other errors

result from the assumption of equal boundary conditions and frequency measurement errors. Also, the applied model assumes that material properties are constant over the specimen length, which is clearly not the case for the inhomogeneous timber. Considering all these model uncertainties, the estimated axial loads appear quite reasonable and give an incentive for further research.

In addition to the estimated axial loads, the boundary conditions were analysed in more detail. *Figure 8-11* shows the estimated rotational stiffness  $k_{est}$  for different load levels of two timber specimens. The plots show rather random variations of the rotational stiffness. The only trend that can be recognized is that it seems to increase in the range of higher loads. This could however also be related to the choice of the varying clear length that has a high influence on the estimation for the rotational stiffness. Overestimated values of the clear length  $L$  lead to higher values of  $k$  (cf. *Figure 5-10*).



*Figure 8-11* Plots of the estimated rotational stiffness  $k_{est}$  for different load levels and two different timber specimens using the transversal and longitudinal E-moduli

*Figure 8-12* illustrates the correlation of the mean estimated rotational stiffness over different load levels for one specimen and its static E-modulus. The respective values are listed in Appendix C.

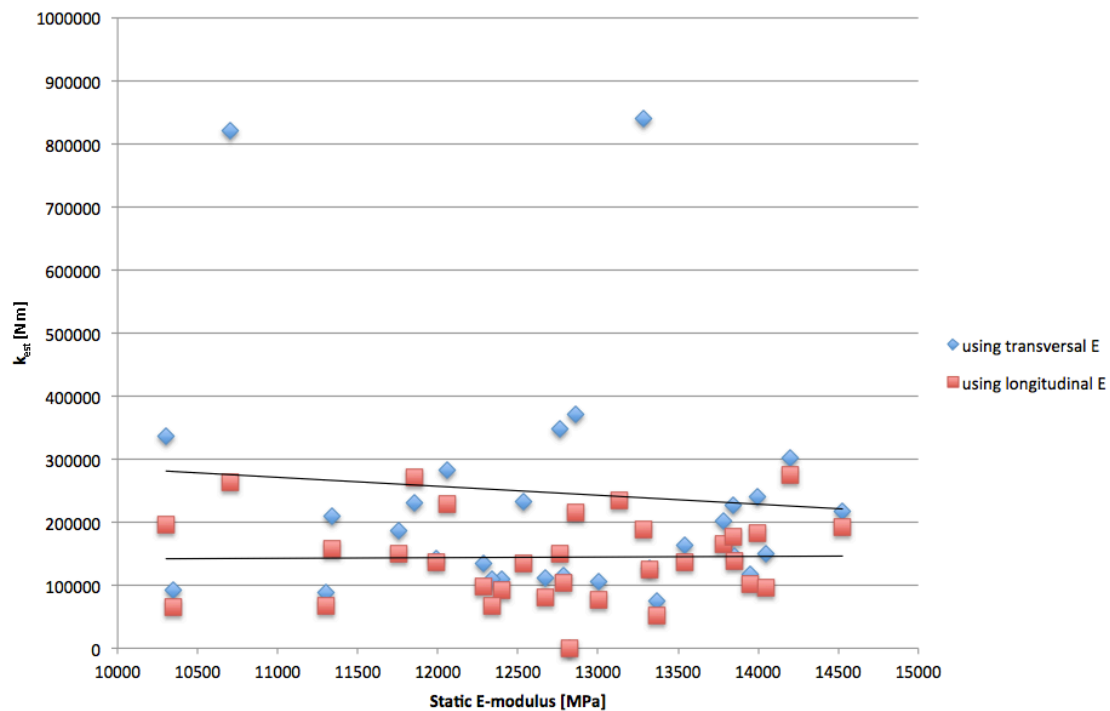


Figure 8-12 Plot of the estimated rotational stiffness  $k_{est}$  averaged over different load levels against the E-moduli of the according timber specimens

It was expected that  $k$  would increase for a higher the specimen stiffness since the boundary conditions were believed to be mainly determined by the material properties. However no such trend could be verified from the data. Maybe this is due to the fact that the range of the E-moduli is rather small and that the errors to  $k$  are rather high. The distribution of the boundary conditions seems rather constant with a mean value of 207695 Nm and a standard deviation of 169567 Nm when using the transversal E-moduli. For comparison, the mean value was 9358 Nm for the Aluminium bar. The difference is due to the smaller dimensions of the bar and the resulting much lower polar moment and bending stiffness.

## 8.4 Determination of ultimate tensile strength

Tensile tests according to CEN/TC (2007) were carried out on some of these specimens to determine an approximate tensile strength and to put it in relation to the E-moduli and the applied loads. The results are shown in Table 8-6 and Figure 8-13. Even though a small correlation between E-moduli and tensile strength is recognisable, the amount of data is too small to make final conclusions on this subject. The mean tensile strength was found to be 25.9 MPa with a standard deviation of 4.7 MPa for this amount of data.

Table 8-6 Results from the ultimate tensile tests

Beam N°	$E_b$	$S_{max}$	$f_{t,0,max}$
[-]	[MPa]	[N]	[MPa]
30	11311	66000	25.1
20	12842	61000	23.2
28	13376	55000	21.0
5	14615	86000	32.8
11	15165	60000	22.9
1	16805	80000	30.5
Mean value	14019	68000	25.9
Std. dev.	1927	12280	4.7

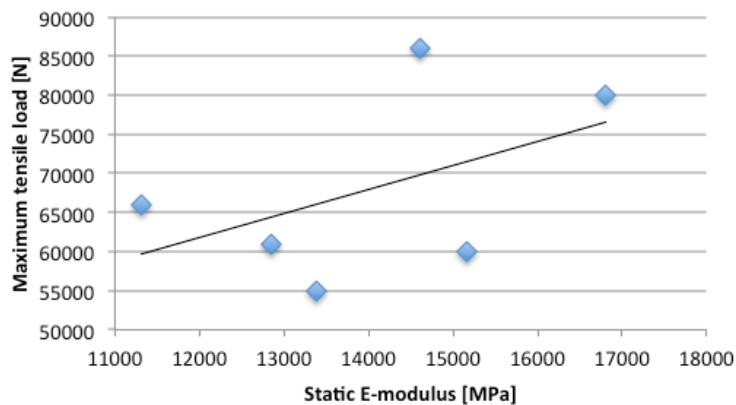


Figure 8-13 Plot of the static E-modulus against the maximum tensile load for the tested specimens

Figure 8-14 illustrates the failure mode of the timber beams. The pressure caused by the friction grips induced local compression at the restraints, leading to a reduced section and hence stress peaks in this area. Resulting cracks at the restraint section of one lamella then relocated the tension on the remaining intact one, which in turn yielded at a knot or otherwise weakened section leading to ultimate failure.



Figure 8-14 Timber specimen after ultimate tensile test: local compression at the restraint (left) and final failure mode (right)

---

---

## 9 Conclusions and further research

### 9.1 Conclusions

The results of the dual parameter estimation showed that it is possible to estimate the axial loads in timber beams using resonance frequency analysis. The sensitivity analysis showed however that the quality of the results is very sensitive to errors in the input parameters, especially the measured frequencies, the clear length and the E-modulus.

It was therefore very important to ensure a high measurement quality and to only use a minimum of resonance frequencies since the precision decreased quickly for higher vibration modes. An error minimisation through additional frequency information was hence not possible in this research. The length of the measurement time and number of excitations was just too small to obtain clear peaks for the higher resonance frequencies of the timber specimens. For the reference aluminium specimen, these factors were however sufficient. This shows that the inhomogeneous character of timber, in association with its natural defects, requires more sophisticated measurement techniques than a homogeneous material. One possibility of improving the frequency resolution would be to use a modal vibration shaker instead of an instrumented hammer. This way more measurements can be made over a longer period of time, resulting in more clear frequency peaks.

The clear length of the beams was another factor that had a strong influence on the test results and caused a high standard deviation from the mean value. The problem was that the available tensile machine was not designed to apply a constant grip pressure on the beam ends. In fact, the grip pressure increased for higher load levels, leading to a varying clear length and also rotational stiffness at the restraints. In addition, these parameters varied for each specimen caused by the difference in material properties. It was therefore not possible to identify the exact clear length for each measurement. Hence, a mean clear length had to be chosen that caused the high spread in results for the parameter estimation. Note that the determination of the restraint length will also be of high importance when applying this method on real structures and therefore needs to be treated with special care.

The best results for the axial load were obtained using the E-modulus obtained from transversal vibration tests with a mean error ranging from 7.6% to 46.6%. When using the longitudinal E-moduli, the mean errors increased to 12.4% to 89.5%. Note, that in both cases the results consistently improved for higher loads. This was in accordance with the results from the sensitivity analysis. It was furthermore attempted to use the static E-modulus for the calculations, which led however to unusable results. This shows that dynamic values need to be used for the estimation of parameters when using the presented resonance frequency method. For the application of the method on real structures, it would therefore be possible to determine the E-modulus using longitudinal frequency measurements or maybe even time of flight measurements.

The model used for the parameter estimation was based on Timoshenko theory. This allowed to include effects of shear deformations and rotary inertia that had a major influence on results, especially for higher vibration modes.

---

## 9.2 Suggestions for further research

The results of the presented research were promising and hence raise the need for further research in this area. In the following, some suggestions are listed.

- Influence of specimen geometry

One of the limitations of this research was the geometry of the specimen. It would be interesting to see how the sensitivity of the results changes for other specimen dimensions, especially bigger sizes. It is hereby important to use a machine that applies constant grip pressure to the specimen ends, so that the restraint length does not vary for different load levels and can be determined with more precision.

- Testing of specimens under compression

Only specimens under tension were analysed in this thesis. The research could be expanded to specimens under compression to see if similar results can be obtained or if there are maybe additional effects that need to be taken into account in this case.

- Tests on real structure

Finally, in-situ tests could be carried out on an existing structure to analyse the applicability of the method under real-life conditions. For this purpose, a modal vibration shaker might be necessary to improve the frequency resolution by increasing the measurement time. Also the frequency plots will probably be more complicated since other structural members might participate in vibration. One solution to this problem could be to attach additional accelerometers in different points of the structure to be able to allocate the frequencies to the respective members.

---

## 10 References

- Akesson, B., & O., F. (1980). *SFVIBAT-II-A Computer Program for Space Frame Vibration Analysis, Publication*. Chalmers Univ. of Technology, Göteborg, Sweden.
- Amabili, M. (2010). Estimation of tensile force in tie-rods using a frequency-based identification method. *Journal of sound and vibration*, 329(11), 2057-2067.
- Avitabile, P. (2001). Experimental modal analysis. *Sound and vibration*, 35(1), 20-31.
- Béliveau, J. G. (1987). System identification of civil engineering structures. *Canadian Journal of Civil Engineering*, 14(1), 7-18.
- Branco, J. M. (2010). Structural analysis of two King-post timber trusses: Non-destructive evaluation and load-carrying tests. *Construction and Building Materials*, 24(3), 371-383.
- Buyleedlumber.com. (2012), from <http://www.buyleedlumber.com/products/fsc-engineered-lvl-and-i-joists-2/>
- Timber Structures - Structural Timber and Glued-laminated Timber - Determination of some Physical and Mechanical Properties (2007).
- Chui, Y., & Smith, I. (1990). Influence of rotatory inertia, shear deformation and support condition on natural frequencies of wooden beams. *Wood science and technology*, 24(3), 233-245.
- Crovella, P., & Kyanka, G. (2011). Use of vibration techniques to determine the rotational stiffness of timber joints.
- Den Hartog, J. P. (1985). *Mechanical vibrations*: Dover Pubns.
- Dossing, O. (1988). Structural Testing Part I: Mechanical Mobility Measurement. *Brüel & Kjaer, Naerum*.
- Friedman, Z., & Kosmatka, J. B. (1993). An improved two-node Timoshenko beam finite element. *Computers & structures*, 47(3), 473-481.
- Haines, D. W. (1996). Determination of Young's modulus for spruce, fir and isotropic materials by the resonance flexure method with comparisons to static flexure and other dynamic methods. *Wood science and technology*, 30(4), 253-263.
- Harris, C. M. (2002). *Harris' shock and vibration handbook* (Vol. 5): McGraw-Hill.
- Howson, W., & Williams, F. (1973). Natural frequencies of frames with axially loaded Timoshenko members. *Journal of sound and vibration*, 26(4), 503-515.
- Ilic, J. (2001). Relationship among the dynamic and static elastic properties of air-dry Eucalyptus delegatensis R. Baker. *European Journal of Wood and Wood Products*, 59(3), 169-175.
- Kjaer, B. (2012). Impact Hammer - Type 8202.
- Leichti, R. J. (2000). The continuum of connection rigidity in timber structures. *Wood and fiber science*, 32(1), 11-19.
- Livingston, T. (1994). *Estimation of axial load in prismatic members using flexural vibrations*. The University of Vermont.

- 
- Maille, N. (2008). *Assessing the Roof Structure of the Breeding Barn Using Truss Member Resonant Frequencies*. The University of Vermont.
- McGuire, J. (1995). Notes on semi-rigid connections. *Finite Element Modeling Continuous Improvement*.
- Ohlsson, S., & Perstorper, M. (1992). Elastic wood properties from dynamic tests and computer modeling. *Journal of Structural Engineering*, 118, 2677.
- Oja, J. (2001). Predicting the stiffness of sawn products by X-ray scanning of Norway spruce saw logs. *Scandinavian Journal of Forest Research*, 16(1), 88-96.
- Paz, M. (1997). *Structural dynamics: theory and computation*: Kluwer Academic Publishers.
- Performancepanels.com. (2012), from [http://www.performancepanels.com/single.cfm?content=app\\_pp\\_atr\\_str1](http://www.performancepanels.com/single.cfm?content=app_pp_atr_str1)
- Ross, R. J. (1994). *Determining in-place modulus of elasticity of stress-laminated timber decks using NDE*.
- Roymech.co.uk. (2010), from [http://www.roymech.co.uk/Useful\\_Tables/Torsion/Torsion.html](http://www.roymech.co.uk/Useful_Tables/Torsion/Torsion.html)
- Sandoz, J. (1989). Grading of construction timber by ultrasound. *Wood science and technology*, 23(1), 95-108.
- Schajer, G. S. (2001). Lumber strength grading using X-ray scanning. *Forest products journal*, 51(1), 43-50.
- Shaker, F. J. (1975). Effect of axial load on mode shapes and frequencies of beams. SIA 265:2003 - Timber structures (2003).
- Strasser, U. (2008). Snow loads in a changing climate: new risks?
- Thelandersson, S., & Larsen, H. J. (2003). *Timber engineering*: Wiley.
- Timoshenko, S. (1974). *Vibration problems in engineering*.
- Tullini, N., & Laudiero, F. (2008). Dynamic identification of beam axial loads using one flexural mode shape. *Journal of sound and vibration*, 318(1), 131-147.
- Wikipedia.org. (2006), from <http://en.wikipedia.org/wiki/Hardwood>
- Wikipedia.org. (2012), from <http://en.wikipedia.org/wiki/Aluminium>, [http://en.wikipedia.org/wiki/Ultimate\\_tensile\\_strength](http://en.wikipedia.org/wiki/Ultimate_tensile_strength)

---

# 11 Appendices

## 11.1 Appendix A – Matlab codes

### 11.1.1 Calculation of transversal frequencies

#### Discrete model – Euler beam theory

The program uses the input parameters to define element mass and stiffness matrices for each finite element, which are then put together to one global matrix. The solution of the according eigenvalue problem then yields the resonance frequencies.

```
%%Remove all variables from the workspace and clear command window
clear all

clc

%%Enter input data
E = 13000*10^6; %%E-modulus in N/m2
G = 760*10^6; %%G-modulus in N/m2
p = 400; %%Specimen density in kg/m3
L = 1.5; %%Clear length in m
H = 0.075; %%Specimen height in m
B = 0.035; %%Specimen width in m
S = 20000; %%Axial load in N
k1 = 10^15; %%Value for translational support in x=0 in N/m
k3 = 10^15; %%Value for translational support in x=L in N/m
k2 = 10000; %%Value for rotational support in x=0 in Nm
k4 = 10000; %%Value for rotational support in x=L in Nm
n = 50; %%Number of finite elements
nnf = 2; %%Number of resonance frequencies

%%Calculation
A = B*H;
Iz = B^3*H/12;
el = L/n;
if (k1 == 0) && (k2 == 0) && (k3 == 0) && (k3 == 0);
    nnf = nnf + 2;
end

%%Connection matrix
```

---

```

for ie = 1:n
    ktr = 2*ie;
    cn(ie,:) = [ktr-1:1:ktr+2];
end
%%Consistent element mass matrix
em = zeros(4);
em = [ 156      22*el      54      -13*el;
      22*el     4*el^2     13*el     -3*el^2;
       54      13*el     156      -22*el;
      -13*el    -3*el^2    -22*el     4*el^2];
em = p*A*el/420 * em;
%%Element stiffness matrix
ek = zeros(4);
ek = [ 6      3*el     -6      3*el;
      3*el    2*el^2   -3*el    el^2;
      -6     -3*el     6      -3*el;
      3*el    el^2    -3*el    2*el^2];
ek = (2*E*Iz/el^3)*ek;
gk = [ 36      3*el     -36      3*el;
      3*el    4*el^2   -3*el    -el^2;
      -36     -3*el     36      -3*el;
      3*el    -el^2    -3*el    4*el^2];
kg = (S/(30*el))*gk;
ek = ek + kg;
%%Global matrix
k = zeros(ktr+2);
m = zeros(ktr+2);
for ie = 1:n
    index = cn(ie,:);
    m(index,index) = m(index,index) + em;
    k(index,index) = k(index,index) + ek;
end
k(1,1) = k(1,1) + k1;
k(2,2) = k(2,2) + k2;
k(ktr+1,ktr+1) = k(ktr+1,ktr+1) + k3;
k(ktr+2,ktr+2) = k(ktr+2,ktr+2) + k4;

```

---

```

%%Solve eigenvalue problem

[v,nu] = eig(k,m);

[w2,ie] = sort(diag(nu));

v = v(:,ie);

%%Print natural frequencies (Hz)

for ie = 1:nnf

    fcalc(ie) = sqrt(w2(ie))/(2*pi);

    fcalc(ie)

end

```

### Discrete model – Timoshenko beam theory

The program uses the same principles as for the Euler theory, except that the mass and stiffness matrices are composed of additional terms to take into account effects from shear deformations and rotary effects.

```

%%Remove all variables from the workspace and clear command window

clear all

clc

%%Enter input data

E = 13000*10^6; %%E-modulus in N/m2

G = 760*10^6; %%G-modulus in N/m2

p = 400; %%Specimen density in kg/m3

L = 1.5; %%Clear length in m

H = 0.075; %%Specimen height in m

B = 0.035; %%Specimen width in m

S = 20000; %%Axial load in N

k1 = 10^15; %%Value for translational support in x=0 in N/m

k3 = 10^15; %%Value for translational support in x=L in N/m

k2 = 10000; %%Value for rotational support in x=0 in Nm

k4 = 10000; %%Value for rotational support in x=L in Nm

n = 50; %%Number of finite elements

nnf = 2; %%Number of resonance frequencies

%%Calculation

```

---

```

A = B*H;

ks = 5/6;

Iz = B^3*H/12;

el = L/n;

fi = 12*E*Iz/(ks*G*A*el^2);

if (k1 == 0) && (k2 == 0) && (k3 == 0) && (k3 == 0);

    nnf = nnf + 2;

end

%%Connection matrix

for ie = 1:n

    ktr = 2*ie;

    cn(ie,:) = [ktr-1:1:ktr+2];

end

%%Consistent mass matrix

em = zeros(4);

emt = [13/35+7/10*fi+1/3*fi^2    (11/210+11/120*fi+1/24*fi^2)*el
        9/70+3/10*fi+1/6*fi^2    -(13/420+3/40*fi+1/24*fi^2)*el;
        (11/210+11/120*fi+1/24*fi^2)*el
        (1/105+1/60*fi+1/120*fi^2)*el^2
        (13/420+3/40*fi+1/24*fi^2)*el
        -(1/140+1/60*fi+1/120*fi^2)*el^2;
        9/70+3/10*fi+1/6*fi^2    (13/420+3/40*fi+1/24*fi^2)*el
        13/35+7/10*fi+1/3*fi^2    -(11/210+11/120*fi+1/24*fi^2)*el;
        -(13/420+3/40*fi+1/24*fi^2)*el
        -(1/140+1/60*fi+1/120*fi^2)*el^2
        -(11/210+11/120*fi+1/24*fi^2)*el
        (1/105+1/60*fi+1/120*fi^2)*el^2];

emr = [6/5    (1/10-1/2*fi)*el    -6/5    (1/10-1/2*fi)*el;
        (1/10-1/2*fi)*el    (2/15+1/6*fi+1/3*fi^2)*el^2
        (-1/10+1/2*fi)*el    -(1/30+1/6*fi-1/6*fi^2)*el^2;
        -6/5    (-1/10+1/2*fi)*el    6/5    (-1/10+1/2*fi)*el;
        (1/10-1/2*fi)*el    -(1/30+1/6*fi-1/6*fi^2)*el^2
        (-1/10+1/2*fi)*el    (2/15+1/6*fi+1/3*fi^2)*el^2];

em = p*A*el/(1+fi)^2*emt + p*A*Iz/((1+fi)^2*el)*emr;

%%Stiffness matrix

ek = zeros(4);

kb = [12    6*el    -12    6*el;
        6*el    (4+fi)*el^2    -6*el    (2-fi)*el^2;
        -12    -6*el    12    -6*el;
        6*el    (2-fi)*el^2    -6*el    (4+fi)*el^2];

kg = [36    3*el    -36    3*el;
        3*el    4*el^2    -3*el    -el^2;
        -36    -3*el    36    -3*el;
        3*el    -el^2    -3*el    4*el^2];

```

---

```

ek = (E*Iz/((1+fi)*el^3))*kb + (S/(30*el))*kg;

%%Global matrix
k = zeros(ktr+2);
m = zeros(ktr+2);
for ie = 1:n
    index = cn(ie,:);
    m(index,index) = m(index,index) + em;
    k(index,index) = k(index,index) + ek;
end
k(1,1) = k(1,1) + k1;
k(2,2) = k(2,2) + k2;
k(ktr+1,ktr+1) = k(ktr+1,ktr+1) + k3;
k(ktr+2,ktr+2) = k(ktr+2,ktr+2) + k4;

%%Solve eigenvalue problem
[v,nu] = eig(k,m);
[w2,ie] = sort(diag(nu));
v = v(:,ie);

%%Print natural frequencies (Hz)
for ie = 1:nmf
    fcalc(ie) = sqrt(w2(ie))/(2*pi);
    fcalc(ie)
end

```

### Continuous model – Timoshenko beam theory

For the entered input parameters, the program determines the lowest transversal frequency for the chosen frequency range by finding the first root of equation (5.20). If no root exists for the entered frequency range, the output will be 'change frequency range'. For higher frequencies, the range needs to be adjusted.

```

%%Remove all variables from the workspace and clear command window
clear all
clc
%%Enter input data

```

---

```

E = 13000*10^6;      %%E-modulus in N/m2
G = 760*10^6;      %%G-modulus in N/m2
p = 400;           %%Specimen density in kg/m3
L = 1.5;           %%Clear length in m
H = 0.075;        %%Specimen height in m
B = 0.035;        %%Specimen width in m
S = 20000;        %%Axial load in N
k1 = 10^15;       %%Value for translational support in x=0 in N/m
k3 = 10^15;       %%Value for translational support in x=L in N/m
k2 = 10000;       %%Value for rotational support in x=0 in Nm
k4 = 10000;       %%Value for rotational support in x=L in Nm
%%Define frequency range of interest
fmin = 20;        %%Minimum frequency
fmax = 77;        %%Maximum frequency
%%Iteration
A = B*H;
ks = 5/6;
Iz = B^3*H/12;
step = 0.01;
i = 0;
for f0 = fmin:step:fmax
    w = 2*pi*f0;
    b2 = A*L^4*p*w^2/(E*Iz);
    r2 = Iz/(A*L^2);
    fi = ks*A*G;
    s2 = (E*Iz)/(fi*L^2);
    p2 = -((L^2*S)/(E*Iz));
    delta = p2/b2+r2*(1-p2*s2)+s2;
    m1 = (sqrt(b2)*sqrt(sqrt((4*(1-p2*s2)*(1-b2*r2*s2))/b2+delta^2)-
        delta))/sqrt(2*(1-p2*s2));
    m2 = (sqrt(b2)*sqrt(sqrt((4*(1-p2*s2)*(1-b2*r2*s2))/b2+delta^2)+
        delta))/sqrt(2*(1-p2*s2));
    H = (b2*s2+m1^2*(1-p2*s2))/(L*m1);
    Z = (m2^2*(1-p2*s2)-b2*s2)/(L*m2);
    c1 = sinh(m1);
    c2 = cosh(m1);

```

---

```

c3 = sin(m2);
c4 = cos(m2);

M = [-k1      -fi*H+fi*m1/L+m1*S/L      -k1      -fi*Z+fi*m2/L+m2*S/L;
      k3*c2-fi*H*c1+fi*m1*c1/L+m1*S*c1/L      -fi*H*c2+fi*m1*c2/L+m1*S*c2/L+k3*c1
      k3*c4+fi*Z*c3-fi*m2*c3/L-m2*S*c3/L      -fi*Z*c4+fi*m2*c4/L+m2*S*c4/L+k3*c3;
      -E*Iz*H*m1/L      H*k2      E*Iz*Z*m2/L      Z*k2;
      -E*Iz*H*m1*c2/L-H*k4*c1      -E*Iz*H*m1*c1/L-H*k4*c2
      E*Iz*Z*m2*c4/L+Z*k4*c3      E*Iz*Z*m2*c3/L-Z*k4*c4];

Det = det(M);

i=i+1;
result(i,1) = f0;
result(i,2) = Det;
sig(i) = sign(Det);
end
sig = sig';
for i=1:length(sig)-1
    diff = sig(i)-sig(i+1);
    if diff==0
        continue
    else break
end
end
%%Print output in [Hz]
if i == (fmax-fmin)/step
    output = 'change frequency range'
elseif abs(result(i,2)) < abs(result(i+1,2))
    f = result(i,1)
else f = result(i+1,1)
end
end

```

### 11.1.2 Calculation of longitudinal E-moduli

After the data from the measurements is imported, the time signals are transformed into frequency data from which the first two resonance frequencies are extracted. These are then used to calculate the dynamic longitudinal E-moduli for the according specimen. The input and output power spectra are plotted along with the frequency response function and the coherence function. The output of the program is the two frequencies and the according E-moduli.

---

```

%%Remove all variables from the workspace, clear command window and
close
%%open windows

clc

clear all

close all

%%File import

[filename, pathname] = uigetfile('*.txt', 'Pick an Input File');

infile=[pathname filename];

importfile(infile)

clear('colheaders');

clear('textdata');

%%Variable declaration

s=data(:,1);           %%time vector
V=data(:,2);           %%input signal
Vl=data(:,3);          %%output signal

specnum = sscanf(filename,'T%f'); %%specimen number for density

SR = 10240;            %%Sampling rate

%%Densities of the 32 specimen in kg/m3

M = [527.7
     511.7
     485.6
     496.5
     515.0
     497.0
     483.6
     466.5
     511.5
     505.4
     532.8
     522.2
     511.7
     464.8
     500.8
     493.0
     447.5
     494.0
     462.0
     460.7
     488.6
     484.1
     460.4
     507.4
     501.3
     465.0
     479.0
     517.1
     447.5
     459.7

```

---

```

    462.2
    471.4];

%%Density extraction

p = M(specnum);

%%Geometry

L=1.5;                                %%Length in m

%%FFT into spectra

[x0,f] = pwelch(V,[ ],[ ],[ ],SR);

[x1,f] = pwelch(V1,[ ],[ ],[ ],SR);

%%Estimation of FRF

[x2,f] = tfestimate(V,V1,[ ],[ ],[ ],SR);

%%Estimation of Coherence function

[x3,f] = mscohere(V,V1,[ ],[ ],[ ],SR);

%%Logging for semi-logarithmic plot

P0=log(x0);

P1=log(x1);

P2=real(log(x2));

P3=real(log(x3));

%%Deleting of initial peaks

P0(1:20)=0;

P1(1:20)=0;

P2(1:20)=0;

P3(1:20)=0;

%%Plotting of input and output spectra, FRF and Coherence function

figure('Color',[1 1 1]);

plot(f,P0);

xlim([0 4200]);

title(['Specimen N°',num2str(specnum),' : Input Power Spectrum']);

xlabel('Frequency [Hz]');

ylabel('Amplitude [dB]');

figure('Color',[1 1 1]);

plot(f,P1);

```

---

```

xlim([0 4200]);

title(['Specimen No', num2str(specnum), ': Output Power Spectrum']);

xlabel('Frequency [Hz]');

ylabel('Amplitude [dB]');

figure('Color',[1 1 1]);

plot(f,P3);

xlim([0 4200]);

title(['Specimen No', num2str(specnum), ': Coherence Function']);

xlabel('Frequency [Hz]');

ylabel('Magnitude [-]');

%%Peak identification for first two frequencies
%%For some specimens, the Minpeakdistance needs to be adjusted

[PKS,LOCS] = findpeaks(P2,'SORTSTR','descend','MINPEAKDISTANCE',400);

for i=1:2

    peaks(i,1) = LOCS(i);

    peaks(i,2) = PKS(i);

end

peaks_sort = sortrows(peaks,1);

f1l=f(peaks_sort(1,1));

b1=P2(peaks_sort(1,1));

f2l=f(peaks_sort(2,1));

b2=P2(peaks_sort(2,1));

%%Printing frequencies

f1l=roundn(f1l,0)

f2l=roundn(f2l,0)

%%Marking of the identified frequencies

figure('Color',[1 1 1]);

plot(f,P2);

xlim([0 4200]);

title(['Specimen No', num2str(specnum), ': Frequency Response
Function']);

xlabel('Frequency [Hz]');

ylabel('Amplitude [dB]');

```

---

```

hold on;

plot(f11,b1+0.05,'k^','markerfacecolor','r');
plot(f21,b2+0.05,'k^','markerfacecolor','r');

text(f11-40,b1+0.3,num2str(f11));
text(f21-40,b2+0.3,num2str(f21));

hold off;

%%Calculation of E-modulus using Euler theory
E1_Euler=round(4*f11^2*L^2*p/(1^2)*10^(-6));
E2_Euler=round(4*f21^2*L^2*p/(2^2)*10^(-6));

%%Print E
E1_Euler
E2_Euler

%%Create output file
fid = fopen('Output.out','w');
fprintf(fid,'%g\n',specnum);
fprintf(fid,'%g\n',f11);
fprintf(fid,'%g\n',f21);
fprintf(fid,'%g\n',E1_Euler);
fprintf(fid,'%g\n',E2_Euler);

%%Plot FRF and Coherence
plotyy(f,P2,f,P3)
[AX,H1,H2] = plotyy(f,P2,f,P3,'plot');
set(get(AX(1),'Ylabel'),'String','Amplitude [dB]');
set(get(AX(2),'Ylabel'),'String','Magnitude [-]');
xlabel('Frequency [Hz]');

title(['Specimen N°',num2str(specnum),' : FRF and Coherence
Function']);

set(AX(1),'XLim',[0 4200]);
set(AX(2),'XLim',[0 4200]);

hold on;

plot(f11,b1+0.05,'k^','markerfacecolor','r');
plot(f21,b2+0.05,'k^','markerfacecolor','r');

```

---

```
text(f1l-40,b1+0.3,num2str(f1l));  
text(f2l-40,b2+0.3,num2str(f2l));  
hold off;
```

### 11.1.3 Calculation of transversal E-moduli

This script works very similar than the one for longitudinal frequencies. It is however distinguished between transversal and torsional frequencies. Also additional functions need to be used to calculate the different material properties. The output is the measured transversal and torsional frequencies as well as the calculated E- and G-moduli according to Euler and Timoshenko theory.

```
%%Remove all variables from the workspace, clear command window and  
%%close open windows  
  
clc  
  
clear all  
  
close all  
  
%%File import  
[filename, pathname] = uigetfile('*.txt', 'Pick an Input File');  
infile=[pathname filename];  
importfile(infile)  
clear('colheaders');  
clear('textdata');  
  
%%Variable declaration  
s=data(:,1); %%time vector  
V=data(:,2); %%input signal  
V2=data(:,4); %%output signal at the edge  
specnum = sscanf(filename,'T%f') %%specimen number for density  
SR=2560; %%Sampling rate  
NFFT=2^16; %%Number of FFT points  
  
%%Densities of the 32 specimen  
M = [527.7  
511.7  
485.6  
496.5  
515.0  
497.0  
483.6  
466.5
```

```

511.5
505.4
532.8
522.2
511.7
464.8
500.8
493.0
447.5
494.0
462.0
460.7
488.6
484.1
460.4
507.4
501.3
465.0
479.0
517.1
447.5
459.7
462.2
471.4];

```

```
%%Density extraction
```

```
p = M(specnum);
```

```
%%Geometry
```

```
L=1.5; %%Length in m
```

```
H=0.075; %%Height in m
```

```
B=0.035; %%Width in m
```

```
A=B*H;
```

```
ks=5/6;
```

```
Iy=B*H^3/12;
```

```
Iz=B^3*H/12;
```

```
Ip=Iy+Iz;
```

```
Kt=H*B^3/3*(1-0.630*B/H+0.052*B^5/H^5);
```

```
%%FFT into spectra
```

```
[x0,f] = pwelch(V,[ ],[ ],NFFT,SR);
```

```
[x2,f] = pwelch(V2,[ ],[ ],NFFT,SR);
```

```
%%Estimation of FRF
```

```
[x4,f] = tfestimate(V,V2,[ ],[ ],NFFT,SR);
```

```
%%Estimation of Coherence function
```

```
[x5,f] = mscohere(V,V2,[ ],[ ],NFFT,SR);
```

```
%%Logging for semi-logarithmic plot
```

---

```

P0=log(x0);
P2=log(x2);
P4=real(log(x4));
P5=log(x5);

%%Reducing data to the deserved range

P0(1:20)=0;
P2(1:20)=0;
P4(1:50)=0;
P4(18049:32769)=0;
P5(1:20)=0;

%%Plotting of input and output spectra, FRF and Coherence function

figure('Color',[1 1 1]);
plot(f,P0);
xlim([0 700]);
title(['Specimen N∞',num2str(specnum),' : Input Power Spectrum']);
xlabel('Frequency [Hz]');
ylabel('Amplitude [dB]');

figure('Color',[1 1 1]);
plot(f,P2);
xlim([0 700]);
title(['Specimen N∞',num2str(specnum),' : Output Power Spectrum']);
xlabel('Frequency [Hz]');
ylabel('Amplitude [dB]');

figure('Color',[1 1 1]);
plot(f,P5);
xlim([0 700]);
title(['Specimen N∞',num2str(specnum),' : Coherence Function']);
xlabel('Frequency [Hz]');
ylabel('Magnitude [-]');

%%Peak identification for first four bending frequencies
%%For some specimens, the Minpeakdistance needs to be adjusted

[PKSb,LOCSb] =
    findpeaks(P4,'SORTSTR','descend','MINPEAKDISTANCE',300);

```

---

```

for i=1:6
    peaksb(i,1) = LOCSb(i);
    peaksb(i,2) = PKSb(i);
end
peaksb_sort = sortrows(peaksb,1);
f1b=f(peaksb_sort(1,1));
b1=P4(peaksb_sort(1,1));
f2b=f(peaksb_sort(2,1));
b2=P4(peaksb_sort(2,1));
f3b=f(peaksb_sort(4,1));
b3=P4(peaksb_sort(4,1));

%%Peak identification for first two torsional frequency
%%For some specimens, the Minpeakdistance needs to be adjusted

[PKSt,LOCSt] =
    findpeaks(P4,'SORTSTR','descend','MINPEAKDISTANCE',500);

for i=1:6
    peakst(i,1) = LOCSt(i);
    peakst(i,2) = PKSt(i);
end
peakst_sort = sortrows(peakst,1);
f1t=f(peakst_sort(3,1));
t1=P4(peakst_sort(3,1));
f2t=f(peakst_sort(5,1));
t2=P4(peakst_sort(5,1));

%%Printing frequencies
f1b=roundn(f1b,-1)
f2b=roundn(f2b,-1)
f3b=roundn(f3b,-1)
f1t=roundn(f1t,-1)
f2t=roundn(f2t,-1)

%%Calculation of G-modulus using Euler theory
G1_Euler=round(4*f1t^2*L^2*p*Ip/(Kt*1^2)*10^(-6));

```

---

```

G2_Euler=round(4*f2t^2*L^2*p*Ip/(Kt*2^2)*10^(-6));
Gm=(G1_Euler+G2_Euler)/2;
%%Calculation of flexural E-modulus using Euler theory
E1_Euler=Euler_b(f1b,p,A,Iz,L);
E2_Euler=Euler_b(f2b,p,A,Iz,L);
E3_Euler=Euler_b(f3b,p,A,Iz,L);
%%Calculation of flexural E-modulus using Timoshenko theory with Gm
E1_Timo=Timo_b(f1b,p,G1_Euler,A,ks,Iz,L);
E2_Timo=Timo_b(f2b,p,G1_Euler,A,ks,Iz,L);
E3_Timo=Timo_b(f3b,p,G1_Euler,A,ks,Iz,L);
%%Print G and E
G1_Euler
G2_Euler
E1_Euler
E2_Euler
E3_Euler
E1_Timo
E2_Timo
E3_Timo
%%Plot of FRF and Coherence
figure('Color',[1 1 1]);
plotyy(f,P4,f,P5)
[AX,H1,H2] = plotyy(f,P4,f,P5,'plot');
set(get(AX(1),'Ylabel'),'String','Amplitude [dB]')
set(get(AX(2),'Ylabel'),'String','Magnitude [-]')
xlabel('Frequency [Hz]');
title(['Specimen N°',num2str(specnum),': FRF and Coherence
Function']);
set(AX(1),'XLim',[0 700]);
set(AX(2),'XLim',[0 700]);
hold on;
%%Marking of the identified frequencies

```

---

```

plot(f1b,b1+0.05,'k^','markerfacecolor','r');
plot(f2b,b2+0.05,'k^','markerfacecolor','r');
plot(f3b,b3+0.05,'k^','markerfacecolor','r');
plot(f1t,t1+0.05,'k^','markerfacecolor','g');
plot(f2t,t2+0.05,'k^','markerfacecolor','g');

text(f1b-40,b1+0.3,num2str(f1b));
text(f2b-40,b2+0.3,num2str(f2b));
text(f3b-40,b3+0.3,num2str(f3b));
text(f1t-40,t1+0.3,num2str(f1t));
text(f2t-40,t2+0.3,num2str(f2t));

hold off

%%%%%%%%%%%%%%%%%%%%%%%%%%%%%%%%%%%%%%%%%%%%%%%%%%%%%%%%%%%%%%%%%%%%%%%%%%%%%%
%%%%%%%%%%%%%%%%%%%%%%%%%%%%%%%%%%%%%%%%%%%%%%%%%%%%%%%%%%%%%%%%%%%%%%%%%%%%%%

function E = Euler_b(f,p,A,Iz,L)

%%Definition of the range for E

Emin = 8000;
Emax = 20000;

%%Calculation

w = 2*pi*f;
i = 0;

for E0 = Emin:Emax

    E0 = E0*10^6;

    a = E0*Iz;

    b = 0;

    c = -A*p*w^2;

    l1 = sqrt(sqrt((-b/(2*a)))^2-c/a)-b/(2*a);
    l2 = sqrt(sqrt((-b/(2*a)))^2-c/a)+b/(2*a);

    c1 = sinh(L*l1);
    c2 = cosh(L*l1);
    c3 = sin(L*l2);
    c4 = cos(L*l2);

    M = [-(a*l2^3-b*l2)    0    a*l1^3+b*l1    0;
          0    -a*l2^2    0    a*l1^2;
          -c4*(a*l2^3-b*l2)    c3*(a*l2^3-b*l2)    c2*(a*l1^3+b*l1)

```

---

```

        c1*(a*l1^3+b*l1);
        -a*c3*l2^2    -a*c4*l2^2    a*c1*l1^2    a*c2*l1^2];

    Det = det(M);

    i=i+1;

    result(i,1) = E0*10^(-6);

    result(i,2) = Det;

    sig(i) = sign(Det);

end

sig = sig';

for i=1:length(sig)-1
    diff = sig(i)-sig(i+1);
    if diff==0
        continue
    else break
    end
end

if abs(result(i,2)) < abs(result(i+1,2))
    E = result(i,1);
else E = result(i+1,1);
end

%%%%%%%%%%%%%%%%%%%%%%%%%%%%%%%%%%%%%%%%%%%%%%%%%%%%%%%%%%%%%%%%%%%%%%%%%%
%%%%%%%%%%%%%%%%%%%%%%%%%%%%%%%%%%%%%%%%%%%%%%%%%%%%%%%%%%%%%%%%%%%%%%%%%%

function E = Timo_b(f,p,G,A,ks,Iz,L)

%%Definition of range for E

Emin = 8000;

Emax = 20000;

%%Calculation

G = G*10^6;

S = 0;

ka = 0;

k = 0;

w = 2*pi*f;

i = 0;

for E0 = Emin:Emax

```

---

```

E0 = E0*10^6;
b2 = A*L^4*p*w^2/(E0*Iz);
r2 = Iz/(A*L^2);
fi = ks*A*G;
s2 = (E0*Iz)/(fi*L^2);
p2 = -(L^2*S)/(E0*Iz);
delta = p2/b2+r2*(1-p2*s2)+s2;
m1 = (sqrt(b2)*sqrt(sqrt((4*(1-p2*s2)*(1-b2*r2*s2))/b2+delta^2)-
delta))/sqrt(2*(1-p2*s2));
m2 = (sqrt(b2)*sqrt(sqrt((4*(1-p2*s2)*(1-
b2*r2*s2))/b2+delta^2)+delta))/sqrt(2*(1-p2*s2));
H = (b2*s2+m1^2*(1-p2*s2))/(L*m1);
Z = (m2^2*(1-p2*s2)-b2*s2)/(L*m2);
c1 = sinh(m1);
c2 = cosh(m1);
c3 = sin(m2);
c4 = cos(m2);
M = [-ka -fi*H+fi*m1/L+m1*S/L -ka -fi*Z+fi*m2/L+m2*S/L;
ka*c2-fi*H*c1+fi*m1*c1/L+m1*S*c1/L
-fi*H*c2+fi*m1*c2/L+m1*S*c2/L+ka*c1
ka*c4+fi*Z*c3-fi*m2*c3/L-m2*S*c3/L
-fi*Z*c4+fi*m2*c4/L+m2*S*c4/L+ka*c3;
-E0*Iz*H*m1/L H*k E0*Iz*Z*m2/L Z*k;
-E0*Iz*H*m1*c2/L-H*k*c1 -E0*Iz*H*m1*c1/L-H*k*c2
E0*Iz*Z*m2*c4/L+Z*k*c3 E0*Iz*Z*m2*c3/L-Z*k*c4];
Det = det(M);
i=i+1;
result(i,1) = E0*10^(-6);
result(i,2) = Det;
sig(i) = sign(Det);
end
sig = sig';
for i=1:length(sig)-1
diff = sig(i)-sig(i+1);
if diff==0
continue

```

---

```

else break
end
end
if abs(result(i,2)) < abs(result(i+1,2))
    E = result(i,1);
else E = result(i+1,1);
end

```

## 11.1.4 Dual parameter estimation

### Extraction of frequencies

This program extracts the frequencies from the tensile tests. It works in the same way as the one for the free-free tests. Furthermore the input and output spectra as well as the frequency response and coherence function are depicted.

```

%%Remove all variables from the workspace, clear command window and
%%close open windows

clc

clear all

close all

%%File import

[filename, pathname] = uigetfile('*.txt', 'Pick an Input File');

infile=[pathname filename];

importfile(infile)

clear('colheaders');

clear('textdata');

%%Variable declaration

s=data(:,1);    %%time vector

V=data(:,2);    %%input signal

V1=data(:,3);   %%output signal at the edge

testnumber = sscanf(filename, 'T%f_%f');    %%specimen number and load
level

specnum = testnumber(1)

level = testnumber(2)

SR=2560; %%Sampling rate

```

---

```

NFFT=2^16; %%Number of FFT points

%%FFT into spectra and Windowing using Welch method
[x0,f] = pwelch(V,[ ],[ ],NFFT,SR);
[x1,f] = pwelch(V1,[ ],[ ],NFFT,SR);

%%Estimation of FRF
[x2,f] = tfestimate(V,V1,[ ],[ ],NFFT,SR);

%%Estimation of Coherence function
[x3,f] = mscohere(V,V1,[ ],[ ],NFFT,SR);

%%Logging for semi-logarithmic plot
P0=log(x0);
P1=log(x1);
P2=real(log(x2));
P3=log(x3);
P2(1:20)=0;
P2(18049:32769)=0;
P3(18049:32769)=0;

%%Plotting of input and output spectra
figure('Color',[1 1 1]);
plot(f,P0);
xlim([0 700]);
title(['Specimen N∞',num2str(specnum),' : Input Power Spectrum']);
xlabel('Frequency [Hz]');
ylabel('Amplitude [dB]');

figure('Color',[1 1 1]);
plot(f,P1);
xlim([0 700]);
title(['Specimen N∞',num2str(specnum),' : Output Power Spectrum']);
xlabel('Frequency [Hz]');
ylabel('Amplitude [dB]');

%%Peak identification for first three bending frequencies
%%For some specimens, the Minpeakdistance needs to be adjusted

[PKSb,LOCSb] =
    findpeaks(P2,'SORTSTR','descend','MINPEAKDISTANCE',1700);

```

---

```

for i=1:5
    peaksb(i,1) = LOCSb(i);
    peaksb(i,2) = PKSb(i);
end
peaksb_sort = sortrows(peaksb,1);
f1b=f(peaksb_sort(1,1));
b1=P2(peaksb_sort(1,1));
f2b=f(peaksb_sort(2,1));
b2=P2(peaksb_sort(2,1));
f3b=f(peaksb_sort(4,1));
b3=P2(peaksb_sort(4,1));

%%Printing frequencies
f1b=roundn(f1b,-1)
f2b=roundn(f2b,-1)
f3b=roundn(f3b,-1)

%%Plot of FRF and Coherence
figure('Color',[1 1 1]);
plotyy(f,P2,f,P3)
[AX,H1,H2] = plotyy(f,P2,f,P3,'plot');
set(get(AX(1),'Ylabel'),'String','Amplitude [dB]')
set(get(AX(2),'Ylabel'),'String','Magnitude [-]')
xlabel('Frequency [Hz]');
title(['Specimen N°',num2str(specnum),' : FRF and Coherence Function
      S = ',num2str(level),' N']);
set(AX(1),'XLim',[0 700]);
set(AX(2),'XLim',[0 700]);
hold on;

%%Marking of the identified frequencies
plot(f1b,b1+0.05,'k^','markerfacecolor','r');
plot(f2b,b2+0.05,'k^','markerfacecolor','r');
plot(f3b,b3+0.05,'k^','markerfacecolor','r');
text(f1b-40,b1+0.3,num2str(f1b));

```

---

```
text(f2b-40,b2+0.3,num2str(f2b));
```

```
text(f3b-40,b3+0.3,num2str(f3b));
```

```
hold off
```

## Parameter estimation

This script uses the entered frequencies to estimate the axial load  $S$  and the rotational stiffness  $k$  at the supports assuming equal boundary conditions. This is done by using each frequency to calculate  $S$  for a range of different  $k$ . The results are two curves of which the crossing point is searched, which finally yields the result for the two unknown parameters. The two curves together with the solutions are depicted.

```
%%Remove all variables from the workspace, clear command window and  
%%close open windows
```

```
clear all
```

```
close all
```

```
clc
```

```
%%Enter input data
```

```
f1 = 134.3; %%First measured frequency
```

```
f2 = 336.7; %%Second measured frequency
```

```
E = 16805*10^6; %%E-modulus in N/m2
```

```
G = 789*10^6; %%G-modulus in N/m2
```

```
p = 527.7; %%Specimen density in kg/m3
```

```
L = 1.255; %%Clear length in m
```

```
H = 0.075; %%Specimen height in m
```

```
B = 0.035; %%Specimen width in m
```

```
ka = 10^15; %%Value for translational support in x=0 in N/m
```

```
%%Definition of range for S and k
```

```
Smin = 0;
```

```
Smax = 1000000;
```

```
kmin = 0;
```

```
kmax = 750000;
```

```
%%Iteration
```

```
A = B*H;
```

```
ks = 5/6;
```

---

```

Iz = B^3*H/12;
iii=1;
n = 150;
diffk = kmax-kmin;
kount = 0;
while diffk > 0.1
%%Approximation of S1
dk = (kmax-kmin)/n;
for j = 1:(n+1)
    k0 = kmin+dk*(j-1);
    resultk(j) = k0;
    count = 0;
    dS = (Smax-Smin)/n;
    for i=1:(n+1)
        S0 = Smin+dS*(i-1);
        b2 = A*L^4*p*(2*pi*f1)^2/(E*Iz);
        r2 = Iz/(A*L^2);
        fi = ks*A*G;
        s2 = (E*Iz)/(fi*L^2);
        p2 = -((L^2*S0)/(E*Iz));
        delta = p2/b2+r2*(1-p2*s2)+s2;
        m1 = (sqrt(b2)*sqrt(sqrt((4*(1-p2*s2)*(1-
            b2*r2*s2))/b2+delta^2)-delta))/sqrt(2*(1-p2*s2));
        m2 = (sqrt(b2)*sqrt(sqrt((4*(1-p2*s2)*(1-
            b2*r2*s2))/b2+delta^2)+delta))/sqrt(2*(1-p2*s2));
        H = (b2*s2+m1^2*(1-p2*s2))/(L*m1);
        Z = (m2^2*(1-p2*s2)-b2*s2)/(L*m2);
        c1 = sinh(m1);
        c2 = cosh(m1);
        c3 = sin(m2);
        c4 = cos(m2);
        M = [-ka    -fi*H+fi*m1/L+m1*S0/L    -ka
            -fi*Z+fi*m2/L+m2*S0/L;
            ka*c2-fi*H*c1+fi*m1*c1/L+m1*S0*c1/L

```

```

        -fi*H*c2+fi*m1*c2/L+m1*S0*c2/L+ka*c1
        ka*c4+fi*Z*c3-fi*m2*c3/L-m2*S0*c3/L -
        fi*Z*c4+fi*m2*c4/L+m2*S0*c4/L+ka*c3;
    -E*Iz*H*m1/L    H*k0    E*Iz*Z*m2/L    Z*k0;
    -E*Iz*H*m1*c2/L-H*k0*c1    -E*Iz*H*m1*c1/L-H*k0*c2
        E*Iz*Z*m2*c4/L+Z*k0*c3    E*Iz*Z*m2*c3/L-Z*k0*c4];

    Det = det(M);

    sig = sign(Det);

    if count == 1

        change = sig/prevsig;

        if change <= 0

            force(1,1) = prevS;

            force(1,2) = S0;

            break

        end
    end

    prevS = S0;

    prevsig = sig;

    count = 1;

end

error = 0.1;

Smin1 = force(1,1);

Smax1 = force(1,2);

diff = Smax1-Smin1;

while diff > error

    count = 0;

    dS1 = (Smax1-Smin1)/n;

    for i=1:(n+1)

        S0 = Smin1+dS1*(i-1);

        b2 = A*L^4*p*(2*pi*f1)^2/(E*Iz);

        r2 = Iz/(A*L^2);

        fi = ks*A*G;

        s2 = (E*Iz)/(fi*L^2);

        p2 = -((L^2*S0)/(E*Iz));

        delta = p2/b2+r2*(1-p2*s2)+s2;

```

```

m1 = (sqrt(b2)*sqrt(sqrt((4*(1-p2*s2)*(1-
b2*r2*s2))/b2+delta^2)-delta))/sqrt(2*(1-p2*s2));

m2 = (sqrt(b2)*sqrt(sqrt((4*(1-p2*s2)*(1-
b2*r2*s2))/b2+delta^2)+delta))/sqrt(2*(1-p2*s2));

H = (b2*s2+m1^2*(1-p2*s2))/(L*m1);

Z = (m2^2*(1-p2*s2)-b2*s2)/(L*m2);

c1 = sinh(m1);

c2 = cosh(m1);

c3 = sin(m2);

c4 = cos(m2);

M = [-ka      -fi*H+fi*m1/L+m1*S0/L      -ka
      -fi*Z+fi*m2/L+m2*S0/L;
      ka*c2-fi*H*c1+fi*m1*c1/L+m1*S0*c1/L
      -fi*H*c2+fi*m1*c2/L+m1*S0*c2/L+ka*c1
      ka*c4+fi*Z*c3-fi*m2*c3/L-m2*S0*c3/L      -
      fi*Z*c4+fi*m2*c4/L+m2*S0*c4/L+ka*c3;
      -E*Iz*H*m1/L      H*k0      E*Iz*Z*m2/L      Z*k0;
      -E*Iz*H*m1*c2/L-H*k0*c1      -E*Iz*H*m1*c1/L-H*k0*c2
      E*Iz*Z*m2*c4/L+Z*k0*c3      E*Iz*Z*m2*c3/L-Z*k0*c4];

Det = det(M);

sig = sign(Det);

if count == 1

    change = sig/prevsig;

    if change <= 0

        force(1,1) = prevS;

        force(1,2) = S0;

        break

    end
end

prevS = S0;

prevsig = sig;

count = 1;

end

Smin1 = force(1,1);

Smax1 = force(1,2);

diff = Smax1-Smin1;

end

resultS1(j) = Smin1;

```

---

```

end

resultk = resultk';
resultS1 = resultS1';

figure(1);

scatter(resultk,resultS1,'o');

hold on;

%%End of Approximation of S1

%%Approximation of S2

dk = (kmax-kmin)/n;

for j = 1:(n+1)

    k0 = kmin+dk*(j-1);

    resultk(j) = k0;

    count = 0;

    dS = (Smax-Smin)/n;

    for i=1:(n+1)

        S0 = Smin+dS*(i-1);

        b2 = A*L^4*p*(2*pi*f2)^2/(E*Iz);

        r2 = Iz/(A*L^2);

        fi = ks*A*G;

        s2 = (E*Iz)/(fi*L^2);

        p2 = -(L^2*S0)/(E*Iz);

        delta = p2/b2+r2*(1-p2*s2)+s2;

        m1 = (sqrt(b2)*sqrt(sqrt((4*(1-p2*s2)*(1-
            b2*r2*s2))/b2+delta^2)-delta))/sqrt(2*(1-p2*s2));

        m2 = (sqrt(b2)*sqrt(sqrt((4*(1-p2*s2)*(1-
            b2*r2*s2))/b2+delta^2)+delta))/sqrt(2*(1-p2*s2));

        H = (b2*s2+m1^2*(1-p2*s2))/(L*m1);

        Z = (m2^2*(1-p2*s2)-b2*s2)/(L*m2);

        c1 = sinh(m1);

        c2 = cosh(m1);

        c3 = sin(m2);

        c4 = cos(m2);

```

---

```

M = [-ka    -fi*H+fi*m1/L+m1*S0/L    -ka
      -fi*Z+fi*m2/L+m2*S0/L;
      ka*c2-fi*H*c1+fi*m1*c1/L+m1*S0*c1/L
      -fi*H*c2+fi*m1*c2/L+m1*S0*c2/L+ka*c1
      ka*c4+fi*Z*c3-fi*m2*c3/L-m2*S0*c3/L    -
      fi*Z*c4+fi*m2*c4/L+m2*S0*c4/L+ka*c3;
      -E*Iz*H*m1/L    H*k0    E*Iz*Z*m2/L    Z*k0;
      -E*Iz*H*m1*c2/L-H*k0*c1    -E*Iz*H*m1*c1/L-H*k0*c2
      E*Iz*Z*m2*c4/L+Z*k0*c3    E*Iz*Z*m2*c3/L-Z*k0*c4];

Det = det(M);

sig = sign(Det);

if count == 1

    change = sig/prevsig;

    if change <= 0

        force(1,1) = prevS;

        force(1,2) = S0;

        break

    end

end

prevS = S0;

prevsig = sig;

count = 1;

end

error = 0.1;

Smin1 = force(1,1);

Smax1 = force(1,2);

diff = Smax1-Smin1;

while diff > error

    count = 0;

    dS1 = (Smax1-Smin1)/n;

    for i=1:(n+1)

        S0 = Smin1+dS1*(i-1);

        b2 = A*L^4*p*(2*pi*f2)^2/(E*Iz);

        r2 = Iz/(A*L^2);

        fi = ks*A*G;

        s2 = (E*Iz)/(fi*L^2);

        p2 = -(L^2*S0)/(E*Iz);

```

---

```

delta = p2/b2+r2*(1-p2*s2)+s2;

m1 = (sqrt(b2)*sqrt(sqrt((4*(1-p2*s2)*(1-
b2*r2*s2))/b2+delta^2)-delta))/sqrt(2*(1-p2*s2));

m2 = (sqrt(b2)*sqrt(sqrt((4*(1-p2*s2)*(1-
b2*r2*s2))/b2+delta^2)+delta))/sqrt(2*(1-p2*s2));

H = (b2*s2+m1^2*(1-p2*s2))/(L*m1);

Z = (m2^2*(1-p2*s2)-b2*s2)/(L*m2);

c1 = sinh(m1);

c2 = cosh(m1);

c3 = sin(m2);

c4 = cos(m2);

M = [-ka      -fi*H+fi*m1/L+m1*S0/L      -ka
      -fi*Z+fi*m2/L+m2*S0/L;
      ka*c2-fi*H*c1+fi*m1*c1/L+m1*S0*c1/L
      -fi*H*c2+fi*m1*c2/L+m1*S0*c2/L+ka*c1
      ka*c4+fi*Z*c3-fi*m2*c3/L-m2*S0*c3/L      -
      fi*Z*c4+fi*m2*c4/L+m2*S0*c4/L+ka*c3;
      -E*Iz*H*m1/L      H*k0      E*Iz*Z*m2/L      Z*k0;
      -E*Iz*H*m1*c2/L-H*k0*c1      -E*Iz*H*m1*c1/L-H*k0*c2
      E*Iz*Z*m2*c4/L+Z*k0*c3      E*Iz*Z*m2*c3/L-Z*k0*c4];

Det = det(M);

sig = sign(Det);

if count == 1

    change = sig/prevsig;

    if change <= 0

        force(1,1) = prevS;

        force(1,2) = S0;

        break

    end

end

prevS = S0;

prevsig = sig;

count = 1;

end

Smin1 = force(1,1);

Smax1 = force(1,2);

diff = Smax1-Smin1;

```

---

```

end
resultS2(j) = Smin1;
end
resultk = resultk';
resultS2 = resultS2';
scatter(resultk,resultS2,'x');
%%End of Approximation of S2
%%Determination of crossing point
diffS = resultS2-resultS1;
signdiff = sign(diffS);
[Y,I] = min(abs(diffS));
if diffS == 0
    kfin = resultk(I);
    Sfin = resultS1(I);
end
if signdiff(I) == signdiff(I+1)
    kmin = resultk(I-1);
    kmax = resultk(I);
    Smin = resultS2(I+1);
    Smax = resultS2(I-2);
else
    kmin = resultk(I);
    kmax = resultk(I+1);
    Smin = resultS2(I+2);
    Smax = resultS2(I-1);
end
diffk = kmax-kmin;
if kount == 0
    resultkplot = resultk;
    resultS1plot = resultS1;
    resultS2plot = resultS2;

```

---

```
end

kount = kount+1;

end

%%Plot of iteration curves

figure(2)

plot(resultkplot.*0.001,resultS1plot.*0.001,'Color',[0 0 1])

hold on

plot(resultkplot.*0.001,resultS2plot.*0.001,'Color',[0
0.498039215803146 0])

scatter(kmin.*0.001,Smax.*0.001,'filled','red')

plot(0:0.1:kmin.*0.001,Smax.*0.001)

plot(kmin.*0.001,0:0.1:Smax.*0.001)

title(['Reference Aluminium Specimen S = 1245 N']);

xlabel('Rotational stiffness k [kNm]');

ylabel('Axial load S [kN]');

legend('f1','f2');

%%Print results

kmin

Smax
```

---

## 11.2 Appendix B – Material properties

### 11.2.1 Density measurements

#### Data

Table 11-1 Weights and densities of the specimen

Beam N°	Weight	$\rho_k$
[-]	[kg]	[kg/m <sup>3</sup> ]
1	2.078	527.7
2	2.015	511.7
3	1.912	485.6
4	1.955	496.5
5	2.028	515.0
6	1.957	497.0
7	1.904	483.6
8	1.837	466.5
9	2.014	511.5
10	1.990	505.4
11	2.098	532.8
12	2.056	522.2
13	2.015	511.7
14	1.830	464.8
15	1.972	500.8
16	1.941	493.0
17	1.762	447.5
18	1.945	494.0
19	1.819	462.0
20	1.814	460.7
21	1.924	488.6
22	1.906	484.1
23	1.813	460.4
24	1.998	507.4
25	1.974	501.3
26	1.831	465.0
27	1.886	479.0
28	2.036	517.1
29	1.762	447.5
30	1.810	459.7
31	1.820	462.2
32	1.856	471.4
	Mean value	488.6
	Std. dev.	24.2
Aluminium	1.976	2643.5

---

## 11.2.2 Moisture measurements

### Data

Table 11-2 *Moisture measurements in three different point and mean moisture contents of the specimen*

Beam N°	w <sub>1</sub>	w <sub>2</sub>	w <sub>3</sub>	w
[-]	[%]	[%]	[%]	[%]
1	12.8	13.2	12.6	12.9
2	12.5	13.0	12.5	12.7
3	11.9	12.9	12.3	12.4
4	12.8	13.5	12.5	12.9
5	12.4	13.8	12.6	12.9
6	11.5	13.1	12.9	12.5
7	12.0	13.0	11.9	12.3
8	12.5	13.1	12.0	12.5
9	12.5	13.3	12.1	12.6
10	12.5	13.6	12.6	12.9
11	12.5	14.0	12.6	13.0
12	12.2	14.0	12.8	13.0
13	13.2	13.6	12.0	12.9
14	12.0	12.6	11.5	12.0
15	12.1	13.5	13.0	12.9
16	13.0	13.2	12.0	12.7
17	12.2	12.5	11.9	12.2
18	13.0	13.1	12.6	12.9
19	12.9	12.5	12.2	12.5
20	11.6	12.4	11.5	11.8
21	13.2	13.1	11.2	12.5
22	13.1	13.5	12.6	13.1
23	13.1	13.2	11.9	12.7
24	13.0	13.3	11.9	12.7
25	12.6	12.9	11.6	12.4
26	11.7	12.1	11.1	11.6
27	9.8	11.0	9.6	10.1
28	13.4	13.6	12.5	13.2
29	12.1	13.1	12.1	12.4
30	11.9	12.7	11.8	12.1
31	12.2	12.5	11.9	12.2
32	11.8	12.4	12.1	12.1
		Mean value	12.5	
		Std. dev.	0.6	

## 11.2.3 Four-point bending tests

### Data

Table 11-3 Results of four-point bending tests

Beam N°	Deflection 1				Deflection 2				Load 1 [N]	Load 2 [N]	E [MPa]
	Supp 1 [mm]	Mid [mm]	Supp 2 [mm]	Tot [mm]	Supp 1 [mm]	Mid [mm]	Supp 2 [mm]	Tot [mm]			
1	0.366	1.295	0.321	0.952	0.408	1.852	0.444	1.426	412.0	606.3	14526
2	0.235	1.372	0.340	1.085	0.272	1.963	0.450	1.602	412.0	606.3	13319
3	0.141	1.467	0.335	1.229	0.175	2.106	0.429	1.804	412.0	606.3	11987
4	0.138	1.393	0.321	1.164	0.172	2.011	0.411	1.720	412.0	606.3	12397
5	0.181	1.359	0.369	1.084	0.216	1.927	0.482	1.578	412.0	606.3	13953
6	0.290	1.364	0.360	1.039	0.359	1.949	0.466	1.537	412.0	606.3	13855
7	0.217	1.495	0.413	1.180	0.259	2.141	0.520	1.752	412.0	606.3	12061
8	0.217	1.448	0.370	1.155	0.278	2.069	0.473	1.694	412.0	606.3	12788
9	0.276	1.401	0.345	1.091	0.320	1.991	0.496	1.583	412.0	606.3	13995
10	0.163	1.323	0.363	1.060	0.199	1.893	0.467	1.560	412.0	606.3	13785
11	0.230	1.261	0.310	0.991	0.272	1.812	0.399	1.477	412.0	606.3	14197
12	0.192	1.342	0.332	1.080	0.234	1.911	0.432	1.578	412.0	606.3	13841
13	0.242	1.398	0.374	1.090	0.285	1.999	0.495	1.609	412.0	606.3	13281
14	0.226	1.400	0.362	1.106	0.268	2.006	0.482	1.631	412.0	606.3	13129
15	0.206	1.385	0.348	1.108	0.247	1.976	0.458	1.624	412.0	606.3	13371
16	0.248	1.381	0.401	1.057	0.292	1.966	0.546	1.547	412.0	606.3	14052
17	0.398	1.687	0.163	1.407	0.437	2.413	0.356	2.017	412.0	606.3	11300
18	0.149	1.375	0.324	1.139	0.188	1.979	0.418	1.676	412.0	606.3	12824
19	0.185	1.814	0.386	1.529	0.255	2.569	0.488	2.198	412.0	606.3	10303
20	0.303	1.563	0.397	1.213	0.344	2.245	0.547	1.800	412.0	606.3	11752
21	0.193	1.477	0.326	1.218	0.270	2.115	0.425	1.768	412.0	606.3	12532
22	0.229	1.408	0.357	1.115	0.278	2.019	0.470	1.645	412.0	606.3	13005
23	0.175	1.433	0.364	1.164	0.214	2.068	0.473	1.725	412.0	606.3	12286
24	0.128	1.400	0.359	1.157	0.171	2.017	0.462	1.701	412.0	606.3	12670
25	0.168	1.321	0.341	1.067	0.210	1.902	0.443	1.576	412.0	606.3	13542
26	0.226	1.481	0.361	1.188	0.288	2.121	0.462	1.746	412.0	606.3	12341
27	0.167	1.689	0.315	1.448	0.218	2.431	0.416	2.114	412.0	606.3	10349
28	0.217	1.423	0.346	1.142	0.260	2.038	0.453	1.682	412.0	606.3	12764
29	0.179	1.370	0.289	1.136	0.219	1.985	0.407	1.672	412.0	606.3	12860
30	0.191	1.696	0.428	1.387	0.220	2.416	0.551	2.031	412.0	606.3	10703
31	0.217	1.528	0.363	1.238	0.268	2.193	0.479	1.820	412.0	606.3	11853
32	0.145	1.548	0.346	1.303	0.178	2.220	0.441	1.911	412.0	606.3	11337
									Mean value		12717
									Std. dev.		1117

---

## 11.2.4 Longitudinal vibration tests

### Data

Table 11-4 Results of the longitudinal tests

Beam N°	$f_{1L}$	$f_{2L}$	$E_{1L}$	$E_{2L}$	$E_{mL}$
[-]	[Hz]	[Hz]	[MPa]	[MPa]	[MPa]
1	1891	3746	16983	16661	16822
2	1793	3528	14805	14330	14568
3	1767	3547	13646	13746	13696
4	1788	3579	14286	14310	14298
5	1788	3555	14818	14644	14731
6	1832	3641	15012	14825	14919
7	1786	3574	13883	13899	13891
8	1779	3539	13288	13146	13217
9	1836	3613	15518	15023	15271
10	1858	3668	15703	15299	15501
11	1793	3573	15416	15304	15360
12	1814	3603	15465	15253	15359
13	1824	3615	15322	15046	15184
14	1846	3707	14255	14371	14313
15	1871	3725	15778	15635	15707
16	1882	3729	15716	15425	15571
17	1749	3436	12320	11887	12104
18	1842	3666	15085	14938	15012
19	1750	3544	12734	13056	12895
20	1776	3536	13078	12961	13020
21	1756	3531	13560	13707	13634
22	1781	3546	13820	13696	13758
23	1789	3603	13262	13448	13355
24	1831	3676	15310	15427	15369
25	1833	3632	15159	14879	15019
26	1784	3534	13319	13067	13193
27	1698	3388	12429	12371	12400
28	1742	3511	14123	14342	14233
29	1902	3778	14570	14371	14471
30	1688	3386	11789	11859	11824
31	1826	3600	13870	13478	13674
32	1786	3578	13533	13579	13556
		Mean value	14308	14187	14247
		Std. dev.	1203	1128	1161
Aluminium	1710	3421	69106	69146	69126

## Correlations

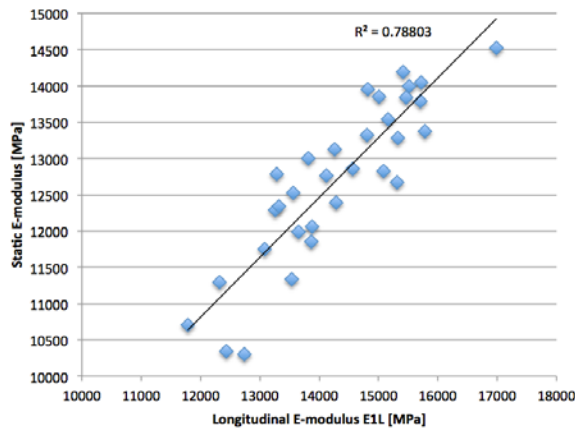


Figure 11-1 Correlation between longitudinal E-modulus found using  $f_{1L}$  and static E-modulus

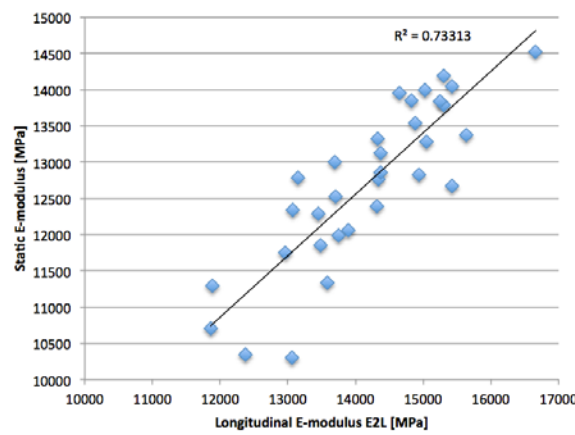


Figure 11-2 Correlation between longitudinal E-modulus found using  $f_{2L}$  and static E-modulus

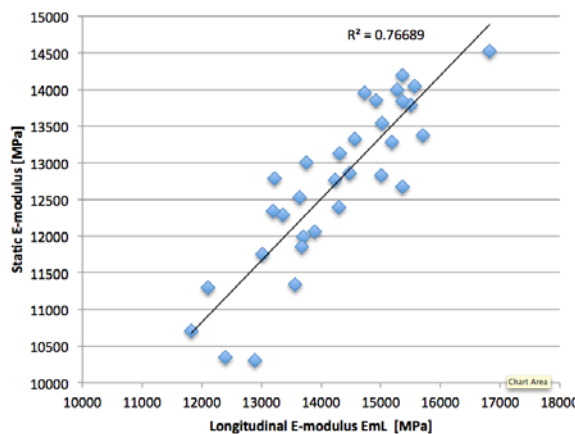
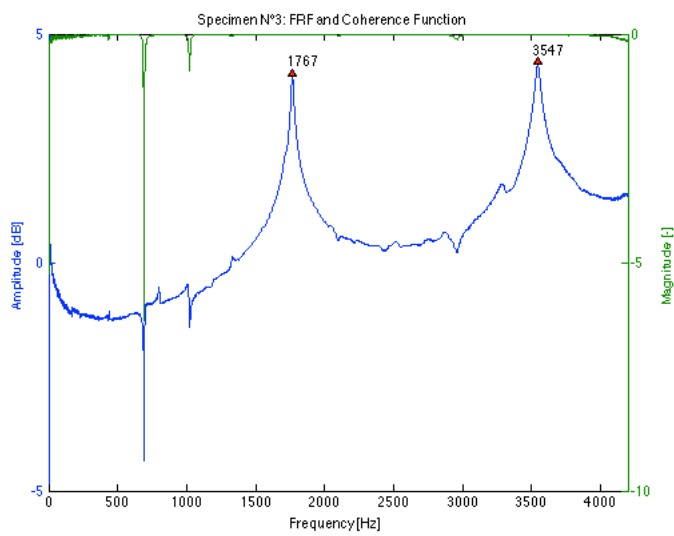
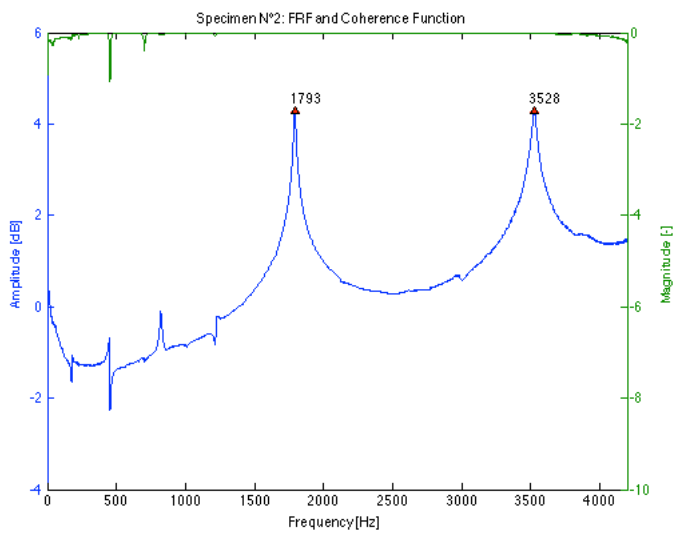
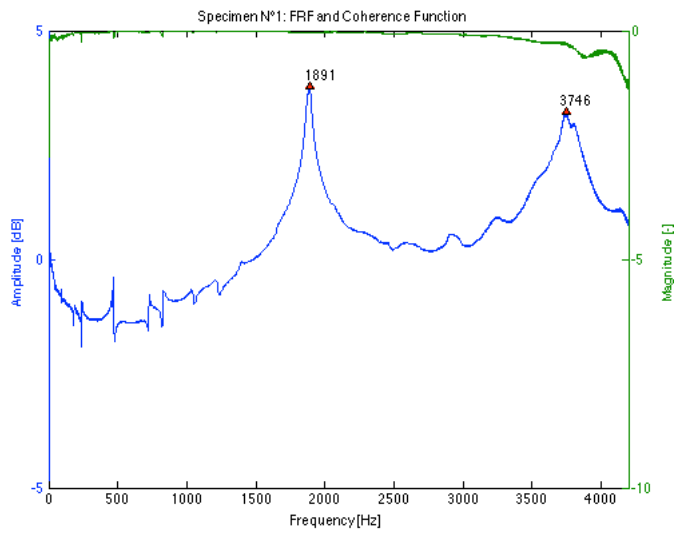
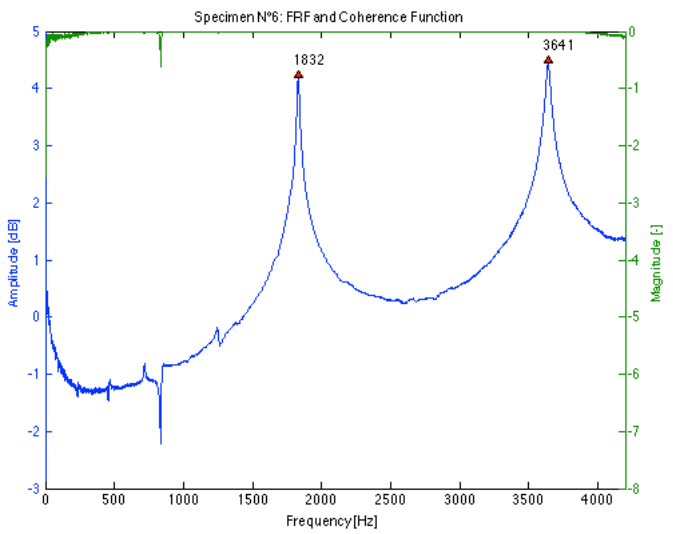
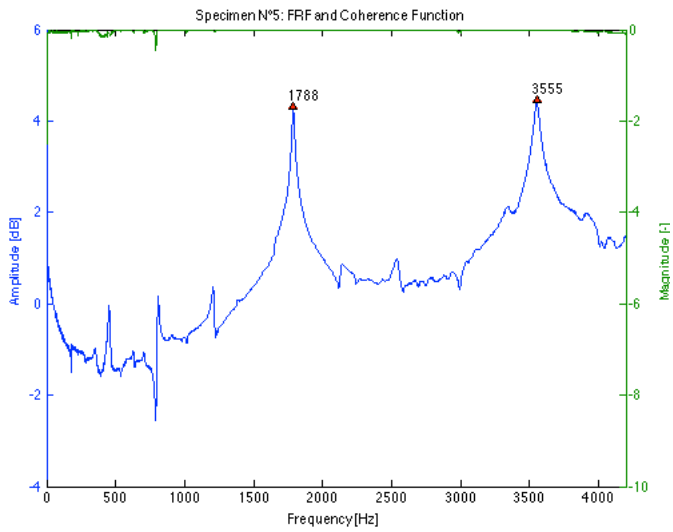
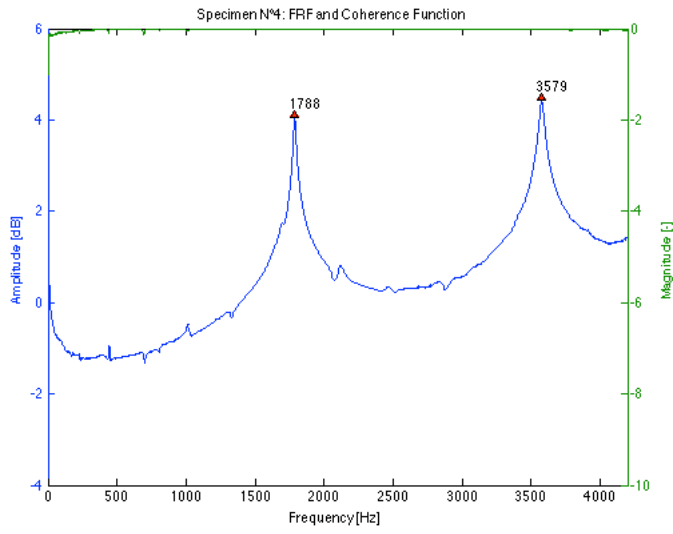
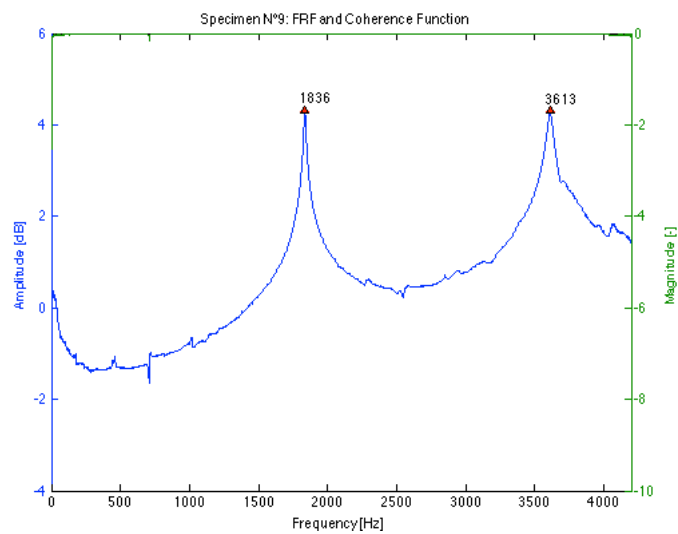
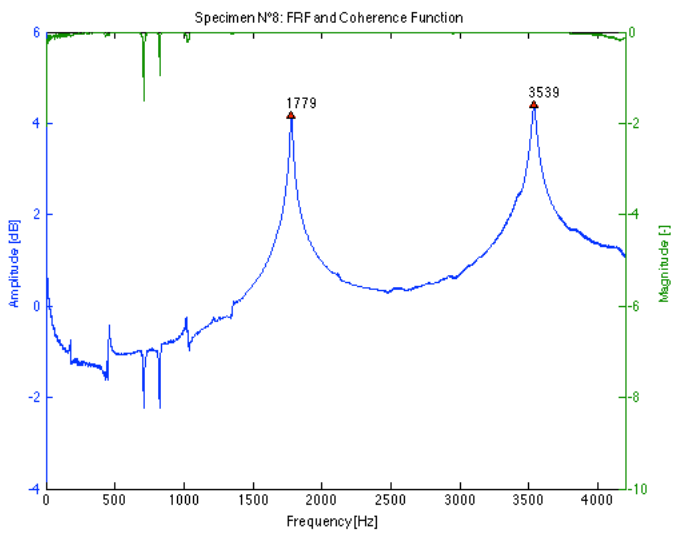
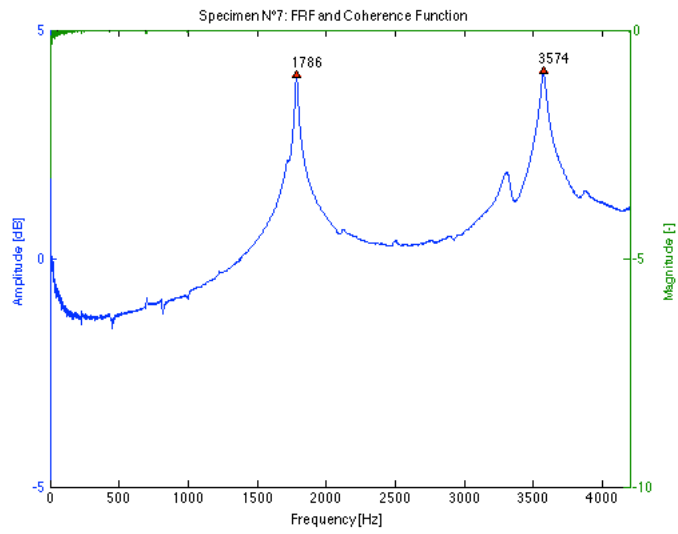


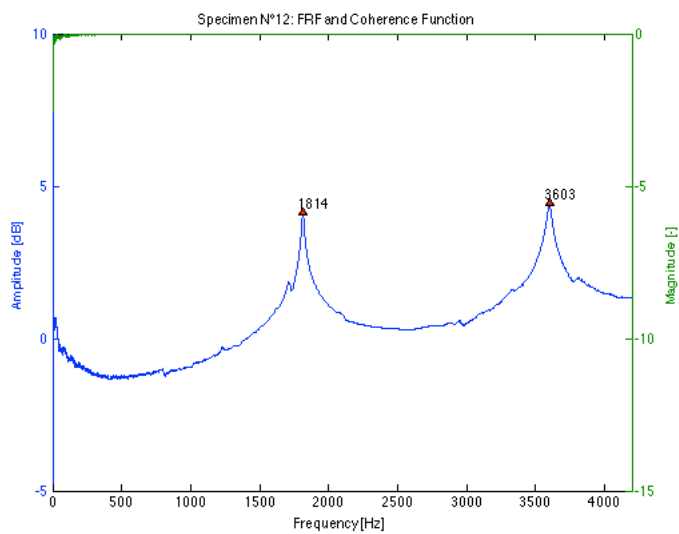
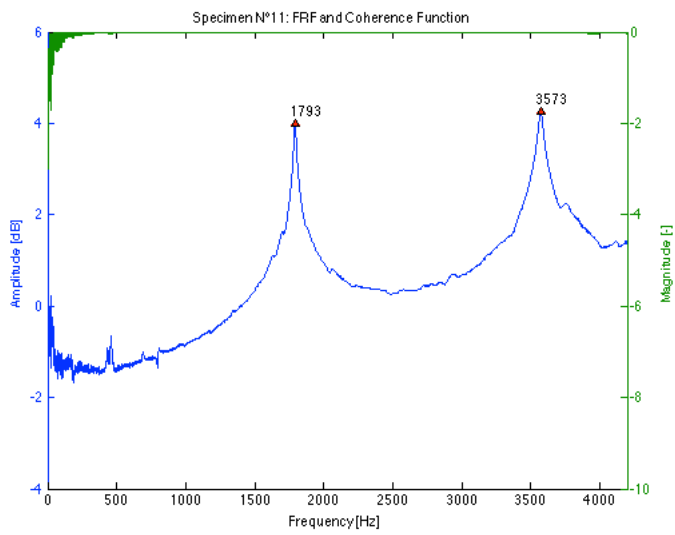
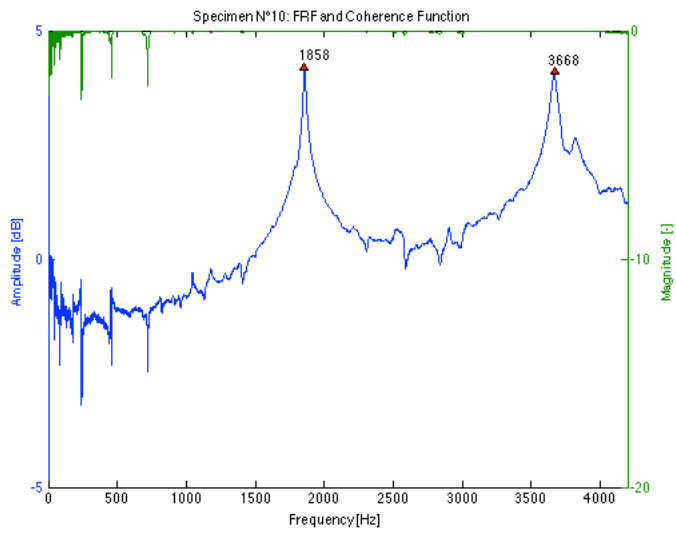
Figure 11-3 Correlation between longitudinal E-modulus found using both frequencies and static E-modulus

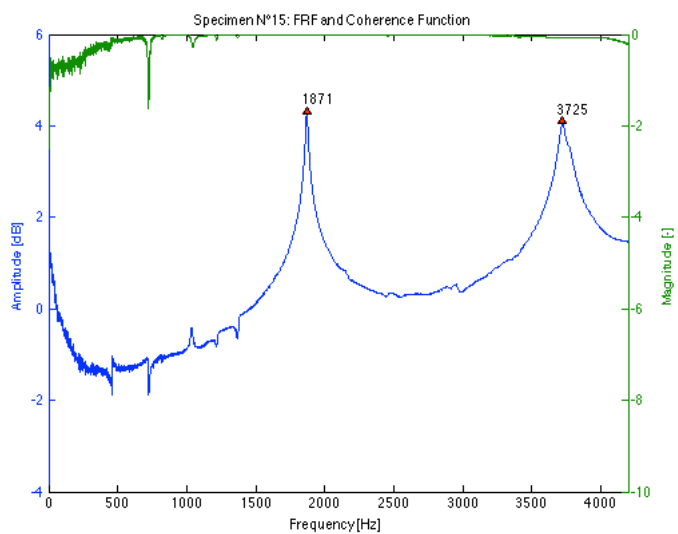
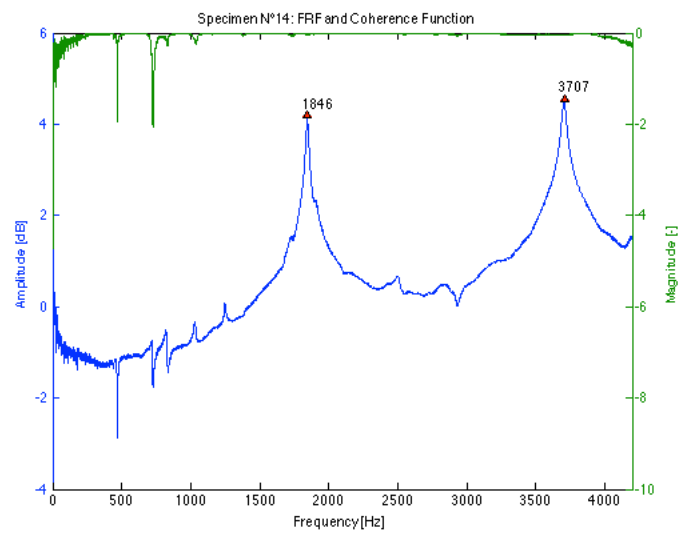
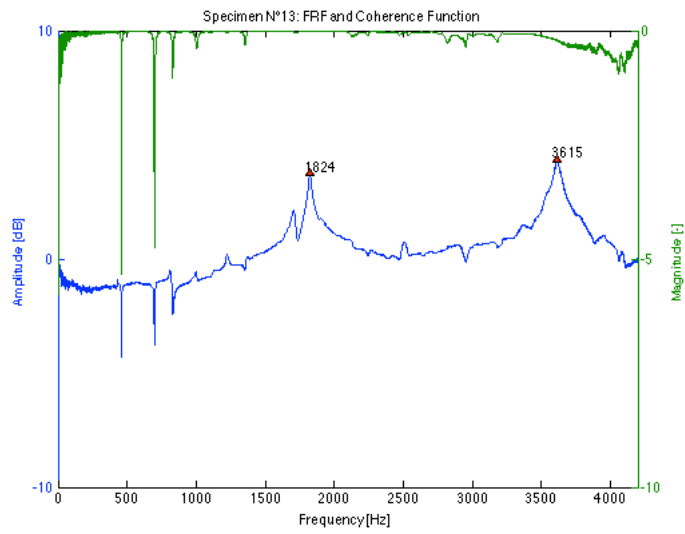
## FRF plots

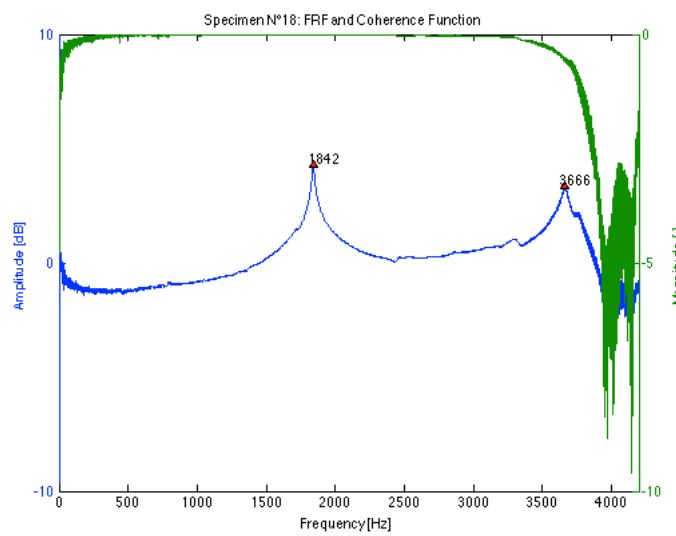
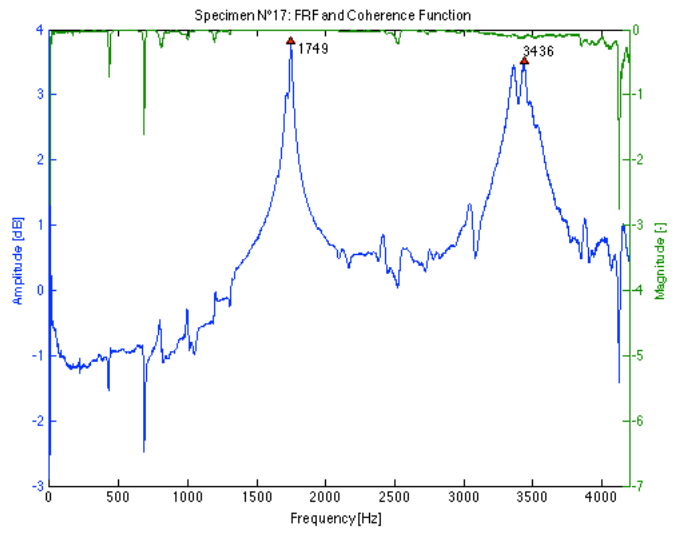
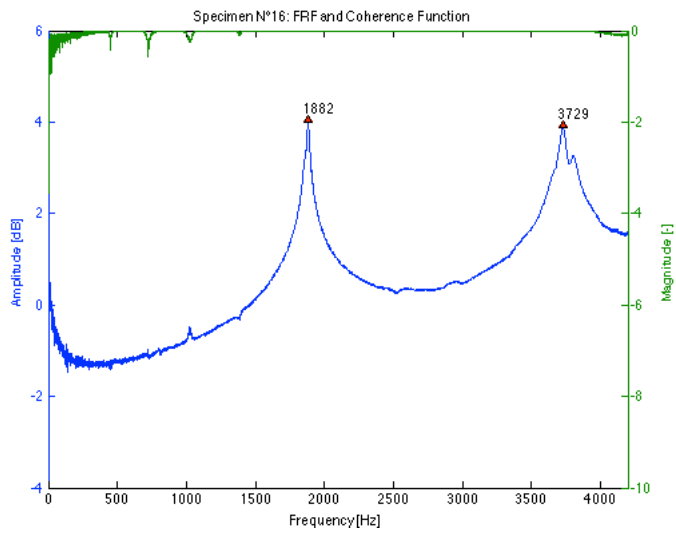


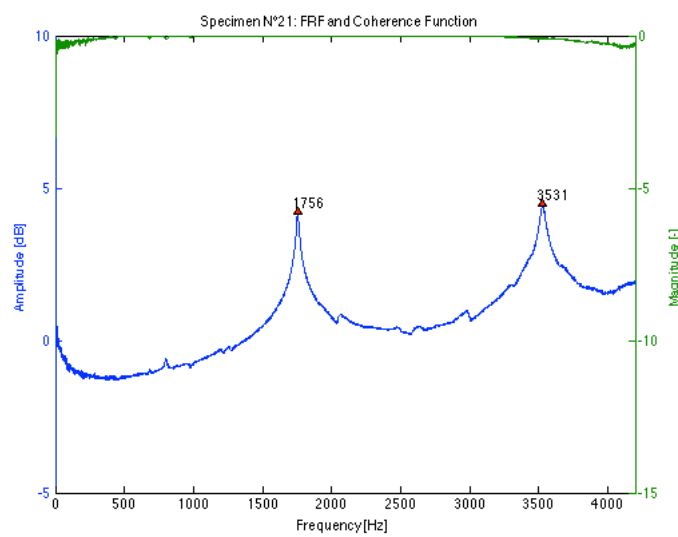
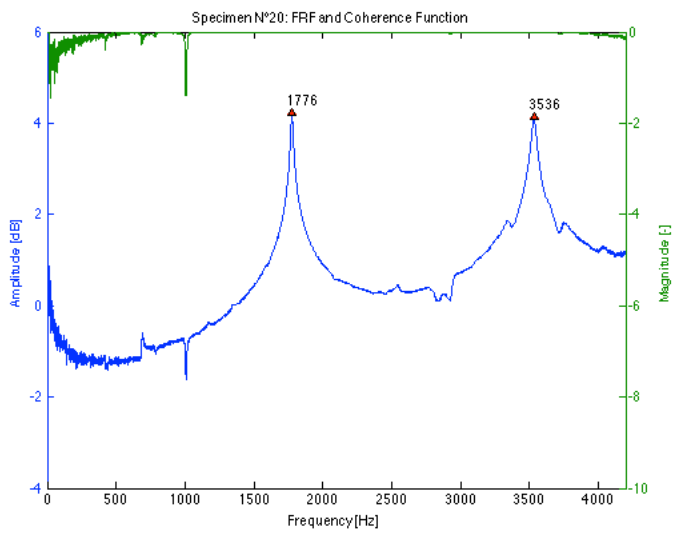
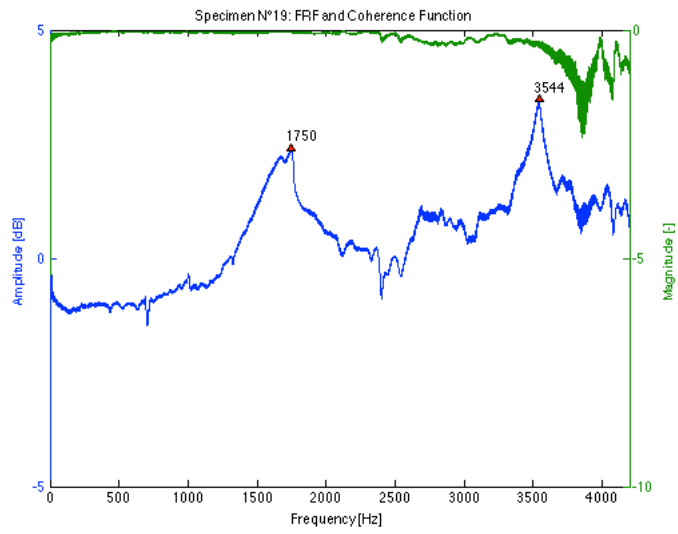


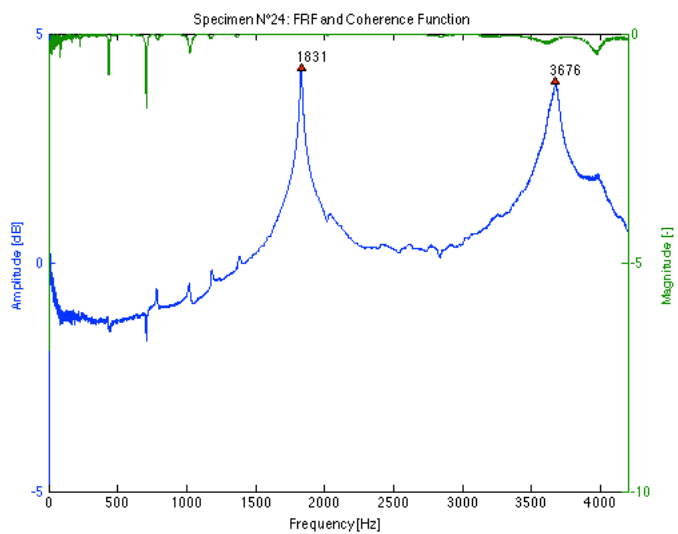
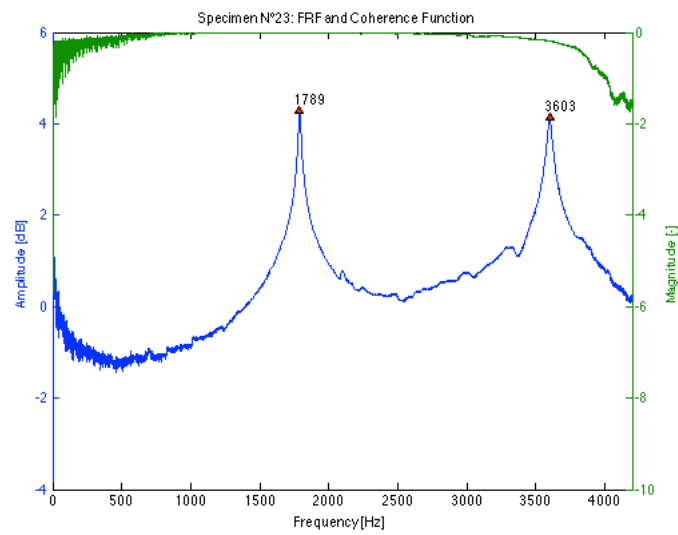
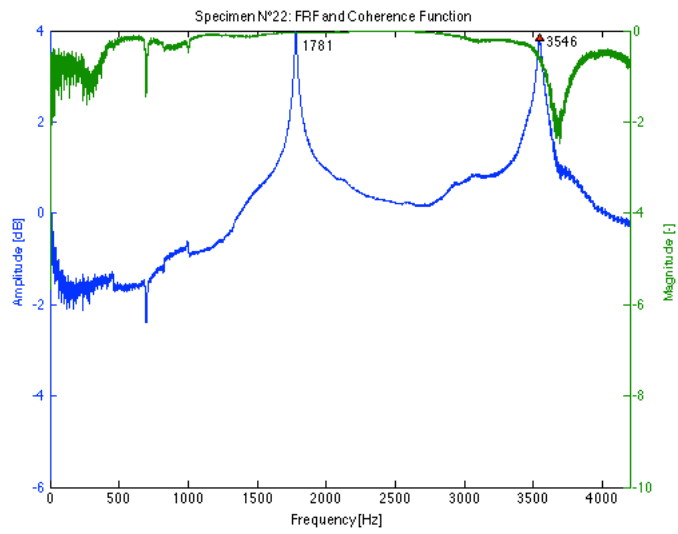


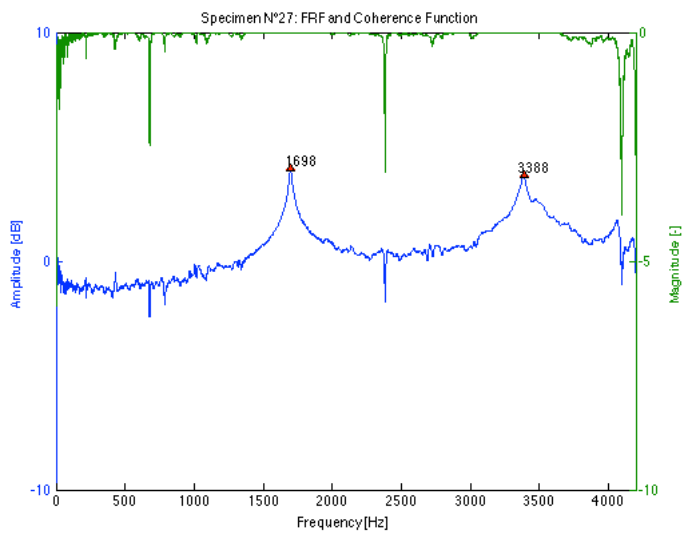
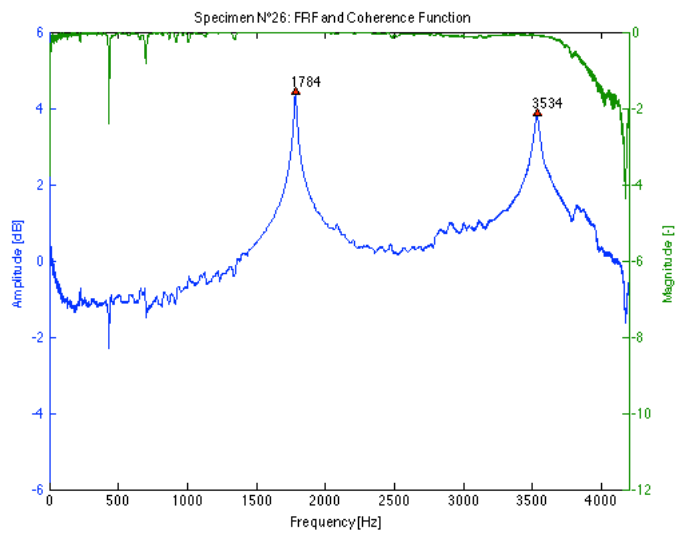
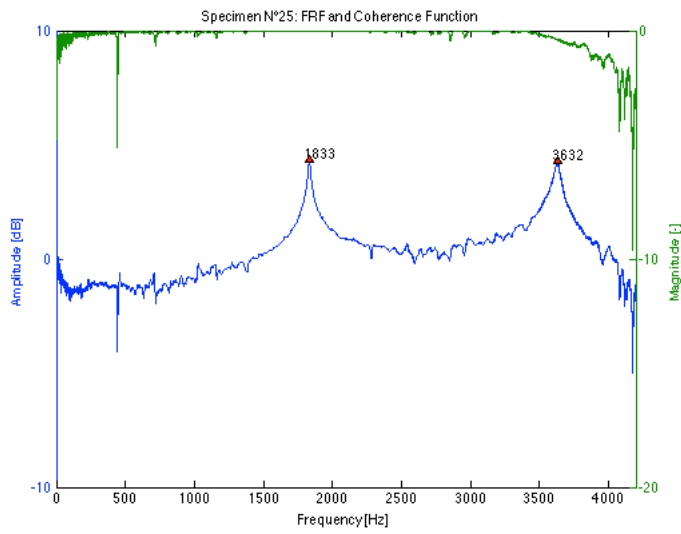


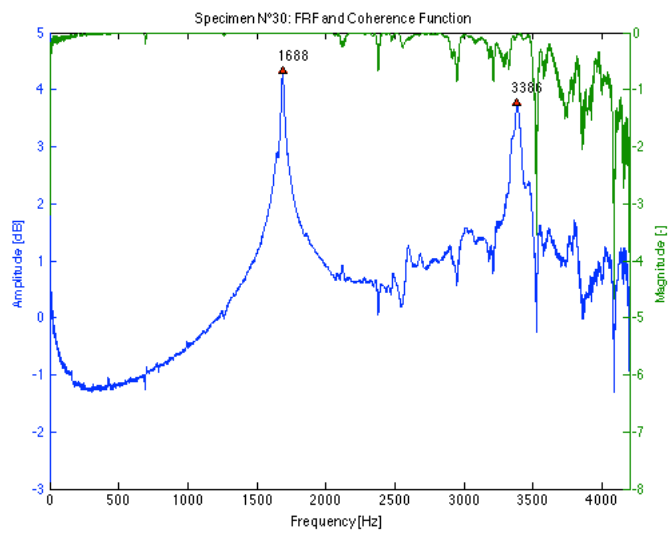
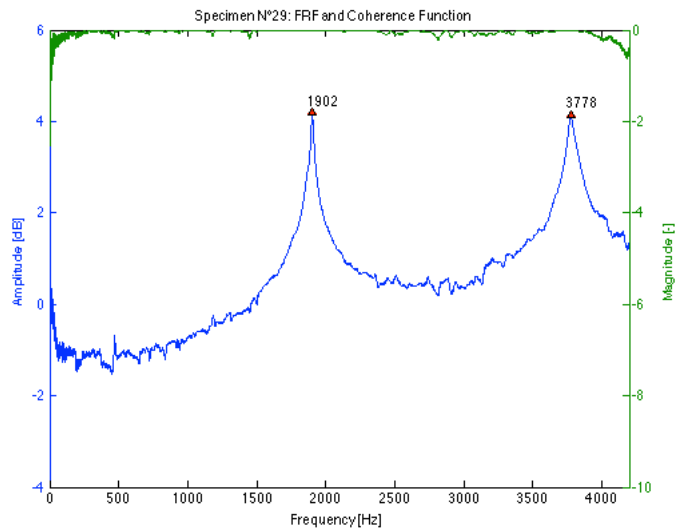
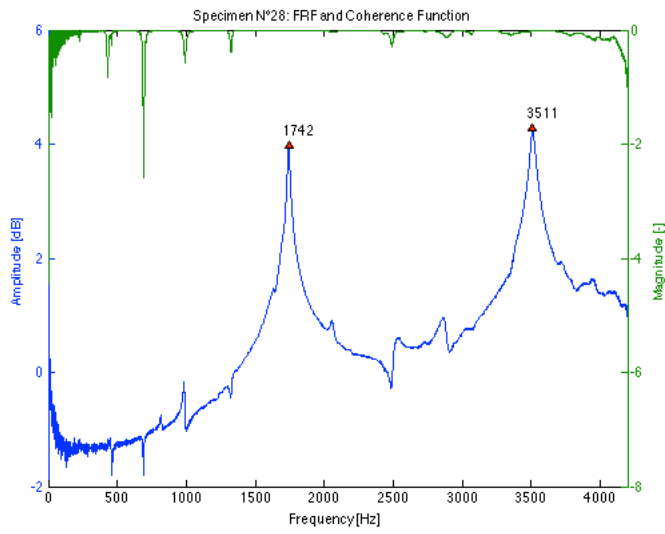


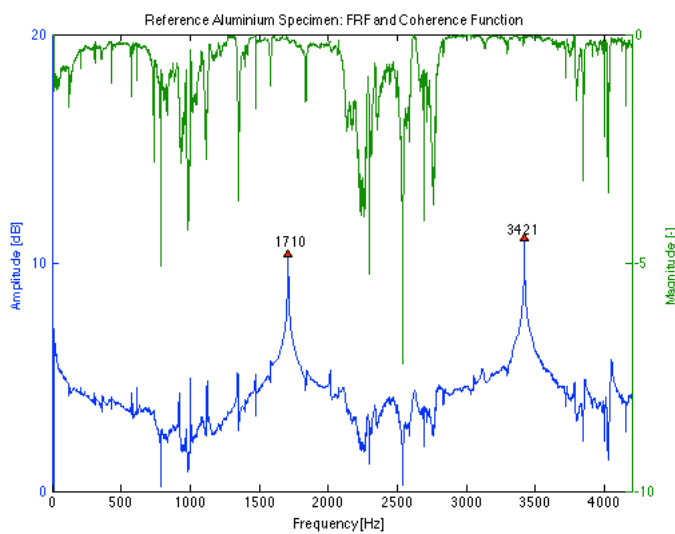
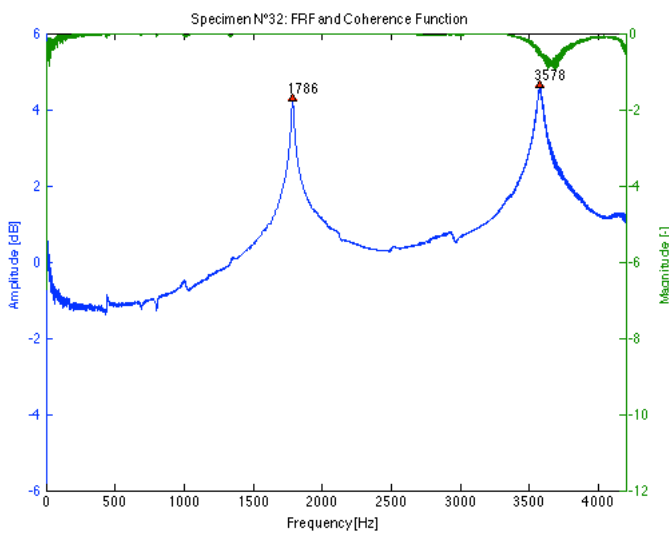
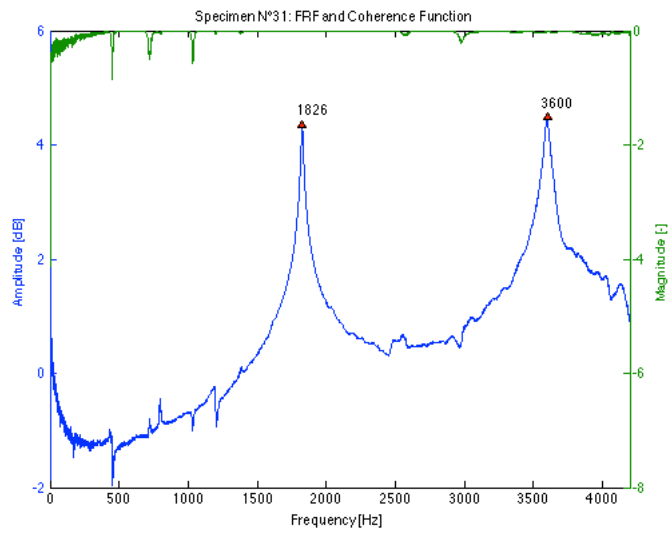












## 11.2.5 Transversal vibration tests

### Data

Table 11-5 Results of transversal tests

Beam N°	f <sub>1b</sub> [Hz]	f <sub>2b</sub> [Hz]	f <sub>3b</sub> [Hz]	f <sub>1t</sub> [Hz]	f <sub>2t</sub> [Hz]	G <sub>1</sub> [MPa]	G <sub>2</sub> [MPa]	G <sub>m</sub> [MPa]	E <sub>1b</sub> [MPa]	E <sub>2b</sub> [MPa]	E <sub>3b</sub> [MPa]	E <sub>mb</sub> [MPa]
1	89.5	240.5	455.4	289.8	587.0	789	809	799	16805	16616	16415	16612
2	85.4	226.6	438.7	309.7	632.6	873	911	892	14794	14139	14472	14468
3	84.0	226.7	442.0	303.9	606.6	798	795	797	13584	13451	14008	13681
4	84.4	229.4	441.0	305.0	617.1	822	841	832	14022	14092	14242	14119
5	84.6	227.1	437.0	304.3	615.9	848	869	859	14615	14316	14489	14473
6	87.0	234.8	452.7	300.1	610.4	796	824	810	14931	14830	15147	14969
7	84.5	227.3	435.5	304.3	614.8	797	813	805	13691	13468	13503	13554
8	84.3	225.9	436.5	301.3	610.1	753	772	763	13147	12836	13116	13033
9	86.5	232.5	439.1	296.9	601.5	802	823	813	15192	14967	14609	14923
10	87.7	237.7	455.2	303.8	611.0	830	839	835	15427	15455	15552	15478
11	84.7	229.7	433.0	297.1	598.4	837	849	843	15165	15198	14756	15040
12	85.6	231.6	437.2	301.4	610.0	844	864	854	15179	15135	14731	15015
13	84.3	229.1	429.4	299.0	602.2	814	825	820	14423	14509	13899	14277
14	85.7	234.7	441.4	296.3	594.7	726	731	729	13548	13873	13433	13618
15	87.4	234.1	450.3	292.0	592.1	760	781	771	15196	14889	15170	15085
16	87.5	235.9	449.3	290.0	587.5	738	757	748	14997	14904	14882	14928
17	82.1	218.7	424.5	322.9	652.9	830	848	839	11937	11452	11708	11699
18	85.7	234.3	439.6	293.9	588.5	759	761	760	14402	14704	14173	14426
19	82.2	224.1	433.1	267.2	587.9	587	710	649	12409	12645	13091	12715
20	83.8	225.2	420.9	287.9	584.4	679	700	690	12842	12646	12064	12517
21	82.0	222.0	423.1	303.9	616.1	803	825	814	13018	12956	12815	12930
22	83.4	222.7	430.5	310.2	628.6	829	851	840	13341	12900	13138	13126
23	83.9	226.8	438.1	301.7	600.7	746	739	743	12850	12772	13043	12888
24	85.6	229.3	445.8	298.1	605.7	802	828	815	14753	14417	14970	14713
25	86.6	232.1	441.9	310.2	626.5	858	875	867	14908	14559	14400	14622
26	82.7	223.3	433.2	306.5	621.3	777	798	788	12601	12473	12819	12631
27	79.4	216.5	426.4	319.4	648.8	869	897	883	11946	12013	12674	12211
28	80.8	223.4	427.9	300.2	612.0	829	861	845	13376	13907	13929	13737
29	89.1	240.7	457.7	288.4	586.3	662	684	673	14124	14123	14094	14114
30	78.9	219.2	422.5	332.9	666.0	906	907	907	11311	11796	11853	11653
31	87.4	233.2	446.2	300.9	611.3	745	768	757	14014	13592	13637	13748
32	84.2	226.8	437.2	307.9	621.6	795	810	803	13246	13055	13247	13183
					Mean value	791	811	801	13931	13834	13877	13881
					Std. dev.	65	59	61	1223	1185	1094	1152
Aluminium	23.2	63.9	125.2	374.7	/	24676	/	/	67289	67223	67211	67241

## Correlations

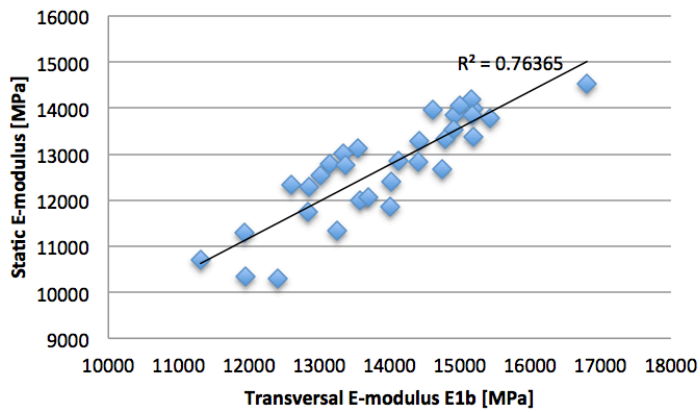


Figure 11-4 Correlation between transversal E-modulus found using  $f_{1b}$  and static E-modulus

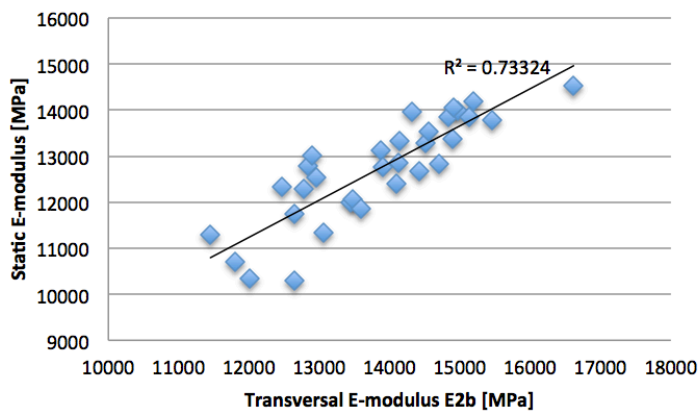


Figure 11-5 Correlation between transversal E-modulus found using  $f_{2b}$  and static E-modulus

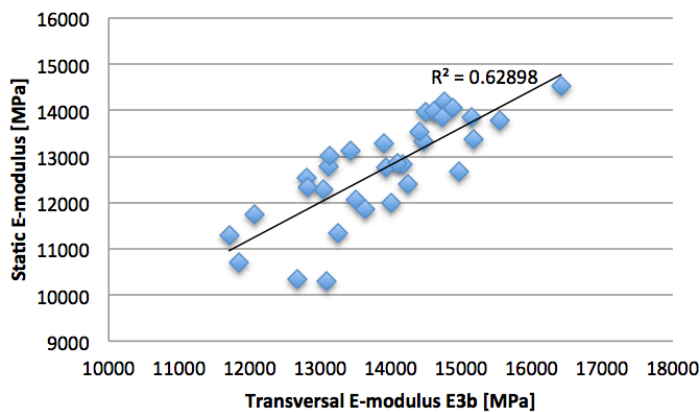


Figure 11-6 Correlation between transversal E-modulus found using  $f_{3b}$  and static E-modulus

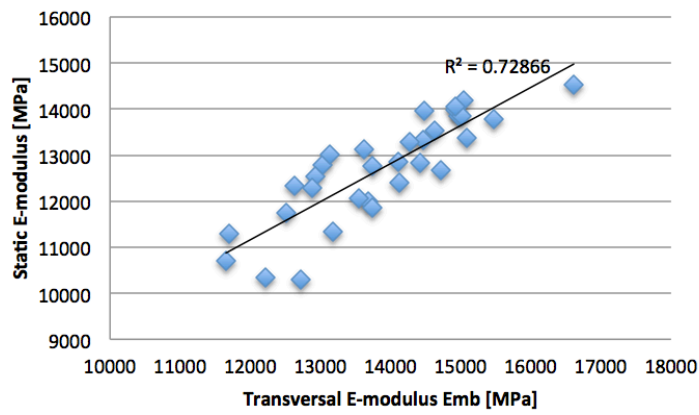
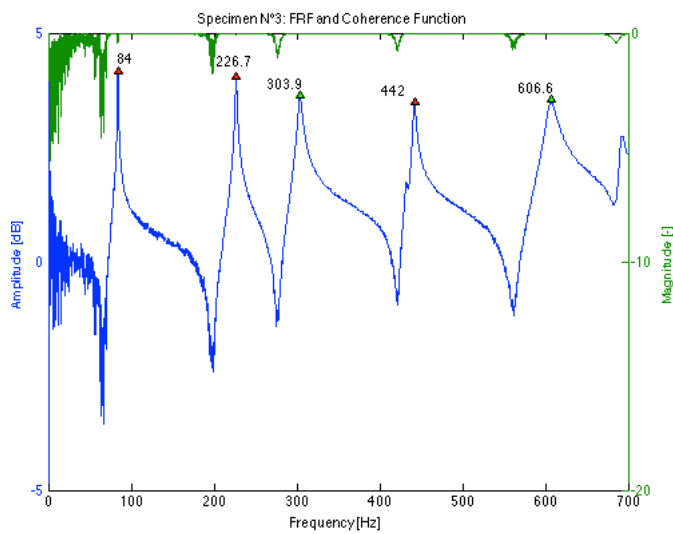
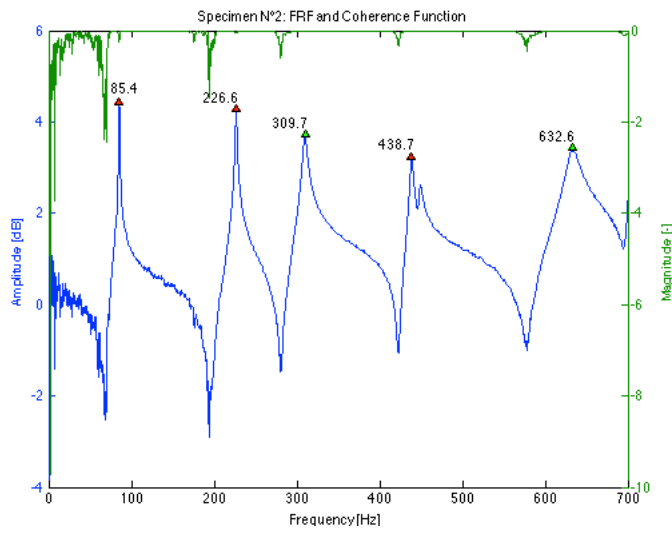
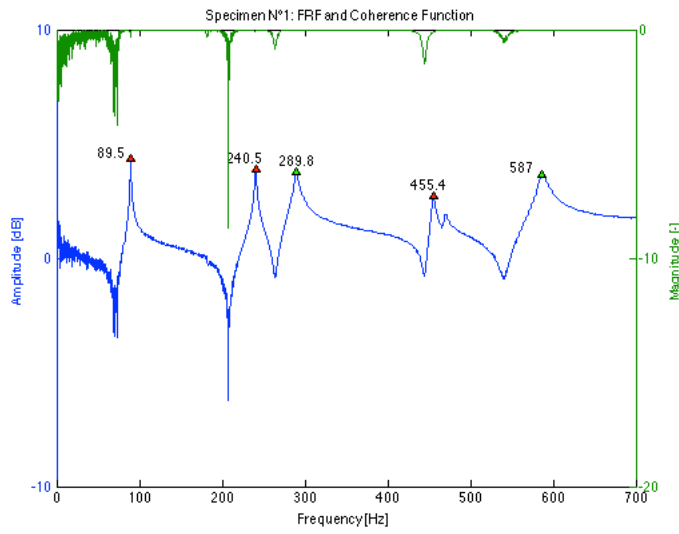
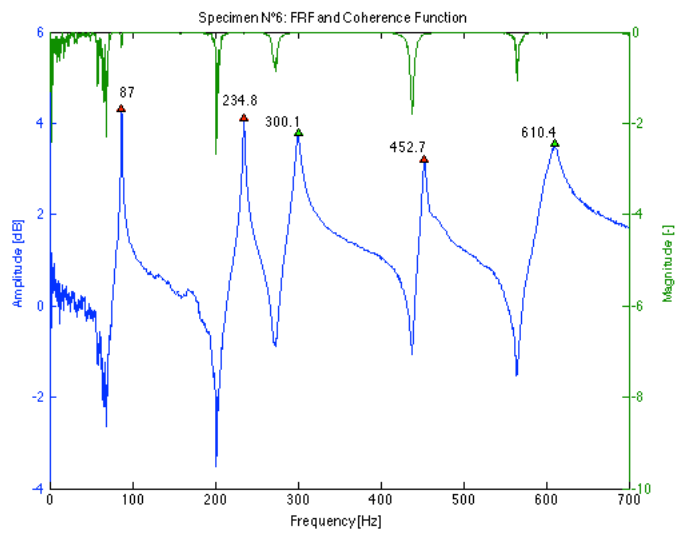
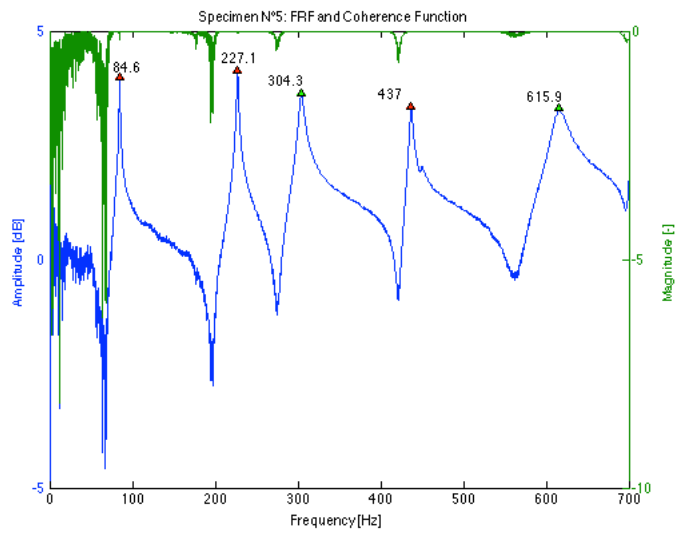
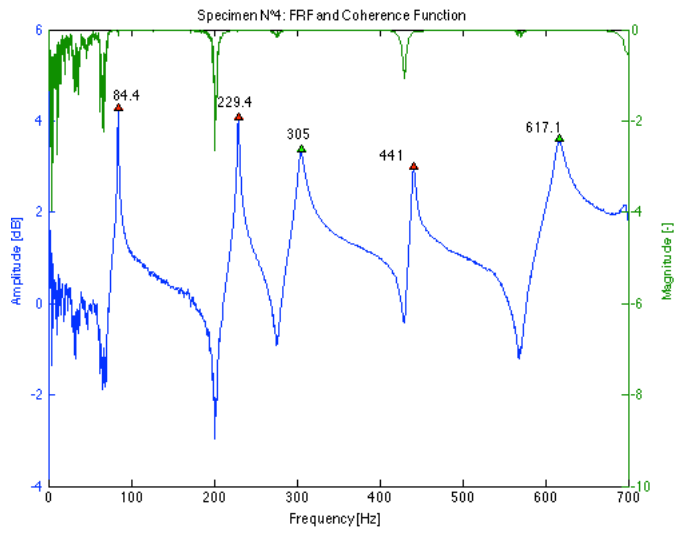
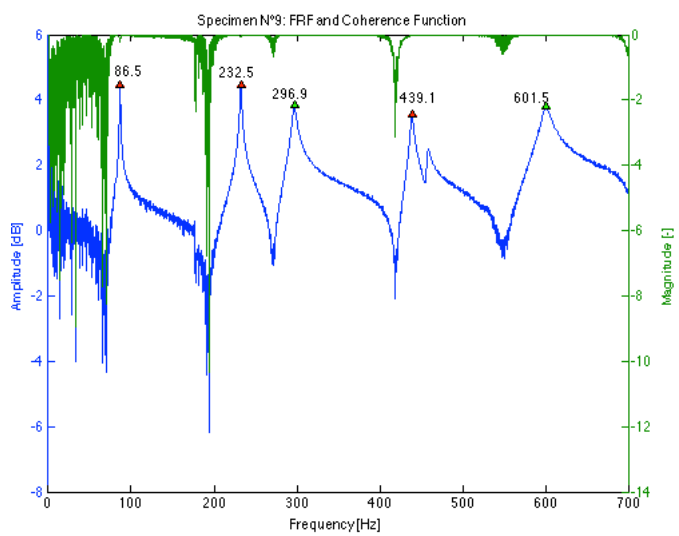
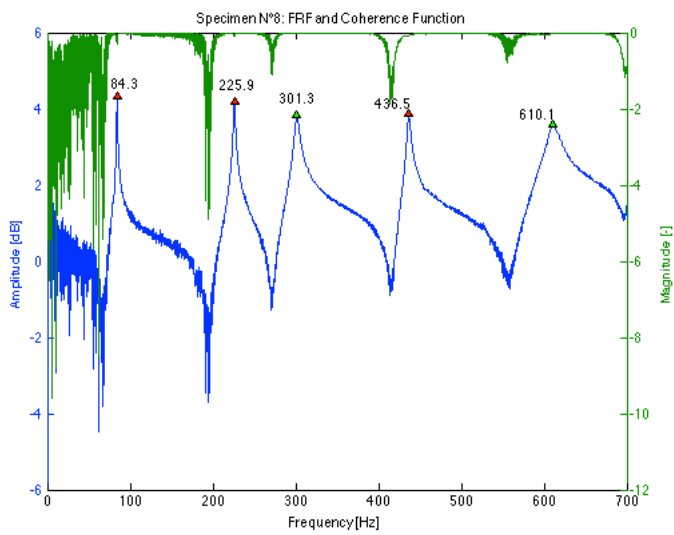
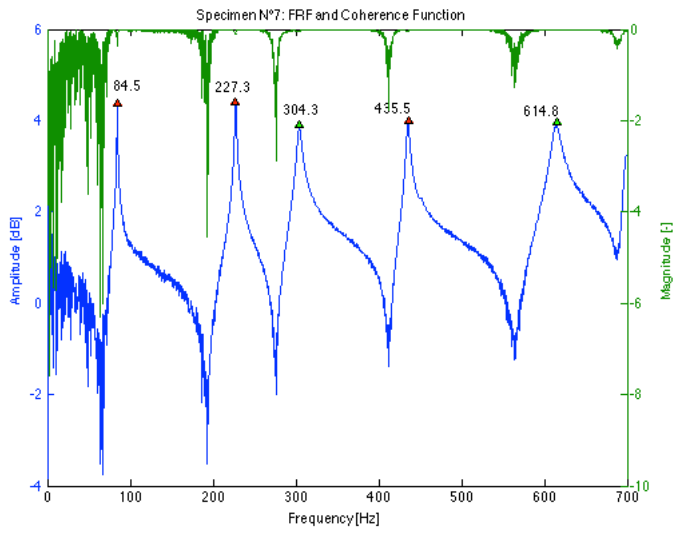


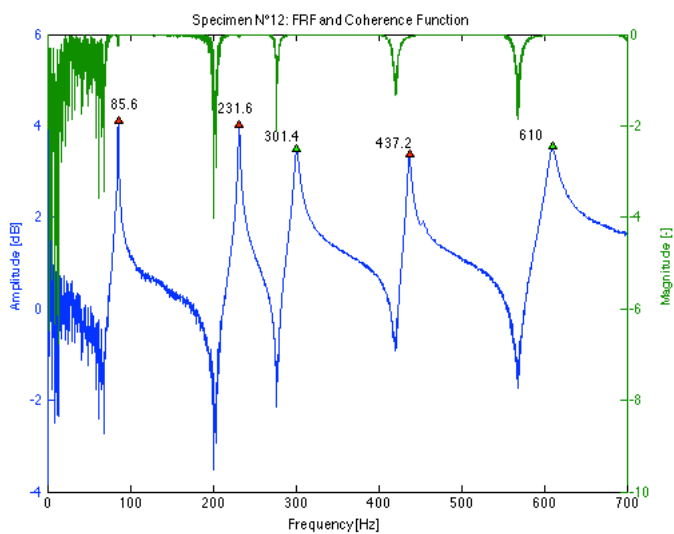
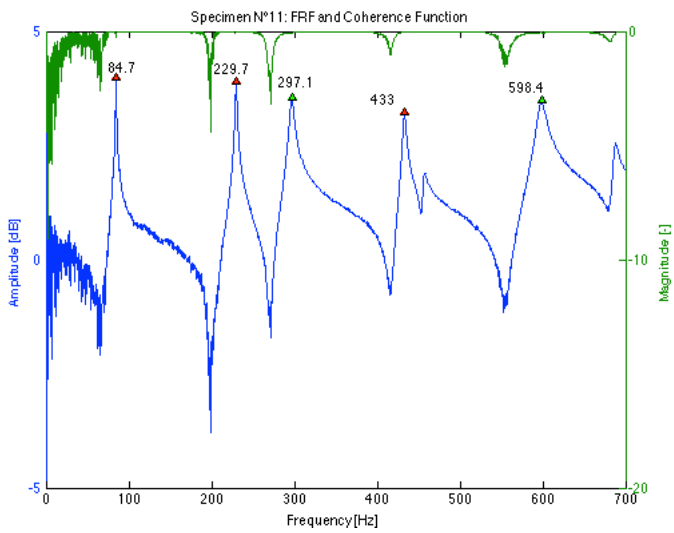
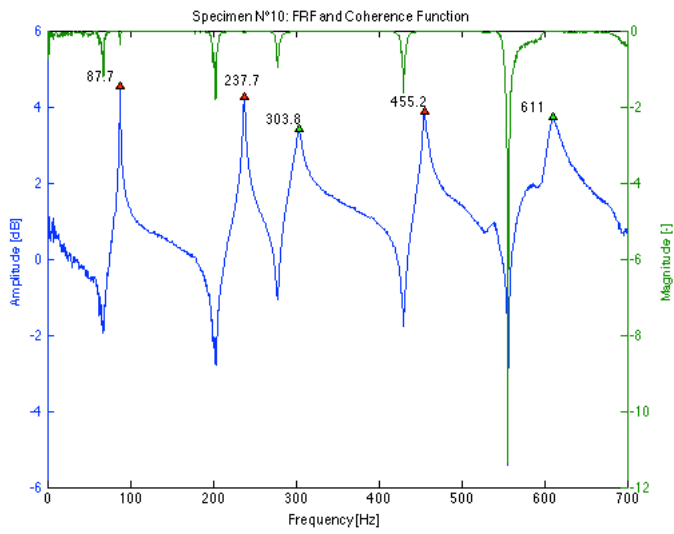
Figure 11-7 Correlation between transversal E-modulus found using all frequencies and static E-modulus

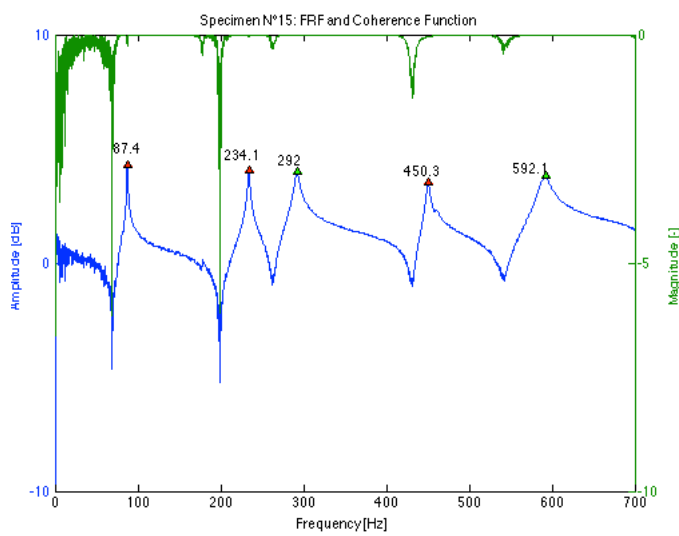
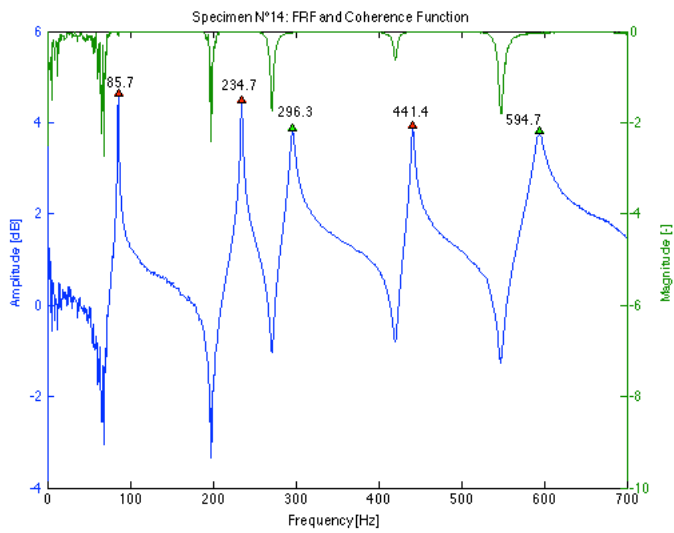
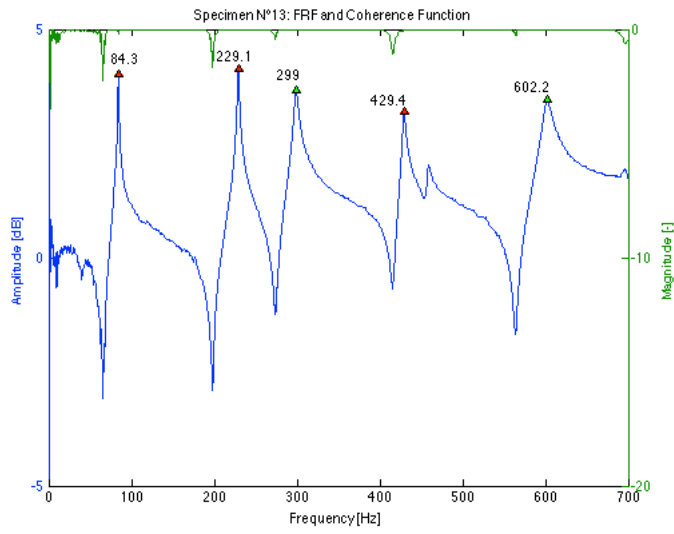
## FRF plots

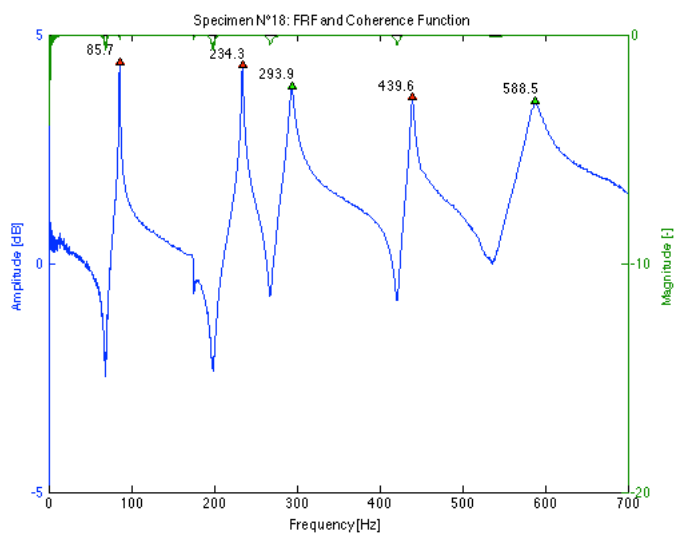
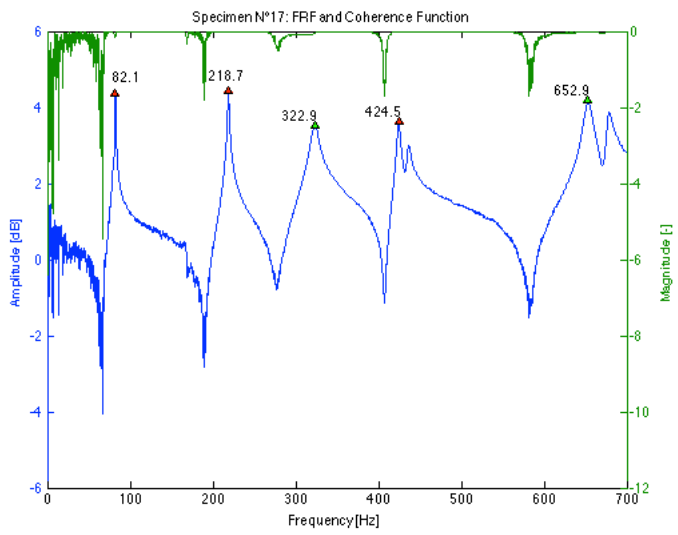
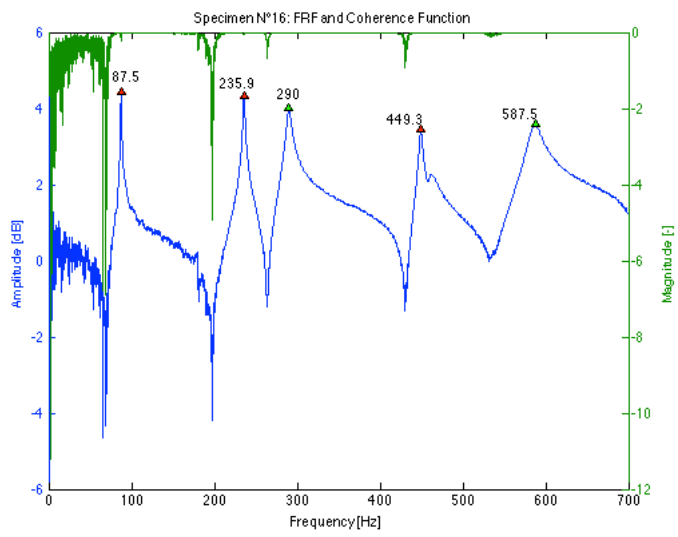


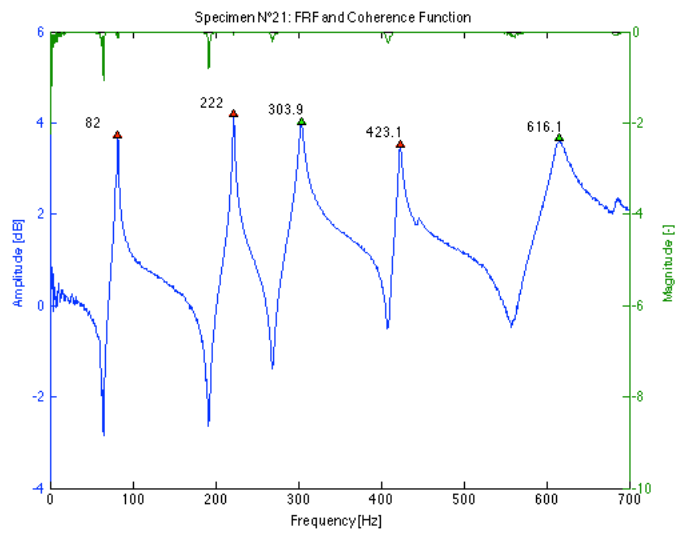
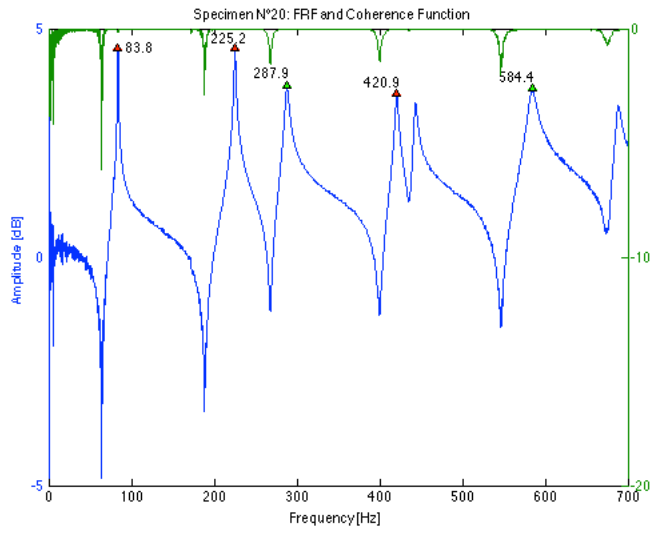
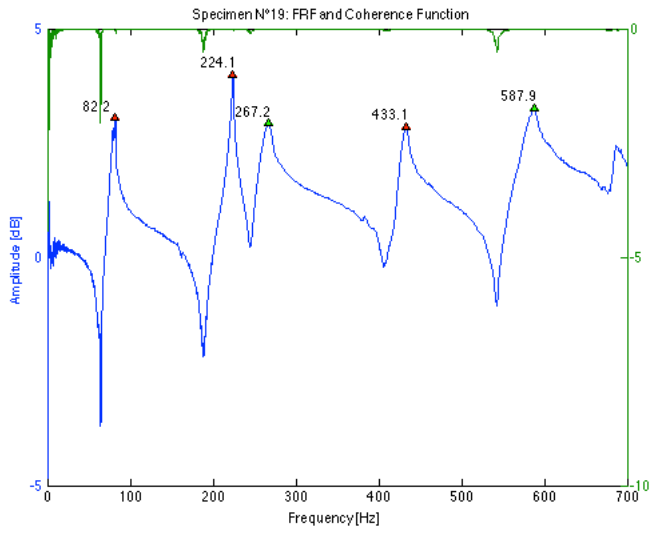


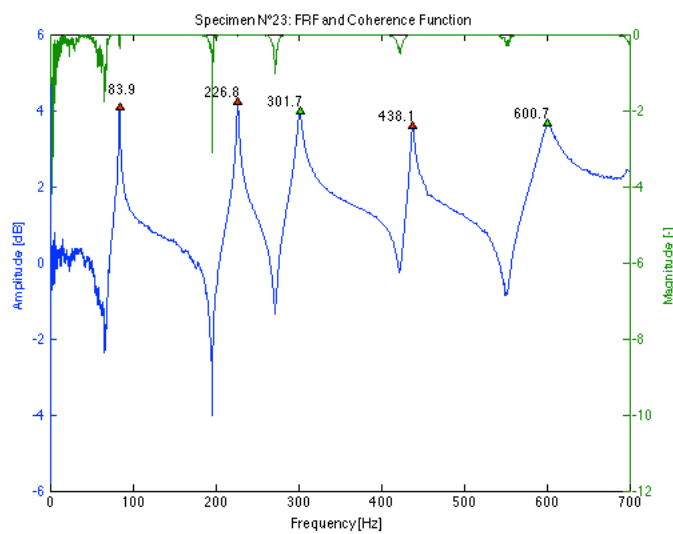
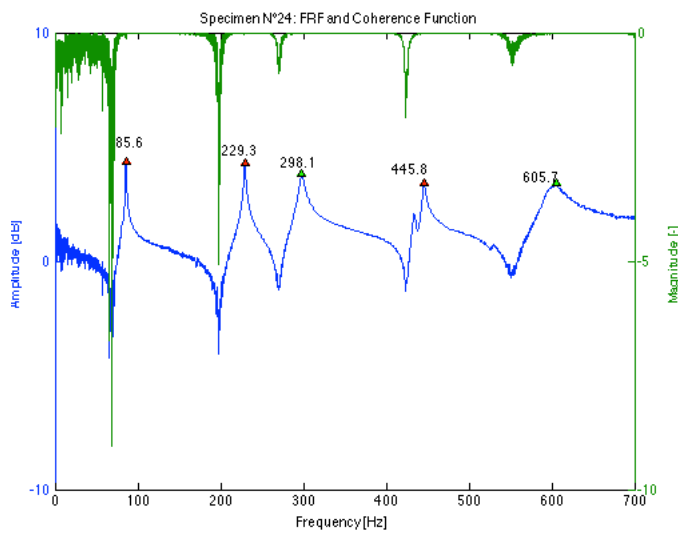
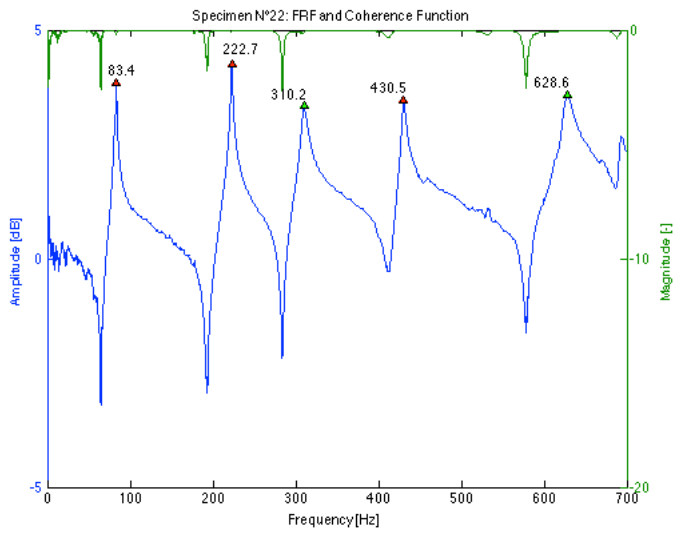


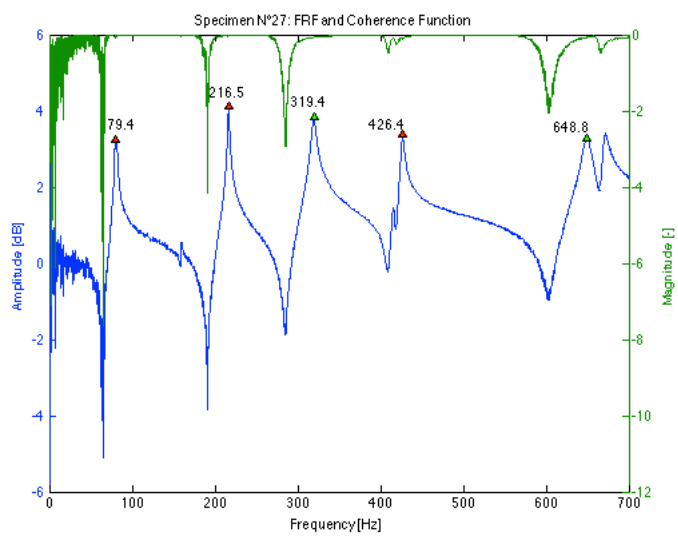
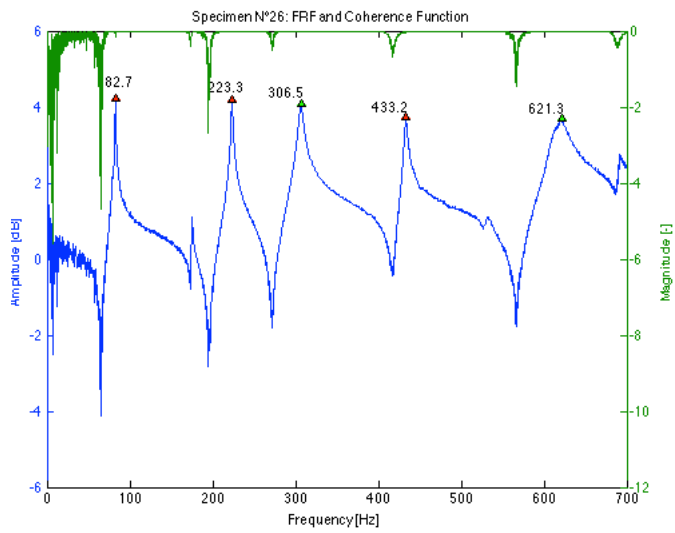
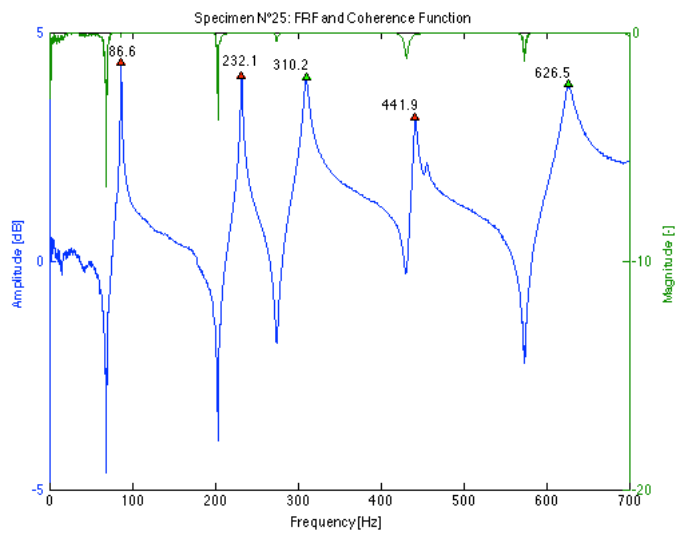


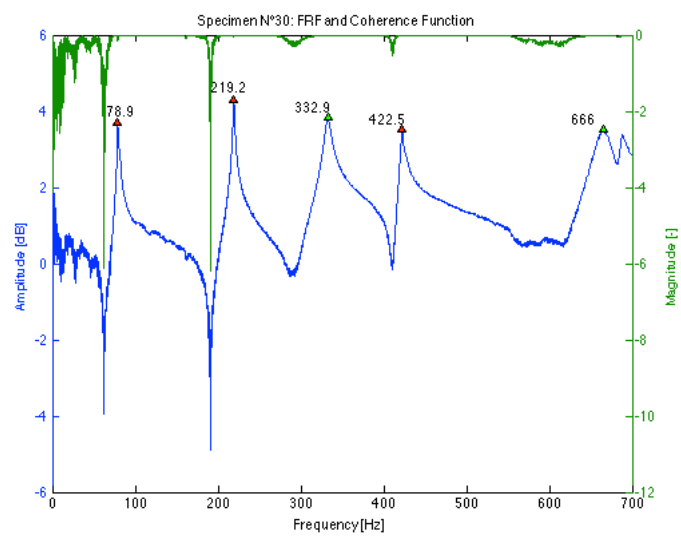
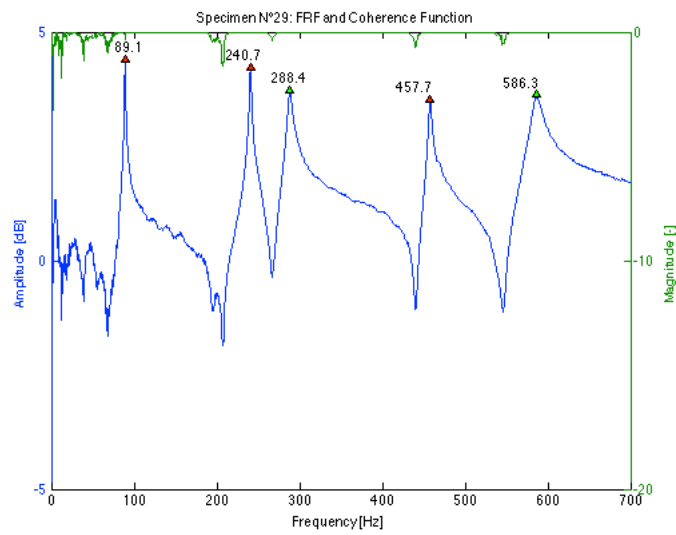
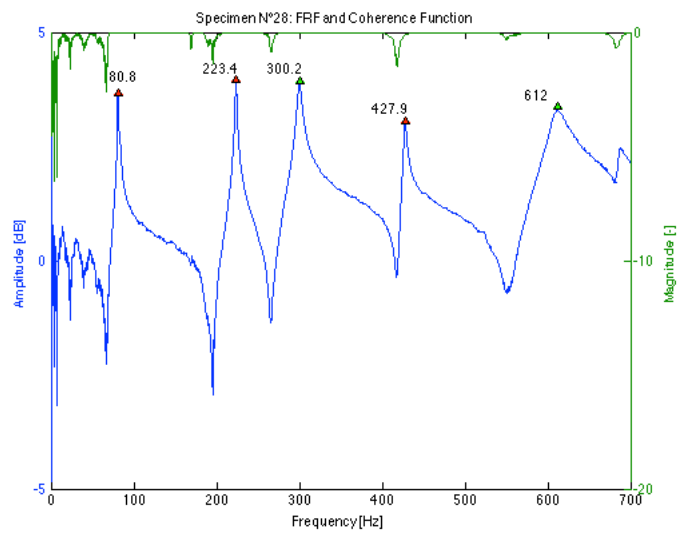


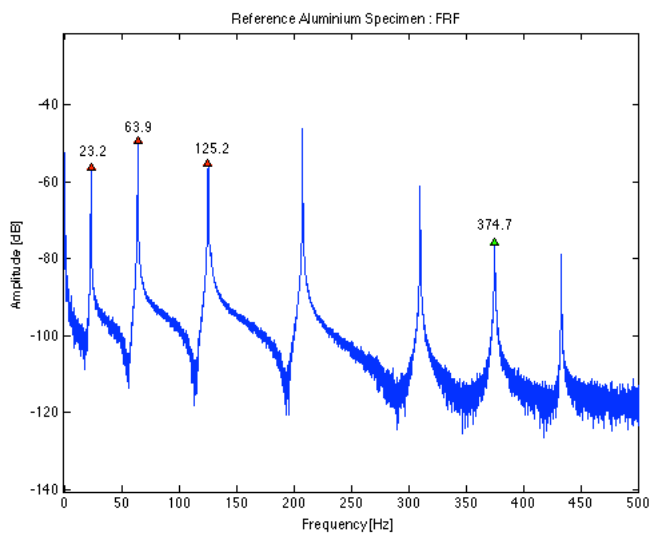
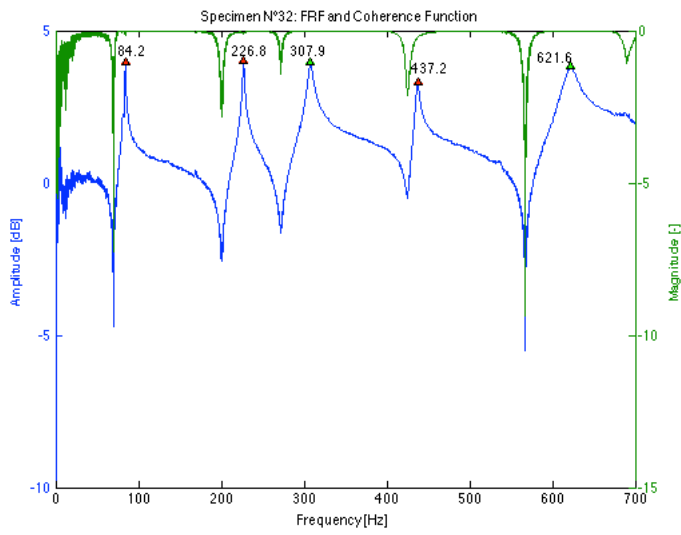
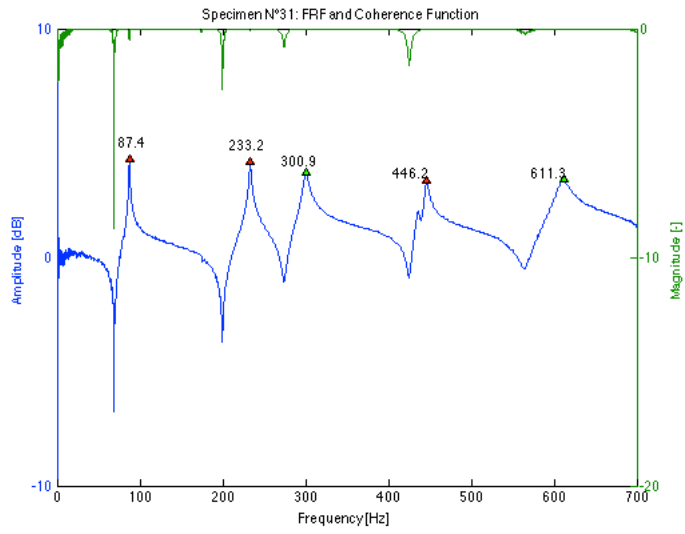












## 11.3 Appendix C - Tension tests

### 11.3.1 Results for each specimen

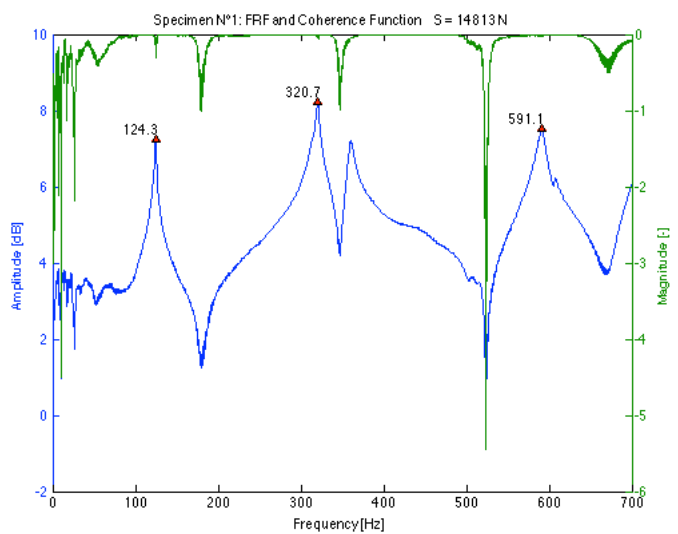
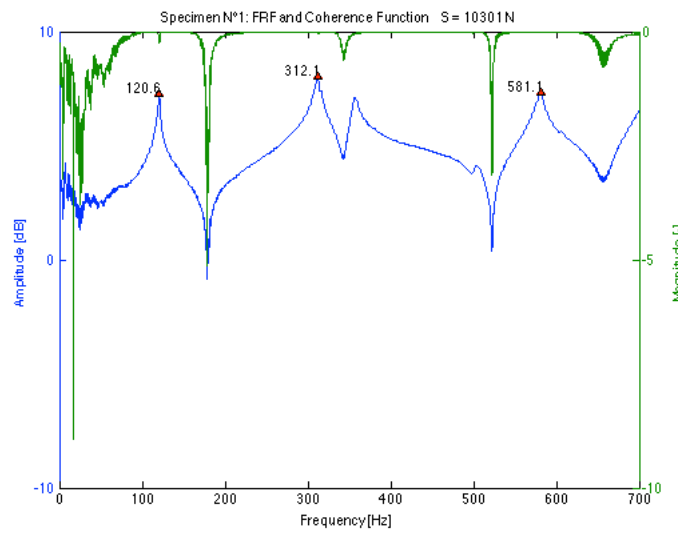
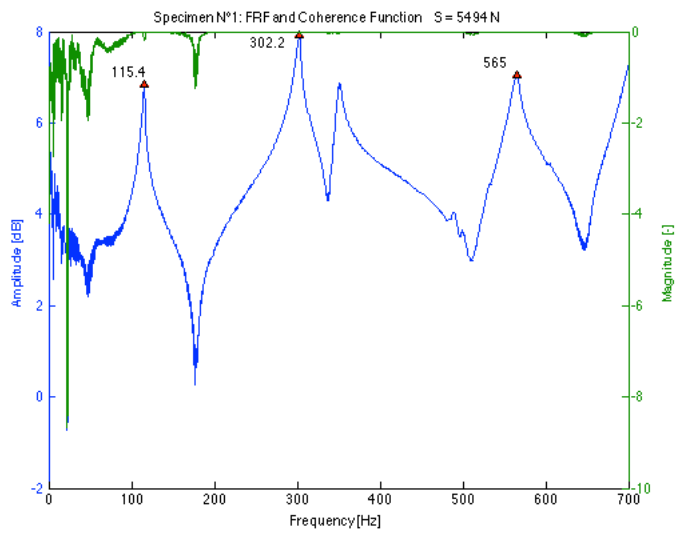
#### T1

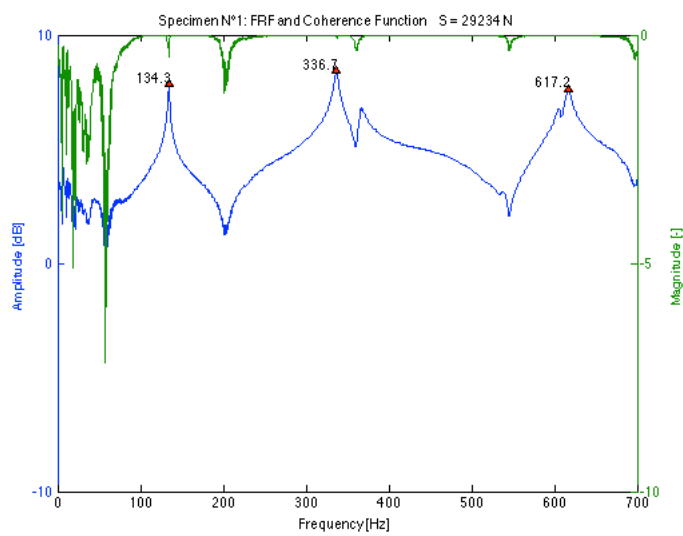
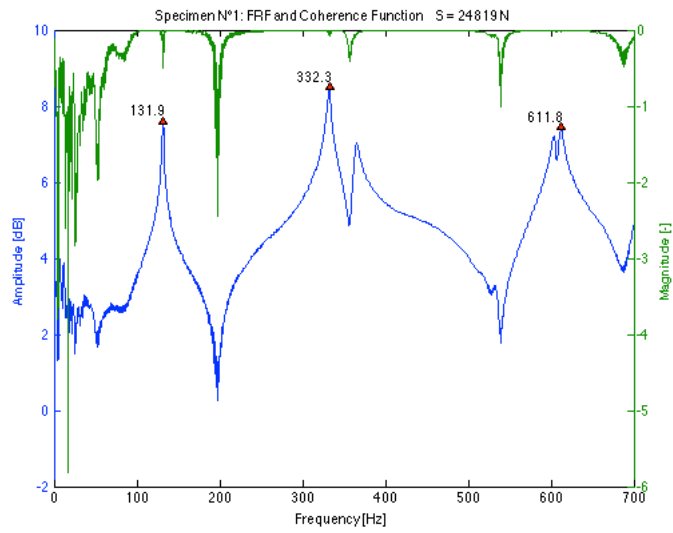
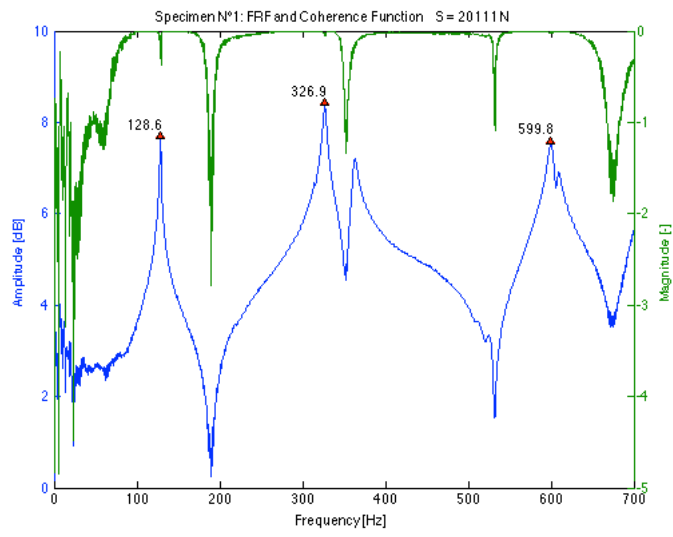
#### Data

Table 11-6 Results of frequency measurements and dual parameter estimation for specimen N°1 using the transversal and longitudinal E-modulus for different load levels

T1		using E <sub>o</sub> using E <sub>l</sub>										
Applied load S	% of yield	S/S <sub>ε</sub>	f <sub>1o</sub>	f <sub>2o</sub>	L	k <sub>est</sub>	S <sub>est</sub>	Error on S	k <sub>est</sub>	S <sub>est</sub>	Error on S	
[N]	[%]	[-]	[Hz]	[Hz]	[m]	[Nm]	[N]	[%]	[Nm]	[N]	[%]	
5494	8.1	0.24	115.4	302.2	1.295	293030	6385	16.2	254060	6715	22.2	
10301	15.1	0.44	120.6	312.1	1.275	209300	13086	27.0	186260	13590	31.9	
14813	21.8	0.61	124.3	320.7	1.255	182890	15242	2.9	164040	15848	7.0	
20111	29.6	0.82	128.6	326.9	1.255	178430	23908	18.9	159880	24607	22.4	
24819	36.5	1.02	131.9	332.3	1.255	199280	29058	17.1	177230	29751	19.9	
29234	43.0	1.20	134.3	336.7	1.255	243740	31557	7.9	213650	32188	10.1	

## FRF plots





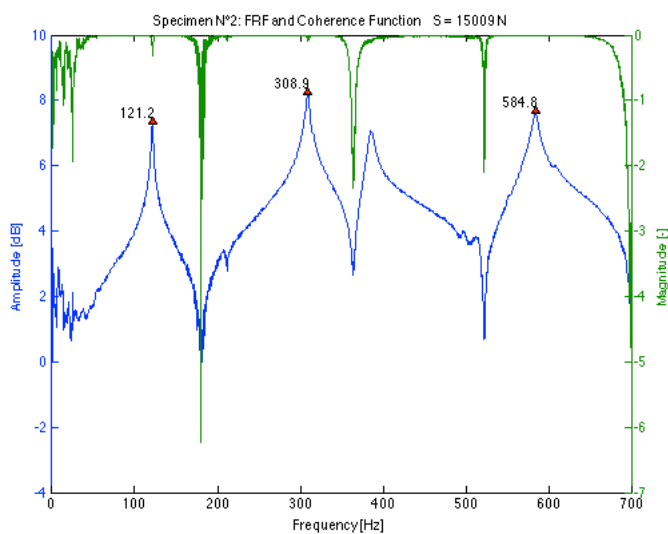
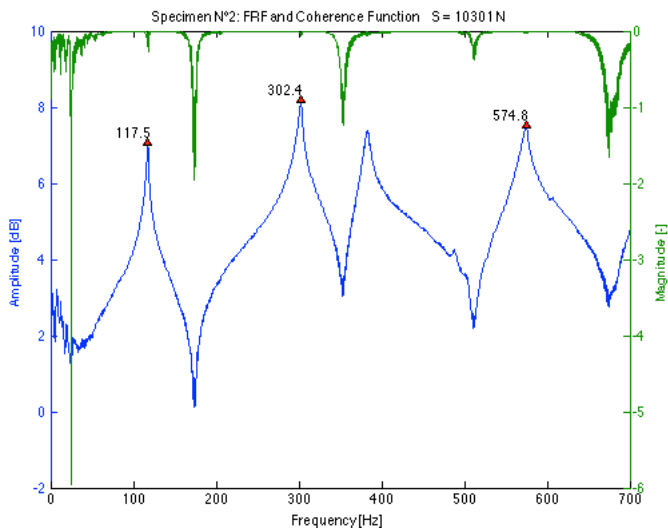
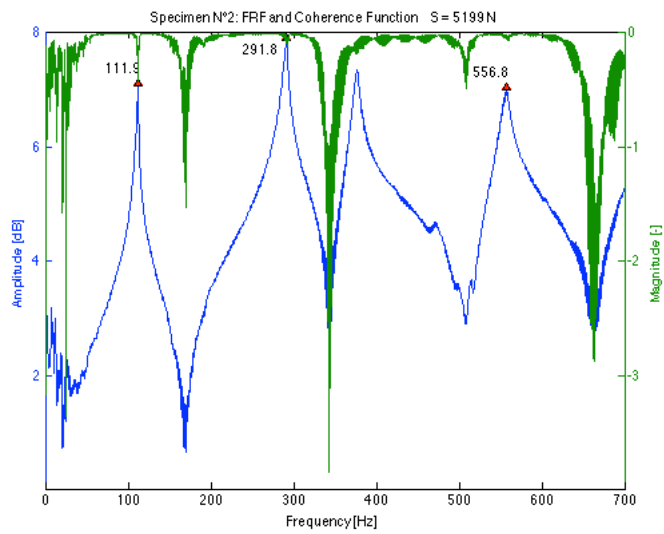
## T2

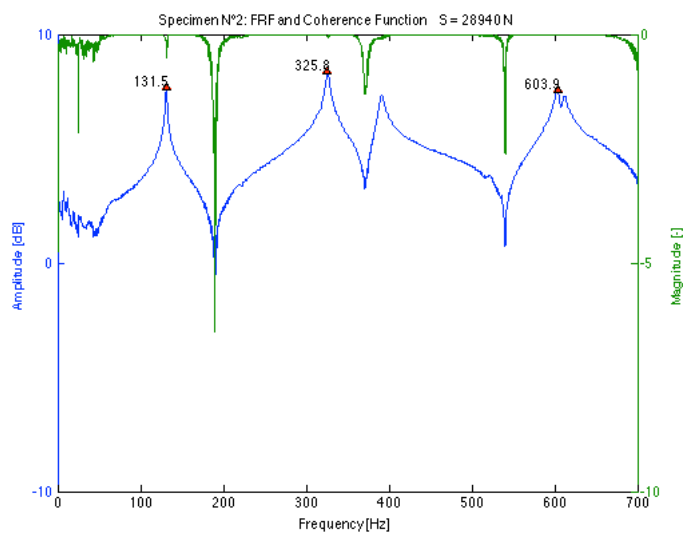
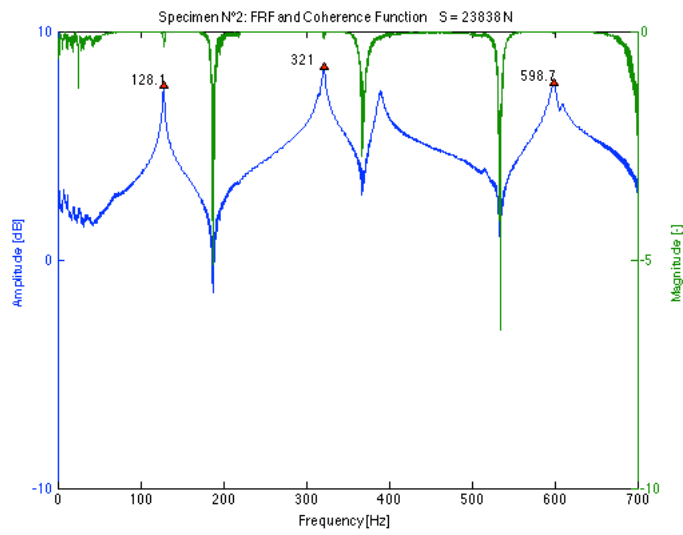
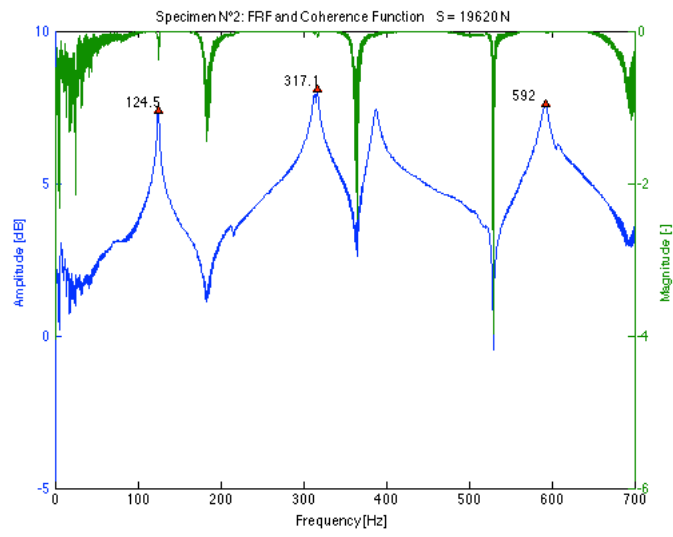
### Data

Table 11-7 Results of frequency measurements and dual parameter estimation for specimen N°2 using the transversal and longitudinal E-modulus for different load levels

T2		using $E_b$							using $E_L$			
Applied load S	% of yield	$S/S_e$	$f_{1b}$	$f_{2b}$	L	$k_{est}$	$S_{est}$	Error on S	$k_{est}$	$S_{est}$	Error on S	
[N]	[%]	[-]	[Hz]	[Hz]	[m]	[Nm]	[N]	[%]	[Nm]	[N]	[%]	
5199	7.6	0.25	111.9	291.8	1.295	168930	11412	119.5	167610	11440	120.0	
10301	15.1	0.48	117.5	302.4	1.275	133310	18580	80.4	132380	18620	80.8	
15009	22.1	0.67	121.2	308.9	1.255	82973	27006	79.9	82458	27074	80.4	
19620	28.9	0.88	124.5	317.1	1.255	152040	23740	21.0	150890	23780	21.2	
23838	35.1	1.07	128.1	321.0	1.255	113290	34770	45.9	112520	34828	46.1	
28940	42.6	1.29	131.5	325.8	1.255	104930	42756	47.7	104220	42823	48.0	

## FRF plots





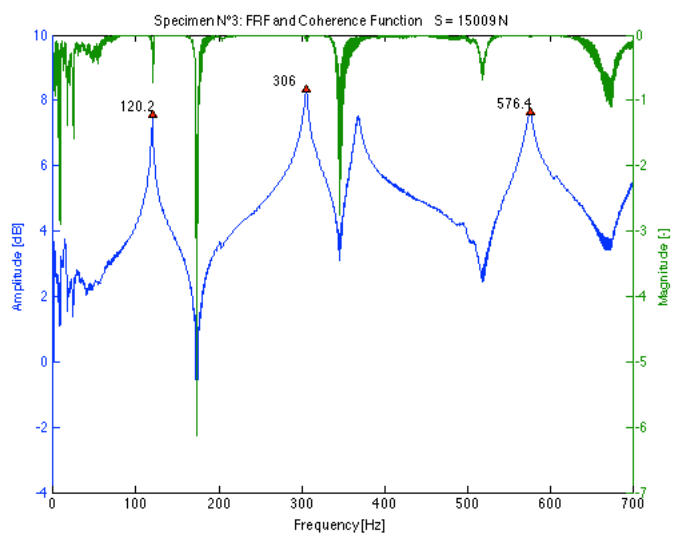
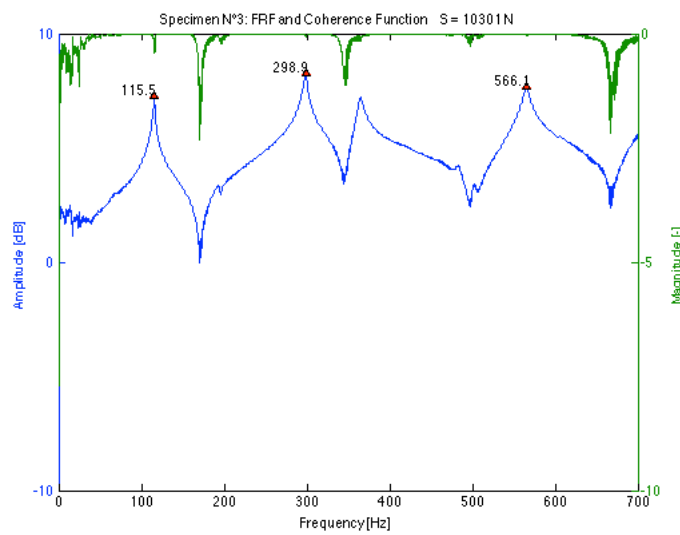
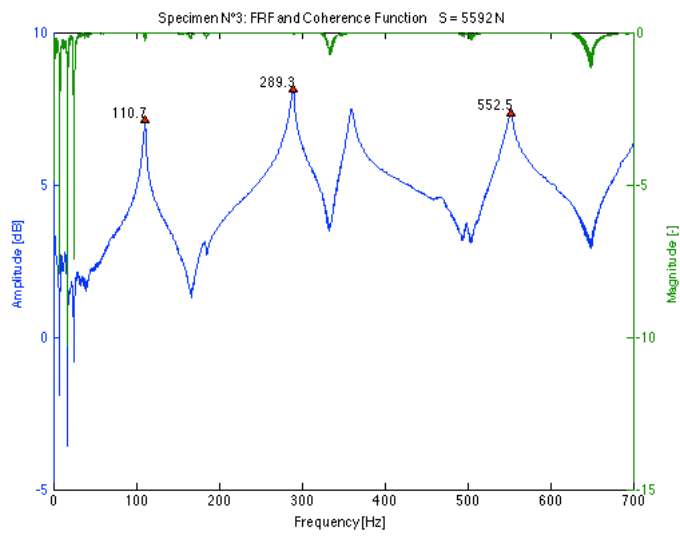
# T3

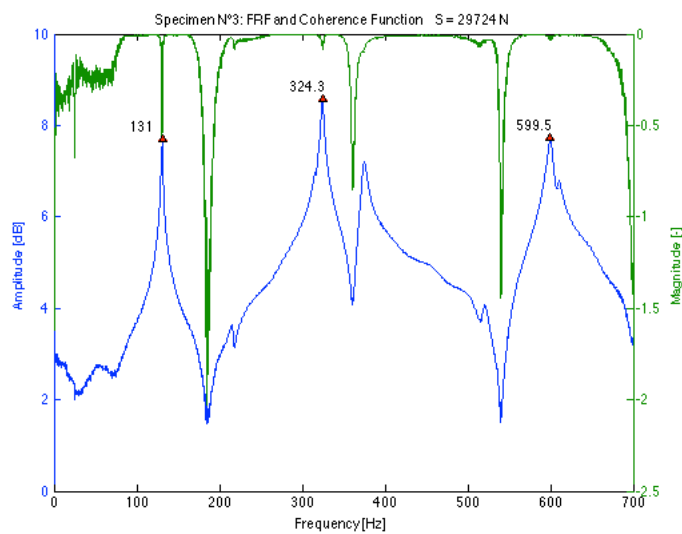
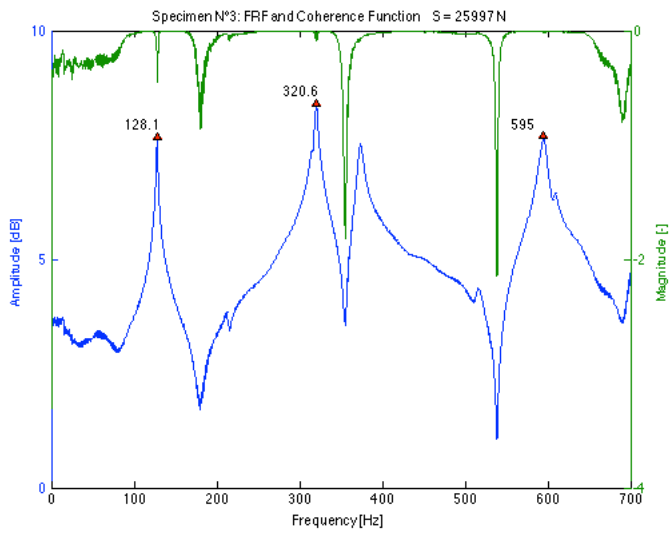
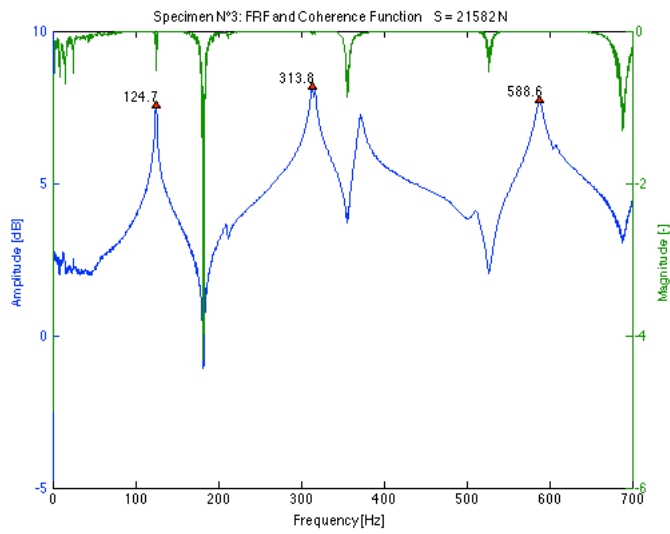
## Data

Table 11-8 Results of frequency measurements and dual parameter estimation for specimen N°3 using the transversal and longitudinal E-modulus for different load levels

T3		using $E_b$							using $E_L$			
Applied load S	% of yield	$S/S_e$	$f_{1b}$	$f_{2b}$	L	$k_{est}$	$S_{est}$	Error on S	$k_{est}$	$S_{est}$	Error on S	
[N]	[%]	[-]	[Hz]	[Hz]	[m]	[Nm]	[N]	[%]	[Nm]	[N]	[%]	
5592	8.2	0.30	110.7	289.3	1.295	216710	8745	56.4	204350	8866	58.5	
10301	15.1	0.53	115.5	298.9	1.275	171170	13397	30.1	162740	13564	31.7	
15009	22.1	0.75	120.2	306.0	1.255	86747	24396	62.5	83441	24747	64.9	
21582	31.7	1.07	124.7	313.8	1.255	105440	29396	36.2	101150	29717	37.7	
25997	38.2	1.29	128.1	320.6	1.255	149050	31055	19.5	142010	31312	20.4	
29724	43.7	1.48	131.0	324.3	1.255	127320	38347	29.0	121630	38661	30.1	

## FRF plots





---

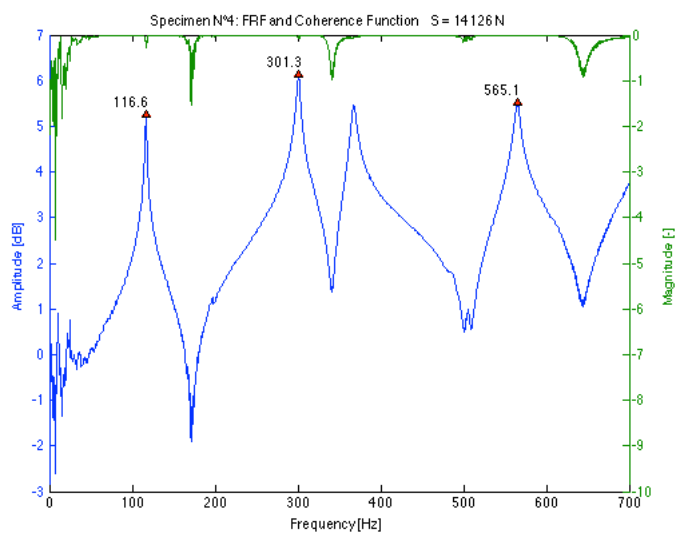
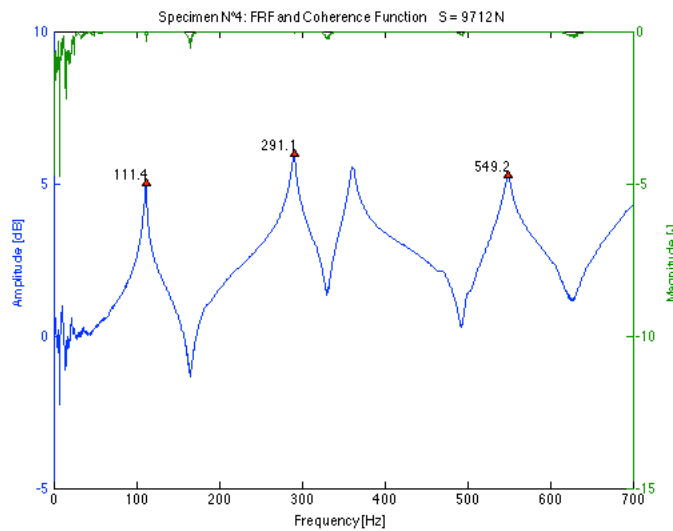
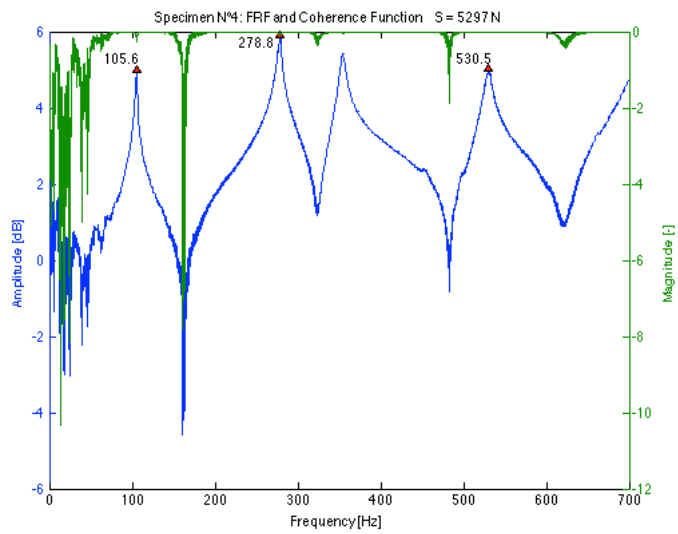
# T4

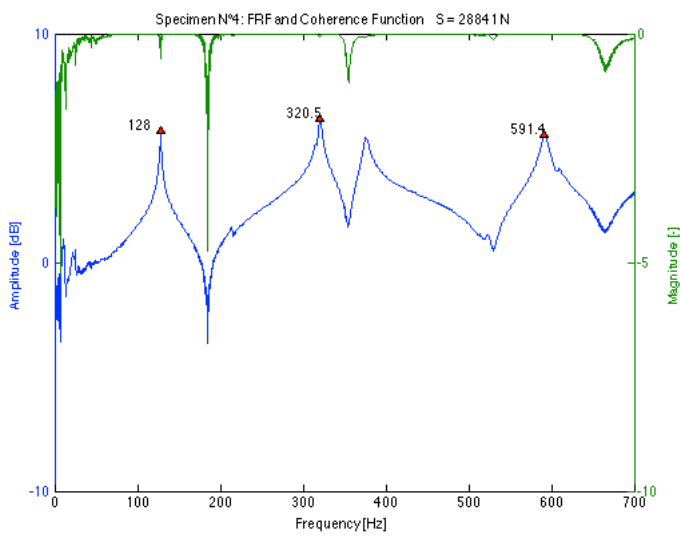
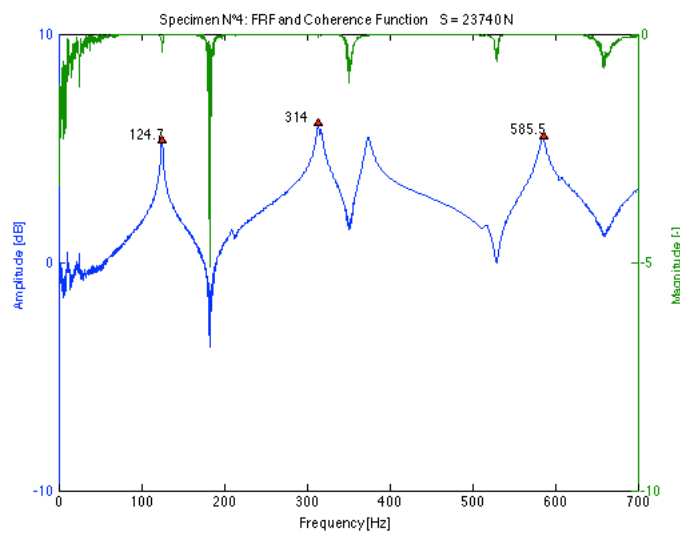
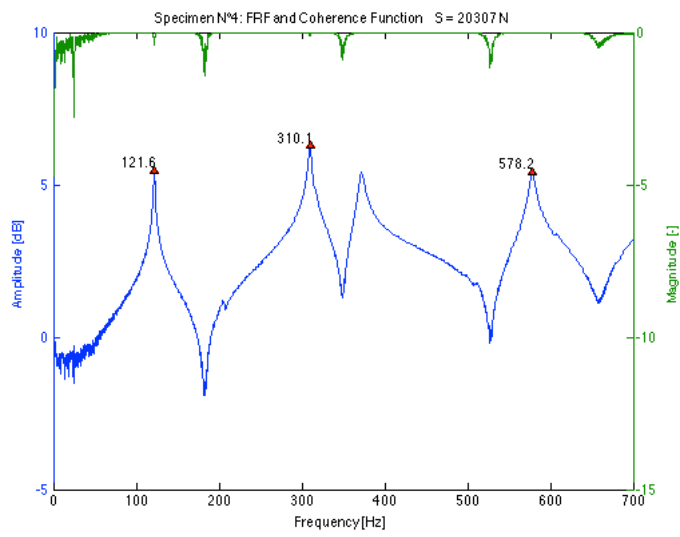
## Data

Table 11-9 Results of frequency measurements and dual parameter estimation for specimen N°4 using the transversal and longitudinal E-modulus for different load levels

T4		using $E_b$							using $E_L$		
Applied load S	% of yield	S/S <sub>c</sub>	f <sub>1b</sub>	f <sub>2b</sub>	L	k <sub>est</sub>	S <sub>est</sub>	Error on S	k <sub>est</sub>	S <sub>est</sub>	Error on S
[N]	[%]	[-]	[Hz]	[Hz]	[m]	[Nm]	[N]	[%]	[Nm]	[N]	[%]
5297	7.8	0.27	105.6	278.8	1.295	101710	7747	46.2	87250	8761	65.4
9712	14.3	0.48	111.4	291.1	1.275	108430	11542	18.8	92573	12613	29.9
14126	20.8	0.68	116.6	301.3	1.255	90174	17759	25.7	77283	19202	35.9
20307	29.9	0.98	121.6	310.1	1.255	116420	22708	11.8	98514	23956	18.0
23740	34.9	1.14	124.7	314.0	1.255	101230	30358	27.9	85890	31896	34.4
28841	42.4	1.39	128.0	320.5	1.255	137020	32173	11.6	114240	33431	15.9

## FRF plots





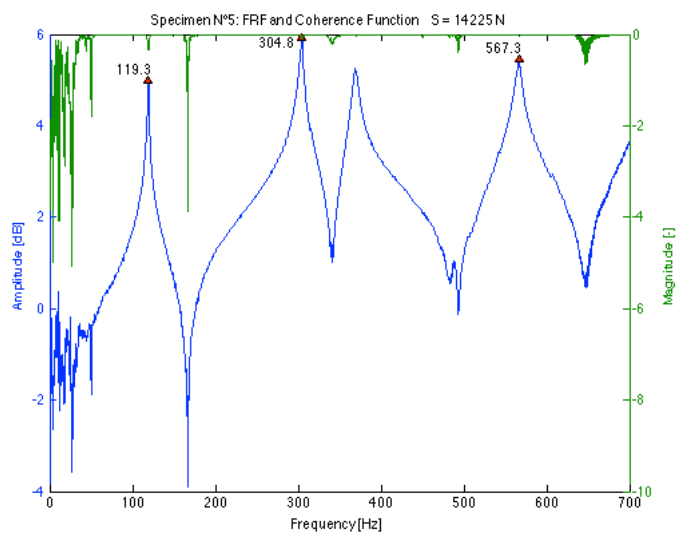
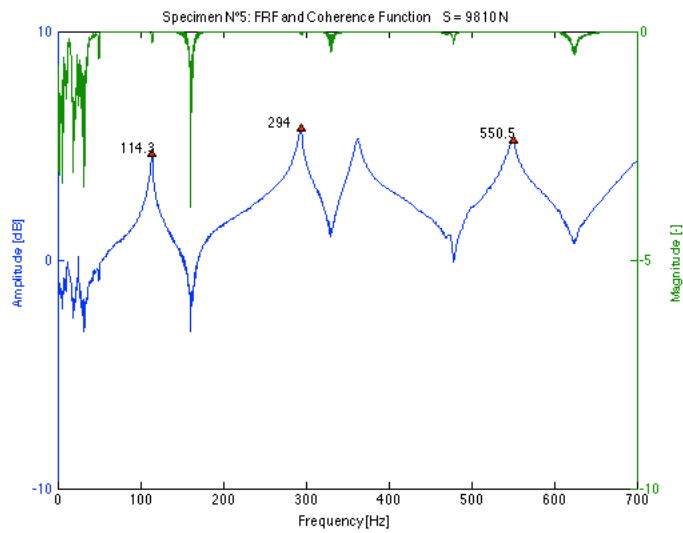
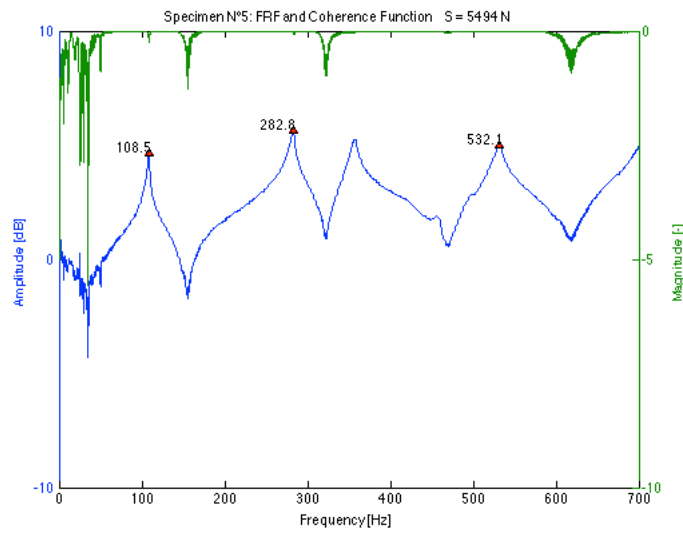
# T5

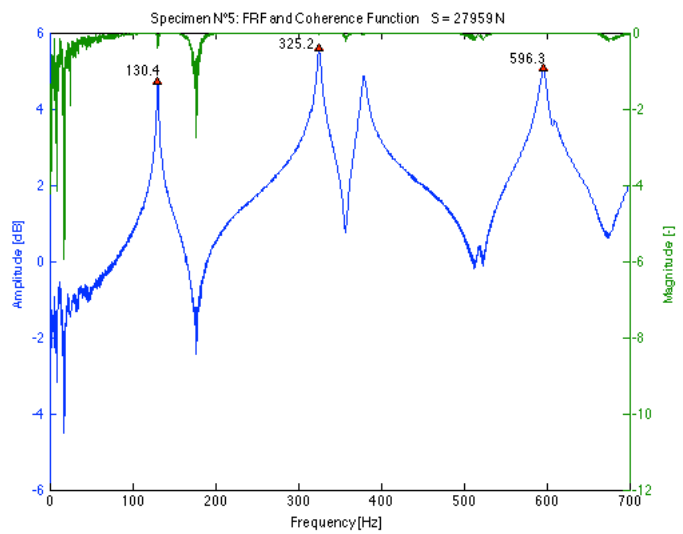
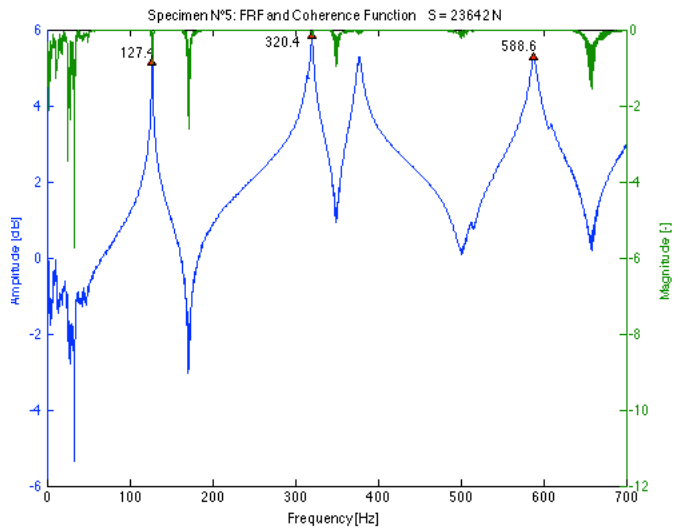
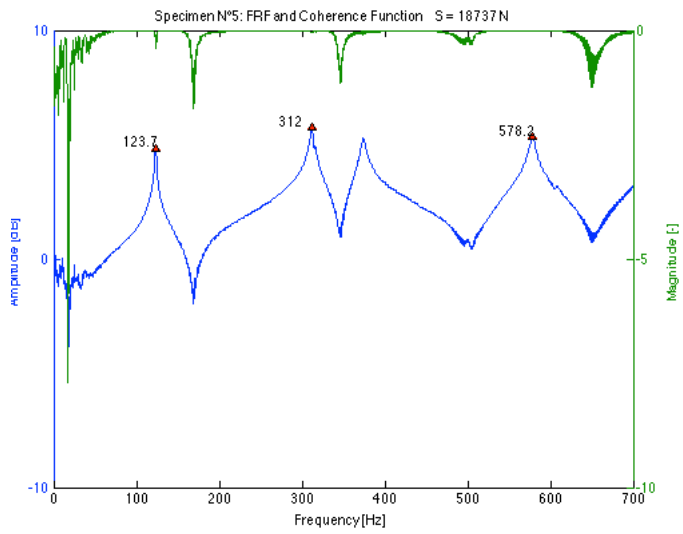
## Data

Table 11-10 Results of frequency measurements and dual parameter estimation for specimen N°5 using the transversal and longitudinal E-modulus for different load levels

T5								using $E_b$		using $E_c$	
Applied load S	% of yield	$S/S_c$	$f_{1b}$	$f_{2b}$	L	$K_{est}$	$S_{est}$	Error on S	$K_{est}$	$S_{est}$	Error on S
[N]	[%]	[-]	[Hz]	[Hz]	[m]	[Nm]	[N]	[%]	[Nm]	[N]	[%]
5494	8.1	0.25	108.5	282.8	1.295	99134	13633	148.2	88456	14515	164.2
9810	14.4	0.43	114.3	294.0	1.275	86171	20905	113.1	76910	22058	124.9
14225	20.9	0.61	119.3	304.8	1.255	83255	25033	76.0	74189	26343	85.2
18737	27.6	0.80	123.7	312.0	1.255	92738	31369	67.4	82321	32652	74.3
23642	34.8	1.01	127.4	320.4	1.255	162980	30157	27.6	141220	30989	31.1
27959	41.1	1.19	130.4	325.2	1.255	173520	35208	25.9	149420	36063	29.0

## FRF plots





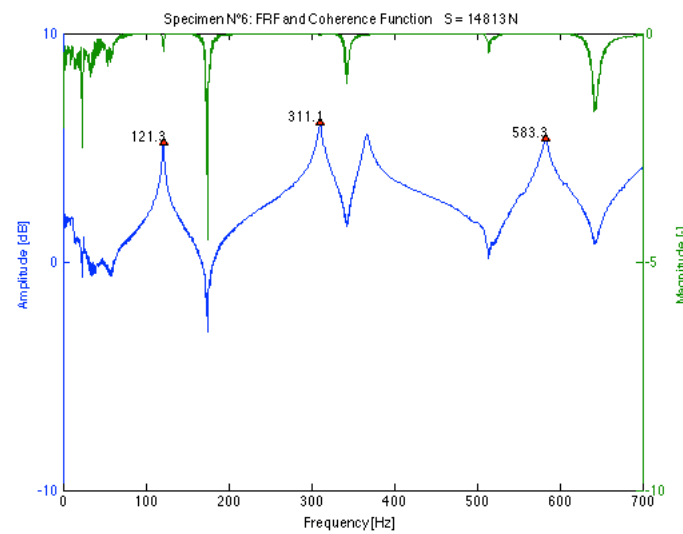
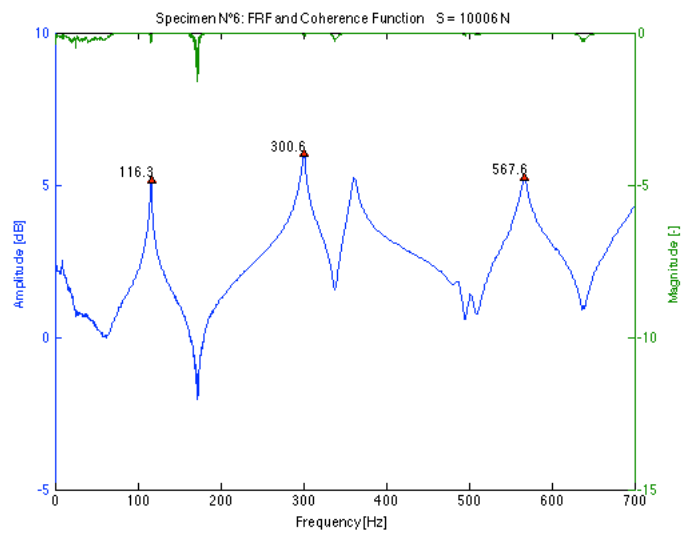
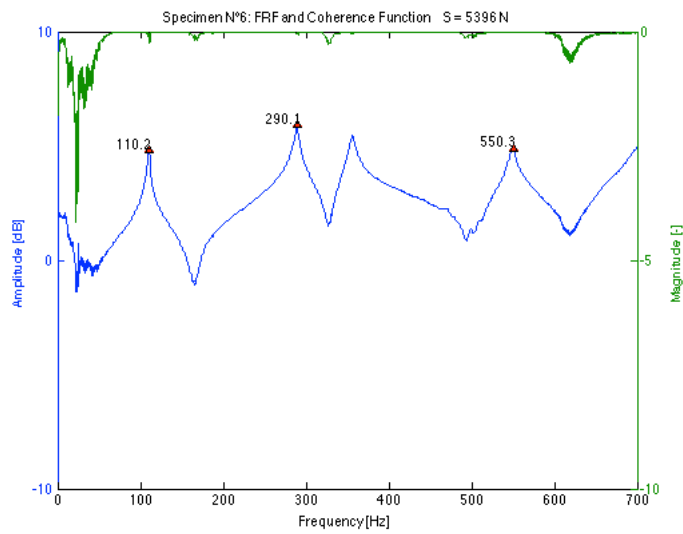
# T6

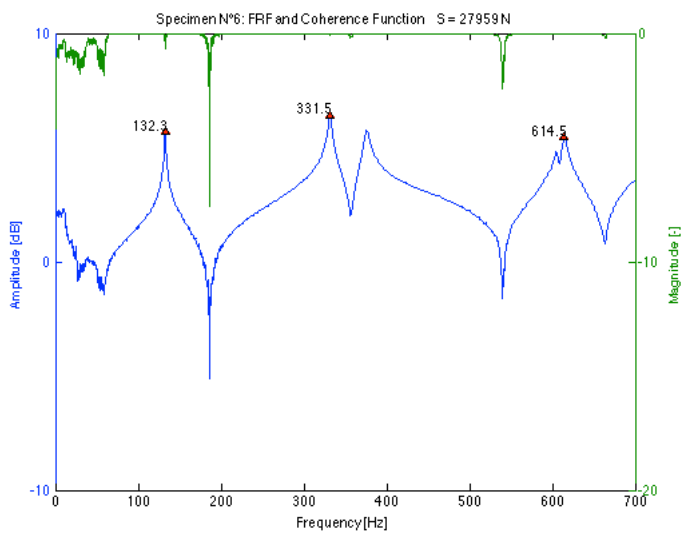
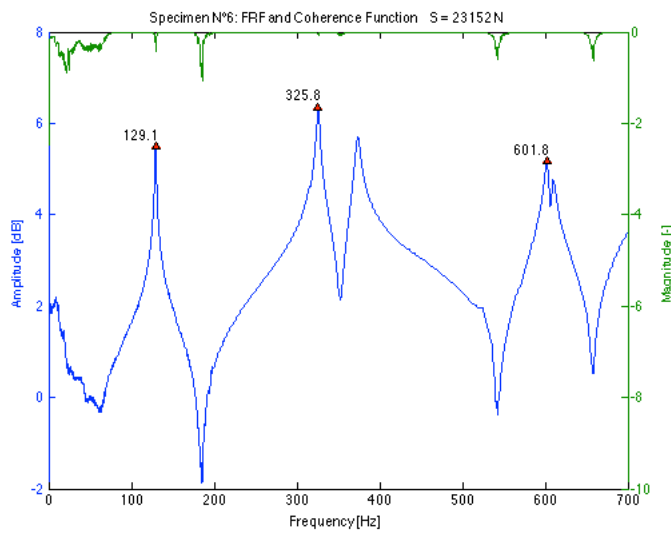
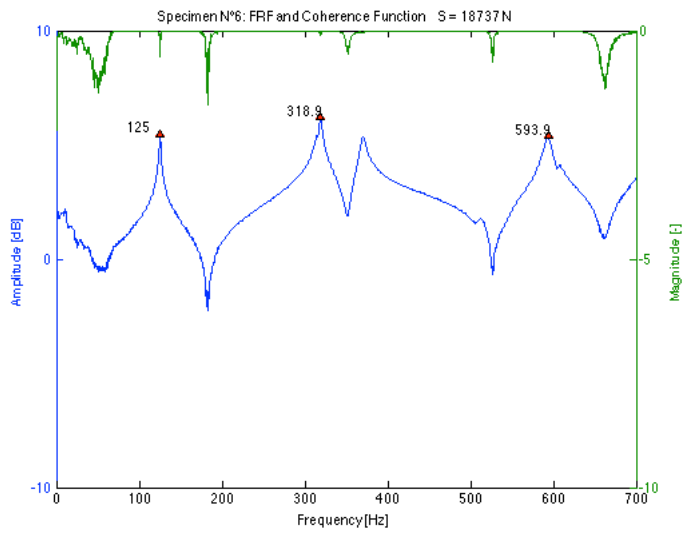
## Data

Table 11-11 Results of frequency measurements and dual parameter estimation for specimen N°6 using the transversal and longitudinal E-modulus for different load levels

T6												
Applied Load S	% of yield	S/S <sub>c</sub>	f <sub>1b</sub>	f <sub>2b</sub>	L	k <sub>est</sub>	using E <sub>b</sub>			using E <sub>c</sub>		
[N]	[%]	[-]	[Hz]	[Hz]	[m]	[Nm]	S <sub>est</sub>	Error on S	k <sub>est</sub>	S <sub>est</sub>	Error on S	
							[N]	[%]	[Nm]	[N]	[%]	
5396	7.9	0.25	110.2	290.1	1.295	149030	6841	26.8	141410	7063	30.9	
10006	14.7	0.44	116.3	300.6	1.275	103310	16825	68.1	98620	17198	71.9	
14813	21.8	0.64	121.3	311.1	1.255	93768	21630	46.0	89528	22083	49.1	
18737	27.6	0.81	125.0	318.9	1.255	144740	21782	16.3	137220	22101	18.0	
23152	34.0	1.00	129.1	325.8	1.255	171770	27198	17.5	161950	27504	18.8	
27959	41.1	1.20	132.3	331.5	1.255	213350	30845	10.3	199480	31127	11.3	

## FRF plots





---

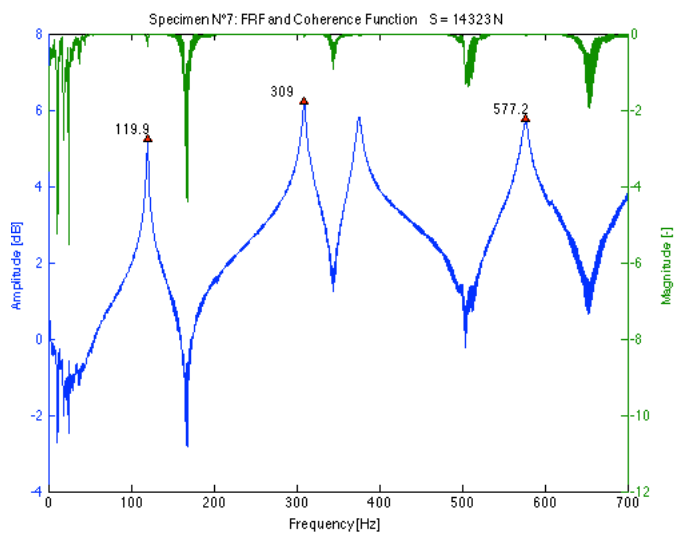
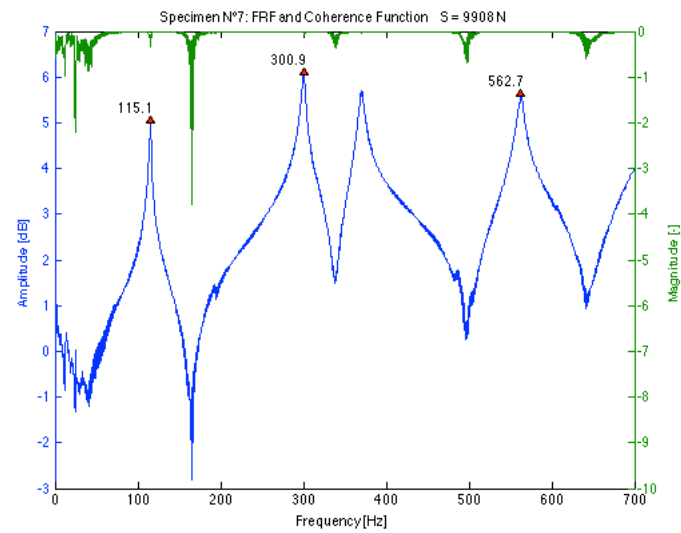
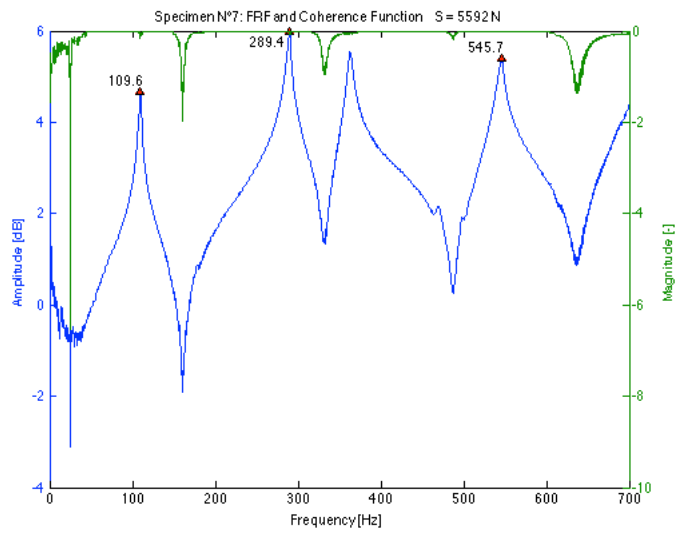
# T7

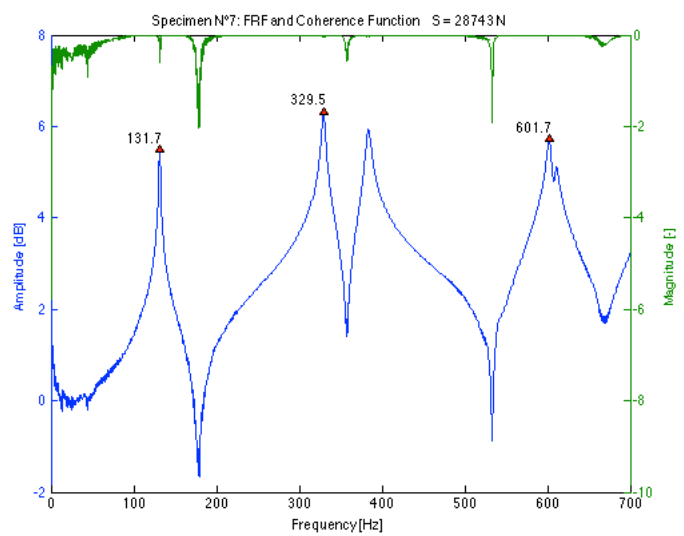
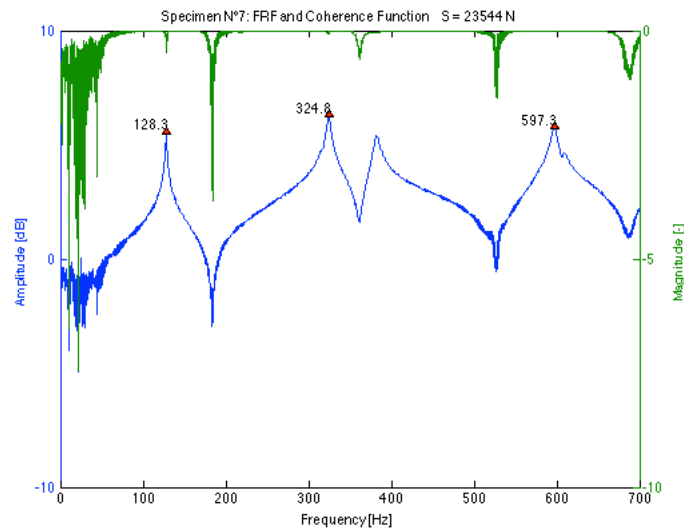
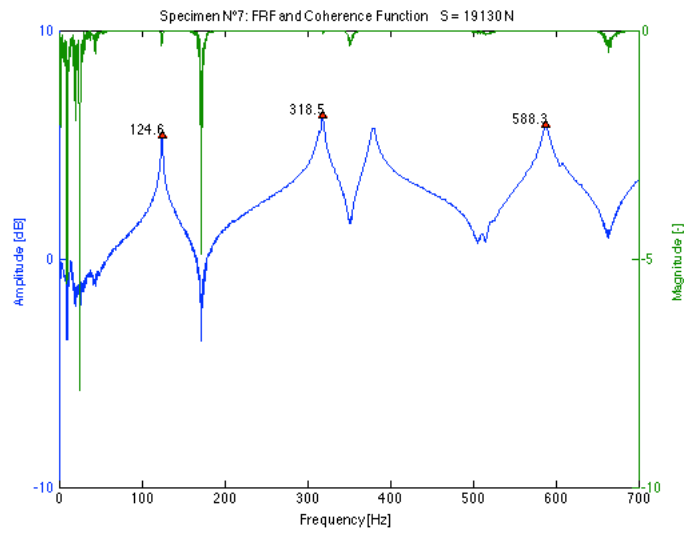
## Data

Table 11-12 Results of frequency measurements and dual parameter estimation for specimen N°7 using the transversal and longitudinal E-modulus for different load levels

T7		using $E_b$							using $E_c$		
Applied load S [N]	% of yield [%]	S/S <sub>c</sub> [-]	f <sub>1b</sub> [Hz]	f <sub>2b</sub> [Hz]	L [m]	k <sub>est</sub> [Nm]	S <sub>est</sub> [N]	Error on S [%]	k <sub>est</sub> [Nm]	S <sub>est</sub> [N]	Error on S [%]
5592	8.2	0.29	109.6	289.4	1.295	287260	4259	-23.8	233840	4546	-18.7
9908	14.6	0.50	115.1	300.9	1.275	279210	8065	-18.6	228300	8409	-15.1
14323	21.1	0.71	119.9	309.0	1.255	147170	15894	11.0	128230	16558	15.6
19130	28.1	0.94	124.6	318.5	1.255	279750	18234	-4.7	228240	18692	-2.3
23544	34.6	1.16	128.3	324.8	1.255	374620	22881	-2.8	291200	23319	-1.0
28743	42.3	1.42	131.7	329.5	1.255	326870	29724	3.4	259430	30256	5.3

## FRF plots





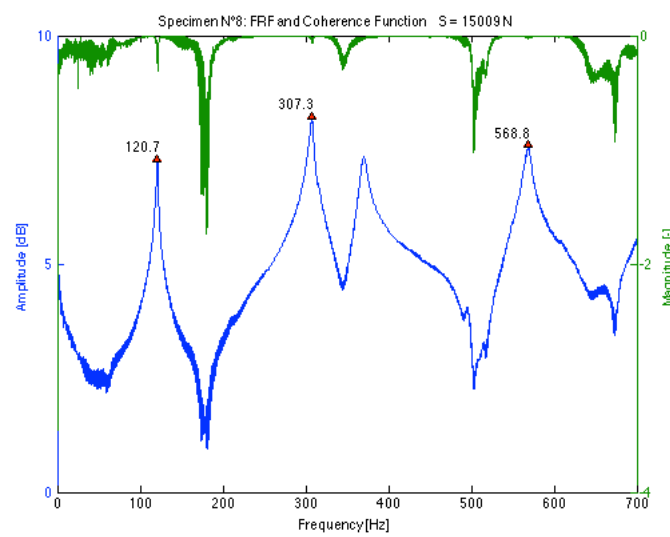
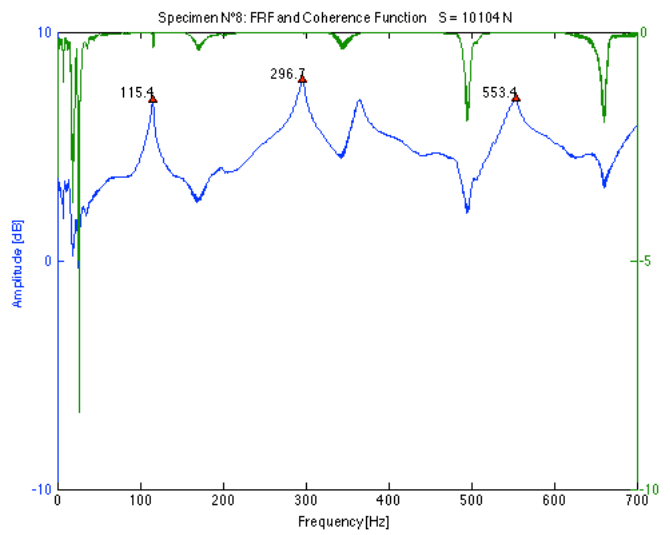
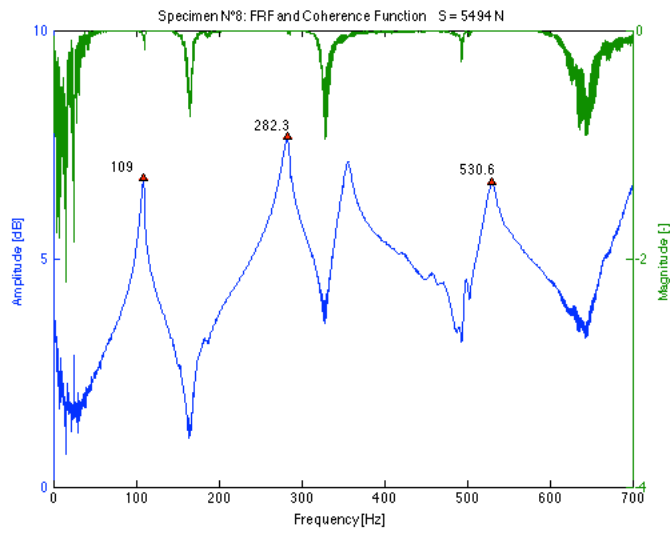
# T8

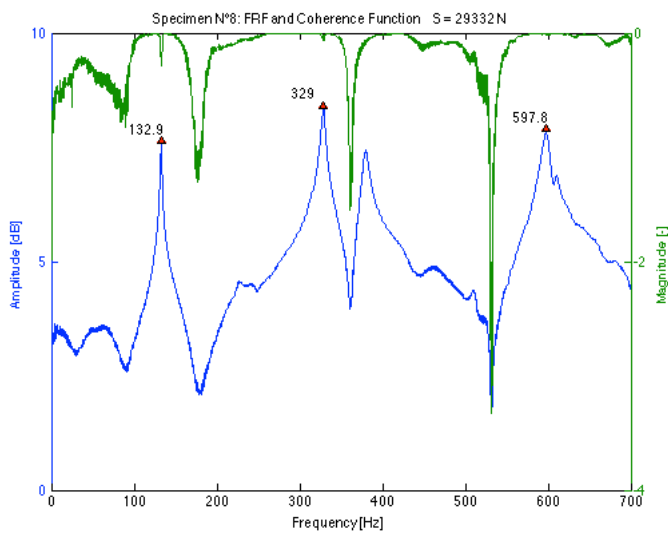
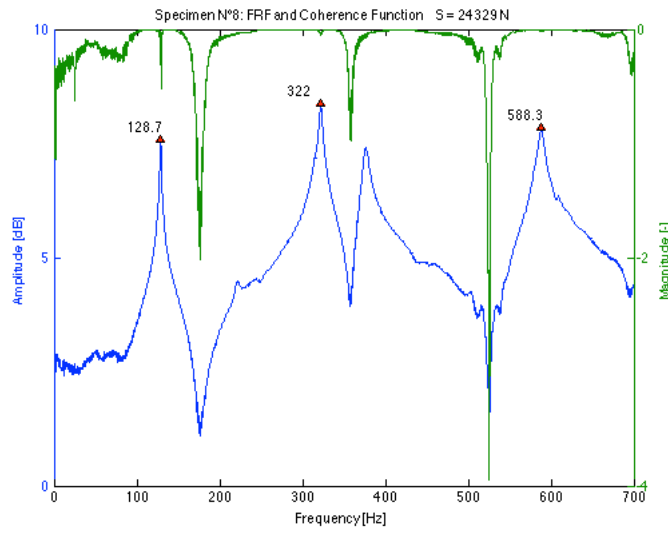
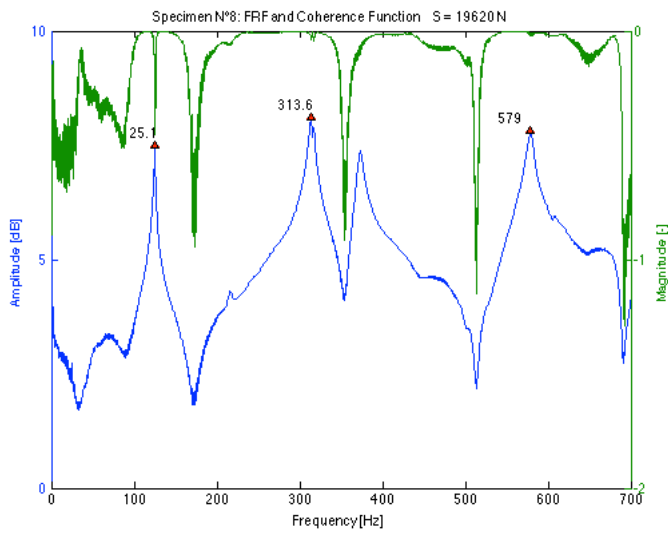
## Data

Table 11-13 Results of frequency measurements and dual parameter estimation for specimen N°8 using the transversal and longitudinal E-modulus for different load levels

T8		using $E_s$										
Applied load S	% of yield	$S/S_c$	$f_{1b}$	$f_{2b}$	L	$k_{est}$	$S_{est}$	Error on S	$k_{est}$	$S_{est}$	Error on S	
[N]	[%]	[-]	[Hz]	[Hz]	[m]	[Nm]	[N]	[%]	[Nm]	[N]	[%]	
5494	8.1	0.27	109.0	282.3	1.295	79109	15349	179.4	72501	16055	192.2	
10104	14.9	0.49	115.4	296.7	1.275	104500	17163	69.9	95073	17764	75.8	
15009	22.1	0.70	120.7	307.3	1.255	89357	22872	52.4	81499	23649	57.6	
19620	28.9	0.91	125.1	313.6	1.255	84086	31319	59.6	76565	32230	64.3	
24329	35.8	1.13	128.7	322.0	1.255	154730	29639	21.8	137800	30213	24.2	
29332	43.1	1.37	132.9	329.0	1.255	180530	35532	21.1	158870	36104	23.1	

## FRF plots





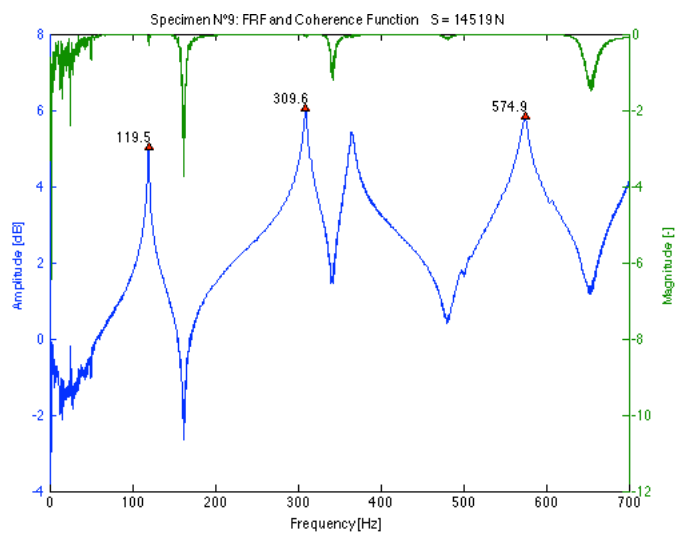
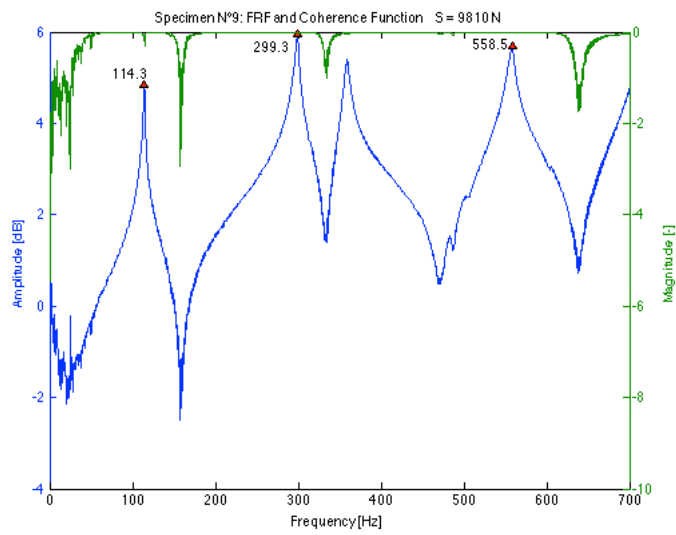
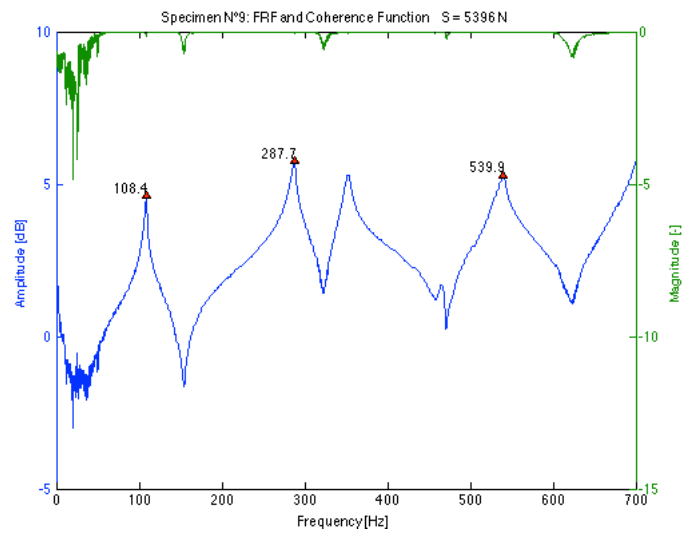
# T9

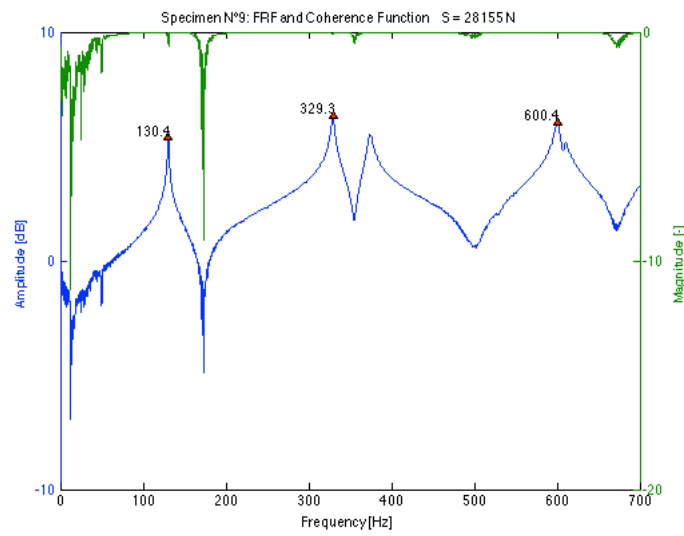
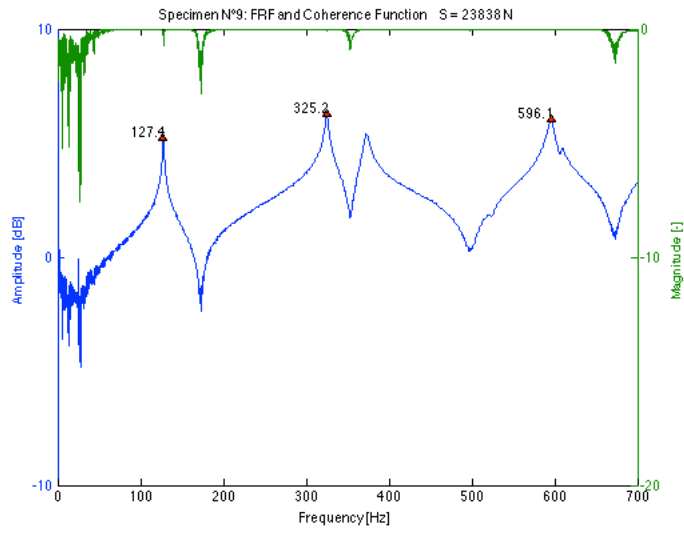
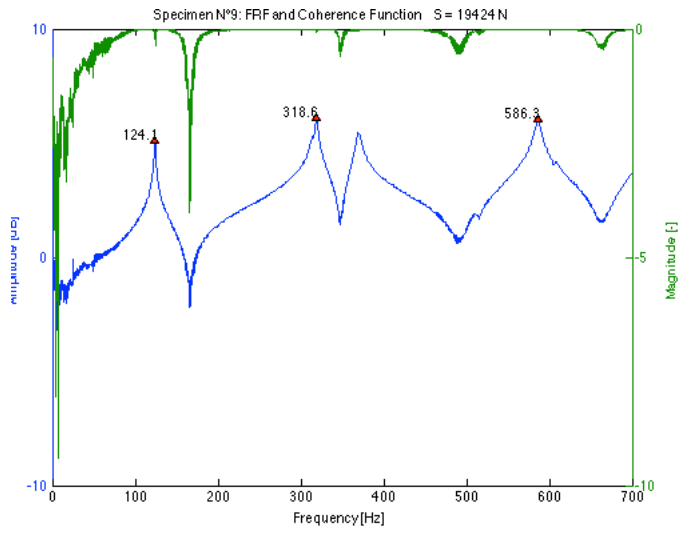
## Data

Table 11-14 Results of frequency measurements and dual parameter estimation for specimen N°9 using the transversal and longitudinal E-modulus for different load levels

T9		using $E_s$							using $E_L$			
Applied load S	% of yield	$S/S_e$	$f_{1b}$	$f_{2b}$	L	$k_{est}$	$S_{est}$	Error on S	$k_{est}$	$S_{est}$	Error on S	
[N]	[%]	[-]	[Hz]	[Hz]	[m]	[Nm]	[N]	[%]	[Nm]	[N]	[%]	
5396	7.9	0.24	108.4	287.7	1.295	187880	2787	-48.3	150930	3535	-34.5	
9810	14.4	0.43	114.3	299.3	1.275	168150	8589	-12.5	136480	9554	-2.6	
14519	21.4	0.62	119.5	309.6	1.255	137750	14400	-0.8	113470	15709	8.2	
19424	28.6	0.83	124.1	318.6	1.255	225610	17059	-12.2	176150	18011	-7.3	
23838	35.1	1.01	127.4	325.2	1.255	380910	19052	-20.1	269650	19785	-17.0	
28155	41.4	1.20	130.4	329.3	1.255	340460	25394	-9.8	246260	26267	-6.7	

## FRF plots





---

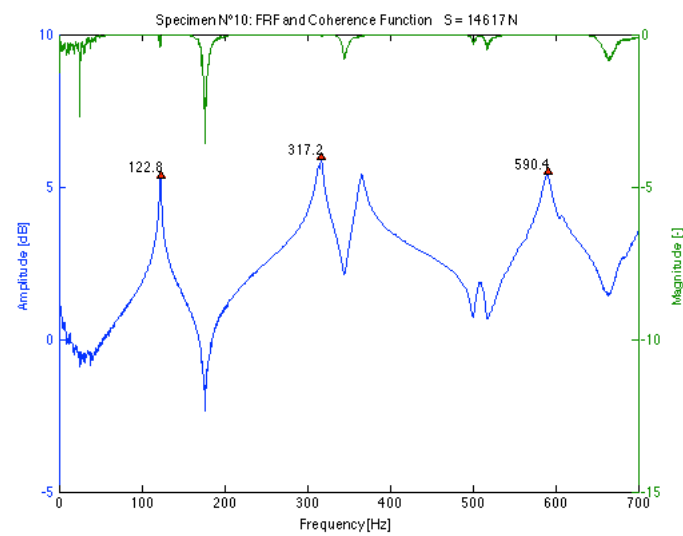
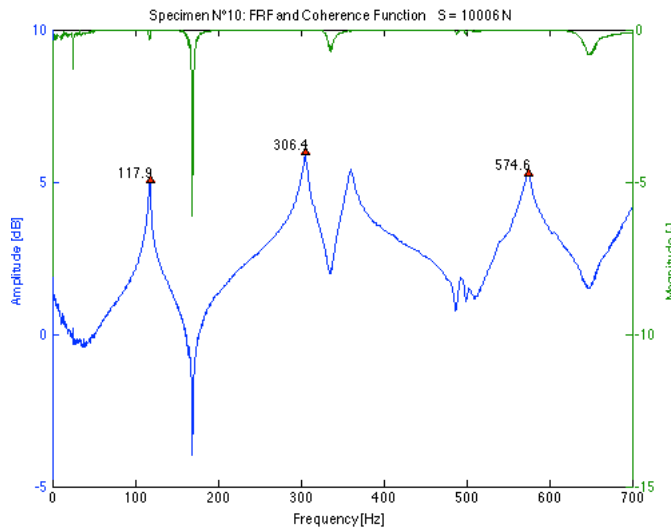
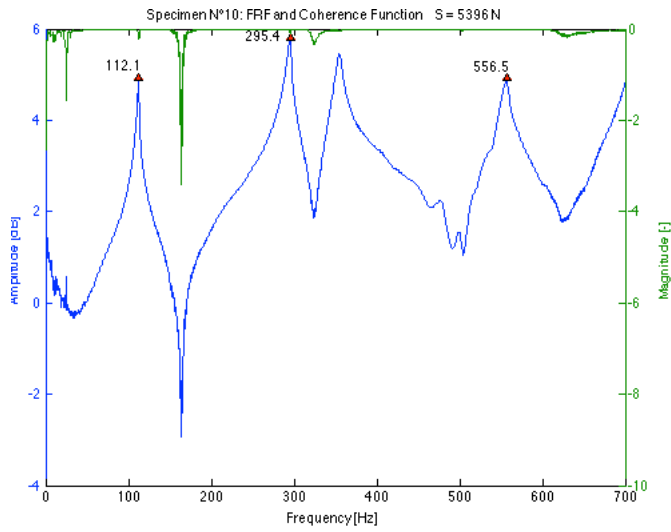
# T10

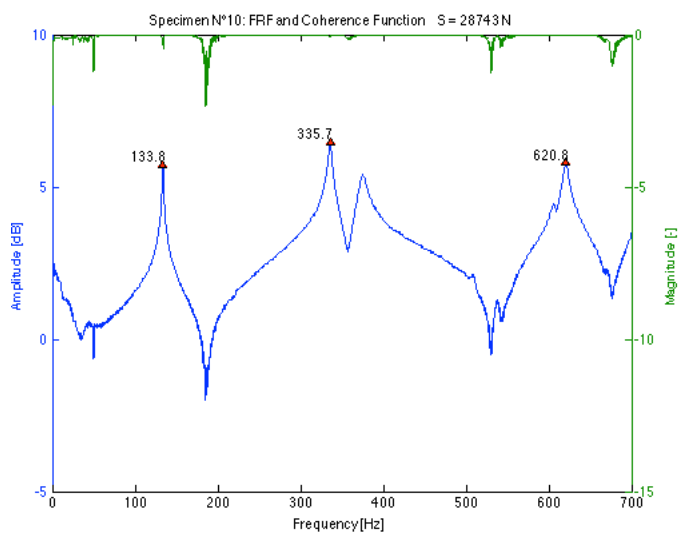
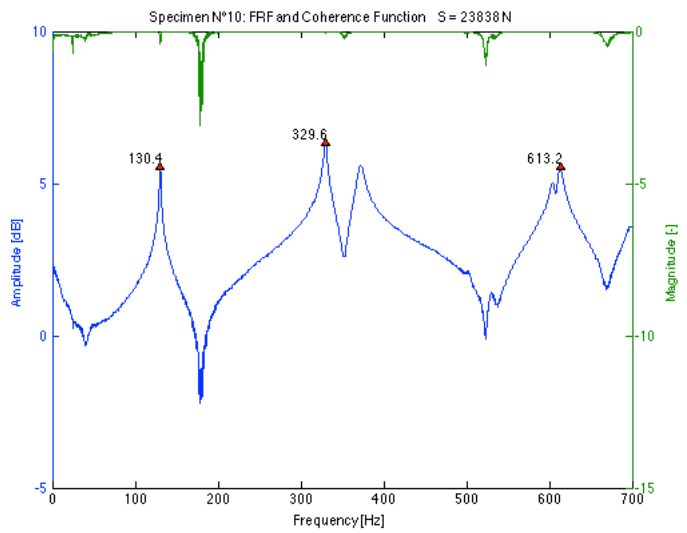
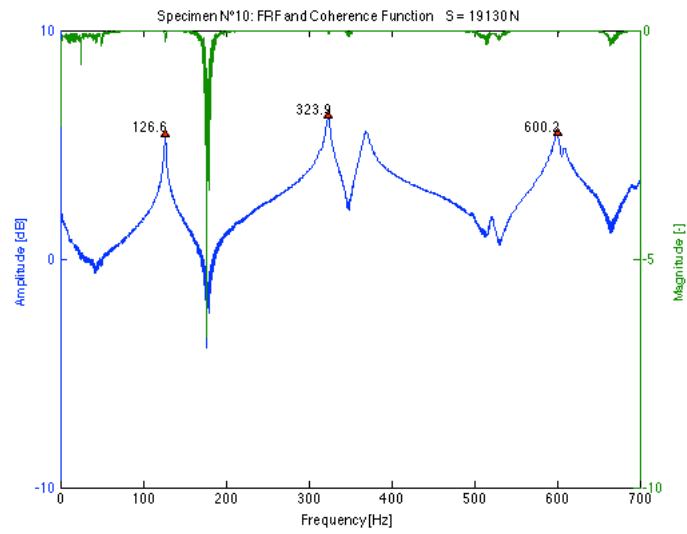
## Data

Table 11-15 Results of frequency measurements and dual parameter estimation for specimen N°10 using the transversal and longitudinal E-modulus for different load levels

T10		using $E_s$							using $E_L$			
Applied load S	% of yield	S/S <sub>e</sub>	f <sub>1b</sub>	f <sub>2b</sub>	L	K <sub>est</sub>	S <sub>est</sub>	Error on S	K <sub>est</sub>	S <sub>est</sub>	Error on S	
[N]	[%]	[-]	[Hz]	[Hz]	[m]	[Nm]	[N]	[%]	[Nm]	[N]	[%]	
5396	7.9	0.25	112.1	295.4	1.295	207760	5692	5.5	170990	6306	16.9	
10006	14.7	0.45	117.9	306.4	1.275	164850	12583	25.8	138530	13460	34.5	
14617	21.5	0.63	122.8	317.2	1.255	159650	15749	7.7	134410	16740	14.5	
19130	28.1	0.83	126.6	323.9	1.255	203540	19853	3.8	167280	20741	8.4	
23838	35.1	1.03	130.4	329.6	1.255	207510	26762	12.3	169700	27736	16.4	
28743	42.3	1.24	133.8	335.7	1.255	271040	30673	6.7	213870	31558	9.8	

## FRF plots





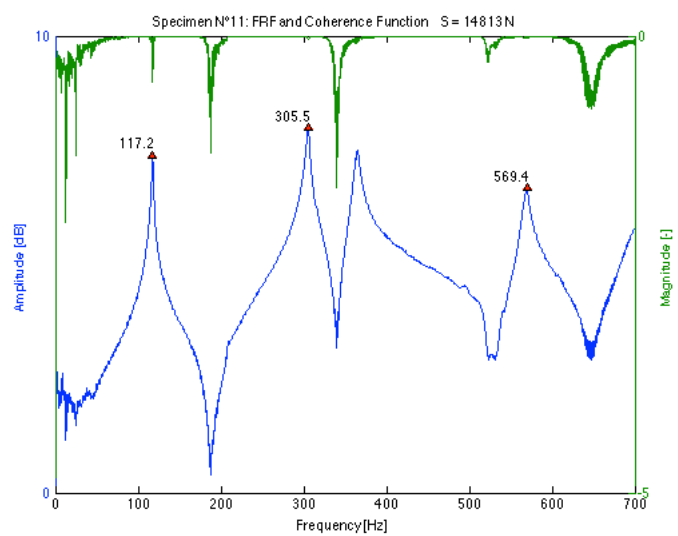
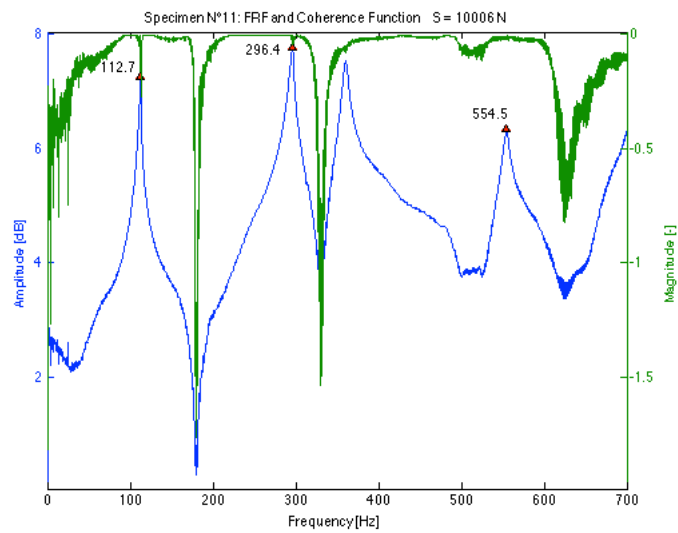
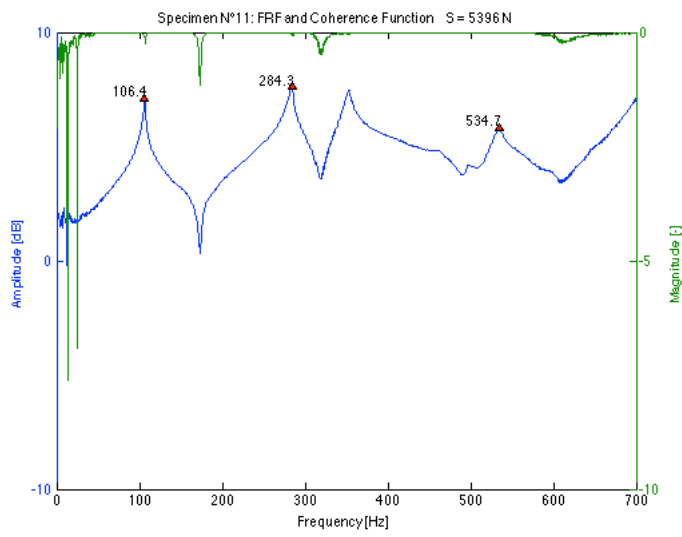
# T11

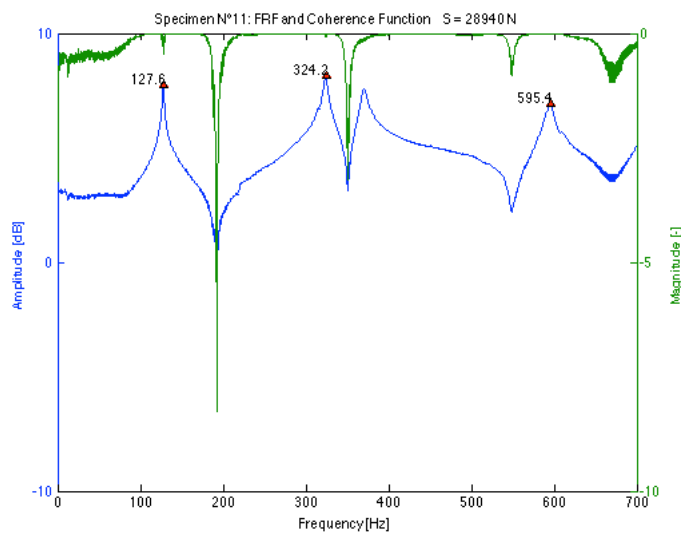
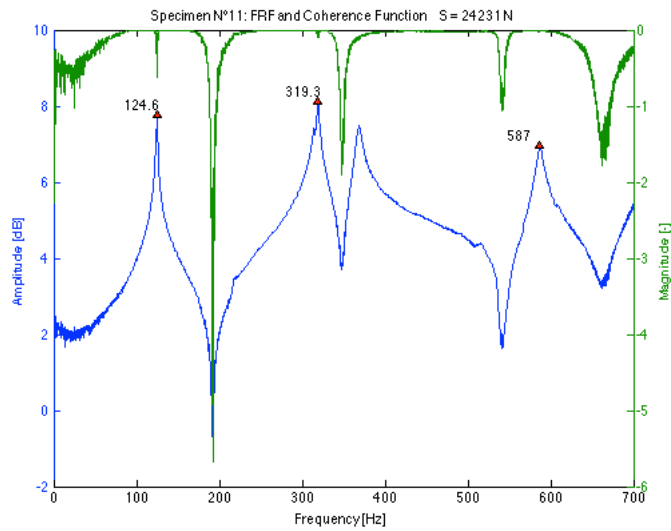
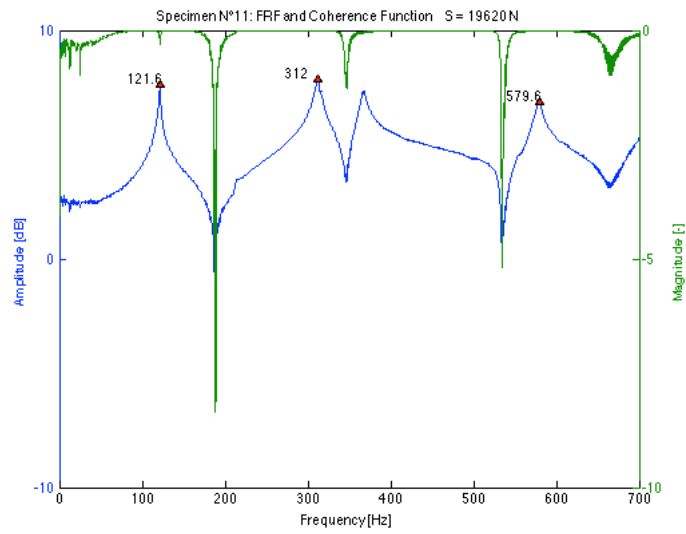
## Data

Table 11-16 Results of frequency measurements and dual parameter estimation for specimen N°11 using the transversal and longitudinal E-modulus for different load levels

T11		using $E_b$							using $E_c$			
Applied load S	% of yield	$S/S_c$	$f_{1b}$	$f_{2b}$	L	$k_{est}$	$S_{est}$	Error on S	$k_{est}$	$S_{est}$	Error on S	
[N]	[%]	[-]	[Hz]	[Hz]	[m]	[Nm]	[N]	[%]	[Nm]	[N]	[%]	
5396	7.9	0.24	106.4	284.3	1.295	288050	-384	-107	230580	-25	-100.5	
10006	14.7	0.43	112.7	296.4	1.275	248730	6040	-39.6	203080	6542	-34.6	
14813	21.8	0.62	117.2	305.5	1.255	188660	10724	-27.6	158740	11437	-22.8	
19620	28.9	0.82	121.6	312.0	1.255	162060	19295	-1.7	193640	18495	-5.7	
24231	35.6	1.02	124.6	319.3	1.255	338090	17875	-26.2	462720	17399	-28.2	
28940	42.6	1.21	127.6	324.2	1.255	585890	21945	-24.2	402890	22425	-22.5	

## FRF plots





---

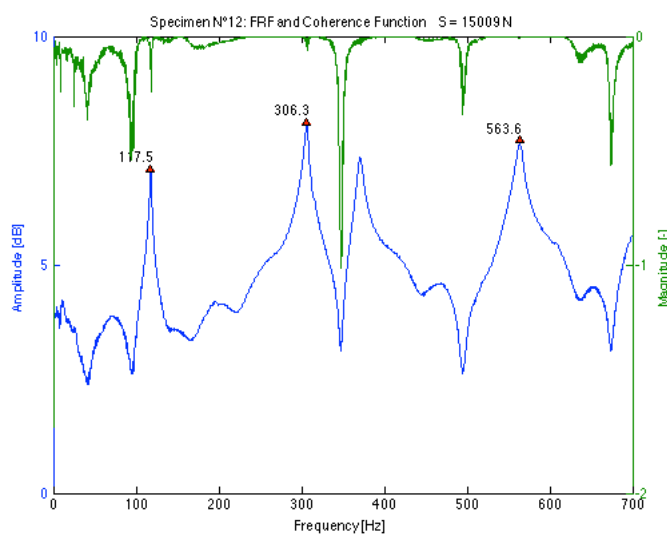
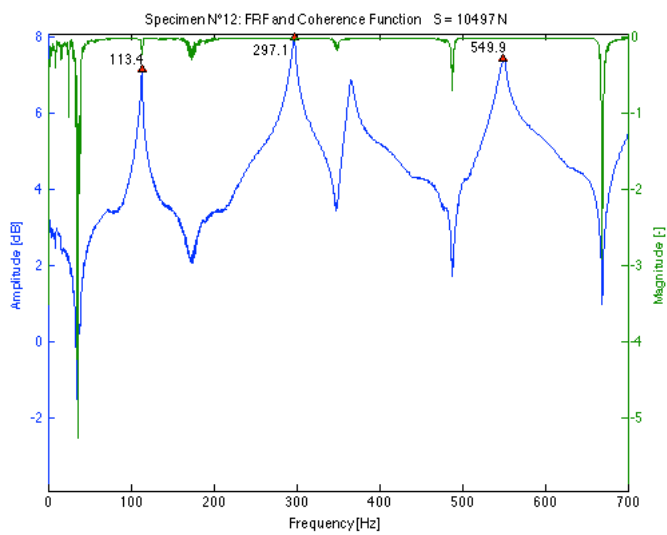
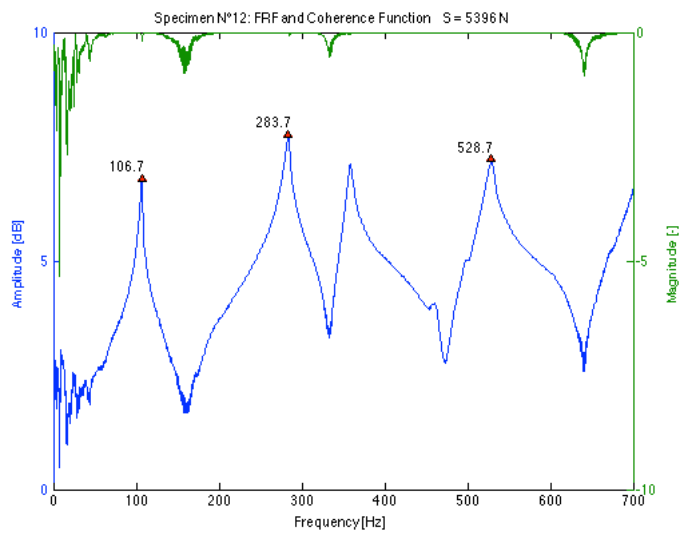
# T12

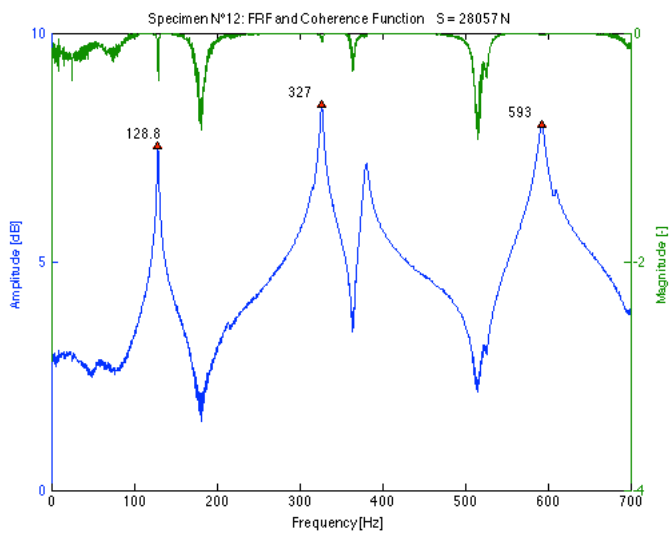
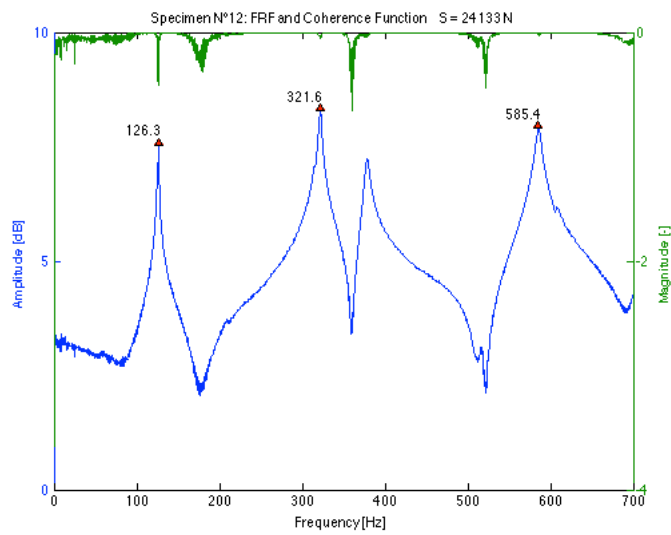
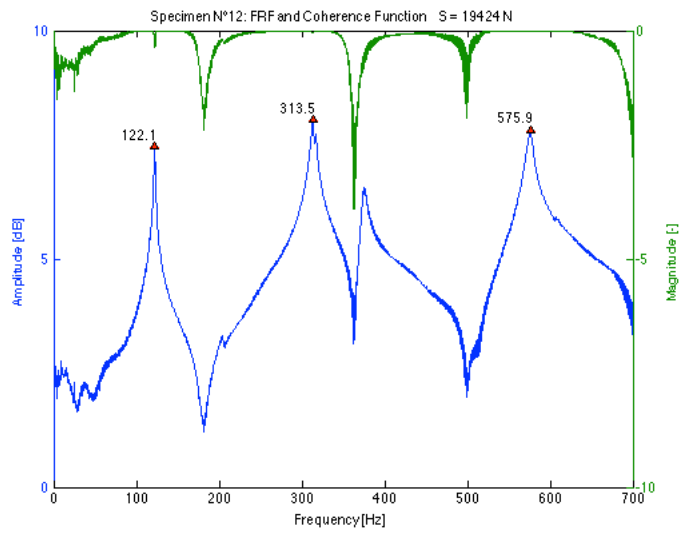
## Data

Table 11-17 Results of frequency measurements and dual parameter estimation for specimen N°12 using the transversal and longitudinal E-modulus for different load levels

T12		using $E_c$										
Applied load S	% of yield	$S/S_c$	$f_{12}$	$f_{20}$	L	$k_{est}$	$S_{est}$	Error on S	$k_{est}$	$S_{est}$	Error on S	
[N]	[%]	[-]	[Hz]	[Hz]	[m]	[Nm]	[N]	[%]	[Nm]	[N]	[%]	
5396	7.9	0.25	106.7	283.7	1.295	159830	3237	-40.0	133860	3973	-26.4	
10497	15.4	0.47	113.4	297.1	1.275	165010	9078	-13.5	137570	9920	-5.5	
15009	22.1	0.65	117.5	306.3	1.255	149120	11769	-21.6	125290	12772	-14.9	
19424	28.6	0.84	122.1	313.5	1.255	165150	18848	-3.0	137190	19883	2.4	
24133	35.5	1.04	126.3	321.6	1.255	260750	21974	-8.9	205070	22781	-5.6	
28057	41.3	1.21	128.8	327.0	1.255	463540	22755	-18.9	325500	23370	-16.7	

## FRF plots





---

## T13

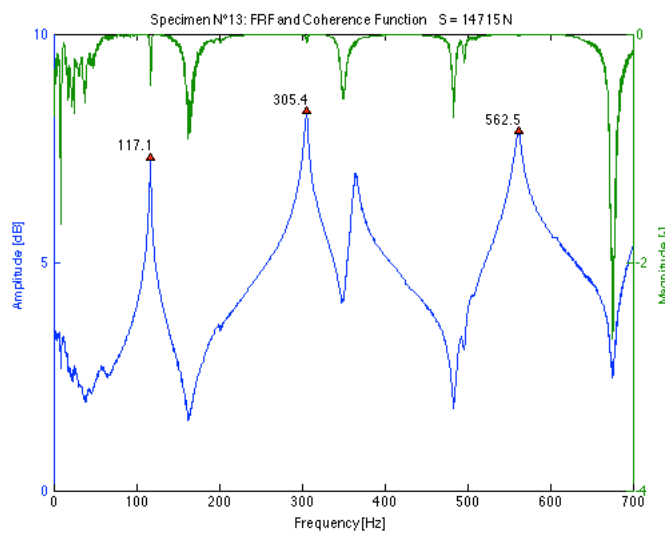
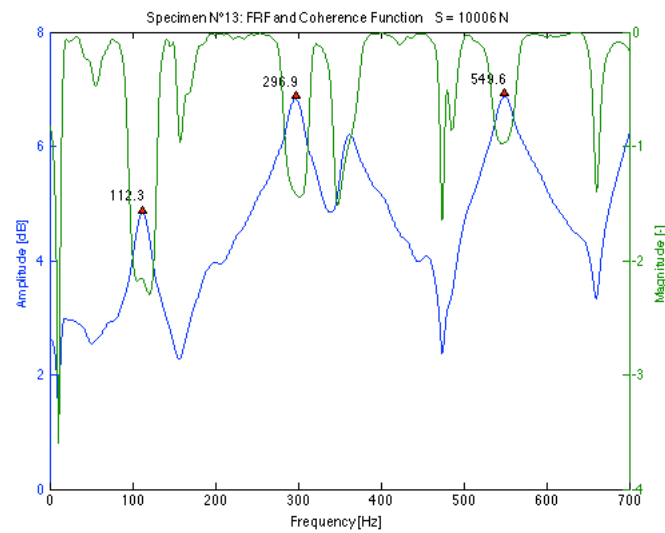
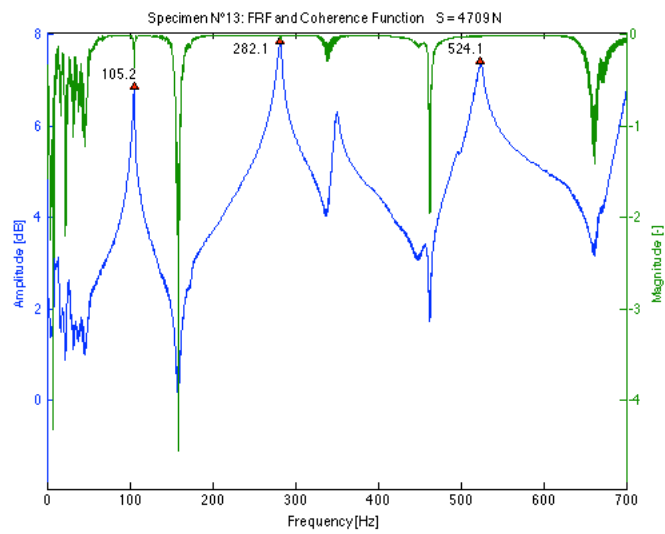
### Data

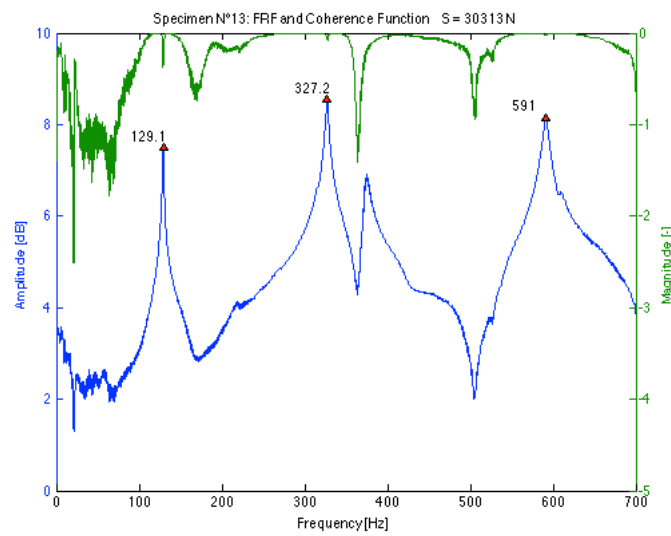
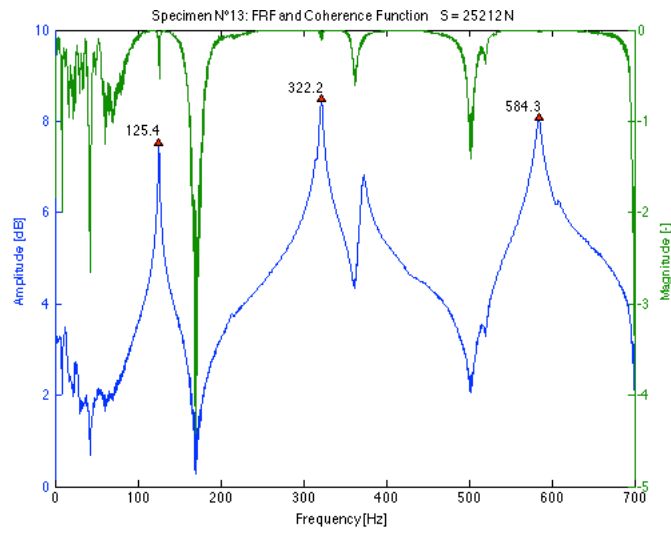
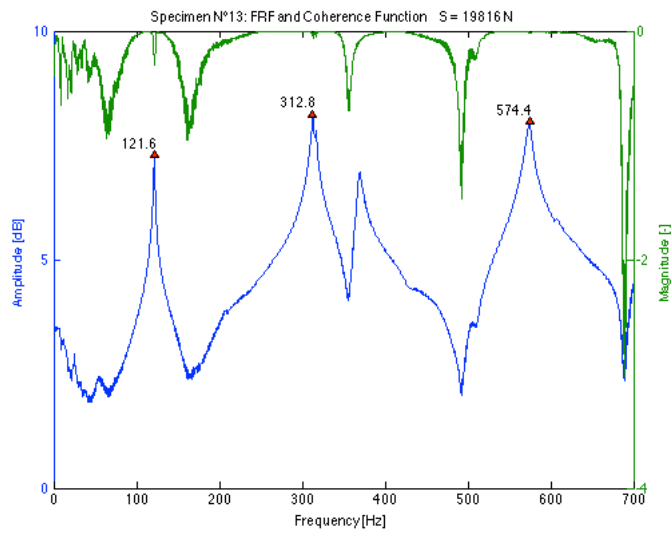
Table 11-18 Results of frequency measurements and dual parameter estimation for specimen N°13 using the transversal and longitudinal E-modulus for different load levels

T13			using $E_b$						using $E_c$		
Applied load S	% of yield	$S/S_c$	$f_{1b}$	$f_{2b}$	L	$K_{est}$	$S_{est}$	Error on S	$K_{est}$	$S_{est}$	Error on S
[N]	[%]	[-]	[Hz]	[Hz]	[m]	[Nm]	[N]	[%]	[Nm]	[N]	[%]
4709	6.9	0.22	105.2	282.1	1.295	252970	-811	-117.2	134500	388	-91.8
10006	14.7	0.46	112.3	296.9	1.275	/	/	/	/	/	/
14715	21.6	0.66	117.1	305.4	1.255	197430	9955	-32.3	108950	12920	-12.2
19816	29.1	0.89	121.6	312.8	1.255	246300	15869	-19.9	126570	18722	-5.5
25212	37.1	1.13	125.4	322.2	1.255	2217100	14807	-41.3	302390	16193	-35.8
30313	44.6	1.36	129.1	327.2	1.255	1286700	22243	-26.6	267150	24057	-20.6

The results for the second load levels were not calculated since the according coherence function showed strong irregularities.

## FRF plots





---

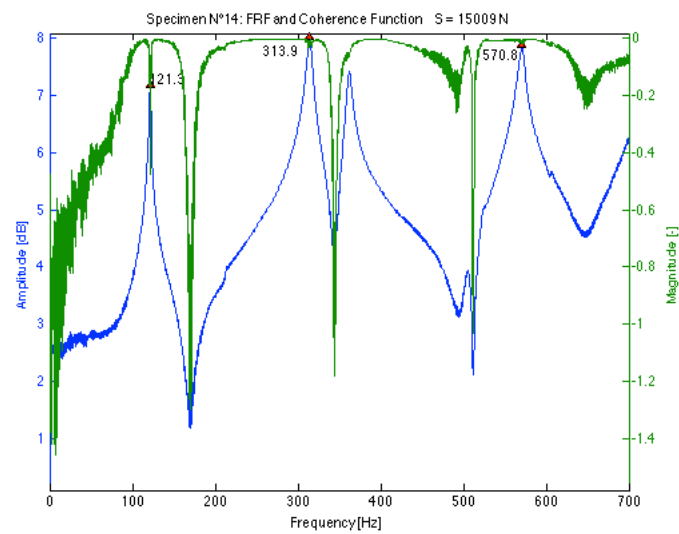
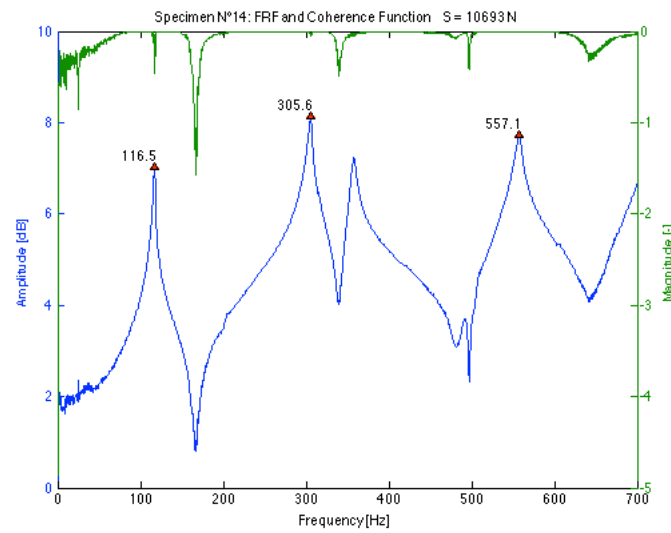
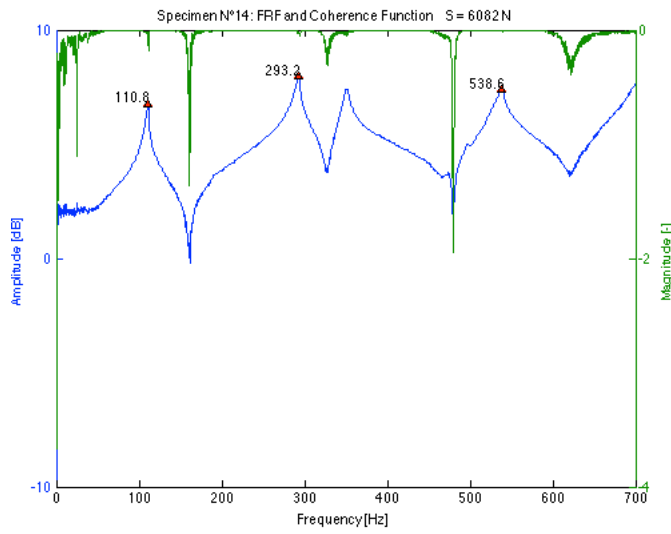
# T14

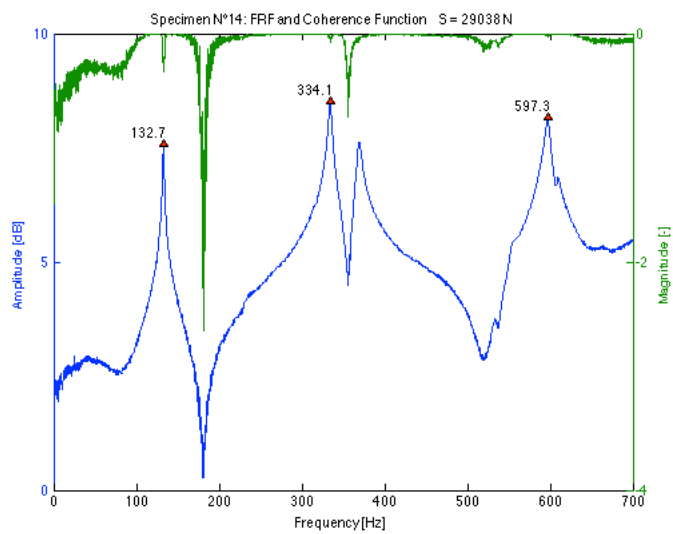
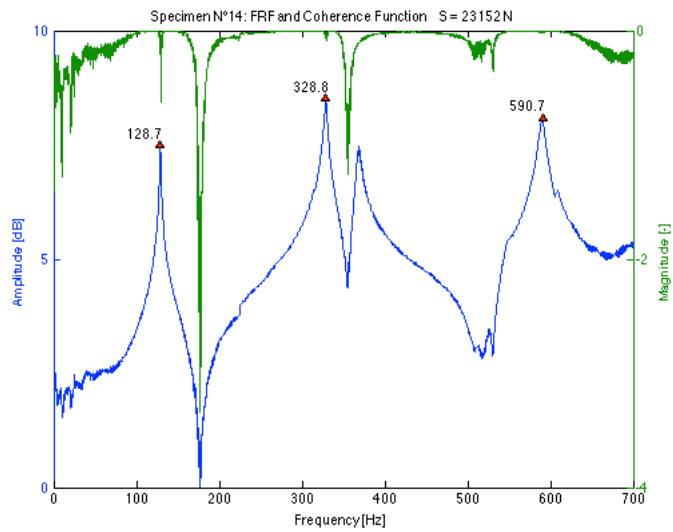
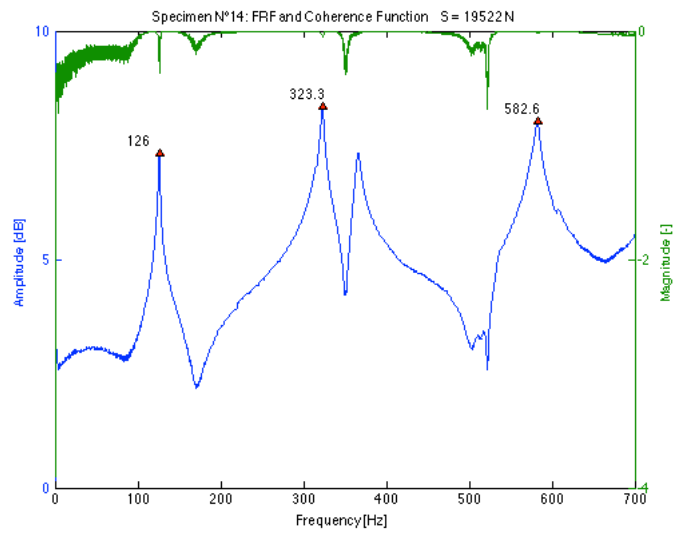
## Data

Table 11-19 Results of frequency measurements and dual parameter estimation for specimen N°14 using the transversal and longitudinal E-modulus for different load levels

T14		using $E_v$						using $E_L$			
Applied load S	% of yield	S/S <sub>c</sub>	f <sub>10</sub>	f <sub>20</sub>	L	K <sub>est</sub>	S <sub>est</sub>	Error on S	K <sub>est</sub>	S <sub>est</sub>	Error on S
[N]	[%]	[-]	[Hz]	[Hz]	[m]	[Nm]	[N]	[%]	[Nm]	[N]	[%]
6082	8.9	0.29	110.8	293.2	1.295	432000	2041	-66.4	192430	3049	-49.9
10693	15.7	0.50	116.5	305.6	1.275	546540	4866	-54.5	217110	5907	-44.8
15009	22.1	0.68	121.3	313.9	1.255	226240	11536	-23.1	128100	13600	-9.4
19522	28.7	0.89	126.0	323.3	1.255	584960	14202	-27.3	222910	15594	-20.1
23152	34.0	1.05	128.7	328.8	1.255	3306700	15795	-31.8	355010	16855	-27.2
29038	42.7	1.32	132.7	334.1	1.255	1238300	23595	-18.7	289740	25062	-13.7

## FRF plots





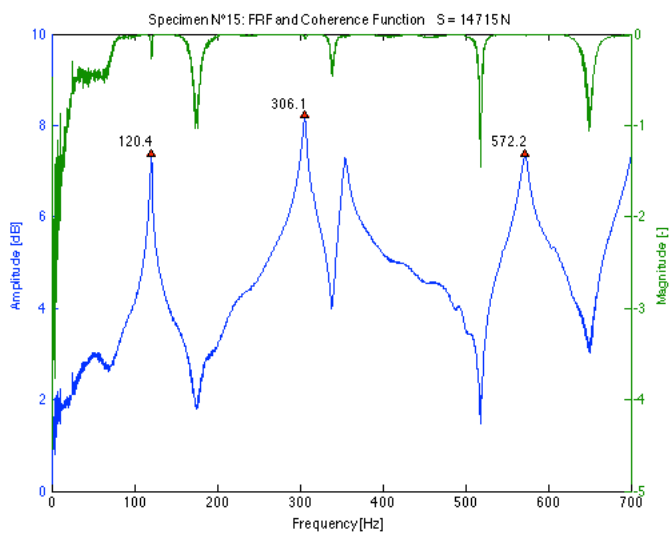
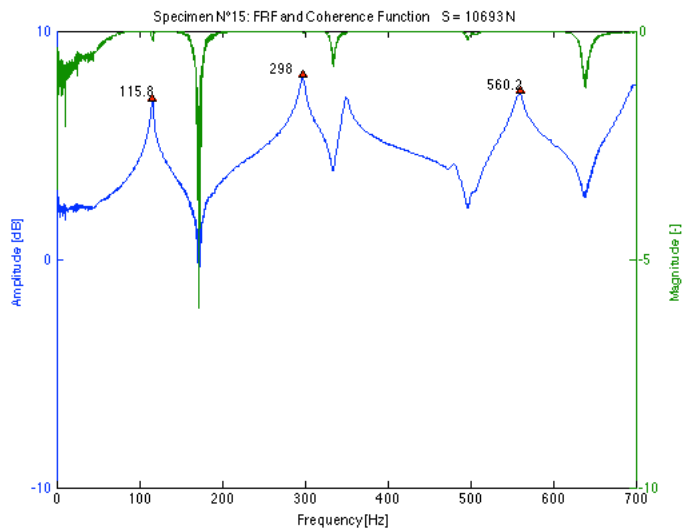
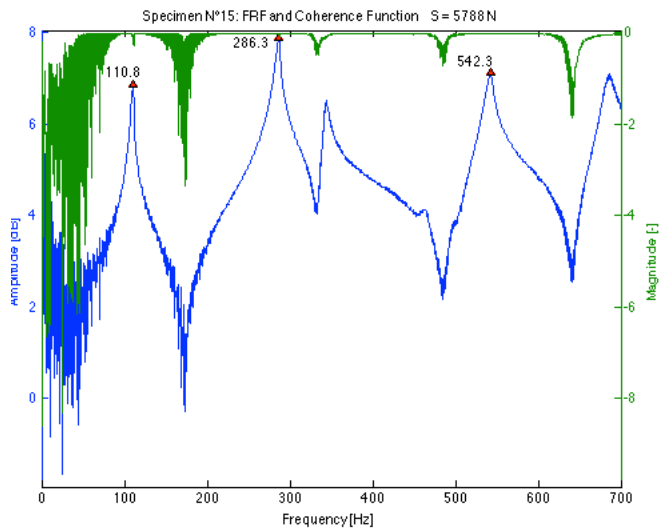
# T15

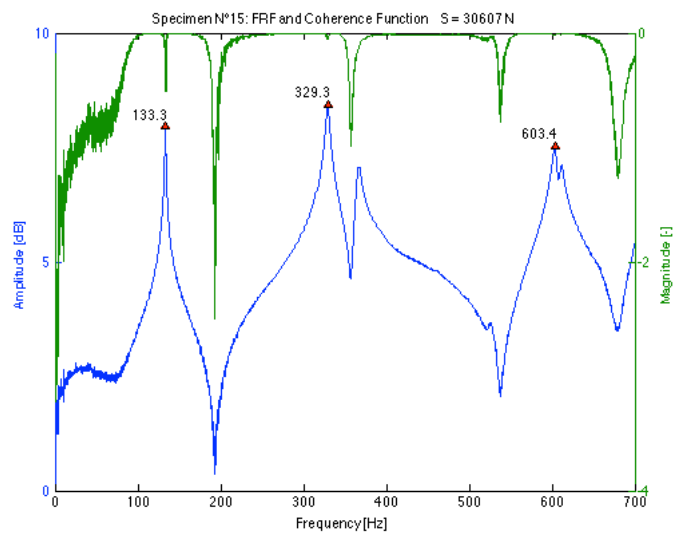
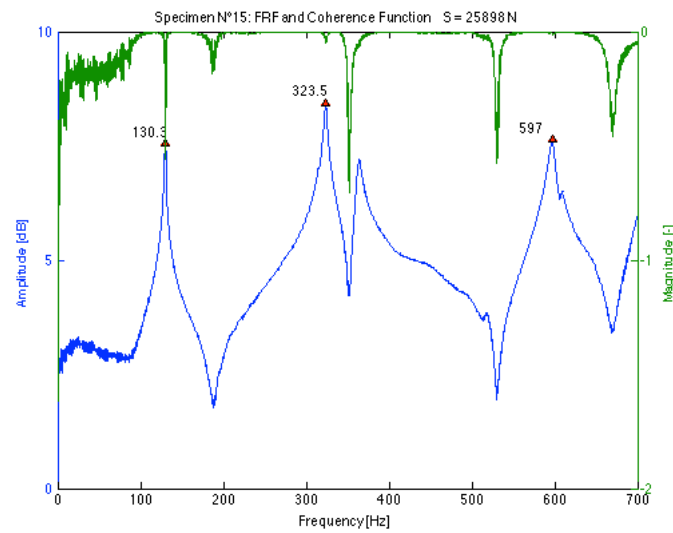
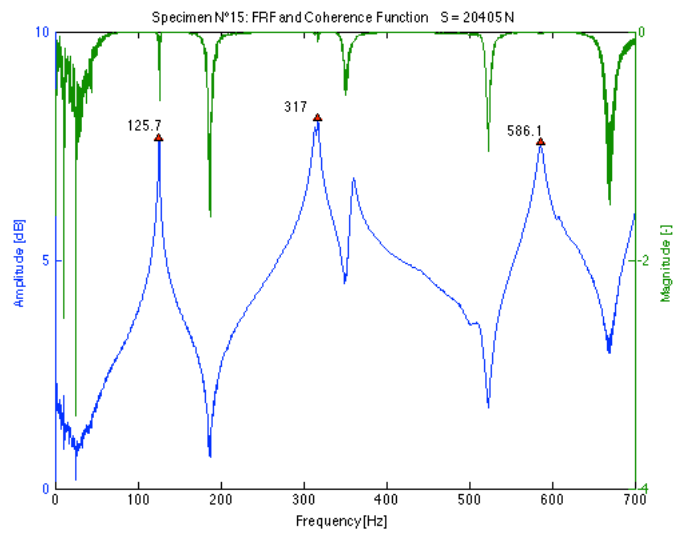
## Data

Table 11-20 Results of frequency measurements and dual parameter estimation for specimen N°15 using the transversal and longitudinal E-modulus for different load levels

T15						using $E_b$			using $E_L$		
Applied load S [N]	% of yield [%]	$S/S_c$ [-]	$f_{1b}$ [Hz]	$f_{2b}$ [Hz]	L [m]	$k_{est}$ [Nm]	$S_{est}$ [N]	Error on S [%]	$k_{est}$ [Nm]	$S_{est}$ [N]	Error on S [%]
5788	8.5	0.27	110.8	286.3	1.295	65496	20152	248.2	46958	25173	334.9
10693	15.7	0.49	115.8	298.0	1.275	76306	20984	96.2	55064	25552	139.0
14715	21.6	0.66	120.4	306.1	1.255	48963	33279	126.2	31403	42606	189.5
20405	30.0	0.91	125.7	317.0	1.255	85542	31379	53.8	60929	36229	77.6
25898	38.1	1.15	130.3	323.5	1.255	77102	42345	63.5	53693	48368	86.8
30607	45.0	1.36	133.3	329.3	1.255	97838	43716	42.8	68711	48616	58.8

## FRF plots





---

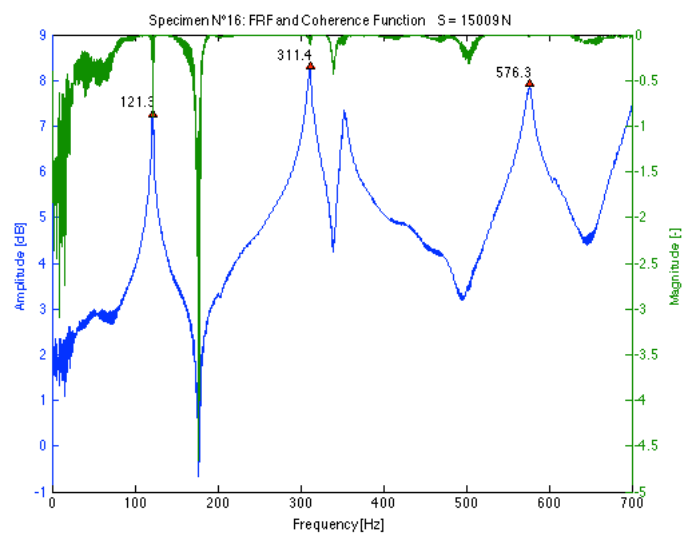
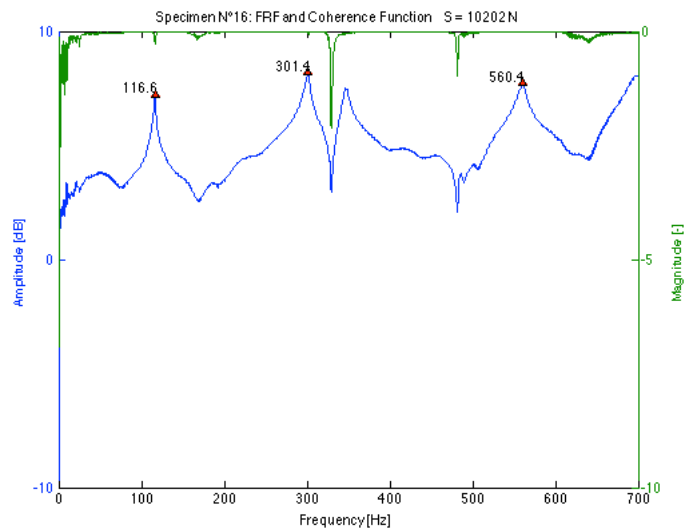
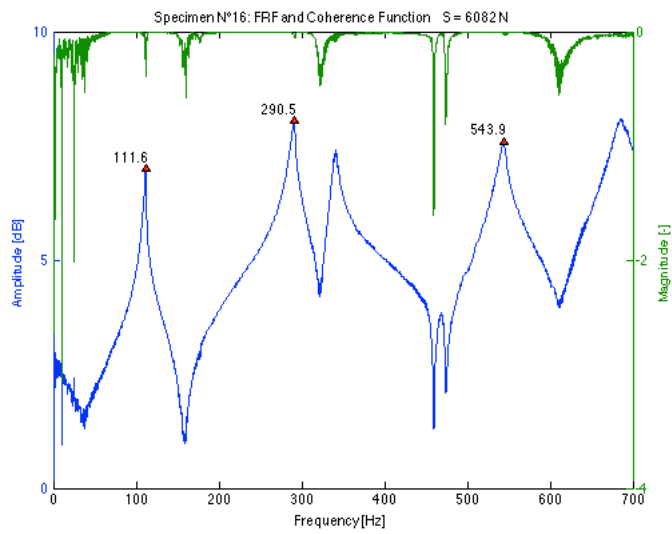
# T16

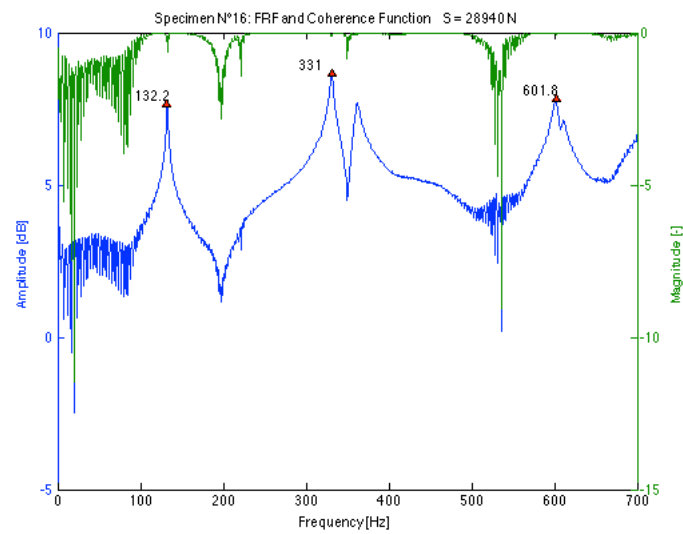
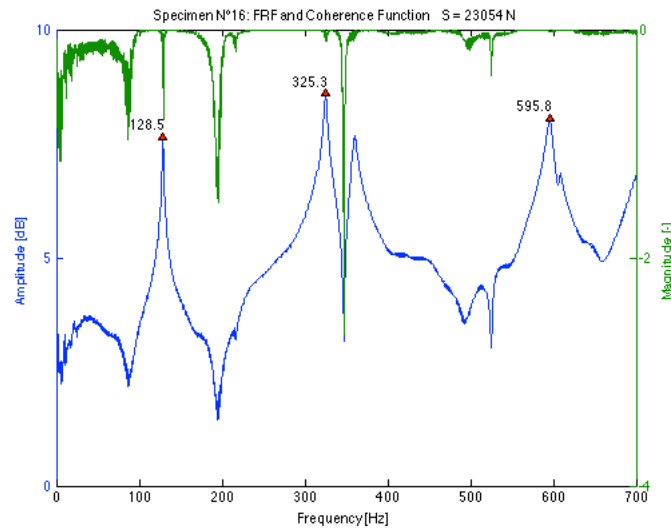
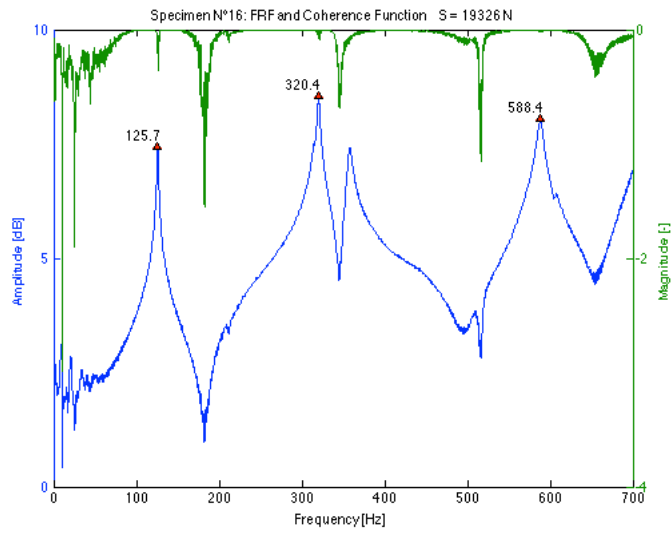
## Data

Table 11-21 Results of frequency measurements and dual parameter estimation for specimen N°16 using the transversal and longitudinal E-modulus for different load levels

T16			using $E_v$						using $E_L$		
Applied load S	% of yield	S/S <sub>e</sub>	f <sub>1b</sub>	f <sub>2b</sub>	L	k <sub>est</sub>	S <sub>est</sub>	Error on S	k <sub>est</sub>	S <sub>est</sub>	Error on S
[N]	[%]	[-]	[Hz]	[Hz]	[m]	[Nm]	[N]	[%]	[Nm]	[N]	[%]
6082	8.9	0.27	111.6	290.5	1.295	112470	12035	97.9	75586	15508	155.0
10202	15.0	0.45	116.6	301.4	1.275	113420	15234	49.3	75729	19035	86.6
15009	22.1	0.64	121.3	311.4	1.255	101830	19495	29.9	67748	24165	61.0
19326	28.4	0.82	125.7	320.4	1.255	167610	20447	5.8	106100	23600	22.1
23054	33.9	0.98	128.5	325.3	1.255	199860	23591	2.3	121900	26521	15.0
28940	42.6	1.23	132.2	331.0	1.255	208670	30022	3.7	125120	33150	14.5

## FRF plots





---

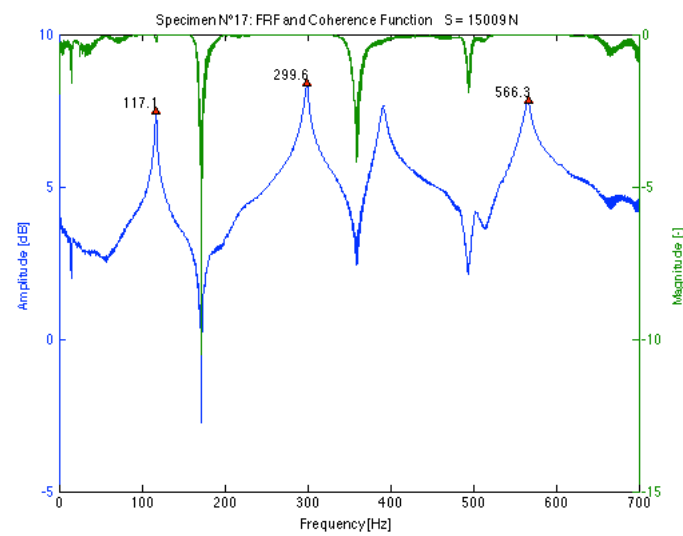
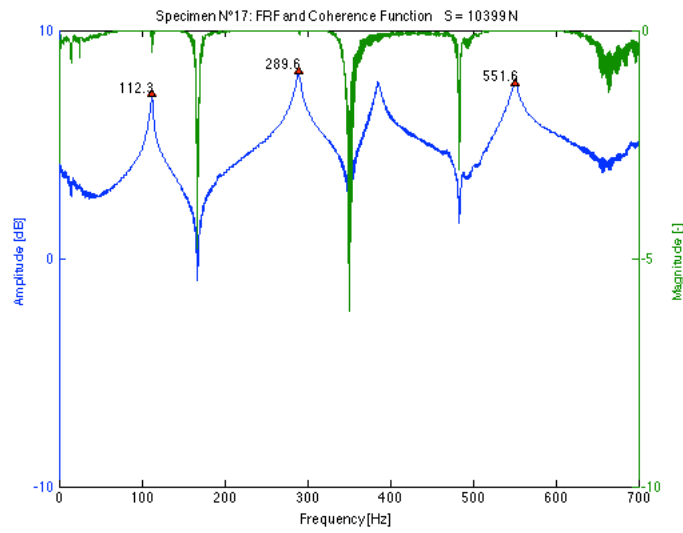
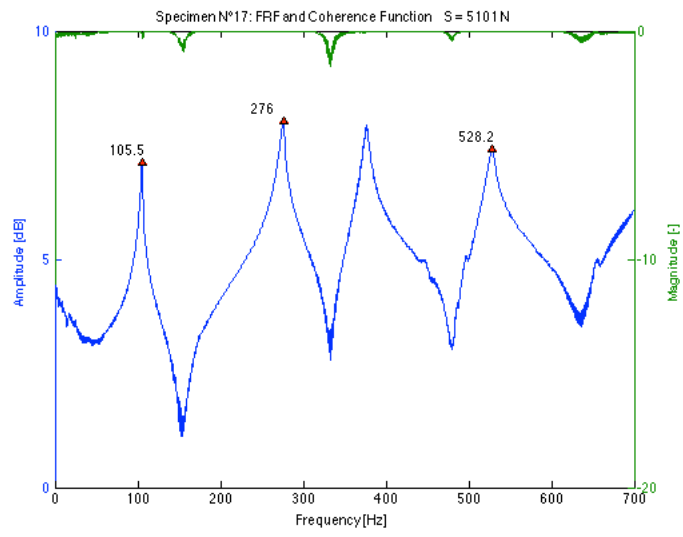
# T17

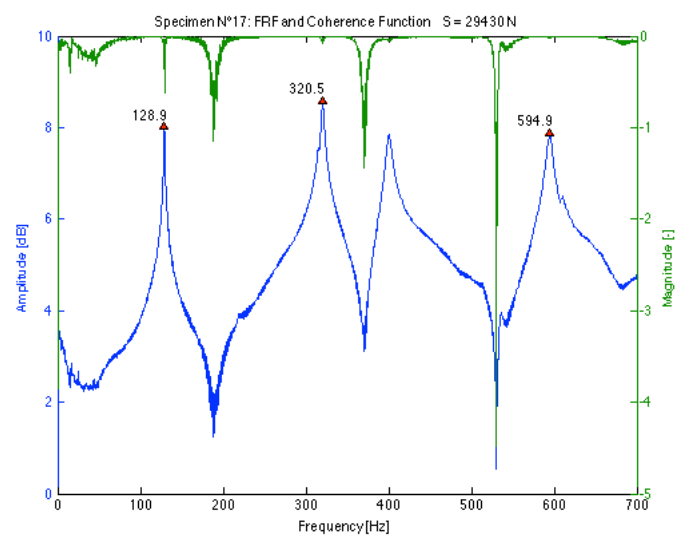
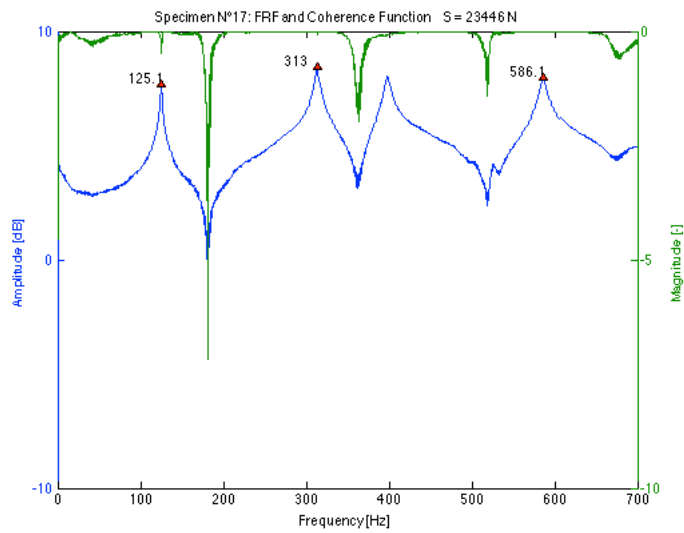
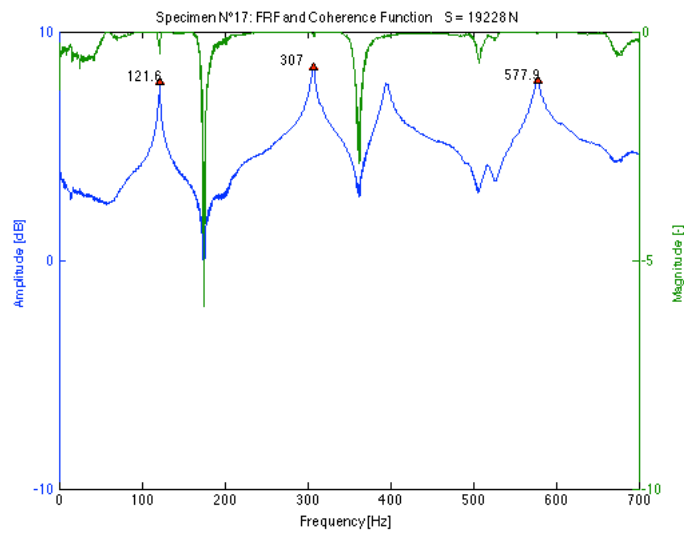
## Data

Table 11-22 Results of frequency measurements and dual parameter estimation for specimen N°17 using the transversal and longitudinal E-modulus for different load levels

T17			using $E_b$						using $E_L$			
Applied load S	% of yield	$S/S_e$	$f_{1b}$	$f_{2b}$	L	$k_{est}$	$S_{est}$	Error on S	$k_{est}$	$S_{est}$	Error on S	
[N]	[%]	[-]	[Hz]	[Hz]	[m]	[Nm]	[N]	[%]	[Nm]	[N]	[%]	
5101	7.5	0.29	105.5	276.0	1.295	78229	11450	124.5	61031	13239	159.5	
10399	15.3	0.57	112.3	289.6	1.275	80616	16946	63.0	62483	18939	82.1	
15009	22.1	0.79	117.1	299.6	1.255	71751	21283	41.8	55576	23738	58.2	
19228	28.3	1.01	121.6	307.0	1.255	80504	26803	39.4	61827	29206	51.9	
23446	34.5	1.24	125.1	313.0	1.255	91633	30780	31.3	69664	33071	41.1	
29430	43.3	1.55	128.9	320.5	1.255	129860	32992	12.1	95318	34851	18.4	

## FRF plots





---

## T18

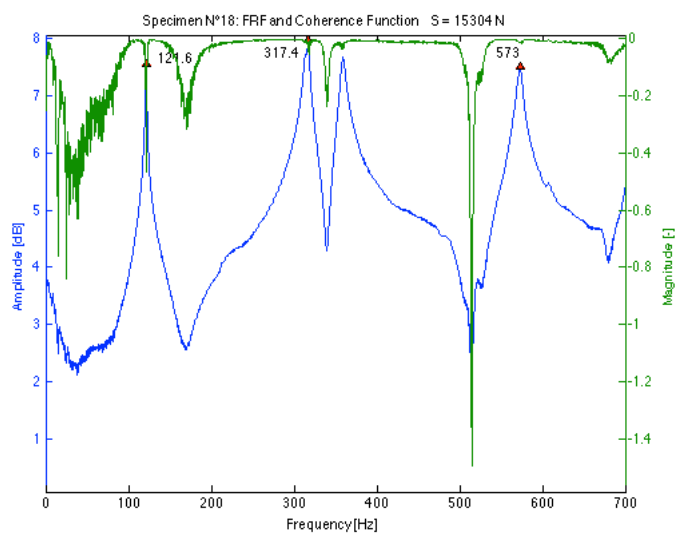
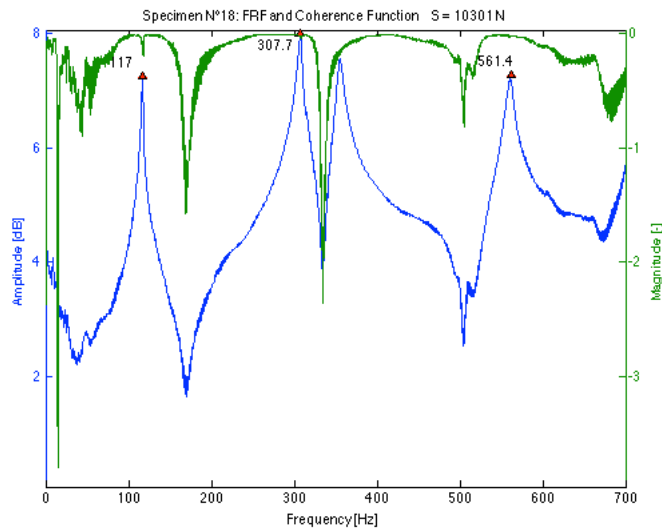
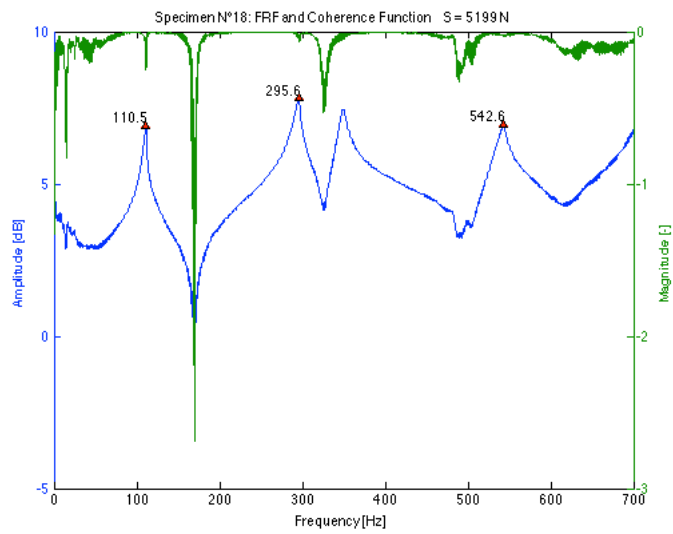
### Data

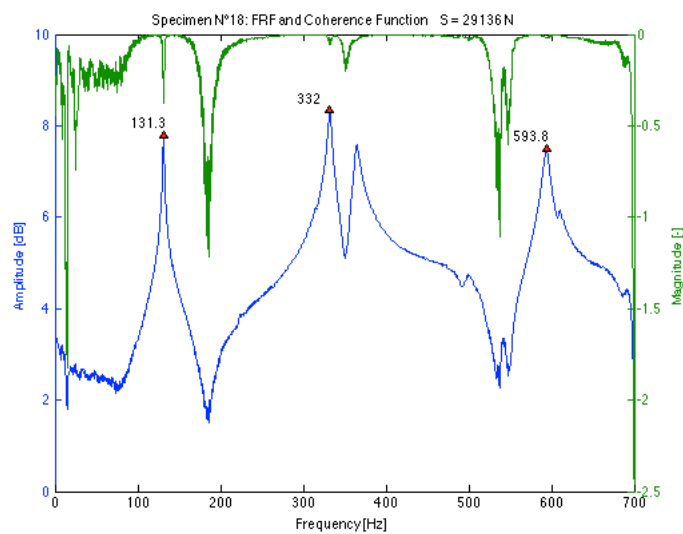
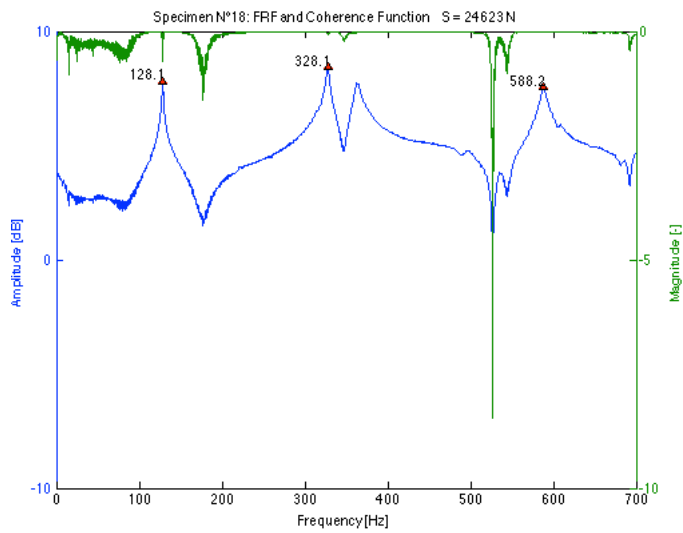
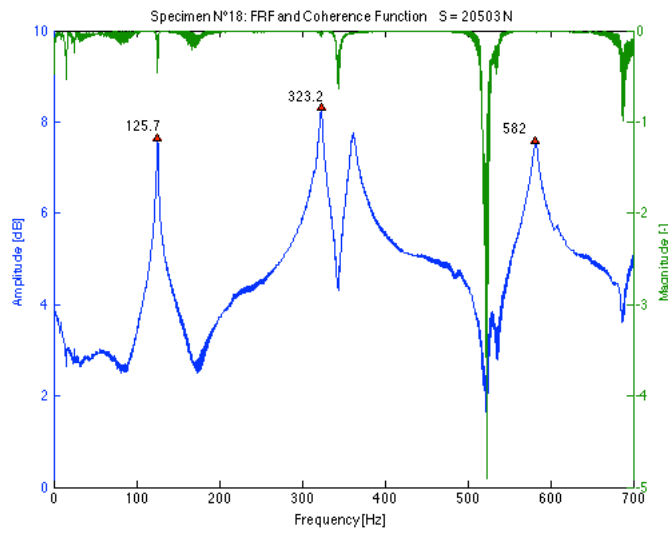
Table 11-23 Results of frequency measurements and dual parameter estimation for specimen N°18 using the transversal and longitudinal E-modulus for different load levels

T18			using $E_v$						using $E_L$		
Applied load S	% of yield	$S/S_e$	$f_{1b}$	$f_{2b}$	L	$k_{est}$	$S_{est}$	Error on S	$k_{est}$	$S_{est}$	Error on S
[N]	[%]	[-]	[Hz]	[Hz]	[m]	[Nm]	[N]	[%]	[Nm]	[N]	[%]
5199	7.6	0.26	110.5	295.6	1.295	/	/	/	/	/	/
10301	15.1	0.49	117.0	307.7	1.275	/	/	/	/	/	/
15304	22.5	0.71	121.6	317.4	1.255	/	/	/	/	/	/
20503	30.2	0.95	125.7	323.2	1.255	/	/	/	/	/	/
24623	36.2	1.14	128.1	328.1	1.255	/	/	/	/	/	/
29136	42.8	1.35	131.3	332.0	1.255	/	/	/	/	/	/

The results for this specimen were very erroneous for undeclared reasons, which is why they were not considered in following calculations.

## FRF plots





---

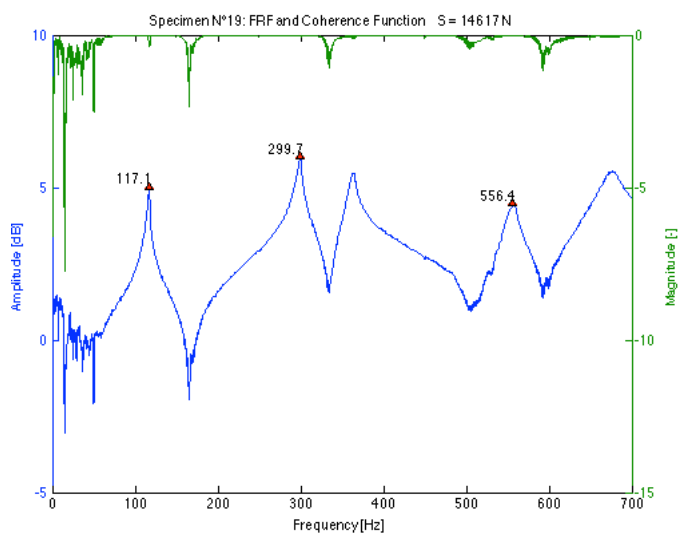
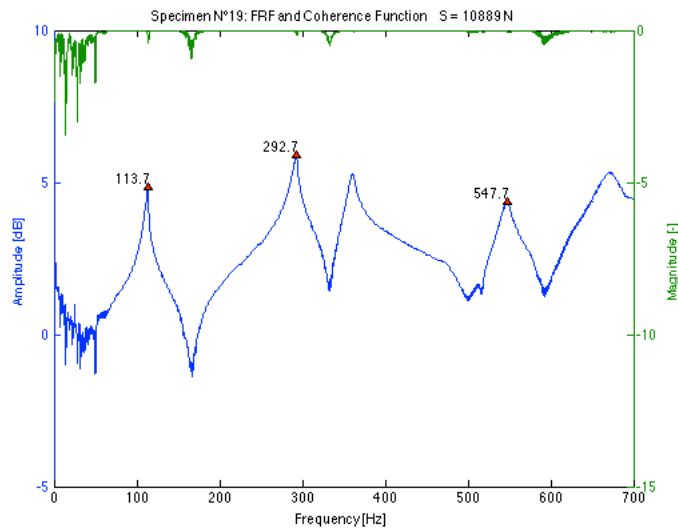
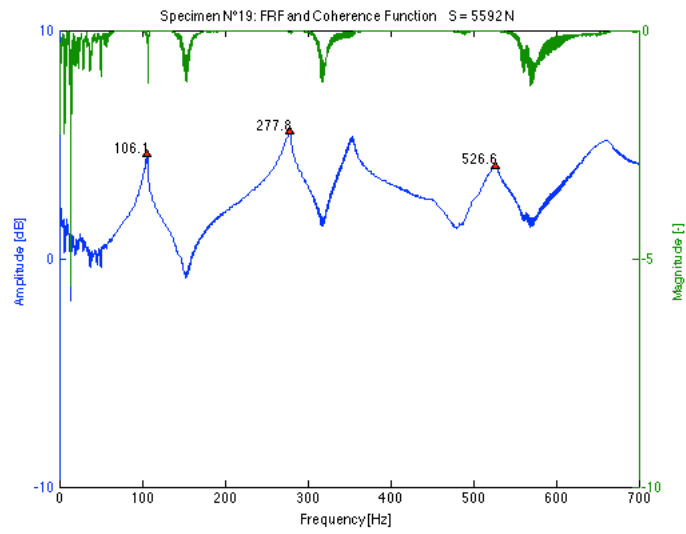
# T19

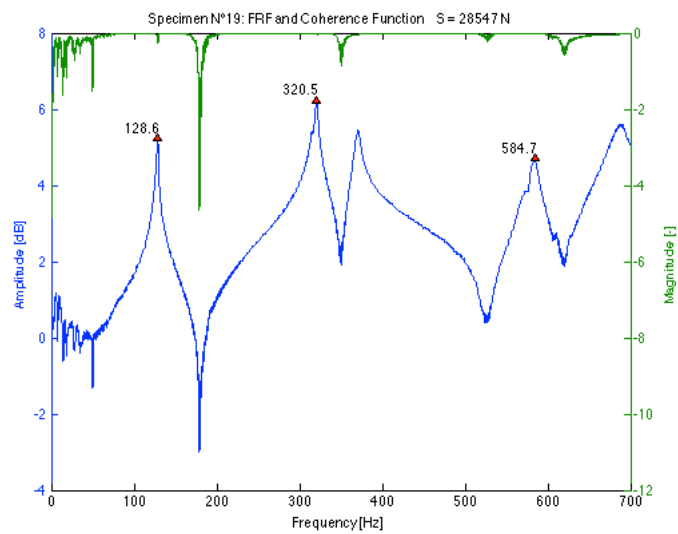
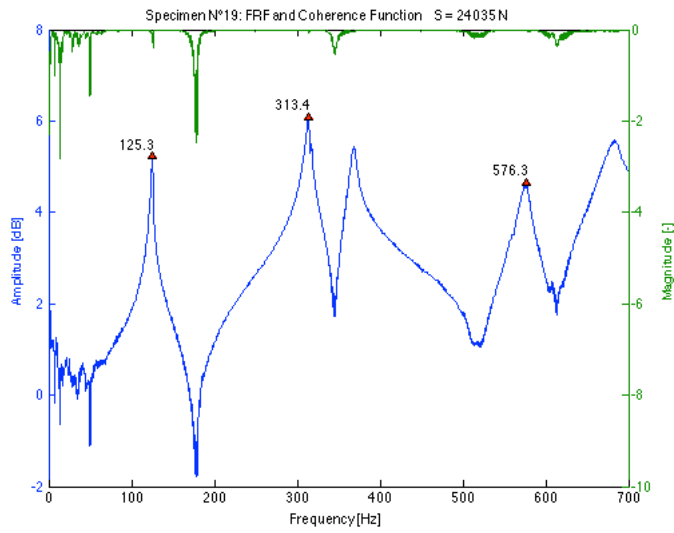
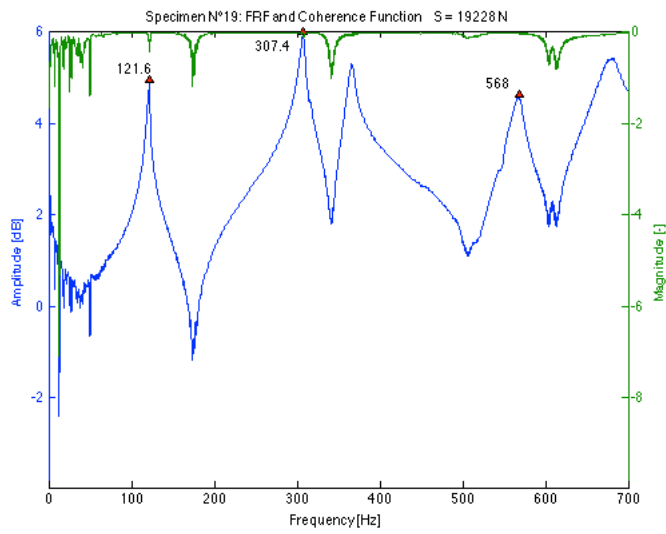
## Data

Table 11-24 Results of frequency measurements and dual parameter estimation for specimen N°19 using the transversal and longitudinal E-modulus for different load levels

T19		using $E_b$							using $E_L$		
Applied load S	% of yield	S/S <sub>c</sub>	f <sub>1b</sub>	f <sub>2b</sub>	L	k <sub>est</sub>	S <sub>est</sub>	Error on S	k <sub>est</sub>	S <sub>est</sub>	Error on S
[N]	[%]	[-]	[Hz]	[Hz]	[m]	[Nm]	[N]	[%]	[Nm]	[N]	[%]
5592	8.2	0.34	106.1	277.8	1.295	216190	4859	-13.1	155940	5521	-1.3
10889	16.0	0.65	113.7	292.7	1.275	253510	10741	-1.4	176280	11479	5.4
14617	21.5	0.84	117.1	299.7	1.255	162820	14086	-3.6	122670	15190	3.9
19228	28.3	1.11	121.6	307.4	1.255	220640	18914	-1.6	157250	19922	3.6
24035	35.3	1.39	125.3	313.4	1.255	260200	23897	-0.6	178260	24921	3.7
28547	42.0	1.65	128.6	320.5	1.255	906830	24803	-13.1	388940	25503	-10.7

## FRF plots





---

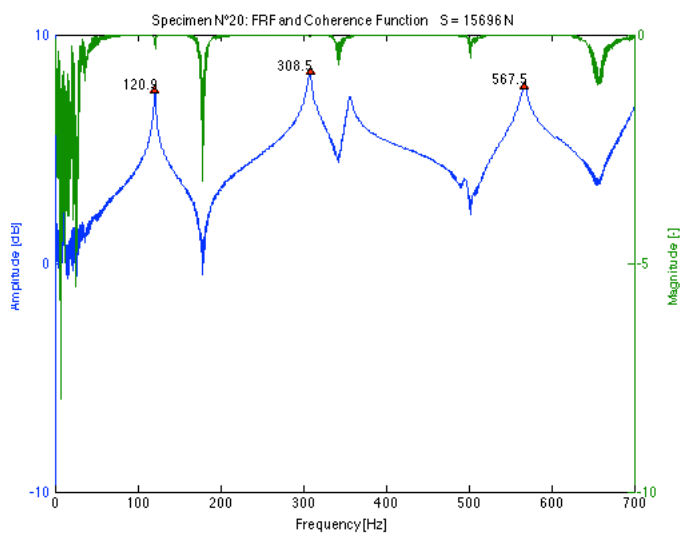
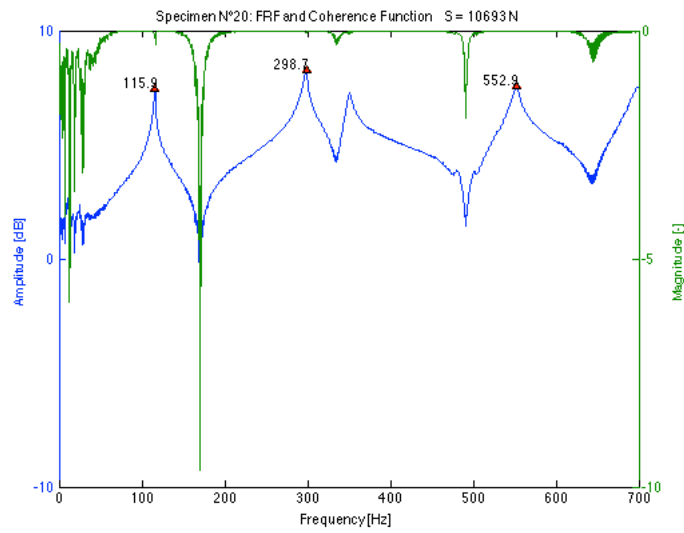
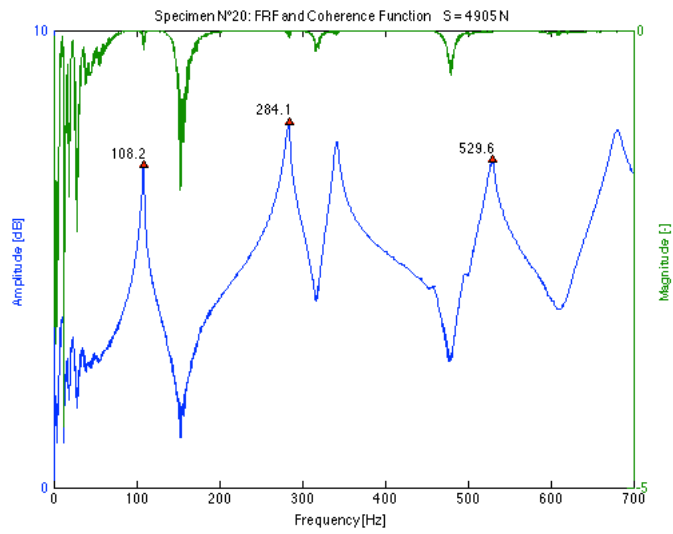
## T20

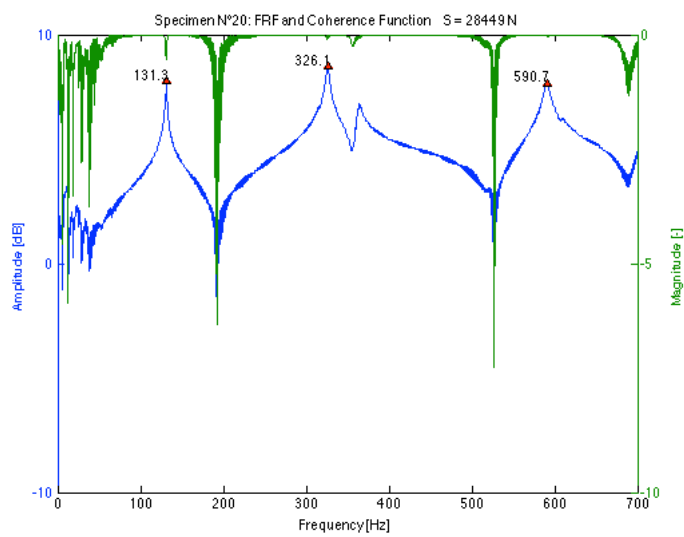
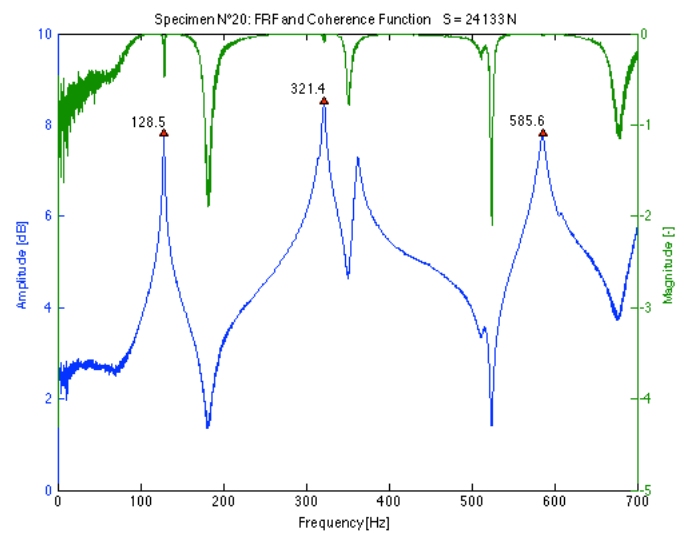
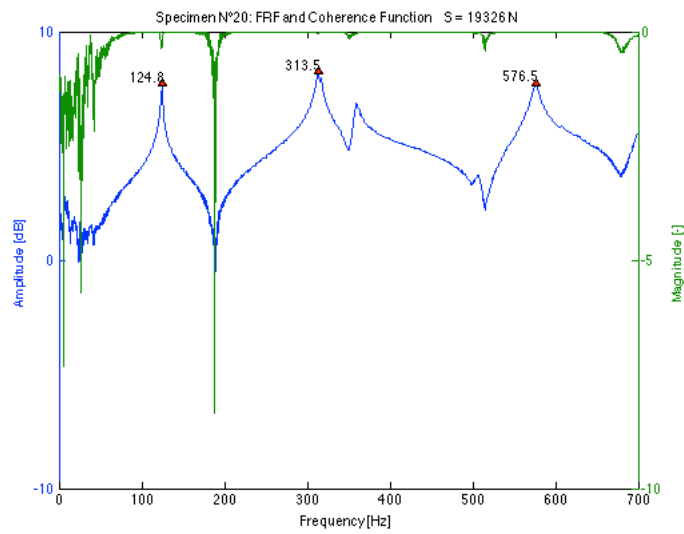
### Data

Table 11-25 Results of frequency measurements and dual parameter estimation for specimen N°20 using the transversal and longitudinal E-modulus for different load levels

T20		using $E_b$							using $E_L$		
Applied load S	% of yield	$S/S_c$	$f_{1b}$	$f_{2b}$	L	$k_{est}$	$S_{est}$	Error on S	$k_{est}$	$S_{est}$	Error on S
[N]	[%]	[-]	[Hz]	[Hz]	[m]	[Nm]	[N]	[%]	[Nm]	[N]	[%]
4905	7.2	0.26	108.2	284.1	1.295	195480	5541	13.0	157540	6034	23.0
10693	15.7	0.56	115.9	298.7	1.275	191620	12724	19.0	154470	13348	24.8
15696	23.1	0.80	120.9	308.5	1.255	144550	17986	14.6	119930	18863	20.2
19326	28.4	0.98	124.8	313.5	1.255	120830	26385	36.5	101210	27526	42.4
24133	35.5	1.22	128.5	321.4	1.255	216640	27019	12.0	170720	27820	15.3
28449	41.8	1.44	131.3	326.1	1.255	251560	30742	8.1	193290	31536	10.9

## FRF plots





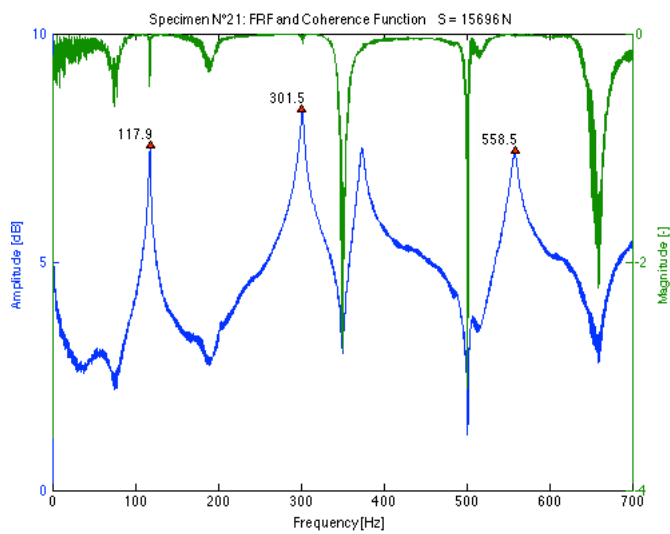
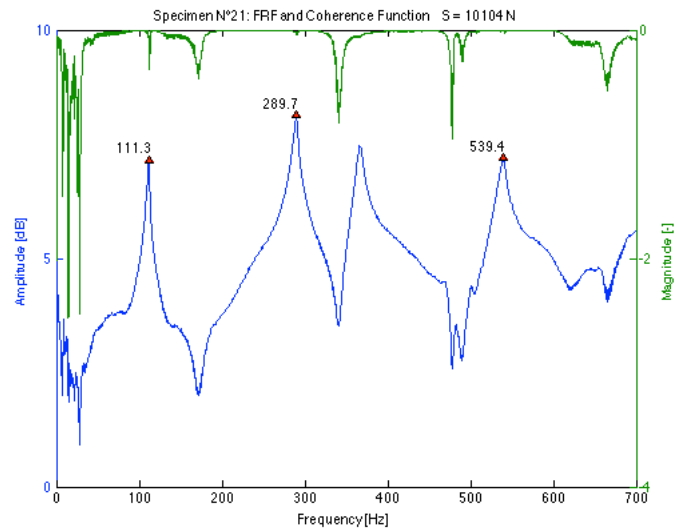
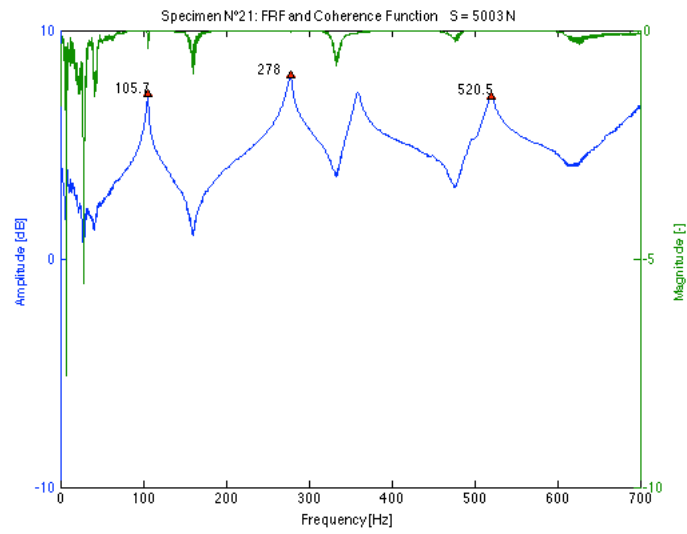
# T21

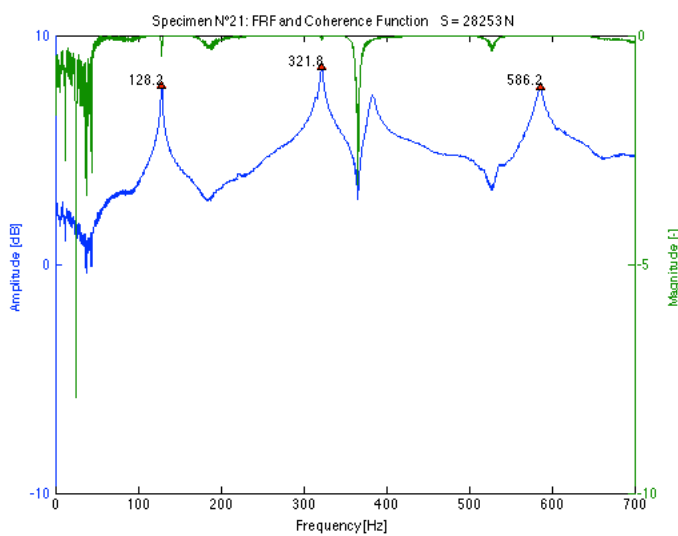
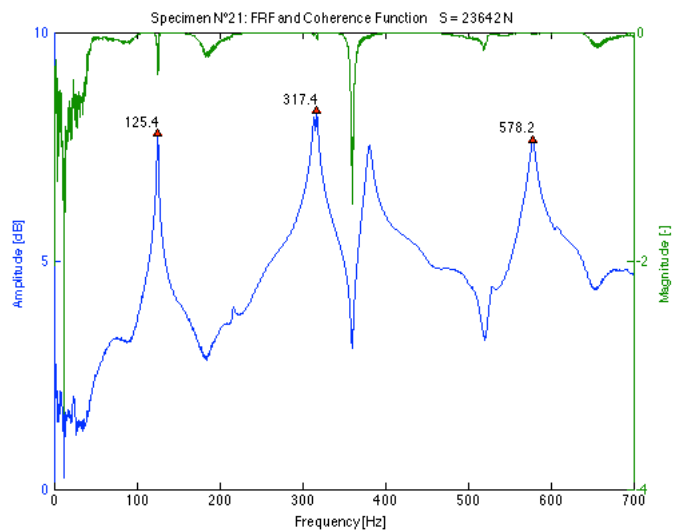
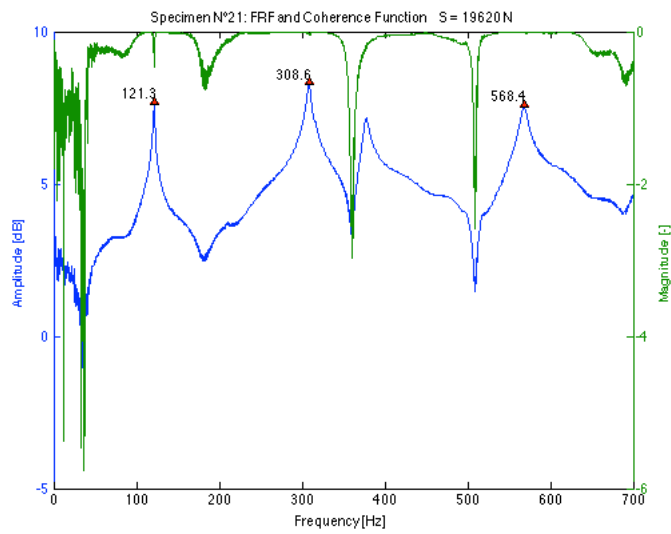
## Data

Table 11-26 Results of frequency measurements and dual parameter estimation for specimen N°21 using the transversal and longitudinal E-modulus for different load levels

T21			using $E_b$						using $E_c$			
Applied load S	% of yield	S/S <sub>c</sub>	f <sub>10</sub>	f <sub>20</sub>	L	k <sub>est</sub>	S <sub>est</sub>	Error on S	k <sub>est</sub>	S <sub>est</sub>	Error on S	
[N]	[%]	[-]	[Hz]	[Hz]	[m]	[Nm]	[N]	[%]	[Nm]	[N]	[%]	
5003	7.4	0.25	105.7	278.0	1.295	145350	7332	46.5	99544	8933	78.5	
10104	14.9	0.50	111.3	289.7	1.275	147710	11291	11.7	100630	13084	29.5	
15696	23.1	0.75	117.9	301.5	1.255	109870	20299	29.3	77163	23027	46.7	
19620	28.9	0.93	121.3	308.6	1.255	169600	21291	8.5	111790	23324	18.9	
23642	34.8	1.12	125.4	317.4	1.255	389600	22619	-4.3	201010	23980	1.4	
28253	41.5	1.34	128.2	321.8	1.255	432760	27026	-4.3	212940	28459	0.7	

## FRF plots





---

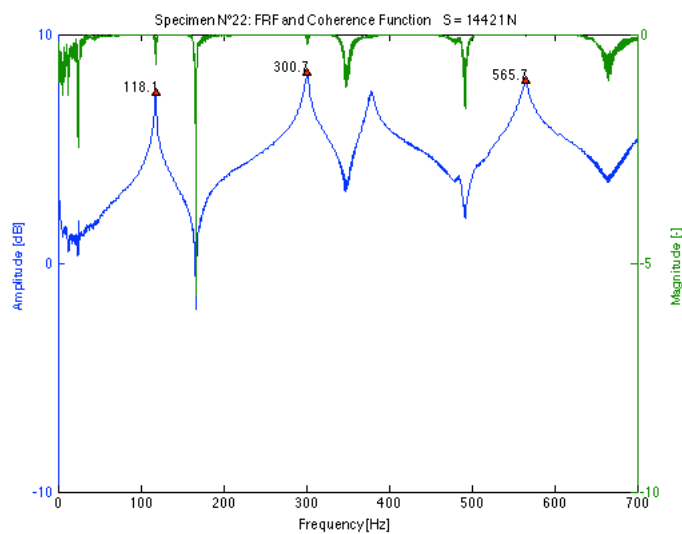
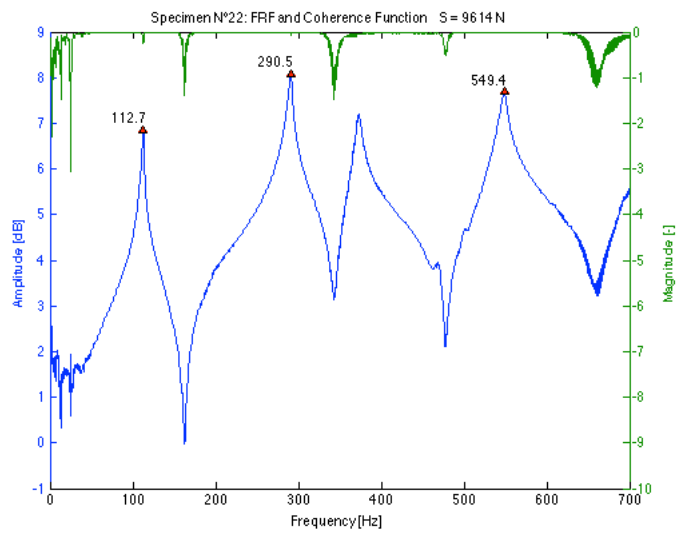
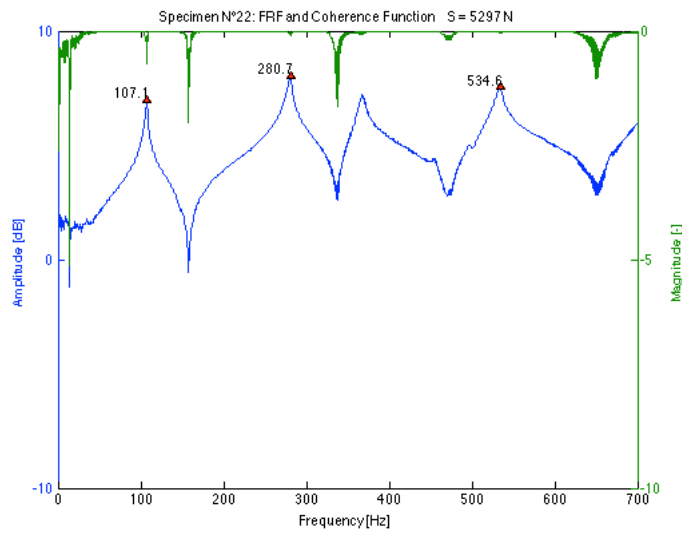
## T22

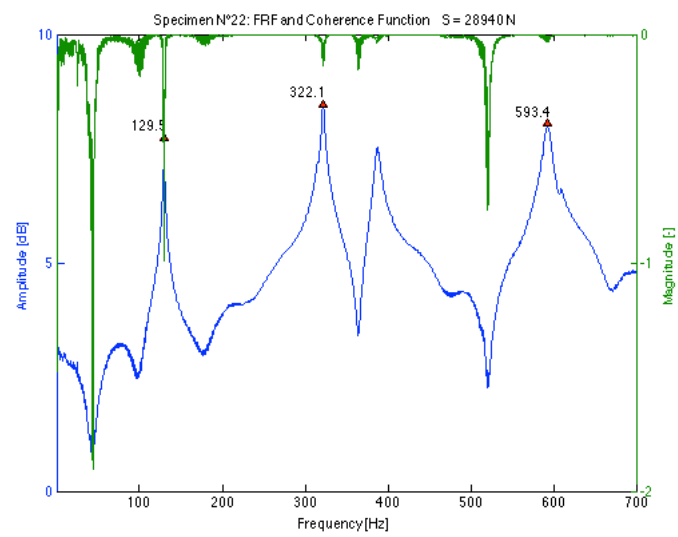
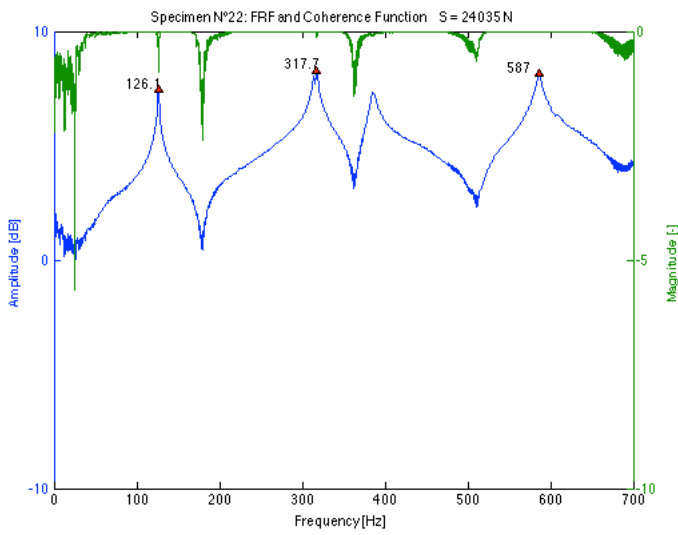
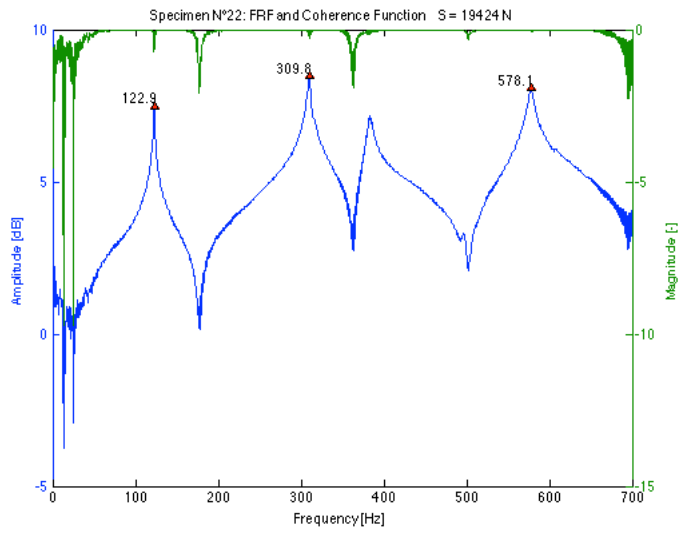
### Data

Table 11-27 Results of frequency measurements and dual parameter estimation for specimen N°22 using the transversal and longitudinal E-modulus for different load levels

T22		using $E_s$							using $E_L$		
Applied load S	% of yield	$S/S_e$	$f_{1b}$	$f_{2b}$	L	$k_{est}$	$S_{est}$	Error on S	$k_{est}$	$S_{est}$	Error on S
[N]	[%]	[-]	[Hz]	[Hz]	[m]	[Nm]	[N]	[%]	[Nm]	[N]	[%]
5297	7.8	0.26	107.1	280.7	1.295	110570	9975	88.3	82239	11805	122.8
9614	14.1	0.45	112.7	290.5	1.275	79331	18802	95.6	59602	21725	126.0
14421	21.2	0.66	118.1	300.7	1.255	62527	26903	86.6	46204	31142	116.0
19424	28.6	0.89	122.9	309.8	1.255	87276	29635	52.6	64623	32869	69.2
24035	35.3	1.10	126.1	317.7	1.255	162090	27256	13.4	113350	29246	21.7
28940	42.6	1.33	129.5	322.1	1.255	137550	35229	21.7	97810	37700	30.3

## FRF plots





---

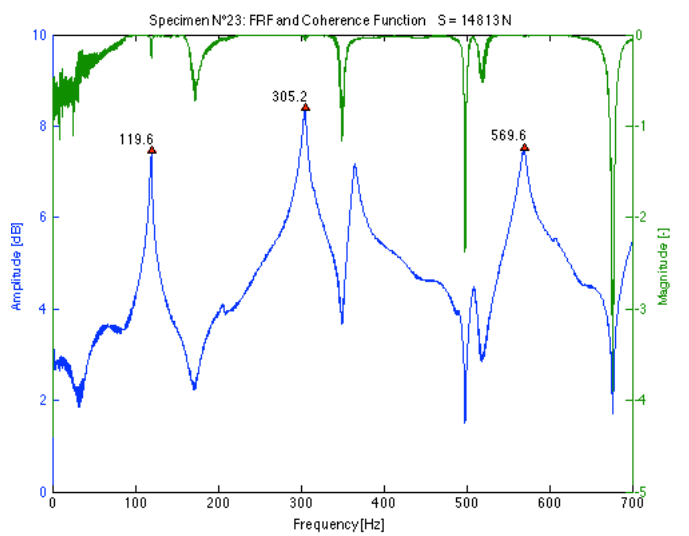
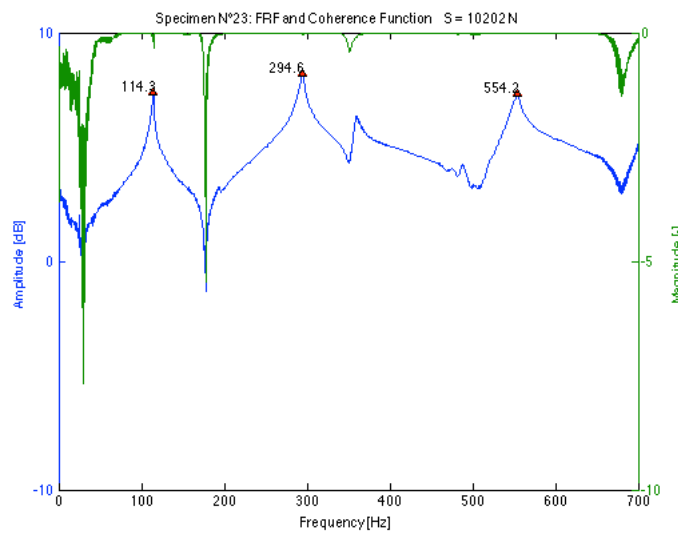
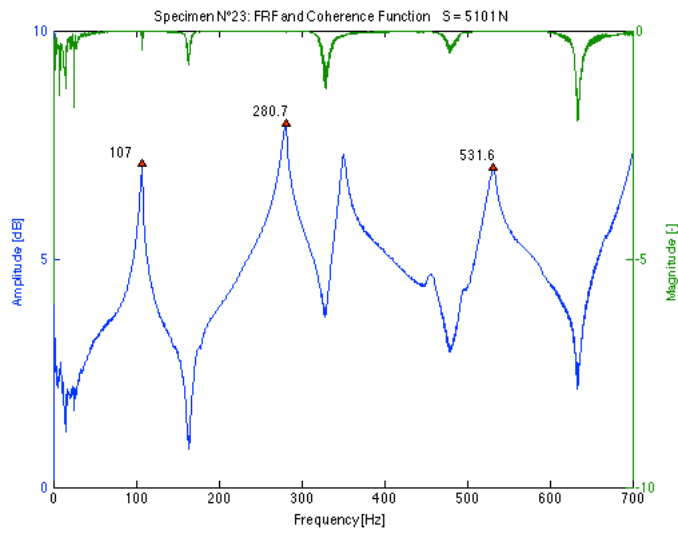
## T23

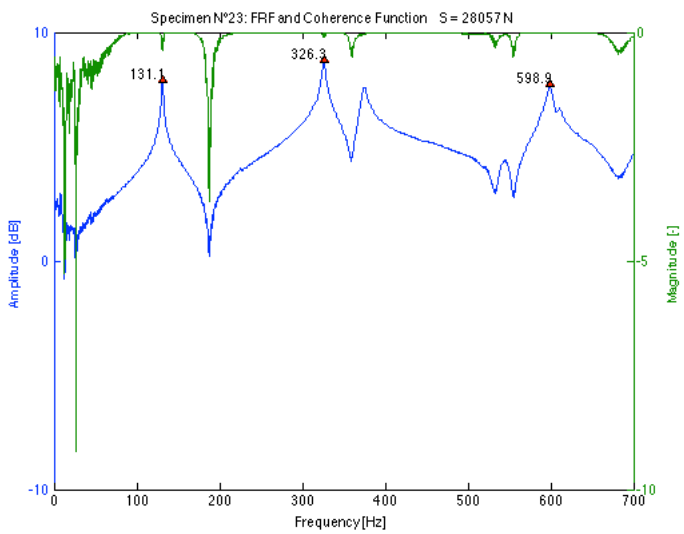
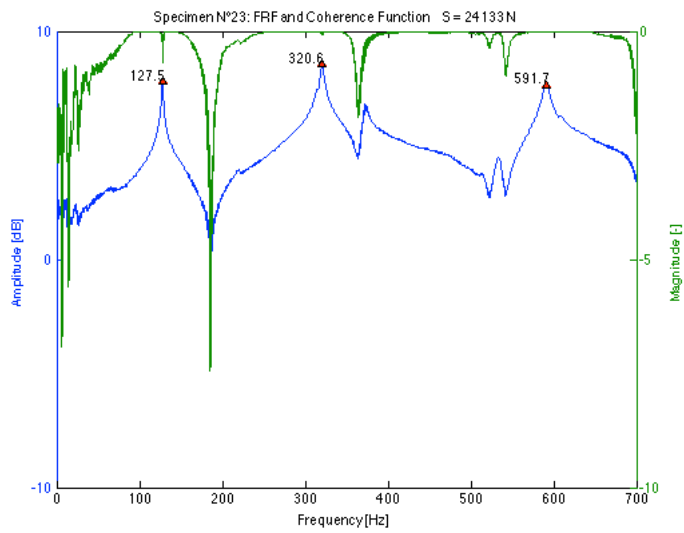
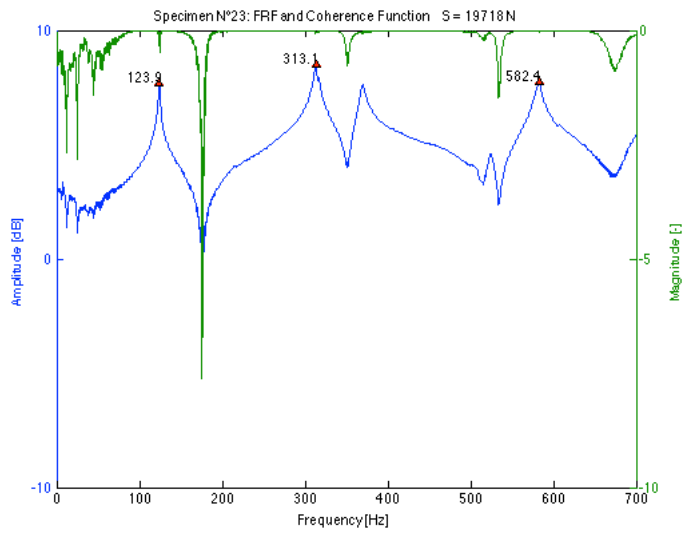
### Data

Table 11-28 Results of frequency measurements and dual parameter estimation for specimen N°23 using the transversal and longitudinal E-modulus for different load levels

T23		using $E_v$						using $E_L$			
Applied load S	% of yield	S/S <sub>y</sub>	f <sub>1b</sub>	f <sub>2b</sub>	L	k <sub>est</sub>	S <sub>est</sub>	Error on S	k <sub>est</sub>	S <sub>est</sub>	Error on S
[N]	[%]	[-]	[Hz]	[Hz]	[m]	[Nm]	[N]	[%]	[Nm]	[N]	[%]
5101	7.5	0.26	107.0	280.7	1.295	106580	8649	69.5	81515	10197	99.9
10202	15.0	0.51	114.3	294.6	1.275	101940	15877	55.6	77761	17782	74.3
14813	21.8	0.72	119.6	305.2	1.255	87557	21415	44.6	66997	23875	61.2
19718	29.0	0.96	123.9	313.1	1.255	116200	24782	25.7	87000	26842	36.1
24133	35.5	1.17	127.5	320.6	1.255	187150	25900	7.3	131040	27431	13.7
28057	41.3	1.36	131.1	326.3	1.255	201590	31444	12.1	138530	33052	17.8

## FRF plots





---

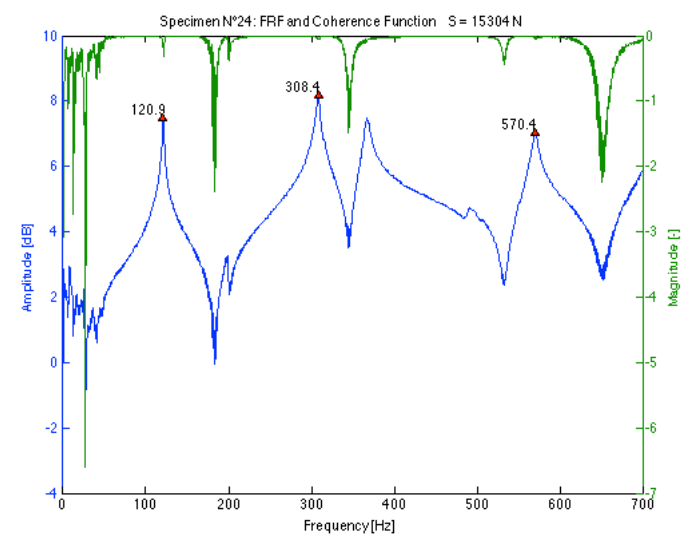
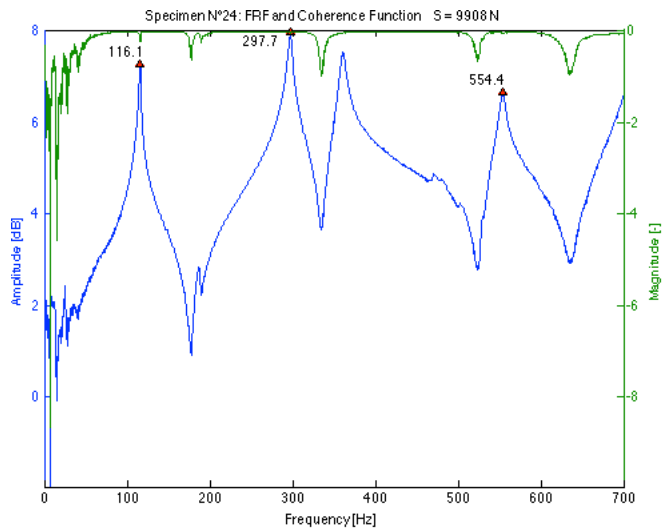
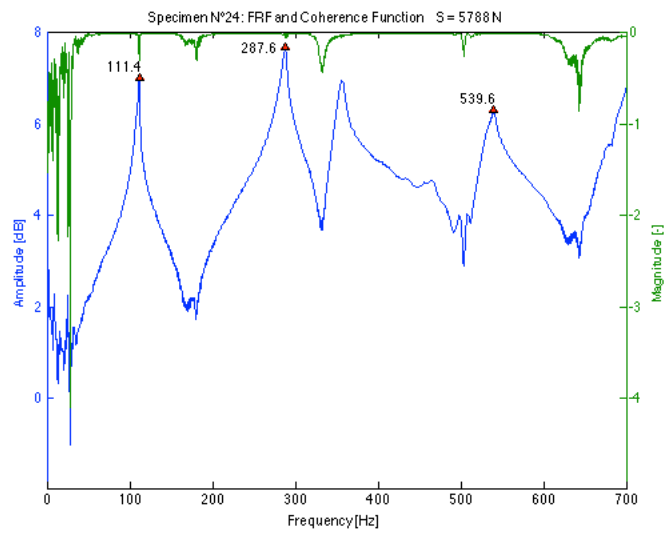
## T24

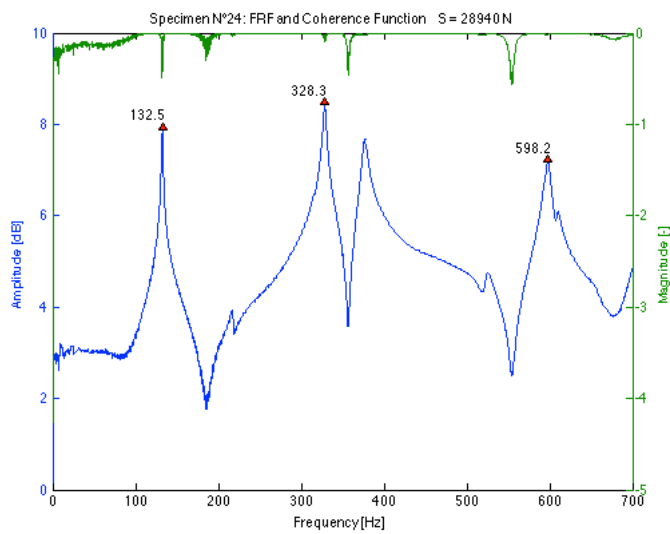
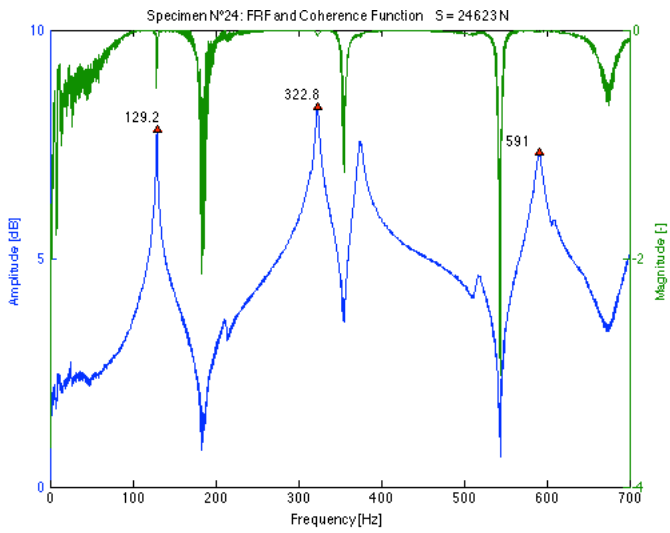
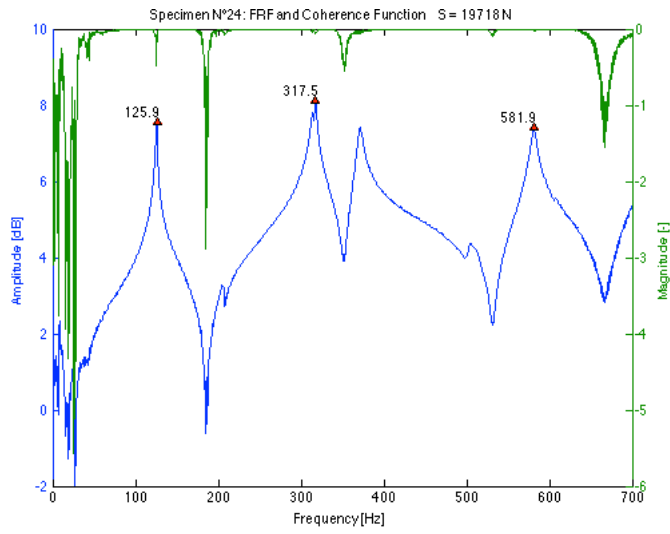
### Data

Table 11-29 Results of frequency measurements and dual parameter estimation for specimen N°24 using the transversal and longitudinal E-modulus for different load levels

T24			using $E_v$						using $E_L$			
Applied load S	% of yield	$S/S_e$	$f_{1b}$	$f_{2b}$	L	$k_{est}$	$S_{est}$	Error on S	$k_{est}$	$S_{est}$	Error on S	
[N]	[%]	[-]	[Hz]	[Hz]	[m]	[Nm]	[N]	[%]	[Nm]	[N]	[%]	
5788	8.5	0.29	111.4	287.6	1.295	94778	17641	204.8	69711	20706	257.7	
9908	14.6	0.48	116.1	297.7	1.275	89645	21619	118.2	65642	25179	154.1	
15304	22.5	0.72	120.9	308.4	1.255	89401	24740	61.7	65109	28636	87.1	
19718	29.0	0.93	125.9	317.5	1.255	121180	29133	47.7	86727	32309	63.9	
24623	36.2	1.16	129.2	322.8	1.255	129240	34490	40.1	91513	37716	53.2	
28940	42.6	1.36	132.5	328.3	1.255	143060	39510	36.5	99770	42694	47.5	

## FRF plots





---

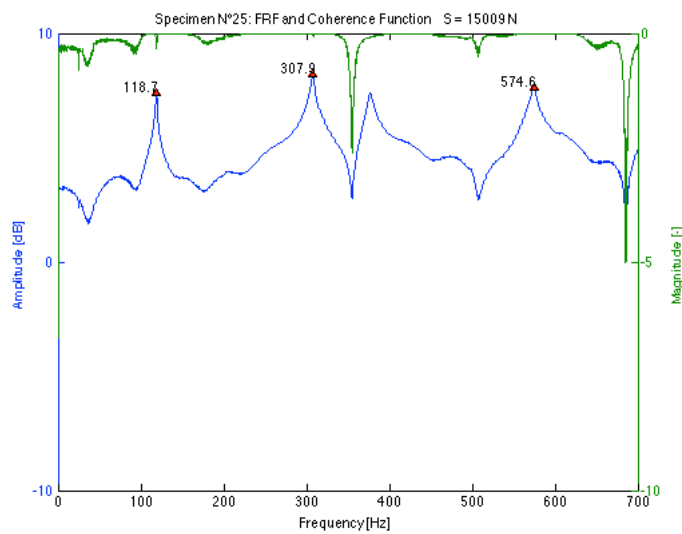
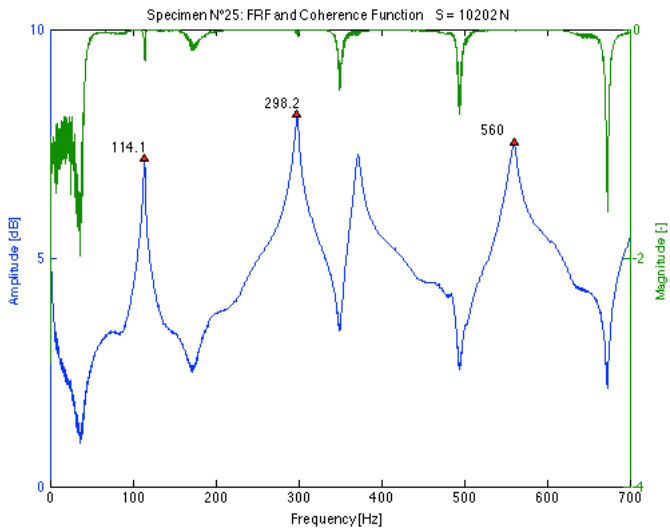
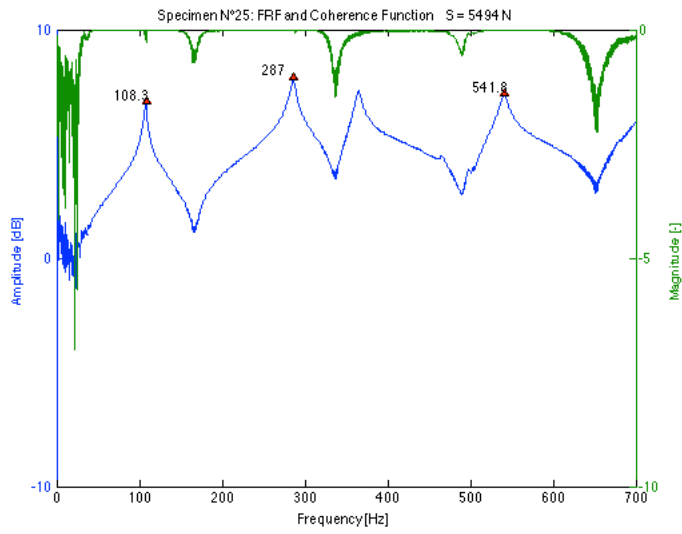
## T25

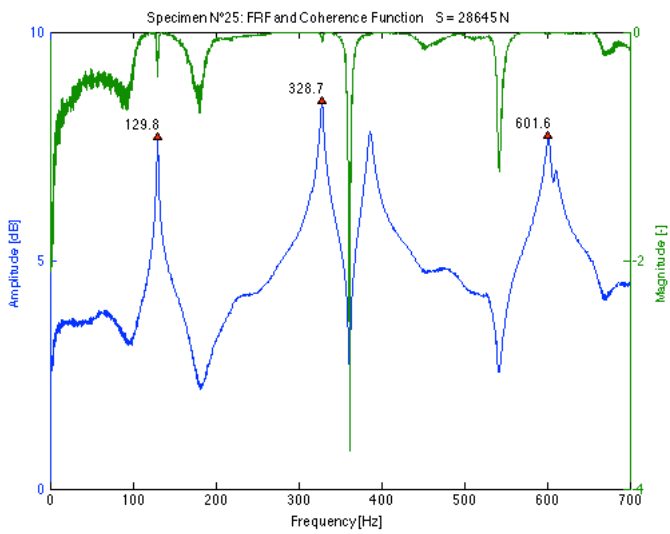
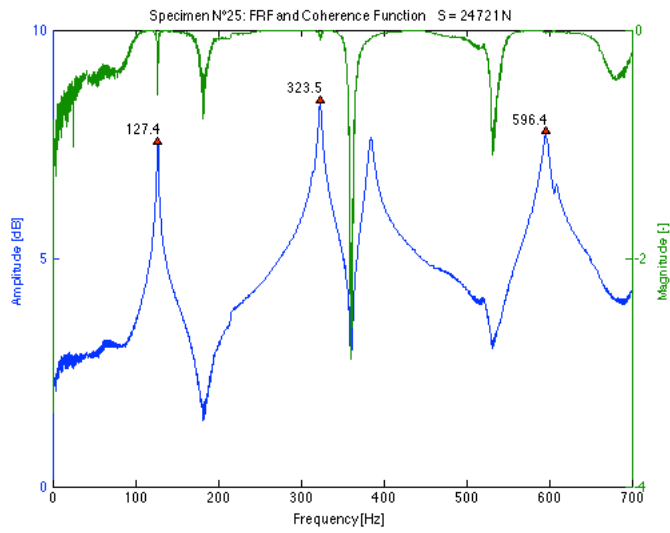
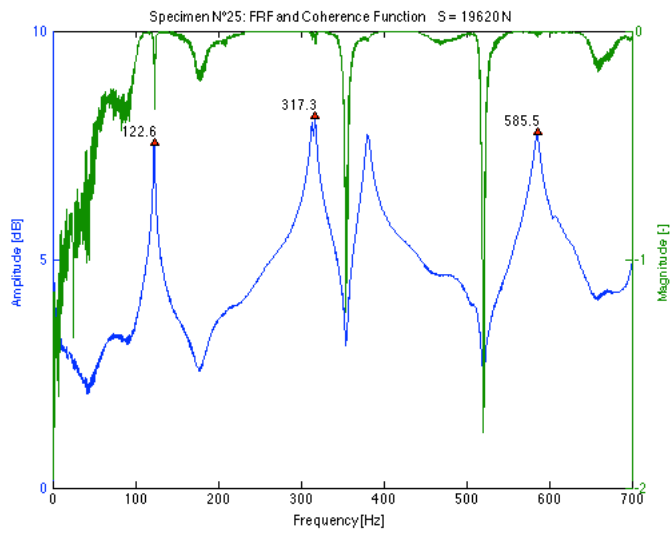
### Data

Table 11-30 Results of frequency measurements and dual parameter estimation for specimen N°25 using the transversal and longitudinal E-modulus for different load levels

T25		using $E_b$						using $E_L$			
Applied load S	% of yield	$S/S_e$	$f_{1b}$	$f_{2b}$	L	$k_{est}$	$S_{est}$	Error on S	$k_{est}$	$S_{est}$	Error on S
[N]	[%]	[-]	[Hz]	[Hz]	[m]	[Nm]	[N]	[%]	[Nm]	[N]	[%]
5494	8.1	0.26	108.3	287.0	1.295	133170	5503	0.2	114880	6266	14.1
10202	15.0	0.46	114.1	298.2	1.275	115140	12002	17.6	99877	13013	27.5
15009	22.1	0.66	118.7	307.9	1.255	100960	16432	9.5	87850	17698	17.9
19620	28.9	0.86	122.6	317.3	1.255	204540	14199	-27.6	169880	14900	-24.1
24721	36.4	1.09	127.4	323.5	1.255	170310	24850	0.5	143370	25796	4.3
28645	42.1	1.26	129.8	328.7	1.255	251660	25309	-11.6	203020	26055	-9.0

## FRF plots





---

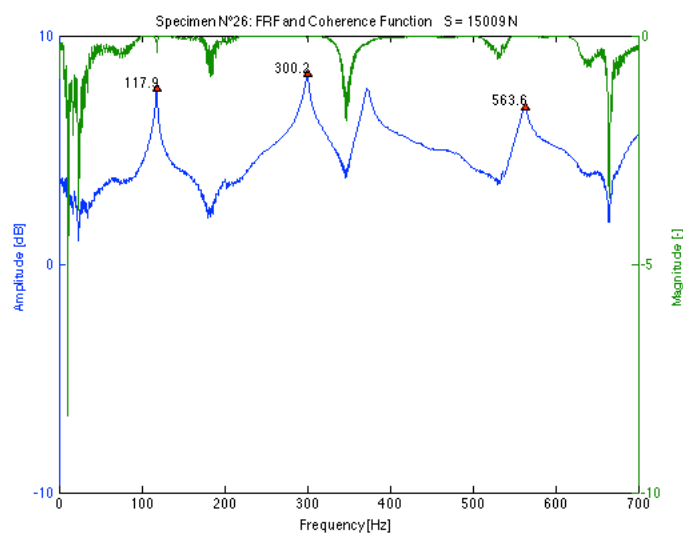
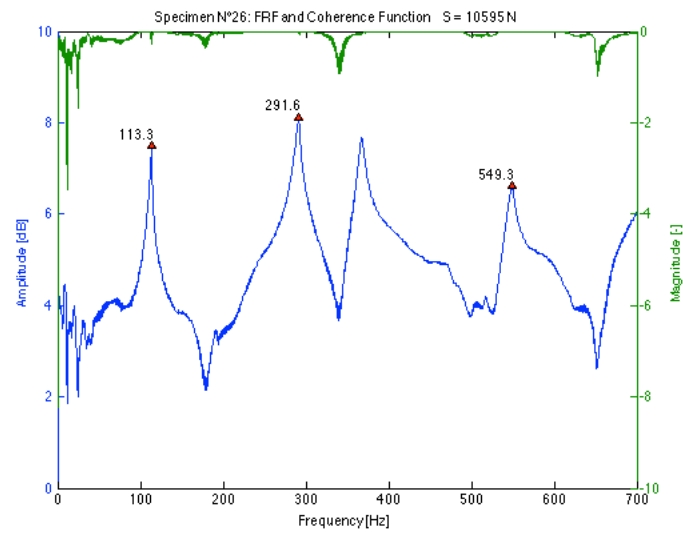
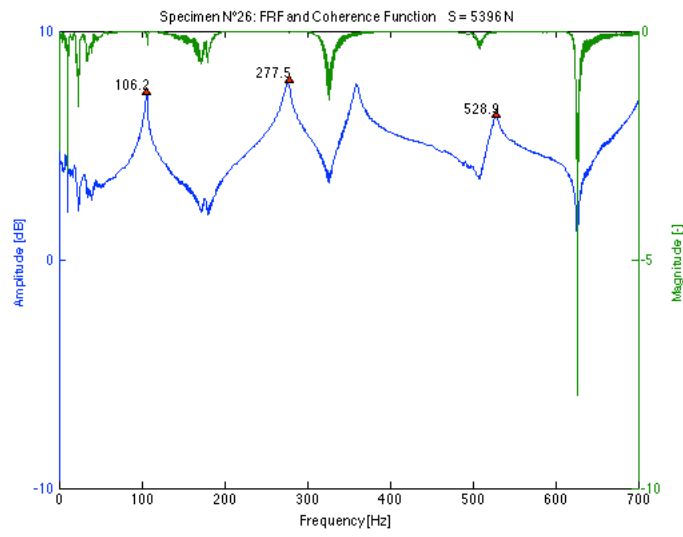
## T26

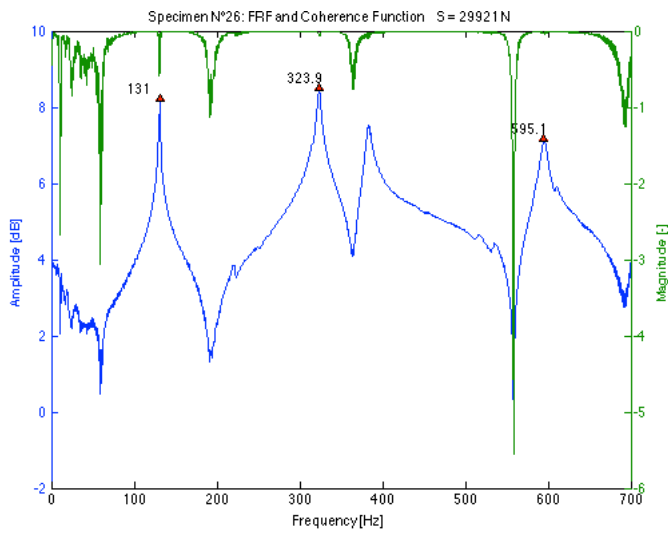
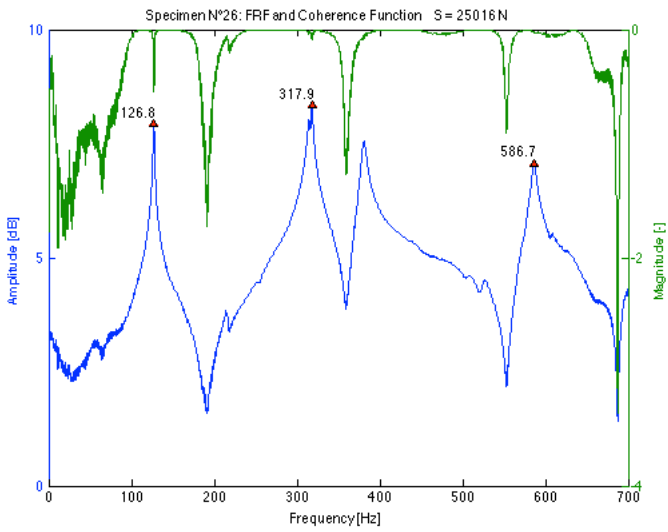
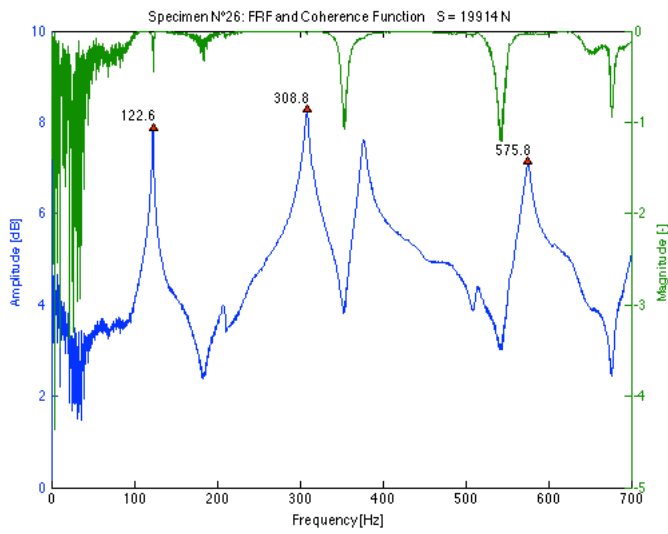
### Data

Table 11-31 Results of frequency measurements and dual parameter estimation for specimen N°26 using the transversal and longitudinal E-modulus for different load levels

T26			using $E_s$						using $E_L$			
Applied load S	% of yield	$S/S_e$	$f_{1b}$	$f_{2b}$	L	$k_{est}$	$S_{est}$	Error on S	$k_{est}$	$S_{est}$	Error on S	
[N]	[%]	[-]	[Hz]	[Hz]	[m]	[Nm]	[N]	[%]	[Nm]	[N]	[%]	
5396	7.9	0.28	106.2	277.5	1.295	90729	11075	105.3	58087	14604	170.7	
10595	15.6	0.53	113.3	291.6	1.275	95042	17034	60.8	59988	20943	97.7	
15009	22.1	0.72	117.9	300.2	1.255	69279	24077	60.4	43110	30101	100.5	
19914	29.3	0.96	122.6	308.8	1.255	91681	27723	39.2	56856	32628	63.8	
25016	36.8	1.21	126.8	317.9	1.255	164600	28060	12.2	94086	31305	25.1	
29921	44.0	1.44	131.0	323.9	1.255	150250	36279	21.3	86548	40137	34.1	

## FRF plots





---

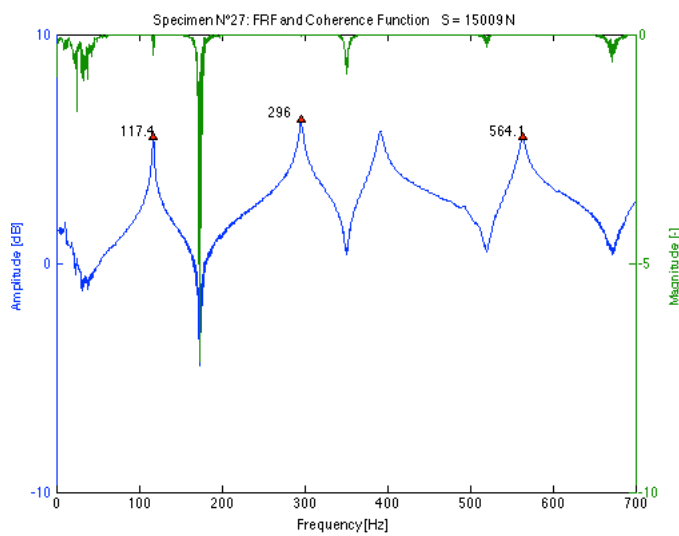
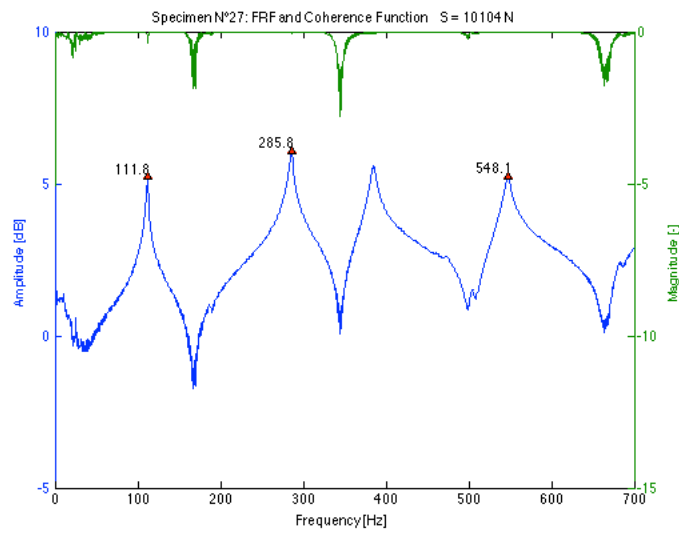
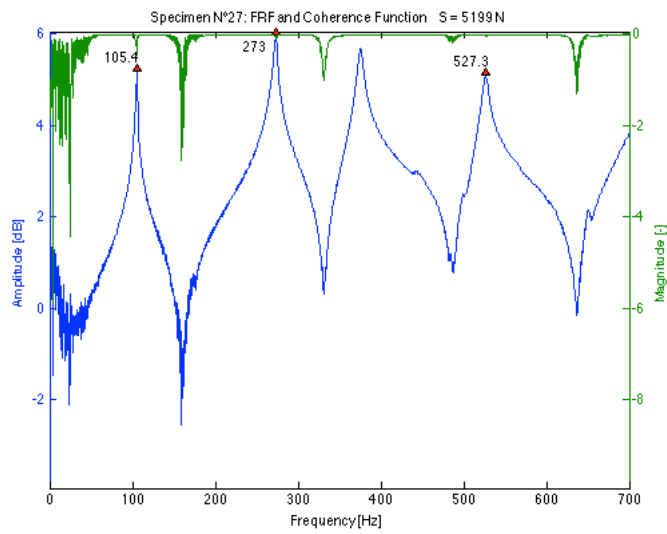
## T27

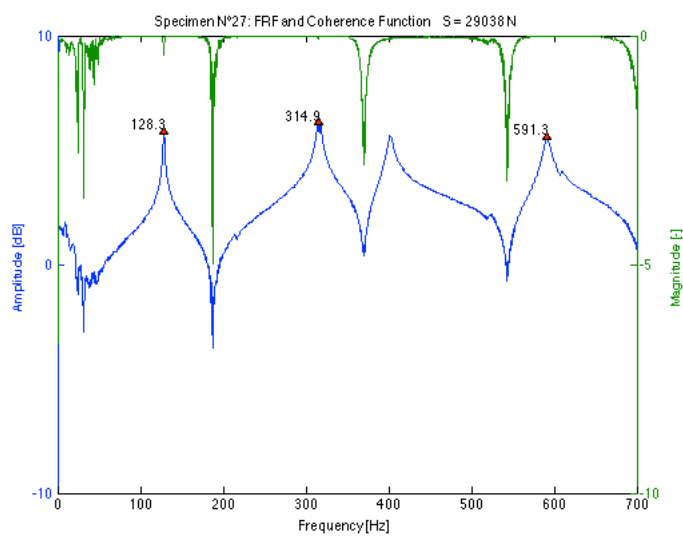
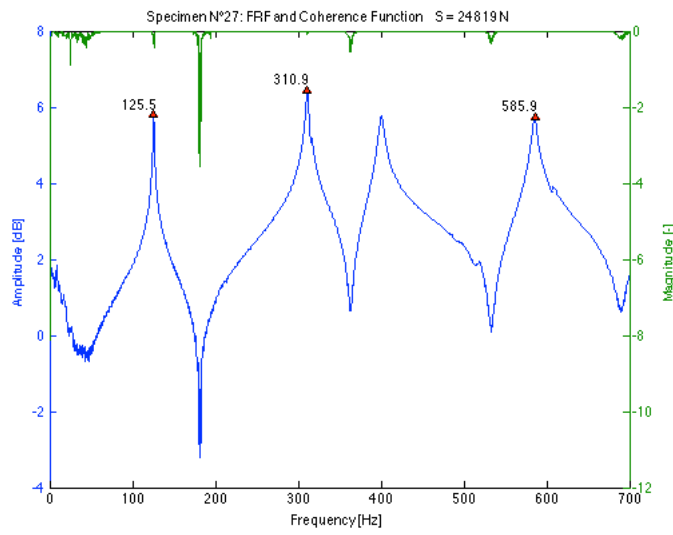
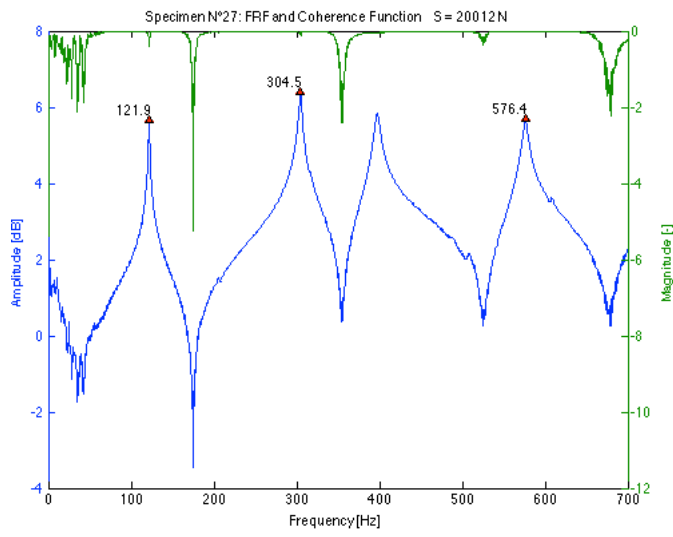
### Data

Table 11-32 Results of frequency measurements and dual parameter estimation for specimen N°27 using the transversal and longitudinal E-modulus for different load levels

T27			using $E_v$						using $E_L$		
Applied load S	% of yield	S/S <sub>e</sub>	f <sub>1b</sub>	f <sub>2b</sub>	L	k <sub>est</sub>	S <sub>est</sub>	Error on S	k <sub>est</sub>	S <sub>est</sub>	Error on S
[N]	[%]	[-]	[Hz]	[Hz]	[m]	[Nm]	[N]	[%]	[Nm]	[N]	[%]
5199	7.6	0.32	105.4	273.0	1.295	91265	14771	184.1	66117	16923	225.5
10104	14.9	0.60	111.8	285.8	1.275	91160	20447	102.4	65672	22908	126.7
15009	22.1	0.86	117.4	296.0	1.255	67947	28891	92.5	48971	32573	117.0
20012	29.4	1.15	121.9	304.5	1.255	92657	32125	60.5	65857	35109	75.4
24819	36.5	1.43	125.5	310.9	1.255	111210	36119	45.5	77413	38883	56.7
29038	42.7	1.67	128.3	314.9	1.255	103870	41990	44.6	72371	45108	55.3

## FRF plots





---

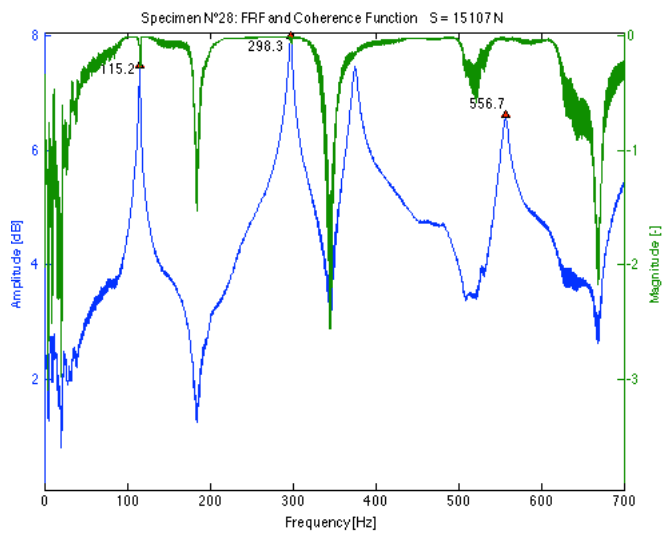
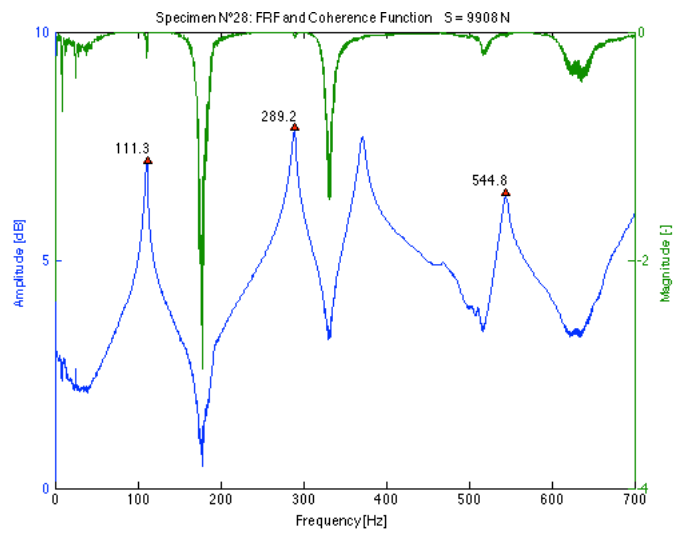
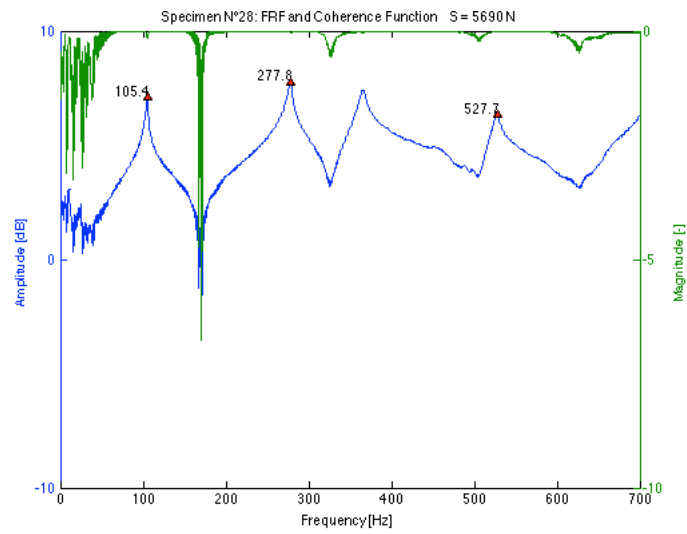
## T28

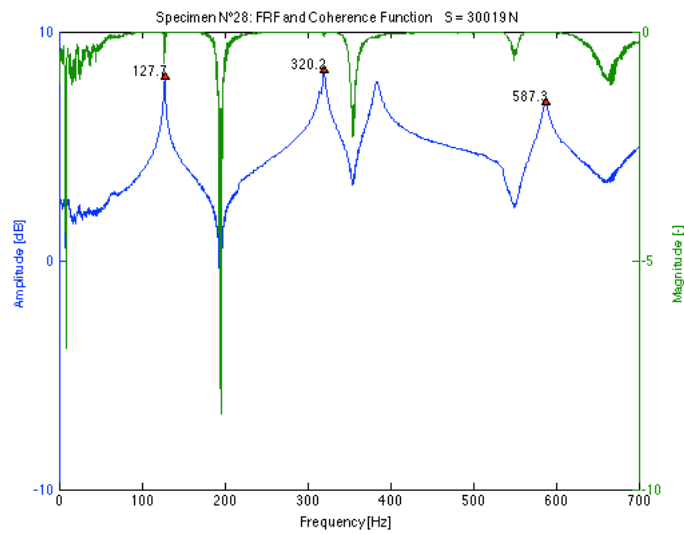
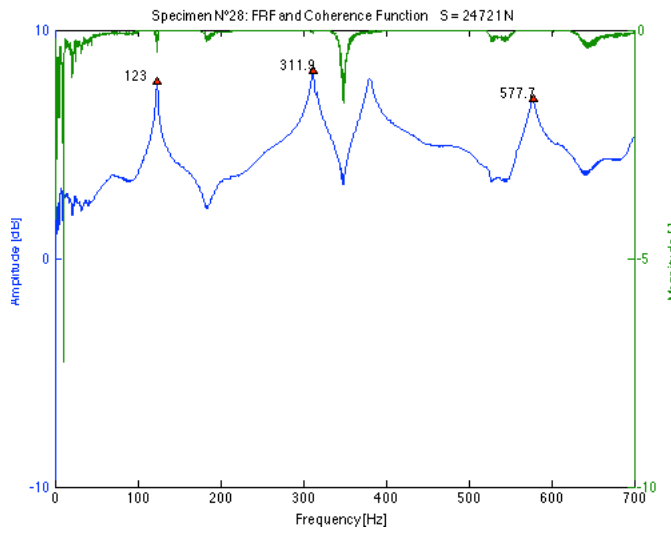
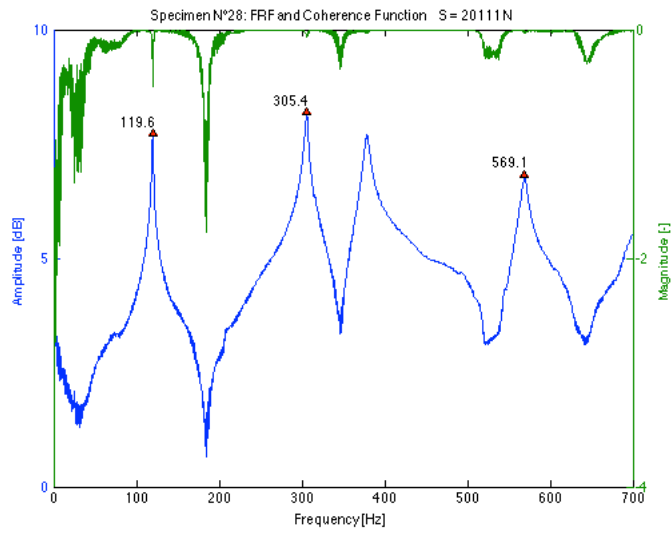
### Data

Table 11-33 Results of frequency measurements and dual parameter estimation for specimen N°28 using the transversal and longitudinal E-modulus for different load levels

T28			using $E_b$						using $E_c$			
Applied load S	% of yield	$S/S_c$	$f_{1b}$	$f_{2b}$	L	$K_{est}$	$S_{est}$	Error on S	$K_{est}$	$S_{est}$	Error on S	
[N]	[%]	[-]	[Hz]	[Hz]	[m]	[Nm]	[N]	[%]	[Nm]	[N]	[%]	
5690	8.4	0.28	105.4	277.8	1.295	247590	5658	-0.6	132740	7247	27.4	
9908	14.6	0.48	111.3	289.2	1.275	208080	11577	16.8	117250	13699	38.3	
15107	22.2	0.70	115.2	298.3	1.255	196410	13251	-12.3	112500	15630	3.5	
20111	29.6	0.94	119.6	305.4	1.255	234880	19436	-3.4	126900	21828	8.5	
24721	36.4	1.15	123.0	311.9	1.255	388610	22356	-9.6	172930	24347	-1.5	
30019	44.1	1.40	127.7	320.2	1.255	814050	28182	-6.1	240180	29981	-0.1	

## FRF plots





---

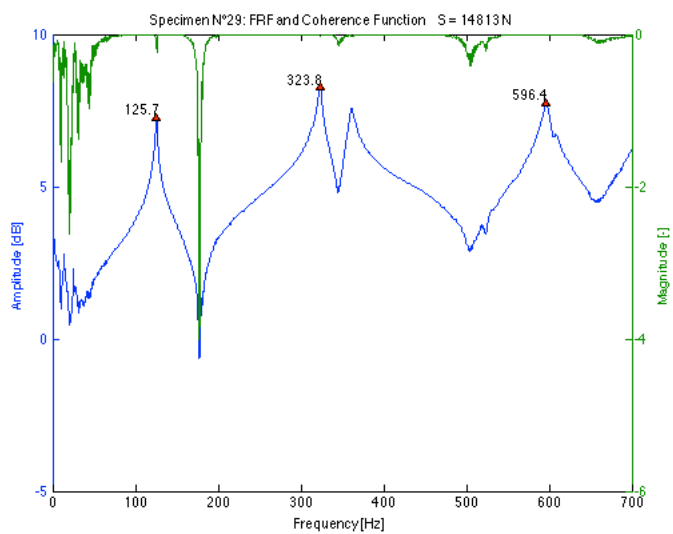
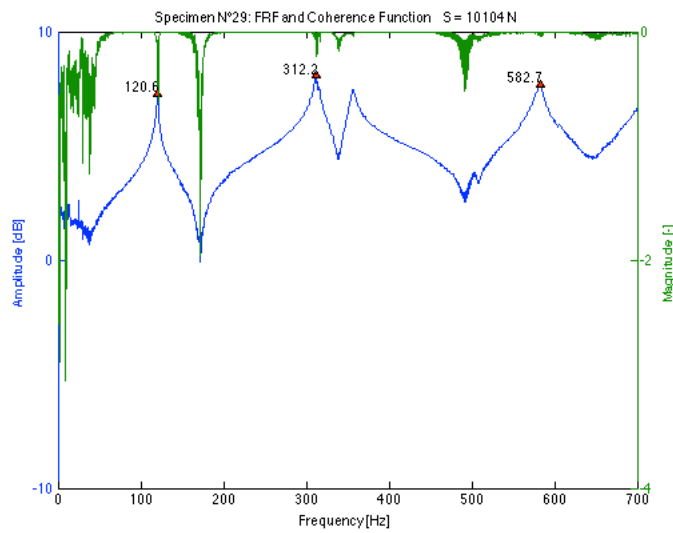
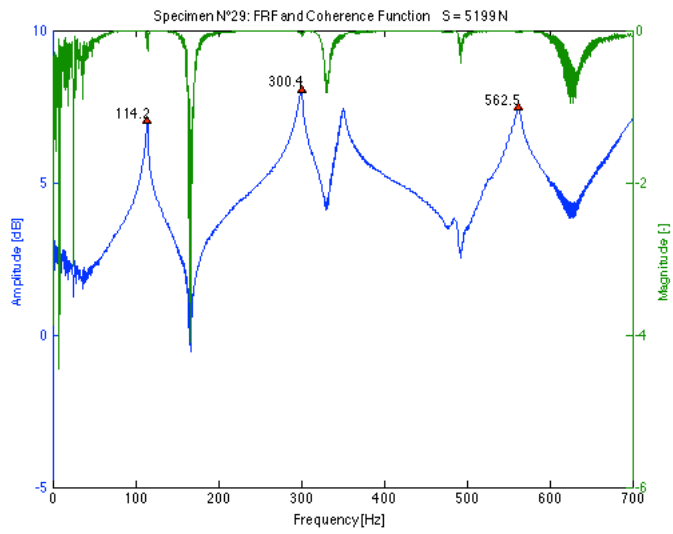
## T29

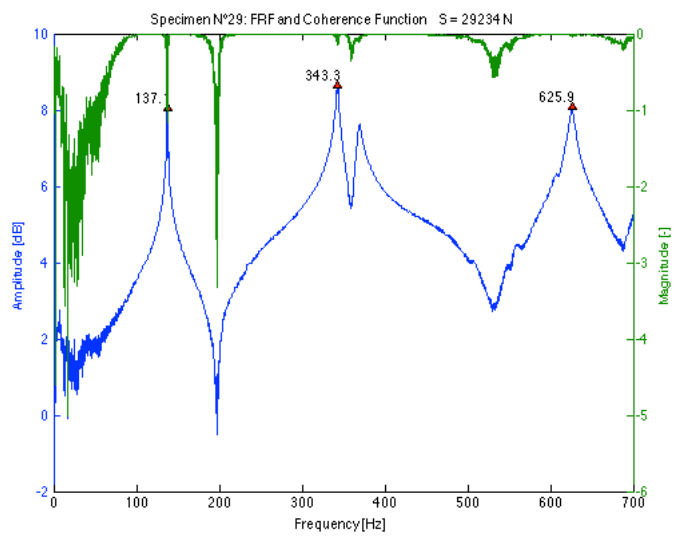
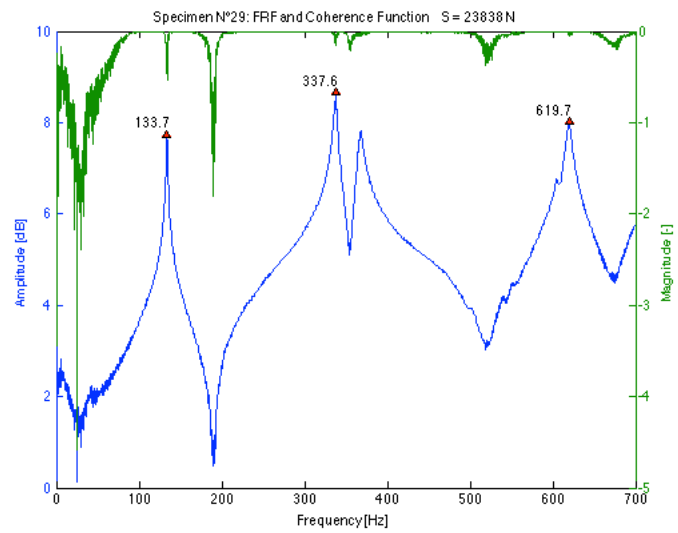
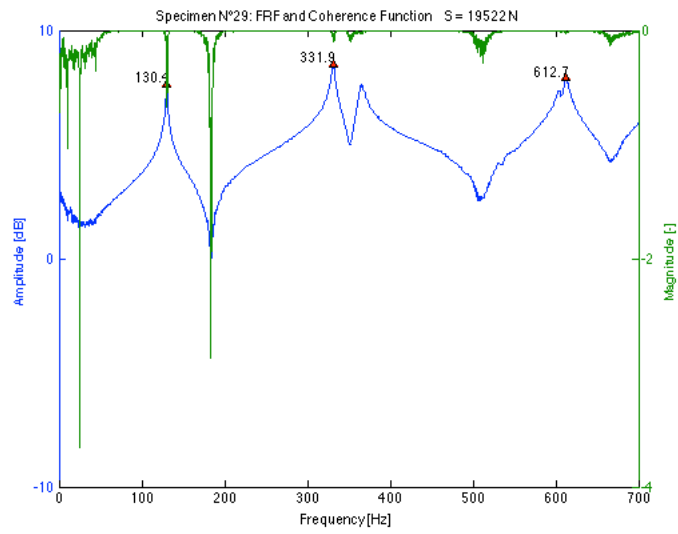
### Data

Table 11-34 Results of frequency measurements and dual parameter estimation for specimen N°29 using the transversal and longitudinal E-modulus for different load levels

T29			using $E_v$						using $E_L$		
Applied load S	% of yield	S/S <sub>y</sub>	f <sub>1b</sub>	f <sub>2b</sub>	L	k <sub>est</sub>	S <sub>est</sub>	Error on S	k <sub>est</sub>	S <sub>est</sub>	Error on S
[N]	[%]	[-]	[Hz]	[Hz]	[m]	[Nm]	[N]	[%]	[Nm]	[N]	[%]
5199	7.6	0.26	114.2	300.4	1.295	289490	3313	-36.3	189670	4107	-21.0
10104	14.9	0.48	120.6	312.2	1.275	210400	10303	2.0	147540	11527	14.1
14813	21.8	0.69	125.7	323.8	1.255	230300	12187	-17.7	158610	13444	-9.2
19522	28.7	0.90	130.4	331.9	1.255	336480	17243	-11.7	210120	18368	-5.9
23838	35.1	1.10	133.7	337.6	1.255	474000	20998	-11.9	263440	22048	-7.5
29234	43.0	1.35	137.1	343.3	1.255	679870	25426	-13.0	323590	26454	-9.5

## FRF plots





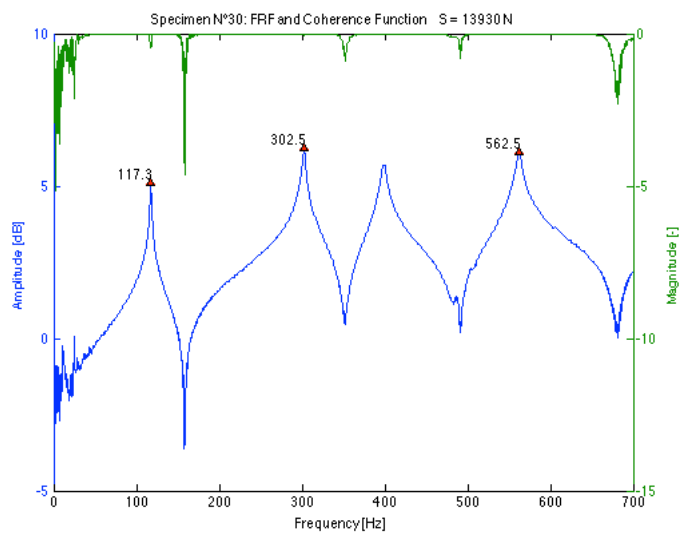
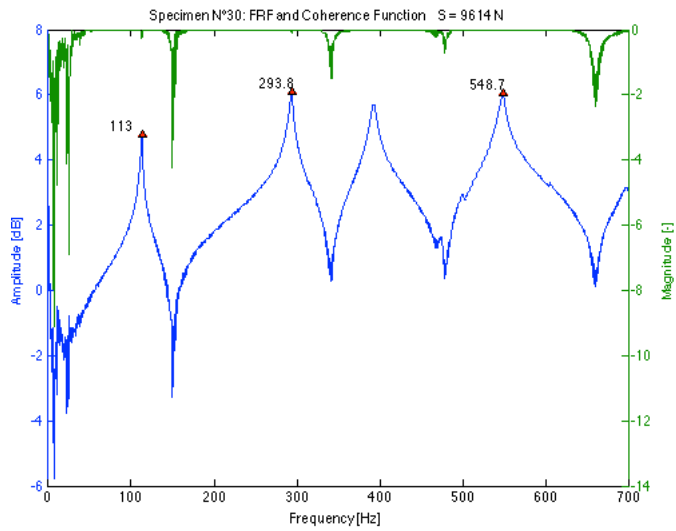
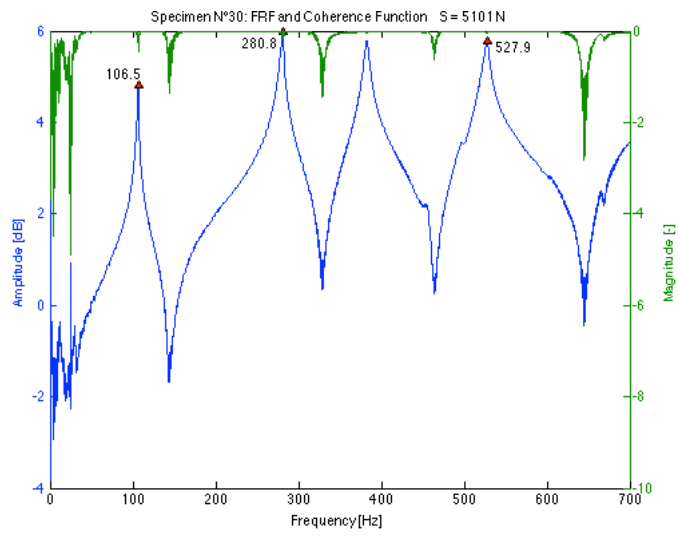
# T30

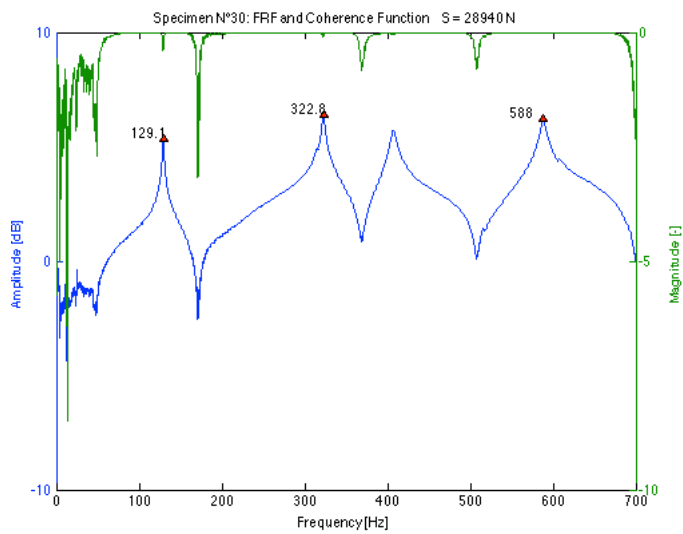
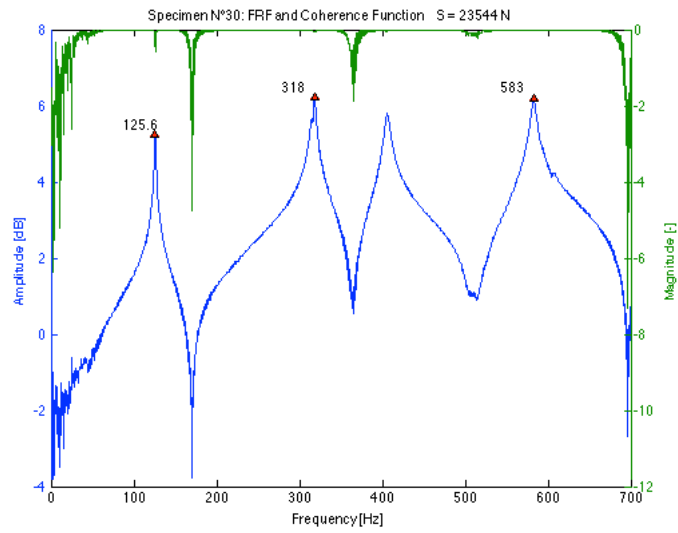
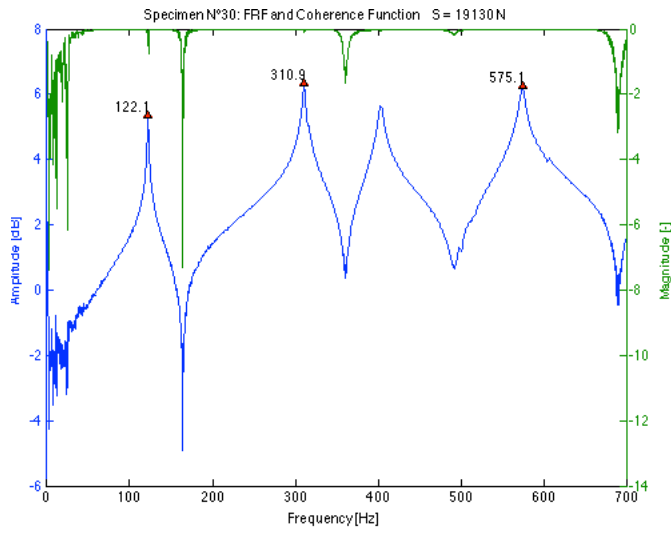
## Data

Table 11-35 Results of frequency measurements and dual parameter estimation for specimen N°30 using the transversal and longitudinal E-modulus for different load levels

T30			using $E_s$						using $E_L$			
Applied load S	% of yield	S/S <sub>e</sub>	f <sub>1b</sub>	f <sub>2b</sub>	L	K <sub>est</sub>	S <sub>est</sub>	Error on S	K <sub>est</sub>	S <sub>est</sub>	Error on S	
[N]	[%]	[-]	[Hz]	[Hz]	[m]	[Nm]	[N]	[%]	[Nm]	[N]	[%]	
5101	7.5	0.30	106.5	280.8	1.295	485920	6040	18.4	214330	6626	29.9	
9614	14.1	0.55	113.0	293.8	1.275	482230	10968	14.1	214020	11707	21.8	
13930	20.5	0.78	117.3	302.5	1.255	277790	14582	4.7	155890	15660	12.4	
19130	28.1	1.06	122.1	310.9	1.255	496570	19727	3.1	216990	20712	8.3	
23544	34.6	1.31	125.6	318.0	1.255	/	/	/	426080	22905	-2.7	
28940	42.6	1.61	129.1	322.8	1.255	2363500	28457	-1.7	354330	29427	1.7	

## FRF plots





---

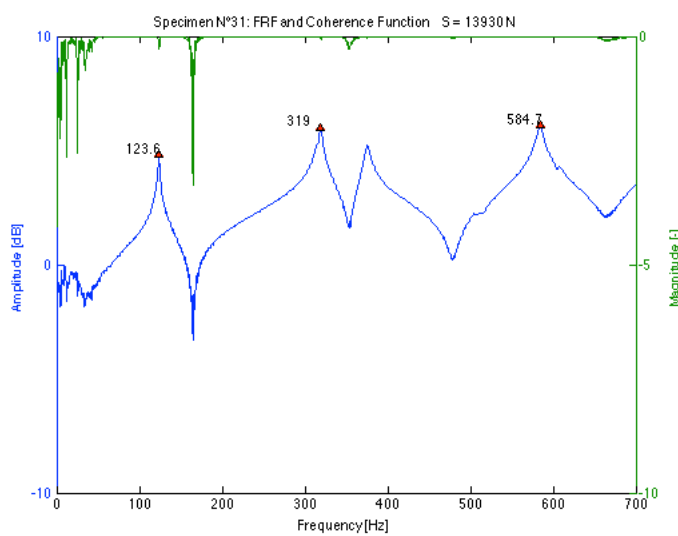
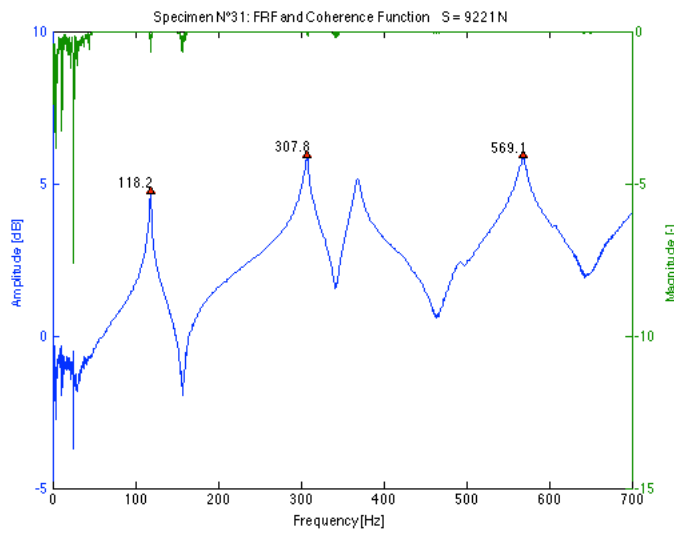
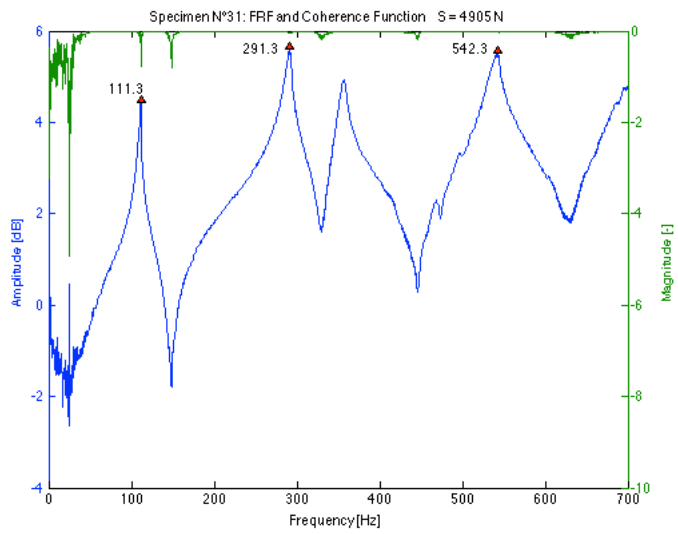
# T31

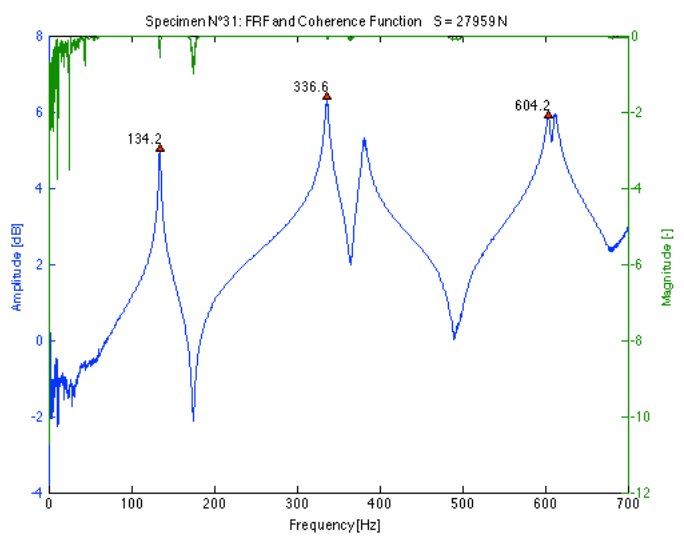
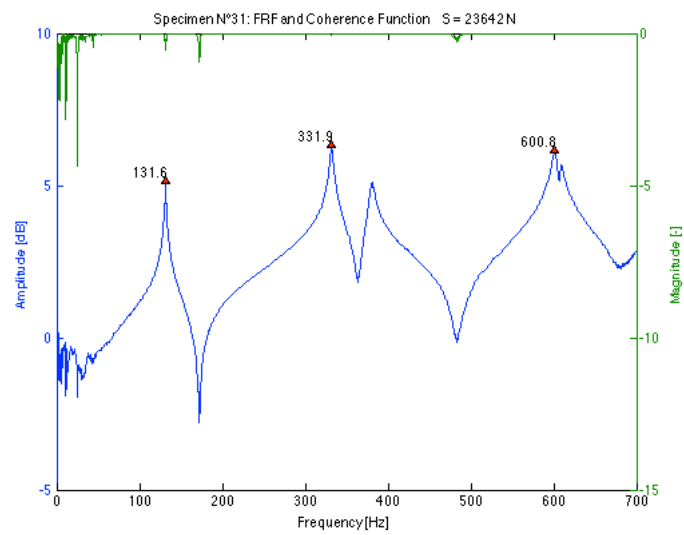
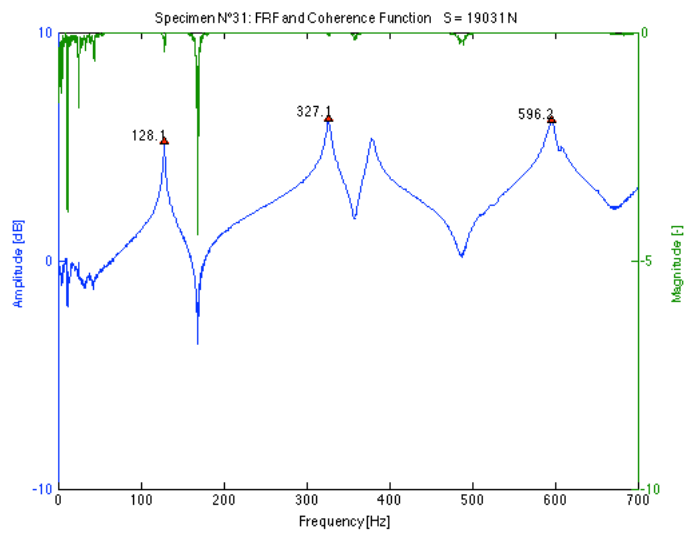
## Data

Table 11-36 Results of frequency measurements and dual parameter estimation for specimen N°31 using the transversal and longitudinal E-modulus for different load levels

T31		using $E_b$							using $E_L$			
Applied load S	% of yield	S/S <sub>c</sub>	f <sub>12</sub>	f <sub>20</sub>	L	K <sub>est</sub>	S <sub>est</sub>	Error on S	K <sub>est</sub>	S <sub>est</sub>	Error on S	
[N]	[%]	[-]	[Hz]	[Hz]	[m]	[Nm]	[N]	[%]	[Nm]	[N]	[%]	
4905	7.2	0.26	111.3	291.3	1.295	116600	9414	91.9	128350	8962	82.7	
9221	13.6	0.48	118.2	307.8	1.275	212770	9360	1.5	244480	9068	-1.7	
13930	20.5	0.70	123.6	319.0	1.255	189440	13596	-2.4	215300	13230	-5.0	
19031	28.0	0.96	128.1	327.1	1.255	282880	17844	-6.2	337210	17535	-7.9	
23642	34.8	1.19	131.6	331.9	1.255	253560	24631	4.2	298400	24252	2.6	
27959	41.1	1.40	134.2	336.6	1.255	329760	27349	-2.2	404410	26999	-3.4	

## FRF plots





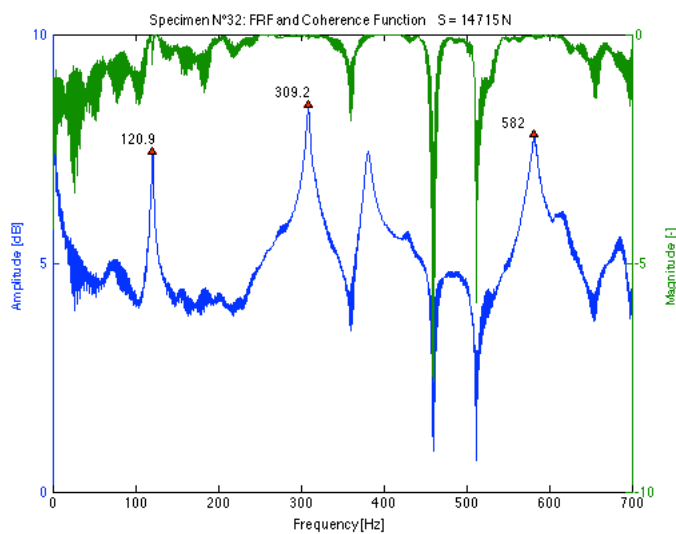
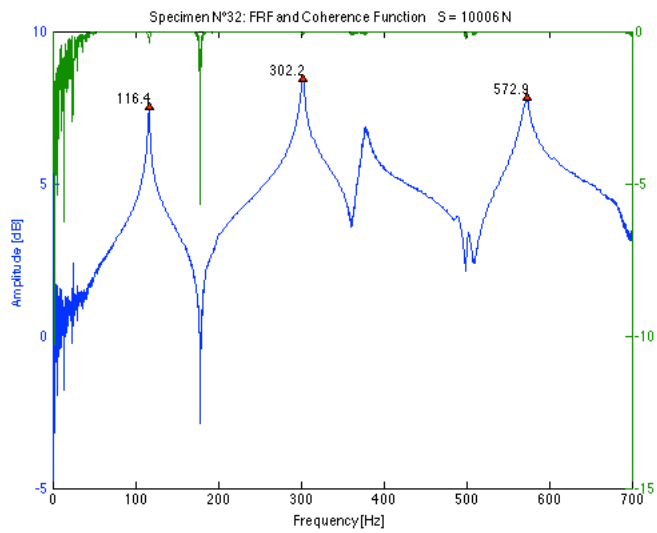
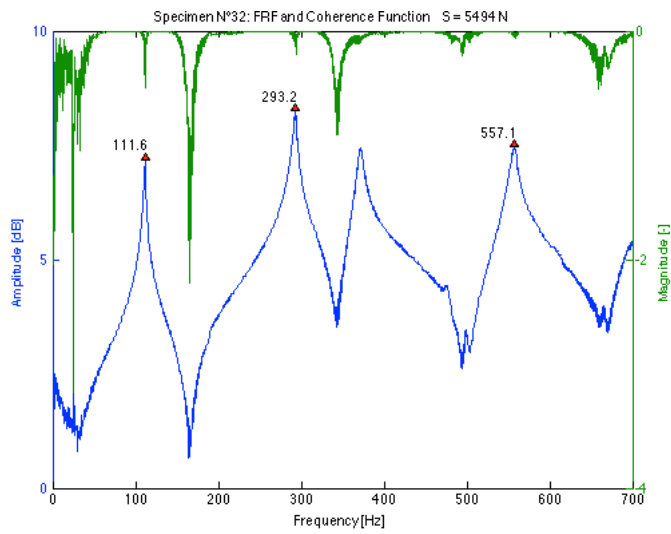
# T32

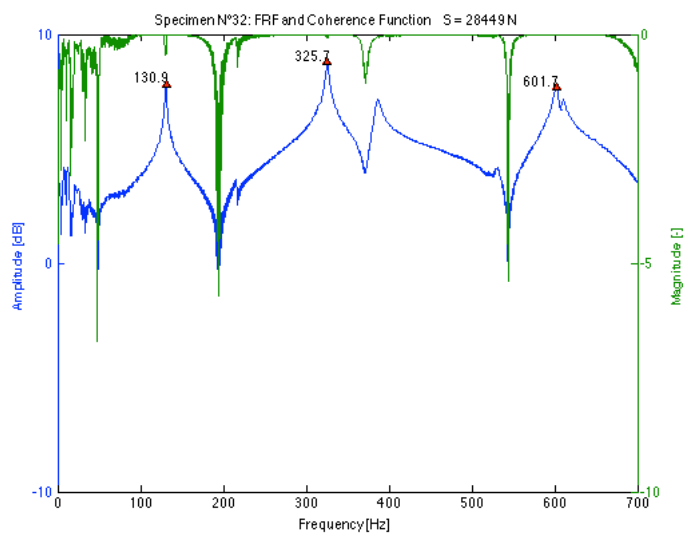
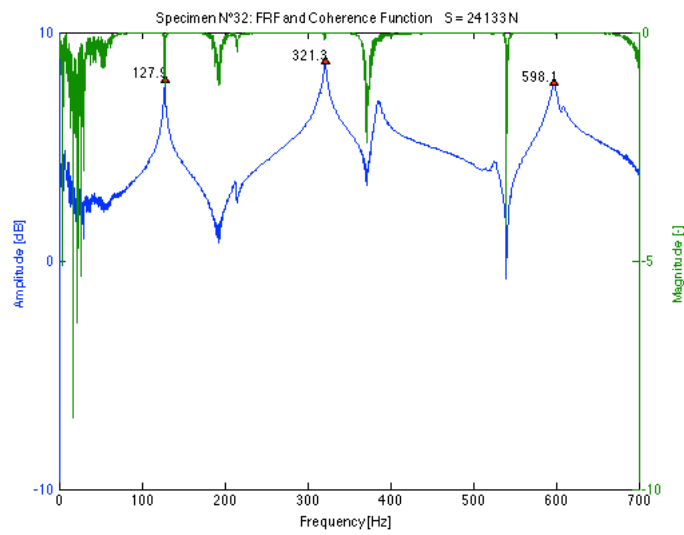
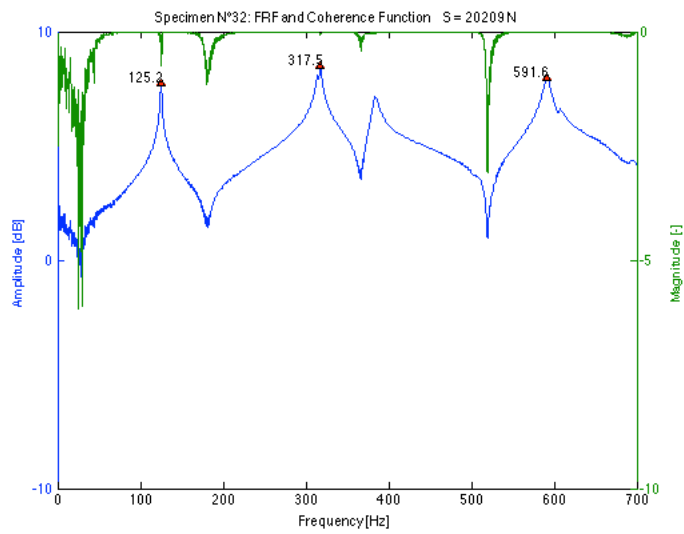
## Data

Table 11-37 Results of frequency measurements and dual parameter estimation for specimen N°32 using the transversal and longitudinal E-modulus for different load levels

T32			using $E_b$						using $E_L$			
Applied load S	% of yield	$S/S_c$	$f_{1b}$	$f_{2b}$	L	$k_{est}$	$S_{est}$	Error on S	$k_{est}$	$S_{est}$	Error on S	
[N]	[%]	[-]	[Hz]	[Hz]	[m]	[Nm]	[N]	[%]	[Nm]	[N]	[%]	
5494	8.1	0.31	111.6	293.2	1.295	414340	5857	6.6	277440	6228	13.4	
10006	14.7	0.54	116.4	302.2	1.275	239450	11170	11.6	181590	11796	17.9	
14715	21.6	0.77	120.9	309.2	1.255	114460	20173	37.1	94453	21471	45.9	
20209	29.7	1.06	125.2	317.5	1.255	170900	22960	13.6	135630	23981	18.7	
24133	35.5	1.27	127.9	321.3	1.255	161960	28156	16.7	129000	29304	21.4	
28449	41.8	1.49	130.9	325.7	1.255	157020	33802	18.8	125120	35073	23.3	

## FRF plots





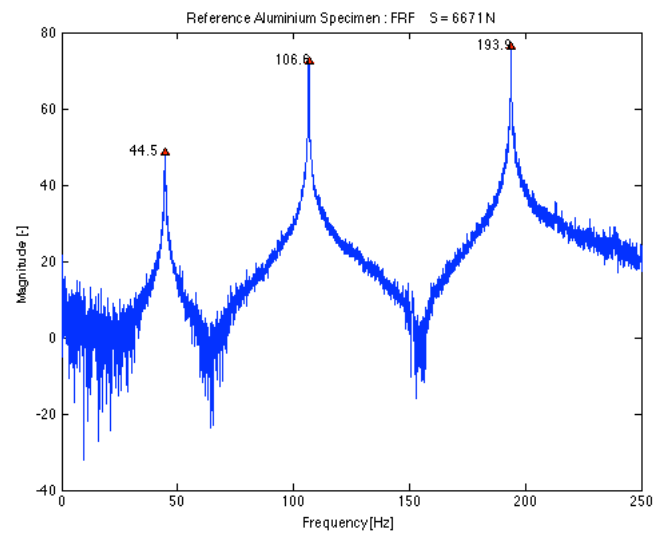
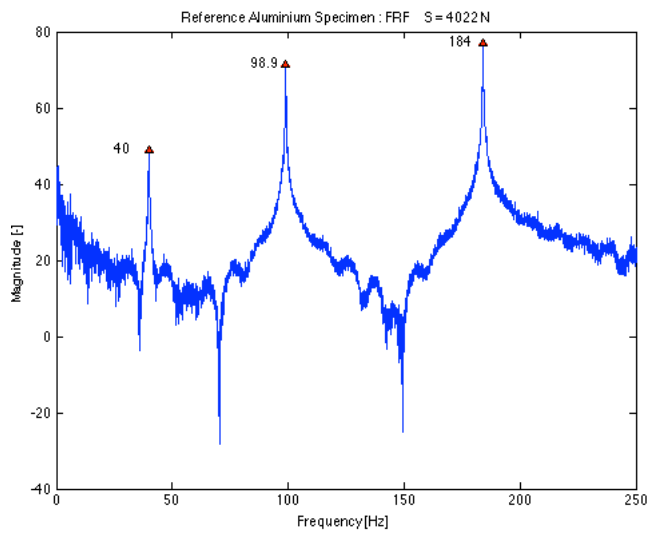
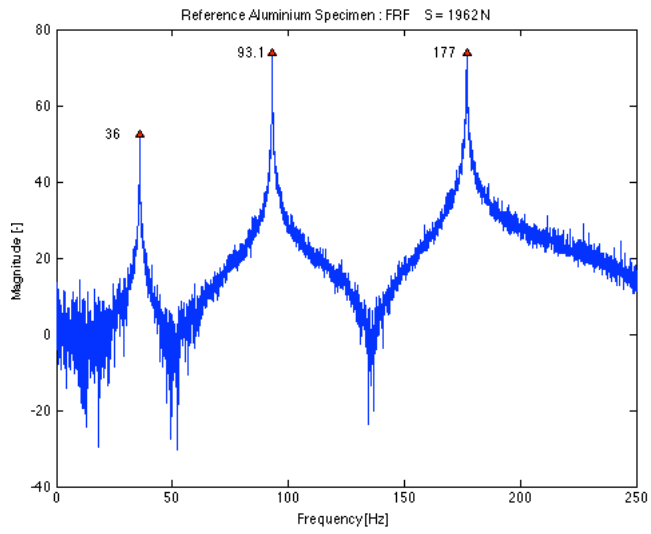
# Aluminium

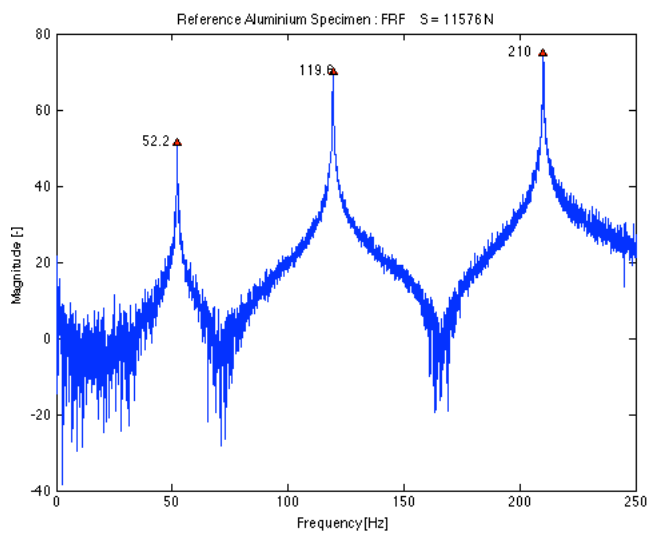
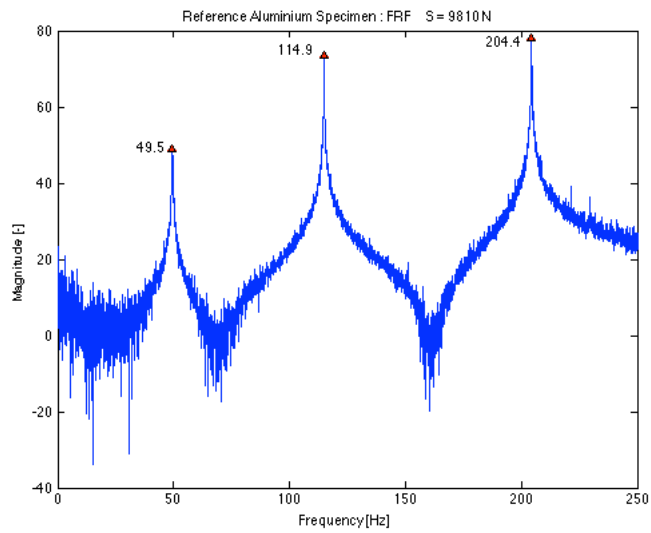
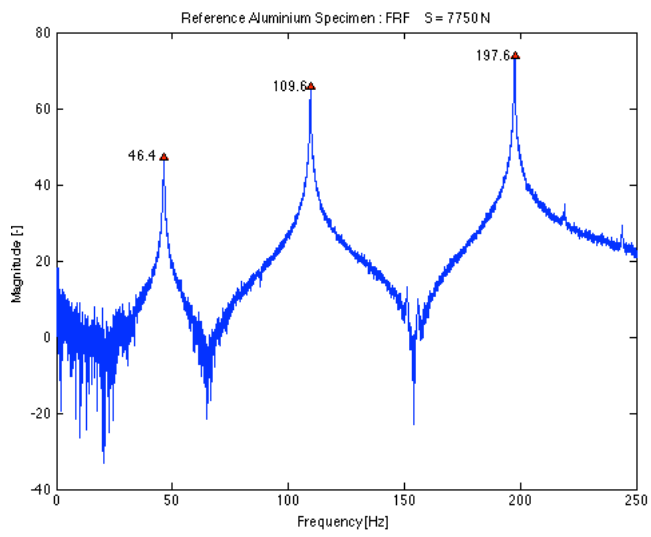
## Data

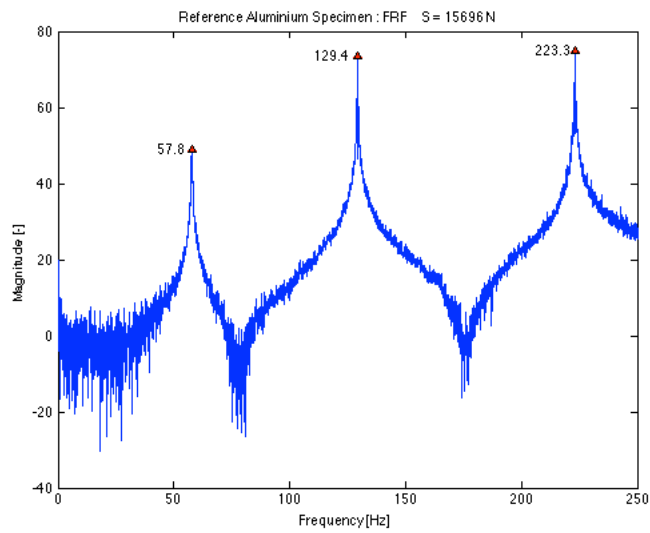
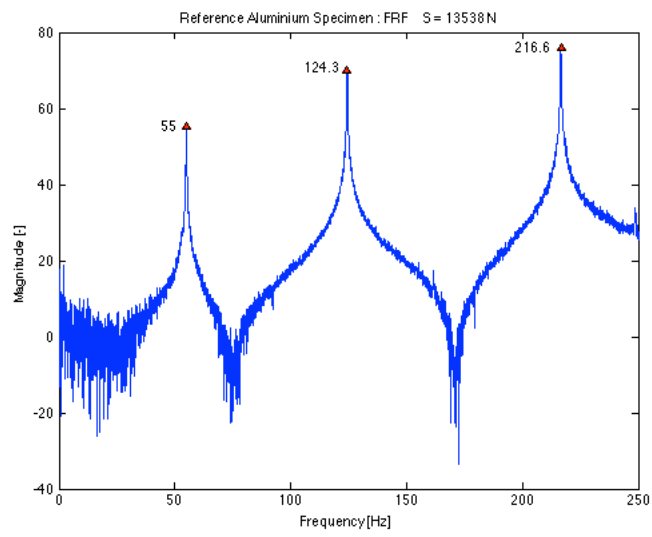
Table 11-38 Results of frequency measurements and dual parameter estimation for the reference aluminium specimen using the transversal and longitudinal E-modulus for different load levels

Aluminium		using $E_b$										
Applied load S	% of yield	$S/S_c$	$f_{1b}$	$f_{2b}$	L	$k_{est}$	$S_{est}$	Error on S	$k_{est}$	$S_{est}$	Error on S	
[N]	[%]	[-]	[Hz]	[Hz]	[m]	[Nm]	[N]	[%]	[Nm]	[N]	[%]	
1962	8.7	1.1	36.0	93.1	1.245	11831	2261	15.2	9365	2356	20.1	
4022	17.9	2.2	40.0	98.9	1.245	10447	4568	13.6	8323	4712	17.2	
6671	29.6	3.6	44.5	106.6	1.245	15288	6884	3.2	11517	7042	5.6	
7750	34.4	4.2	46.4	109.6	1.245	14510	8181	5.6	10979	8363	7.9	
9810	43.6	5.3	49.5	114.9	1.245	16907	10161	3.6	12418	10367	5.7	
11576	51.4	6.2	52.2	119.6	1.245	19800	11982	3.5	14059	12208	5.5	
13538	60.2	7.3	55.0	124.3	1.245	18378	14241	5.2	13167	14508	7.2	
15696	69.8	8.5	57.8	129.4	1.245	24670	16228	3.4	16532	16508	5.2	

## FRF plots







## 11.3.2 Summary of results

Table 11-39 Error on the estimated axial load  $S$  for each specimen and different load levels using the transversal  $E$ -modulus

$E_t$ Beam N*	$S$ [N]					
	5000	10000	15000	20000	25000	30000
1	16.2	27.0	2.9	18.9	17.1	7.9
2	119.5	80.4	79.9	21.0	45.9	47.7
3	56.4	30.1	62.5	36.2	19.5	29.0
4	46.2	18.8	25.7	11.8	27.9	11.6
5	148.2	113.1	76.0	67.4	27.6	25.9
6	26.8	68.1	46.0	16.3	17.5	10.3
7	-23.8	-18.6	11.0	-4.7	-2.8	3.4
8	179.4	69.9	52.4	59.6	21.8	21.1
9	-48.3	-12.5	-0.8	-12.2	-20.1	-9.8
10	5.5	25.8	7.7	3.8	12.3	6.7
11	-107.1	-39.6	-27.6	-1.7	-26.2	-24.2
12	-40.0	-13.5	-21.6	-3.0	-8.9	-18.9
13	-117.2	/	-32.3	-19.9	-41.3	-26.6
14	-66.4	-54.5	-23.1	-27.3	-31.8	-18.7
15	248.2	96.2	126.2	53.8	63.5	42.8
16	97.9	49.3	29.9	5.8	2.3	3.7
17	124.5	63.0	41.8	39.4	31.3	12.1
18	/	/	/	/	/	/
19	-13.1	-1.4	-3.6	-1.6	-0.6	-13.1
20	13.0	19.0	14.6	36.5	12.0	8.1
21	46.5	11.7	29.3	8.5	-4.3	-4.3
22	88.3	95.6	86.6	52.6	13.4	21.7
23	69.5	55.6	44.6	25.7	7.3	12.1
24	204.8	118.2	61.7	47.7	40.1	36.5
25	0.2	17.6	9.5	-27.6	0.5	-11.6
26	105.3	60.8	60.4	39.2	12.2	21.3
27	184.1	102.4	92.5	60.5	45.5	44.6
28	-0.6	16.8	-12.3	-3.4	-9.6	-6.1
29	-36.3	2.0	-17.7	-11.7	-11.9	-13.0
30	18.4	14.1	4.7	3.1	/	-1.7
31	91.9	1.5	-2.4	-6.2	4.2	-2.2
32	6.6	11.6	37.1	13.6	16.7	18.8
Mean value	46.6	34.3	27.8	16.2	9.4	7.6
Std. dev.	89.5	45.0	39.9	26.9	23.7	20.2

Table 11-40 Error on the estimated axial load  $S$  for each specimen and different load levels using the longitudinal  $E$ -modulus

$E_l$ Beam N*	$S$ [N]					
	5000	10000	15000	20000	25000	30000
1	22.2	31.9	7.0	22.4	19.9	10.1
2	120.0	80.8	80.4	21.2	46.1	48.0
3	58.5	31.7	64.9	37.7	20.4	30.1
4	65.4	29.9	35.9	18.0	34.4	15.9
5	164.2	124.9	85.2	74.3	31.1	29.0
6	30.9	71.9	49.1	18.0	18.8	11.3
7	-18.7	-15.1	15.6	-2.3	-1.0	5.3
8	192.2	75.8	57.6	64.3	24.2	23.1
9	-34.5	-2.6	8.2	-7.3	-17.0	-6.7
10	16.9	34.5	14.5	8.4	16.4	9.8
11	-100.5	-34.6	-22.8	-5.7	-28.2	-22.5
12	-26.4	-5.5	-14.9	2.4	-5.6	-16.7
13	-91.8	/	-12.2	-5.5	-35.8	-20.6
14	-49.9	-44.8	-9.4	-20.1	-27.2	-13.7
15	334.9	139.0	189.5	77.6	86.8	58.8
16	155.0	86.6	61.0	22.1	15.0	14.5
17	159.5	82.1	58.2	51.9	41.1	18.4
18	/	/	/	/	/	/
19	-1.3	5.4	3.9	3.6	3.7	-10.7
20	23.0	24.8	20.2	42.4	15.3	10.9
21	78.5	29.5	46.7	18.9	1.4	0.7
22	122.8	126.0	116.0	69.2	21.7	30.3
23	99.9	74.3	61.2	36.1	13.7	17.8
24	257.7	154.1	87.1	63.9	53.2	47.5
25	14.1	27.5	17.9	-24.1	4.3	-9.0
26	170.7	97.7	100.5	63.8	25.1	34.1
27	225.5	126.7	117.0	75.4	56.7	55.3
28	27.4	38.3	3.5	8.5	-1.5	-0.1
29	-21.0	14.1	-9.2	-5.9	-7.5	-9.5
30	29.9	21.8	12.4	8.3	-2.7	1.7
31	82.7	-1.7	-5.0	-7.9	2.6	-3.4
32	13.4	17.9	45.9	18.7	21.4	23.3
Mean value	68.4	48.1	41.5	24.1	14.4	12.4
Std. dev.	102.5	52.6	48.3	30.4	26.2	22.1

Table 11-41 Mean estimated rotational stiffness  $k$  for each specimen using the transversal and longitudinal  $E$ -modulus and comparison with the static  $E$ -modulus

	$k_{est,m}$ using $E_b$ [Nm]	$k_{est,m}$ using $E_L$ [Nm]	$E_{static}$ [MPa]
1	217778	192520	14526
2	125912	125013	13319
3	142740	135887	11987
4	109164	92625	12397
5	116300	102086	13953
6	145995	138035	13855
7	282480	228207	12061
8	115385	103718	12788
9	240127	182157	13995
10	202392	165797	13785
11	301913	275275	14197
12	227233	177413	13841
13	840100	187912	13281
14	1055790	234217	13129
15	75208	52793	13371
16	150643	95364	14052
17	88766	67650	11300
18	/	/	12824
19	336698	196557	10303
20	186780	149527	11752
21	232482	133846	12532
22	106557	77305	13005
23	133503	97141	12286
24	111217	79745	12670
25	162630	136480	13542
26	110264	66446	12341
27	93018	66067	10349
28	348270	150417	12764
29	370090	215495	12860
30	821202	263607	10703
31	230835	271358	11853
32	209688	157206	11337
Mean value	254554	148963	12717
Std. dev.	233373	64211	1117
Alu	16479	12045	70000